Dynamic Covalent Chemistry of Cyclic Oligochalcogenides and Phosphorothioates for Thiol-Mediated Uptake

Laurent, Quentin François Antoine

UNIVERSITÉ DE GENÈVE FACULTÉ DES SCIENCES

Section de chimie et biochimie
Département de chimie organique Professeur Stefan Matile

Dynamic Covalent Chemistry of Cyclic Oligochalcogenides and Phosphorothioates for Thiol-Mediated Uptake

THÈSE

présentée à la Faculté des sciences de l'Université de Genève
pour obtenir le grade de Docteur ès sciences, mention chimie

par
Quentin LAURENT
de
Lyon (FR)

Thèse N° xxxx

GENÈVE
Atelier Repromail – Uni Mail
2022

UNIVERSITÉ DE GENÈVE

FACULTÉ DES SCIENCES

DOCTORAT ÈS SCIENCES, MENTION CHIMIE

Thèse de Monsieur Quentin François Antoine LAURENT

intitulée :

«Dynamic Covalent Chemistry of Cyclic Oligochalcogenides and Phosphorothioates for Thiol-Mediated Uptake»

La Faculté des sciences, sur le préavis de Monsieur S. MATILE, professeur ordinaire et directeur de thèse (Département de chimie organique), Monsieur N. WINSSINGER, professeur ordinaire (Département de chimie organique), Monsieur O. THORN-SESHOLD, docteur (Department of Pharmacy, Ludwig-Maximilians, Universtät München, München, Germany), autorise l'impression de la présente thèse, sans exprimer d'opinion sur les propositions qui y sont énoncées.

Genève, le 1er mars 2022

Thèse - 5638 -

Le Doyen

N.B. - La thèse doit porter la déclaration précédente et remplir les conditions énumérées dans les "Informations relatives aux thèses de doctorat à l'Université de Genève".

Acknowledgements

I would first like to thank my PhD advisor, Prof. Stefan Matile, for these four years. I had a great time in Geneva, worked on extremely exciting and innovative science, and I am truly grateful for that. I also greatly acknowledge the help of Dr. Naomi Sakai, whose day-to-day help in the lab has been extremely important to me, and to everyone in the group.

I greatly thank my jury members, Dr. Oliver Thorn-Seshold and Prof. Nicolas Winssinger, for taking the time to evaluate my work. I hope you will find this thesis and PhD defense enjoyable, and look forward to discussing the science herein with you.

Most of the projects I worked on during these four years would not have been possible without the help of excellent collaborators. I would like to acknowledge the great teamwork by Dr. Mathéo Berthet and Dr. Sofia Barluenga, in the group of Prof. Winssinger, on the collaboration for the antibiotics project. I have been fortunate enough to take part in large collaborations, and I am grateful to have always worked with incredible scientists. A particular thank you goes to the ACCESS platform, Dr. Dimitri Moreau and Stefania Vossio, for their amazing help with cell and microscopy experiments. Especially to Dimitri, who has been the easiest person to collaborate with, taking time to help us with project designs, failed experiments, and so on, on top of being an excellent skiing companion.

I never thought the toughest words to write in this thesis would be the ones coming next. It's difficult to say goodbye to such a group of great friends like the Matile group has been over the years. I am extremely thankful to all the group members, past and present, who made this journey so enjoyable, cheering me up when things weren't good, celebrating when they were, … Everything would have been a lot tougher without them. A special thanks to everyone who I shared the lab with, Éline, Xiaoyu, Andrea, Bumhee, Filipe, and Michael, and those who didn't but still spent some time around my fumehood, Anna, Karolina, Lucia,

Heorhii, Miguel, … A very special thank you to the two most supportive people ever, Lea and Inga, who have been around most of my time in Geneva, are excellent scientists, and even more excellent friends, thank you for always being here. And a special thanks also goes to Andrea and Lucia, for being always great chemists and remaining close friends after they left.

In an international lab in a French-speaking country, it has almost been part of the contract to help others giving phone calls to administrations, insurances, banks, … I have been lucky to share this task with an amazing French team, Rémi and Antoine. Rémi has been here most of my time in Geneva, has spent hours proofreading this thesis, and even worse, has been suffering my "Friday afternoon genius ideas" mayhem for years. I am glad I got to share all this time with a friend like him. Antoine was only here for the first year and a half of my PhD, but has been extremely important to my development as a scientist. His passion for science, knowledge, and mentoring throughout the years, even after he left, even in everyday life, and his friendship have been most important.

I got the chance, when I started, to be offered to supervise the apprentices in our lab. It has been a great pleasure and an important learning process for me to train Samantha and Mélissa over this time. I don't think they realized how much I was learning when teaching them, and I am grateful for this opportunity.

An immense thank you to my family and friends outside the lab, without whom I would not be where I am today. My parents and my brother have always supported my choices, even though they have not a single clue about what chemistry is and what I do, and I will forever be thankful for that. Laura has been the most important person throughout these four years and many more, being the most amazing ~~girlfriend~~ fiancée one can hope for. I cannot express how happy I am I got to share every moment with her.

Finally, thank you to anyone who is reading this thesis, I hope you will find what you are looking for here, and that my writing won't bore you to death.

List of Publications

[1] **Q. Laurent**, N. Sakai, S. Matile, "The Opening of 1,2-Dithiolanes and 1,2-Diselenolanes: Regioselectivity, Rearrangements, and Consequences for Poly(Disulfide)s, Cellular Uptake and Pyruvate Dehydrogenase Complexes", *Helv. Chim. Acta* **2019**, *102*, e1800209.

[2] E. Bartolami, D. Basagiannis, L. Zong, R. Martinent, Y. Okamoto, **Q. Laurent**, T. R. Ward, M. Gonzalez-Gaitan, N. Sakai, S. Matile, "Diselenolane-Mediated Cellular Uptake: Efficient Cytosolic Delivery of Probes, Peptides, Proteins, Artificial Metalloenzymes and Protein-Coated Quantum Dots", *Chem. Eur. J.* **2019**, *25*, 4047–4051.

[3] R. Martinent, **Q. Laurent**, N. Sakai, S. Matile, "Cellular Uptake Mediated by Cyclic Oligochalcogenides", *Chimia* **2019**, *73*, 304–307.

[4] **Q. Laurent***, M. Berthet*, Y. Cheng, N. Sakai, S. Barluenga, N. Winssinger, S. Matile, "Probing for Thiol-Mediated Uptake into Bacteria", *ChemBioChem* **2020**, *21*, 69–73.

[5] J. López-Andarias, J. Saarbach, D. Moreau, Y. Cheng, E. Derivery, **Q. Laurent**, M. Gonzáles-Gaitán, N. Winssinger, N. Sakai, S. Matile, "Cell-Penetrating Streptavidin: A General Tool for Bifunctional Delivery with Spatiotemporal Control, Mediated by Transport Systems Such as Adaptive Benzopolysulfane Networks", *J. Am. Chem. Soc.* **2020**, *142*, 4784–4782.

[6] **Q. Laurent**, R. Martinent, B. Lim, A.-T. Pham, T. Kato, J. López-Andarias, N. Sakai, S. Matile, "Thiol-Mediated Uptake", *JACS Au* **2021**, *1*, 710–728.

[7] **Q. Laurent**, R. Martinent, D. Moreau, N. Winssinger, N. Sakai, S. Matile, "Oligonucleotide Phosphorothioates Enter Cells by Thiol-Mediated Uptake", *Angew. Chem. Int. Ed.* **2021**, *60*, 19102–19106.

[8] R. Martinent, S. Tawffik, J. López-Andarias, D. Moreau, **Q. Laurent**, S. Matile, "Dithiolane Quartets: Thiol-Mediated Uptake Enables

Cytosolic Delivery in Deep Tissue", *Chem. Sci*. **2021**, *12*, 13922–13929.

[9] **Q. Laurent**, N. Sakai, S. Matile, "Orthogonal Dynamic Covalent Chemistry for Ring-Opening Polymerization of Cyclic Oligochalcogenides on Detachable Helical Peptide Templates", *in preparation*.

* These authors contributed equally.

Summary

The great potential of macromolecules such as oligonucleotides or proteins in therapeutic and fundamental studies is often hampered by the low permeability of the cell membrane to such molecules. It is therefore crucial to develop tools to understand and improve the cellular uptake of these biomolecules. Over the past few decades, the field of cellular uptake grew bigger and bigger, and many methods are nowadays available for these purposes. Cell-penetrating peptides (CPPs) have first received attention, being able to either trigger endocytosis and endosomal escape, or to achieve direct cytosolic delivery through counterion-mediated uptake. Thiol-mediated uptake is receiving increasing attention as an innovative way to penetrate cells. Taking advantage of dynamic thiol-disulfide exchanges at the cell surface, both polymeric and small molecule transporters were introduced by our group, achieving excellent cellular uptake properties with minimal toxicity.

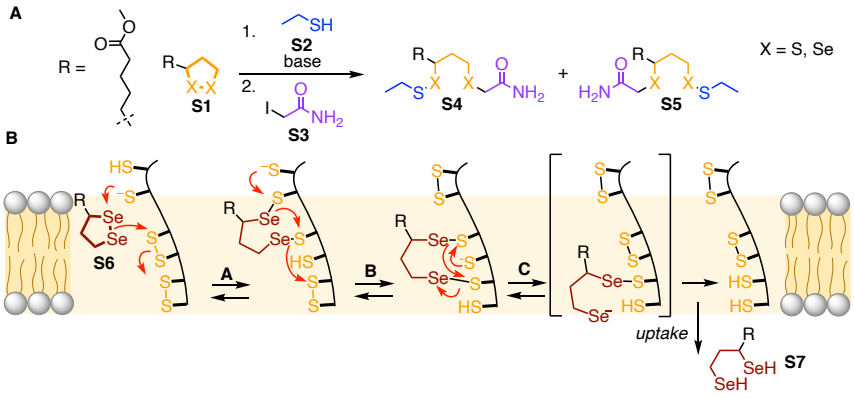

Figure S1. A) Regioselective ring opening of 1,2-dithiolane and 1,2-diselenolane. B) Hypothetic molecular walker mechanism for 1,2-diselenolane uptake.

The purpose of this thesis is to better understand the mechanisms involved in thiol-mediated uptake. Starting from a curiosity question, whether the attack of a thiolate on lipoic acid derivatives was regioselective or not, the ring opening of 1,2-dithiolanes **S1** and 1,2-diselenolanes **S6** was first studied (Figure S1, A). This allowed the clarification of the exact structure of cell-penetrating poly(disulfide)s and, more importantly, led to a hypothetical molecular walker mechanism to account for the excellent uptake properties of small molecule transporters (Figure S1, B).

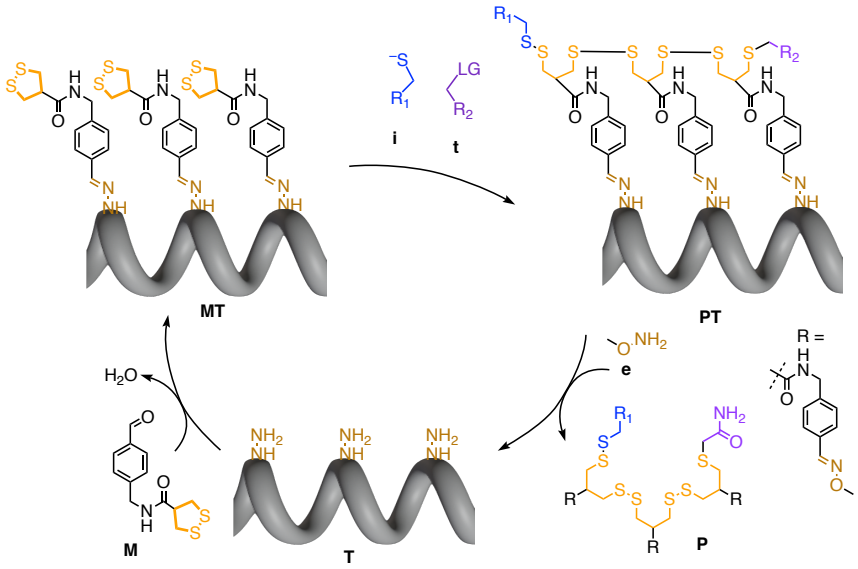

Figure S2. Templated ring-opening oligomerization of 1,2-dithiolanes on a 3_{10}-helix template.

The lessons learned from the ring opening of cyclic disulfides and diselenides were then applied to their controlled ring-opening oligomerization on a peptide foldamer template. Using orthogonal dynamic covalent chemistries, disulfide- and diselenide-containing monomers **M** could be loaded on a 3_{10}-helix template **T**, the ring-opening oligomerization performed with an initiator **i** and a terminator **t** (**MT** → **PT**), and the synthesized oligomers **P** detached from the

template with an exchanger **e** (Figure S2). The system was found to respond well to helix uptwisting and denaturation, with the templation efficiency depending on the reaction conditions.

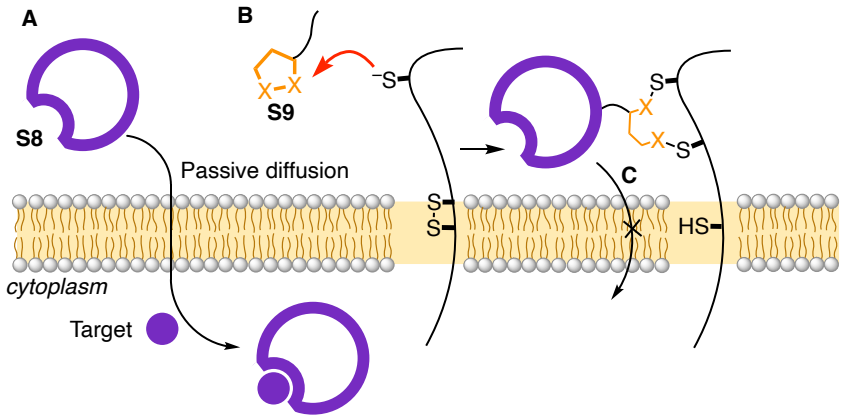

Figure S3. Proposed mechanism for the inactivation of antibiotics **S8** with intracellular targets. Without transporter **S9**, passive diffusion allows the antibiotics to reach its target (A). Upon reaction with exofacial thiols (B), passive diffusion is prohibited and the drug is immobilized at the cell surface (C).

Focusing on applications, the transposition of thiol-mediated uptake into bacteria was envisioned next. Despite countless applications in mammalian cells, bacterial uptake of thiol-mediated uptake transporters had not been reported. To this purpose, a library of antibiotic-transporter conjugates was synthesized and evaluated for their antibiotic activity. Five antibiotics selective for Gram+ bacteria were selected, with different modes of action, in an attempt to make them active against Gram– bacteria by increasing their cellular uptake. Instead of activation in Gram–, the activity was lost in Gram+ bacteria for antibiotics with an intracellular mode of action, but maintained for those acting on the extracellular milieu. Immobilization at the cell surface was proposed as a general mechanism to explain these results (Figure S3). This provided proof that non-trivial mechanisms are at play during thiol-mediated uptake.

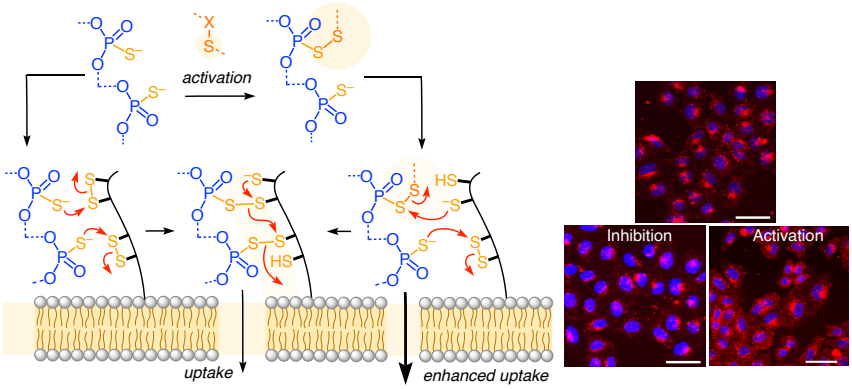

Figure S4. Mechanism of uptake of OPS forming pseudo-disulfide with disulfide-rich membrane proteins, activation of uptake by pseudo-disulfide formation and CLSM images of HeLa Kyoto cells incubated with OPS with inhibition or activation prior to uptake.

Finally, the dynamic covalent chemistry of phosphorothioates was studied. Oligonucleotide phosphorothioates (OPS) are DNA mimics with a sulfur atom replacing one of the non-bridging oxygens in phosphodiesters, which show enhanced cellular uptake as compared to non-modified DNA. Using reported thiol-mediated uptake inhibitors to inhibit the uptake of a fluorescently-labelled OPS, it was shown that OPS enter cells by thiol-mediated uptake. The dynamic covalent chemistry of the phosphorothioate moiety was studied by HPLC-MS with a model compound. Pseudo-disulfides were shown to form with both activated and non-activated disulfides, hinting towards OPS forming transient pseudo-disulfides with disulfide-rich membrane proteins during uptake (Figure S4). Such pseudo-disulfides could further improve the cytosolic uptake of OPS, seemingly bypassing endocytosis.

Résumé

Le potentiel de macromolécules comme les oligonucléotides ou les protéines tant pour une visée thérapeutique que fondamentale est souvent entravé par la faible perméabilité des membranes cellulaires. Il est donc crucial de développer des outils pour mieux comprendre et améliorer la perméabilité cellulaire. Cet axe de recherche a récemment pris de plus en plus d'importance, et de nombreuses méthodes sont aujourd'hui disponibles pour transporter de larges molécules directement dans le cytosol. Parmi ces méthodes, les peptides perméables (CPPs) ont d'abord été développés, étant capables soit de déclencher un processus d'endocytose et d'échappement endosomal, soit de délivrer la molécule cible directement dans le cytosol. Le concept de transport induit par les thiols reçoit aujourd'hui de plus en plus d'attention comme manière innovante de pénétrer dans les cellules. Basé sur des échanges covalents dynamiques entre thiols et disulfures à la surface des cellules, des transporteurs polymériques et des petites molécules ont été développées dans notre équipe, permettant d'atteindre d'excellents niveaux de pénétration cellulaire sans déclencher de toxicité.

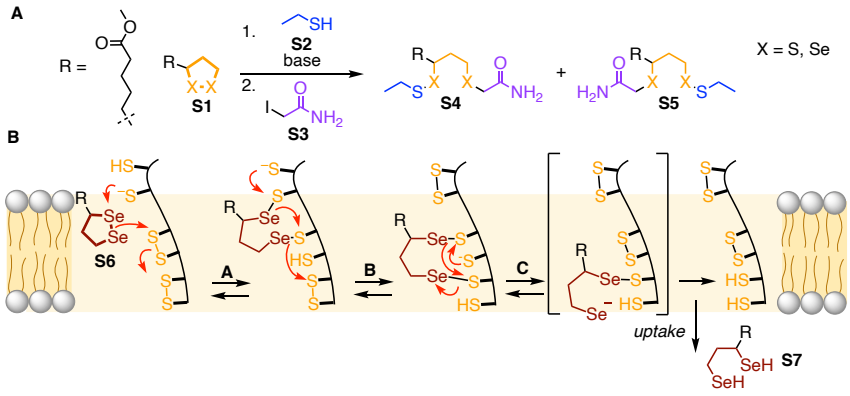

Figure S1. A) Ouverture régiosélective des 1,2-dithiolanes et 1,2-disélénolanes. B) Modèle de marcheur moléculaire.

Le but de cette thèse est d'améliorer notre compréhension des mécanismes impliqués dans le transport induit par les thiols. L'ouverture des 1,2-dithiolanes et disélénolanes par des thiols a d'abord été étudié (Figure S1, A), afin d'étudier la régiosélectivité de cette réaction. Cette étude a permis de clarifier la structure exacte des poly(disulfure)s et, plus important encore, a permis de développer un modèle hypothétique de marcheur moléculaire pour expliquer les excellentes propriétés de transport de ces petites molécules (Figure S1, B).

Les enseignements tirés de cette étude sur l'ouverture des disulfures et disélénures ont ensuite été appliqués à leur oligomérisation sur un modèle peptidique. En utilisant des chimies covalentes dynamiques orthogonales, des monomères **M** ont d'abord pu être attachés sur le modèle **T**. L'oligomérisation a ensuite pu être réalisée avec un initiateur **i** et un terminateur **t** (**MT** → **PT**), et les oligomères ont finalement pu être détachés du modèle par un échangeur **e** (Figure S2). Le système ainsi développé répond aux modifications de l'hélicité du modèle peptidique, l'efficacité du modèle dépendant des conditions de réaction.

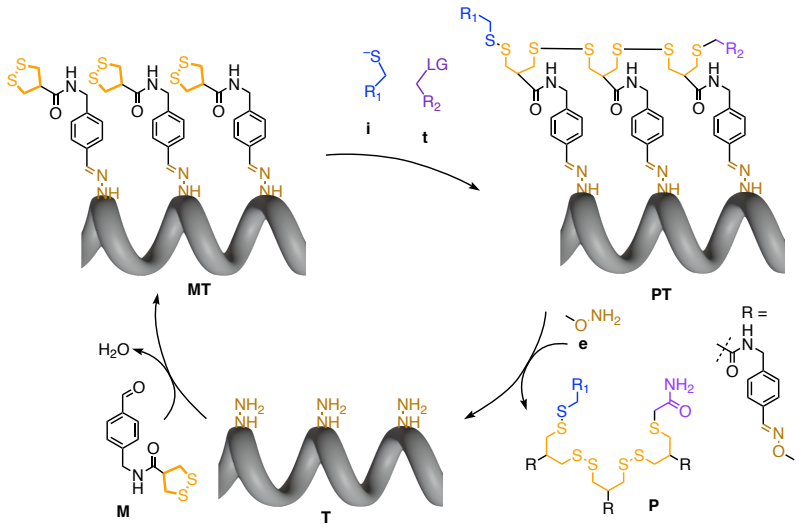

Figure S2. Oligomérisation par ouverture de cycle de 1,2-dithiolanes sur un modèle peptidique hélical.

En se focalisant plus sur de potentielles applications, nous nous sommes ensuite intéressés au transport induit par les thiols dans les bactéries. En effet, malgré de nombreuses applications dans des cellules eucaryotes, l'utilisation de cette méthode dans les bactéries n'avait encore jamais été reportée. Dans ce but, nous avons synthétisé une série de conjugués antibiotique-transporteur, et avons évalué leur activité antibiotique. Cinq antibiotiques avec différents modes d'action ont été sélectionnés, tous actifs contre les bactéries Gram+, le but étant de les rendre actifs contre les bactéries Gram– en augmentant leur perméabilité cellulaire. En lieu et place d'une activation dans les bactéries Gram–, nous avons observé une perte d'activité contre les bactéries Gram+ pour les antibiotiques ayant un mode d'action intracellulaire, activité toutefois maintenue pour ceux ayant une cible extracellulaire. Nous avons proposé une immobilisation à la surface des cellules bactériennes comme mécanisme général pour expliquer ces résultats (Figure S3). Cette étude a ainsi prouvé que des mécanismes non triviaux sont à l'œuvre durant le transport induit par des thiols.

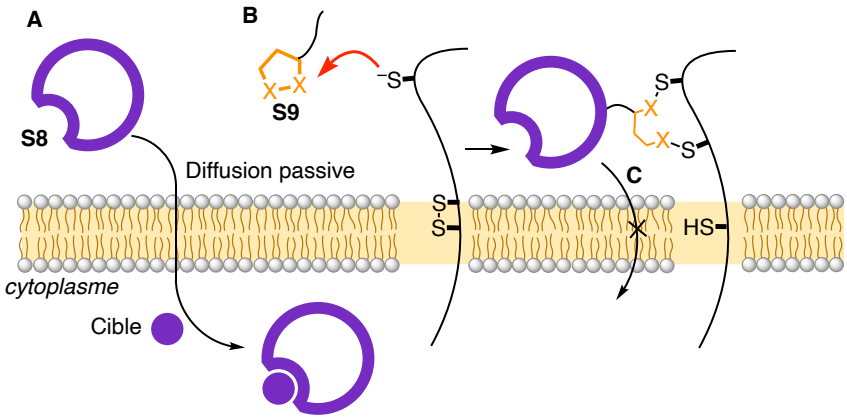

Figure S3. Mécanisme proposé pour l'inactivation des antibiotiques ayant un mode d'action intracellulaire. Sans transporteur, la diffusion passive permet aux antibiotiques d'atteindre leur cible (A). Après réaction avec des thiols à la surface (B), cette diffusion passive n'est plus possible, et l'antibiotique est immobilisé à la surface (C).

Enfin, nous avons étudié la chimie covalente dynamique des phosphorothioates. Les oligonucléotides phosphorothioates (OPS) sont des analogues de l'ADN où un atome de soufre vient remplacer un oxygène non-pontant des liaisons phosphodiesters, et ont une capacité de pénétration cellulaire bien supérieur à celle de l'ADN non modifié. En utilisant des inhibiteurs de transport induit par les thiols pour inhiber le transport d'un OPS marqué par un fluorophore, nous avons pu montrer que les OPS entrent dans les cellules par ce mécanisme. La chimie covalente dynamique du motif phosphorothioate a ensuite pu être étudiée par HPLC-MS grâce à un composé modèle. En montrant l'existence de pseudo-disulfures après réaction avec des disulfures activés ou non, nous avons proposé que de tels pseudo-disulfures se forment à la surface des cellules avec des protéines riches en ponts disulfures. En pré-activant un OPS en formant ces pseudo-disulfures, nous avons pu montrer que cette formation entrainait une augmentation du transport cellulaire d'OPS, tout en évitant l'endocytose (Figure S4).

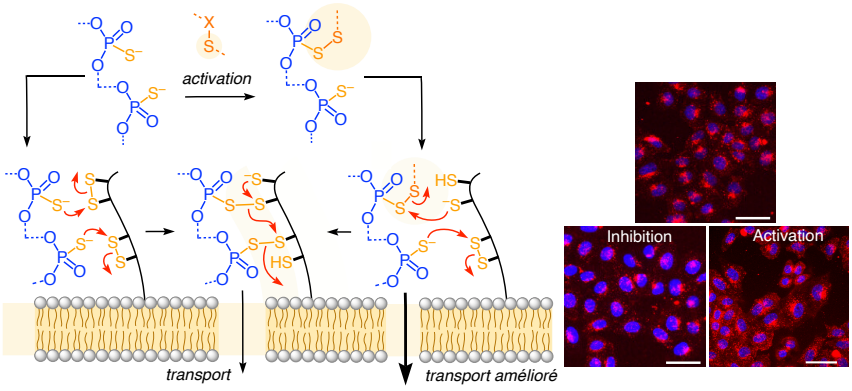

Figure S4. Mécanisme de transport cellulaire des OPS, formant des pseudo-disulfures avec des protéines membranaires riches en ponts disulfures, activation du transport cellulaire par préformation de pseudo-disulfures et images de microscopie confocale de cellules HeLa incubées avec OPS avec inhibition ou activation préalable.

Table of Contents

Chapter 1

INTRODUCTION

1.1. Cellular Uptake in Mammalian Cells

1.1.1. Composition of the Plasma Membrane

All cells, whether they are mammalian, bacterial, yeasts, or even some viruses, are held together by a lipid envelope: the plasma membrane (Figure 1). The lipid content varies from one cell to another and these variations account, in part, for different membrane properties and processes, such as fluidity, cell survival, …[1] Viewed as only its lipid components, the very hydrophobic plasma membrane is impermeable to hydrophilic molecules. In medicinal chemistry, Lipinski's rule of five for orally-active drugs is a good example of the importance of lipophilicity for passive diffusion through lipid bilayers.[2] In Gram-negative bacteria, for example, the presence of two plasma membranes further complicates passive diffusion, making a lot of antibiotics inactive in Gram– strains.[3]

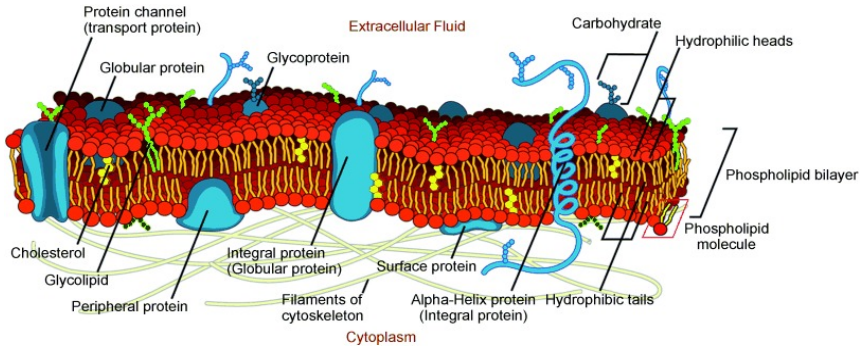

Figure 1. A schematic representation of a plasma membrane.[4]

However, restraining the plasma membrane to only lipids is a gross over-simplification. Membrane are embedded with countless (glyco)proteins, enzymes, channels, etc. which regulate most exchange processes between the extracellular and intracellular milieu by mechanisms more complex than simple passive diffusion (Figure 1, blue).[5] Carriers, channels and proteins are responsible for the cellular uptake of many components. Even for drugs which abide by Lipinski's rule of five, specific carriers have been shown to help their uptake.[6] One mechanism of resistance to anticancer drugs is active efflux through protein channels,[7] highlighting how crucial it is not to limit the plasma membrane to only its lipid components.

Because of this complexity, cellular delivery remains one of the major challenges in medicinal chemistry and chemical biology, and is still not fully understood. Promising new therapeutics such as peptides, antibodies or oligonucleotides so far often fail to deliver on their promises, precisely because only a small portion of the administered drug can reach its target.[8] Therefore, more efficient drug delivery would be highly beneficial for society. For example, for mRNA Covid-19 vaccines based on lipid nanoparticles, only a small portion of the injected mRNA gets uptaken and translated into the Spike protein to build immunity.[9] This highlights how much room for improvement still exists, and how important these problematics are.

1.1.2. Endocytic Processes and Limitations

Passive diffusion and ion-channel-mediated uptake are used by cells to get nutrients from the extracellular milieu, but they are not enough for the whole variety of molecules and particles cells need to survive.[10] To do so, a cellular process called endocytosis takes place: the materials that need to be internalized, once in close proximity to the cell, are surrounded by parts of the membrane, creating vesicles that then traffic within the cell (Figure 2). Endocytosis can be divided in four categories: phagocytosis, macropinocytosis, caveolin-mediated, and clathrin-mediated endocytosis.[11]

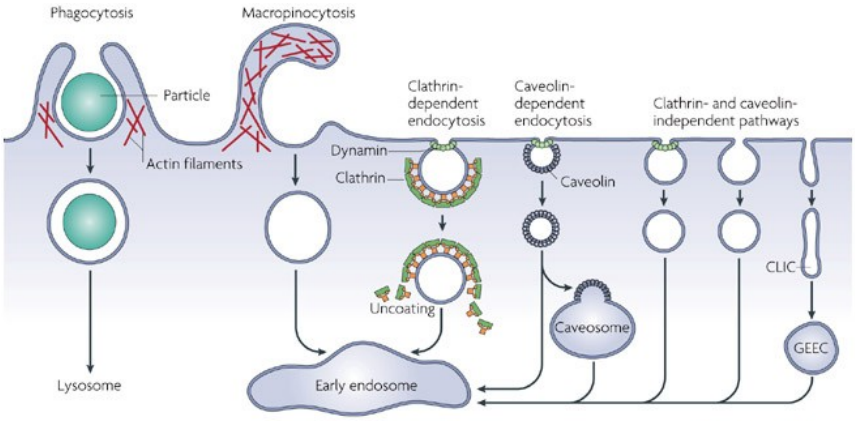

Figure 2. The different types of endocytosis: phagocytosis, pinocytosis and receptor-mediated endocytosis. Adapted from reference.[12]

Phagocytosis is well-known for white blood cells (namely, macrophages).[13] It is the mechanism by which cells internalize materials of large diameter, up to a micron, such as infectious microorganisms (bacteria, viruses), cell debris, apoptotic cells, … Of crucial importance for the balance of living organisms, the large sizes involved and the rapid degradation of the internalized material make phagocytosis somewhat less interesting for chemical biology applications.

Macropinocytosis is a non-specific process by which small particles are encapsulated in vesicles within the cell after invagination of the cell membrane.[14] Unlike clathrin- and caveolin-mediated endocytosis, macropinocytosis is not specific: the cell engulfs parts of its surrounding fluids, including all substances in close proximity. Thanks to this absence of specificity, macropinocytosis is responsible for the cellular uptake of a lot of non-targeted drug delivery systems, which will be uptaken if the concentration in proximity to the cell is high enough.[15] However, this is a double-edged sword, because targeting possibilities are very limited with macropinocytosis, and a cell type-dependent uptake is unlikely.

Receptor-mediated endocytosis (clathrin- or caveolin-mediated) takes advantage of specific receptors that trigger the recruitment of specific proteins responsible for membrane invagination and formation of coated vesicles.[16] Because it is only activated by receptor binding, specificity arises from the ligands used for binding, and this pathway can be hijacked to deliver various cargos. For example, conjugation of a wide variety of impermeable structures with RGD cyclic peptides have been shown to increase cellular uptake.[17,18] Because receptor-mediated endocytosis differs from one cell type to another, it is possible to harness these differences to selectively delivery drugs to cancer cells over healthy cells.[19]

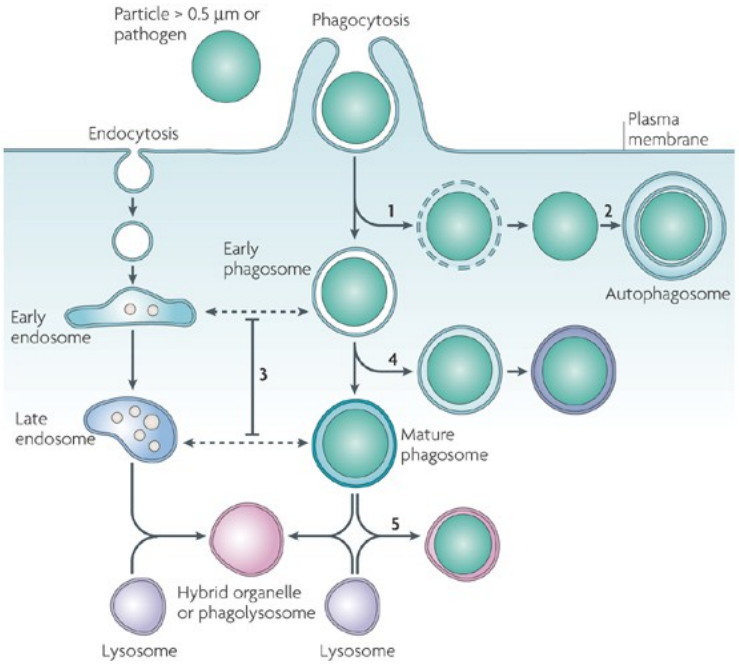

Figure 3. The endolysosomal network after endocytosis and phagocytosis, leading to degradation in lysosomes. Adapted from reference.[12]

All of these endocytic pathways are energy-dependent. In all cases, after internalization, the formed vesicles join the endolysosomal network and trafficking (Figure 3). Going from early to late endosome and then to lysosomes, entrapped cargos go through gradual acidification from around 6.5 to 5.5 to 4.5. Through this network, cargos that cannot escape end up being degraded in lysosomes, either by the acidic pH alone or by enzymes.[12] To reach the desired effect, whether it is gene transfection, protein inhibition or any cytosolic task, the payload has to escape the endolysosomal network.[20] Several mechanisms can lead do endosomal escape, depending on the properties of the carrier used (Figure 4). Using pH buffering carriers, the so-called proton sponge effect can take place and results in osmolysis of the endosome after swelling (Figure 4, A).[21] Alternatively, membrane-disrupting agents have been described, to directly disrupt either the plasma membrane or the endosome membrane, resulting in both cases in pore formation and cytosolic delivery (Figure 4, B).[15] Finally, membrane fusion, in the endolysosomal network or at the plasma membrane, can also lead to cytosolic delivery (Figure 4, C).[22]

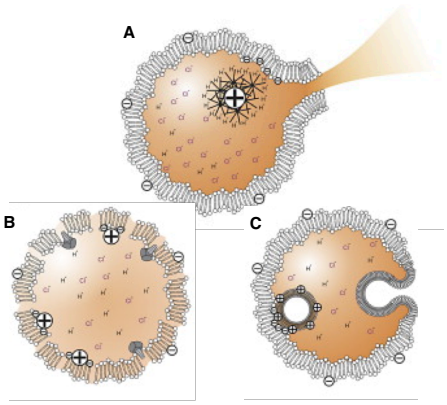

Figure 4. Three mechanisms of endosomal escape: osmolysis by proton sponge effect (A), pore formation by membrane-disrupting agents (B) and membrane fusion (C). Adapted from reference.[22]

Low endosomal escape is usually the bottleneck in drug delivery development, and novel methods to either bypass endocytosis or facilitate endosomal escape are always needed.[20] Several artificial delivery systems have been developed throughout the past few decades, and will be described in the following section.

1.2. Artificial Delivery Systems: Carriers, Cell-Penetrating Peptides and Mimics

1.2.1. Nano-Sized Carriers: Liposomes, Nanoparticles, Polyplexes and Others

A large variety of nanocarriers have been developed to overcome the limitations of endocytosis. Due to their amphiphilic character, lipids have attracted much attention as delivery vehicles for both hydrophilic and hydrophobic payloads. Composed of a lipid bilayer of various composition, with a hydrophilic core and hydrophobic membrane, liposomes are among the most widely used lipid-based carriers (Figure 5, A).[23] They are usually biodegradable, biocompatible and have low immunogenicity, which are all desirable qualities of a drug-delivery system. Liposomes are also easy to derivatize on their surface, either with targeting ligands to trigger endocytosis or with polyethyleneglycol (PEG) chains to prevent their clearance from the body. Cellular uptake of such structures is usually achieved through membrane fusion after endocytosis (Figure 4, C). Among the various drug delivery systems developed over the years, liposomes are the most advanced in terms of applications, with multiple liposomal formulations of drugs currently on the market.[24]

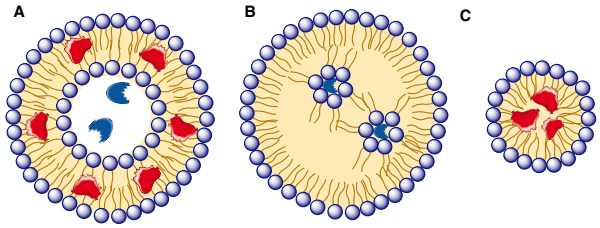

Figure 5. Schematic representation of a liposome (A), lipid nanoparticle (B) and micelle (C) encapsulating hydrophilic (blue) and hydrophobic (red) payloads.

Less ordered lipid structures, such as lipid nanoparticles with non-continuous bilayer (Figure 5, B),[25] micelles (Figure 5, C)[26] or unstructured lipoplexes are also used to deliver cargos inside cells with good efficiency. The variety of structures is important for the drug-delivery field, the efficiency of uptake being often cargo-dependent and poorly predictable.

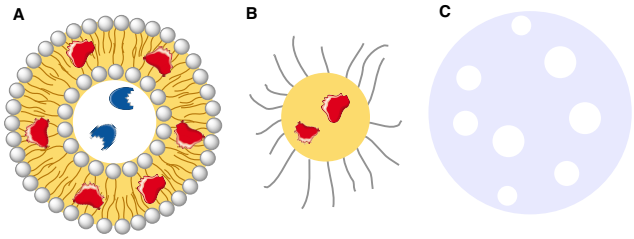

Figure 6. Polymer-based drug-delivery vehicles with polymersomes (A) and polymer nanospheres (B). C) Hollow inorganic nanoparticles.

Synthetic and natural polymers are also popular as building blocks for drugs delivery. The large structural variety offered by polymers resulted in a wide range of polymeric nanoparticles of various sizes and aspects (Figure 6, A, B).[27,28] Nanocapsules, with cavities surrounded by a polymer shell, and nanospheres, composed of a solid matrix can both encapsulate cargos of choice, whether it is proteins, antibodies or oligonucleotides to name a few. Thanks to the large variety of chemistries in polymer science, the encapsulation, stability

in biological media, and retention/release properties of such systems can be finely tuned to fit the desired application.

Inorganic nanoparticles, mostly made of gold or silica, have excellent encapsulation properties thanks to precise formulations and engineering to vary their size and geometry (Figure 6, C).[28] Due to the possible magnetic or plasmonic properties, inorganic nanoparticles can fill the needs for specific applications, such as theranostic and photothermal therapies that are out of reach for organic materials. However, they are less tunable in terms of biocompatibility, solubility and toxicity as compared to organic polymers, which hampers their application in clinical settings.

Taking advantage of the proton sponge effect for endosomal escape (Figure 4, A), polycationic polymers with high buffering capacity are often used to deliver different cargos into the cytosol.[29] Poly(ethyleneimine) (PEI) and poly(amidoamine) dendrimers (PAMAM) are among the most popular, used either alone or in combination with other polymers for gene delivery for example. Commercially available transfection agents such as JetPEI and Lipofectamine are based on similar structures. Taking advantage of the acidification from early to late endosomes to lysosomes, the secondary and tertiary amines in polycationic polymers become protonated through influx of protons into endosomes by proton pumps followed by counterion and water, without changes of the pH.[30] This disrupts the osmotic balance of the endosome, building internal pressure which eventually leads to endosome lysis. However, this process is quite damaging for cells as it disrupts the endocytic processes needed for cell survival, and applications in clinical settings are quite limited.

A more recent class of promising drug delivery vehicles is based on DNA nanostructures.[31,32] Using DNA not for its genetic information, but for its self-assembly properties, allowed the creation of various sizes and geometries of nanostructures with very precise control over the past four decades. Recently, it was observed that some of these structures display good cellular uptake

properties, which is highly counterintuitive considering the polyanionic nature of DNA.[33] Cages, tetrahedra, nanotubes and spherical nucleic acids have been shown to encapsulate different drug cargos efficiently and to deliver them into cancer cells with good biocompatibility and high tunability. Whereas the mechanism by which the delivered drug can reach the cytosol is still unclear, applications of these structures start to appear.

1.2.2. Cell-Penetrating Peptides

Cell-penetrating peptides (CPPs) originated from the isolation of the Tat protein of the HIV virus. Lebleu *et al.* identified that a small cationic peptide (**1**, RKKRRQRRR sequence) was responsible for the facilitated uptake of HIV particles in human cells, and showed that the peptide alone was able to bypass endocytosis.[34] It is counterintuitive that a polycationic, highly charged peptide would cross the plasma membrane by passive diffusion, no hydrophobic residues being involved. Instead, studies by Wender, Rothbard *et al.* showed that arginine residues were the most important in the Tat sequence, and oligoarginine peptides were showed to behave similarly, stirring up mechanistic questions to understand how these could penetrate cells (see Figure 8).[35]

Wender *et al.* proposed that the guanidium side chains, with their pK_a ~ 13, remain charged in any physiological conditions and create ion pairs with negatively charged phosphates and carboxylates at the cell surface (Figure 7, A).[36] In contrast, polylysine peptides, with a lower pK_a of the ammonium side chains to minimize charge repulsion, can undergo deprotonation and bind less tightly to negatively charged membranes. This counterion-mediated attraction is the first step for efficient cellular uptake.[37] For example, macropinocytosis would engulf most of the CPP-tagged cargo in close proximity to the cell. However, both Tat and polyarginine peptides were showed to bypass endosomal capture and enter the cytosol, at least partially, in an endocytosis-independent manner.[35]

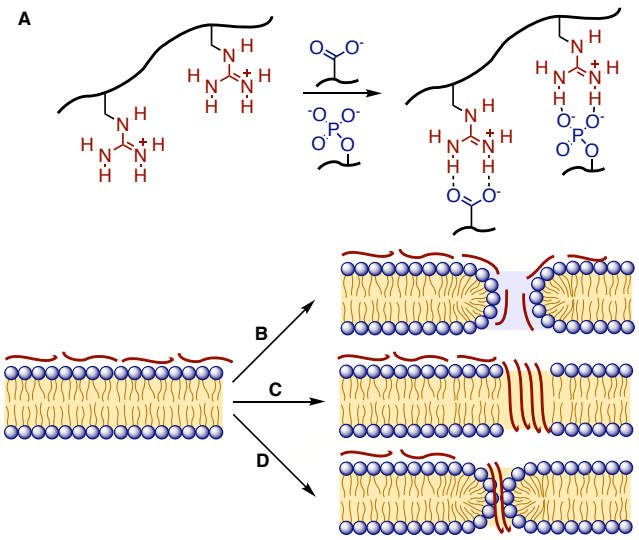

Figure 7. A) Binding of guanidinium to negatively-charged carboxylates and phosphates on the membrane. Carpet (B), barrel stave (C) and toroidal pore (D) models to explain the direct translocation of CPPs.

To explain the cell-penetrating abilities of such peptides, the formation of adaptive, non-leaky micellar pores after tight binding of the cationic CPP to the anionic plasma membrane was proposed (Figure 7, B).[38] Using black lipid membrane experiments and molecular dynamics simulations, Herce *et al.* showed the appearance of current upon incubation with CPPs.[39] Three possible models were proposed to explain their direct translocation: a carpet model (micellar pores), a barrel stave (Figure 7, C) and a toroidal pore (Figure 7, D) models, the latter two relying on CPP aggregation to form the pores. These mechanisms are consistent with the energy-independent uptake of cationic CPPs and are now largely accepted as their way of entry into cells.[40]

Building on the early success of cationic CPPs, many structure-activity relationship studies have been performed to improve their properties. Because of the mechanisms described above, cationic CPPs are often membrane-lytic and toxic. Introduction of hydrophobic residues such as tryptophan or phenylalanine

to make amphipathic peptides proved successful to reduce the toxicity while maintaining the cell-penetrating properties.[41] It was showed that three-dimensional secondary structures, for example for the presentation of the arginine residues on a single face, was desirable and could not be achieved by purely cationic CPPs.[42] Such secondary structures can be favored by macrocyclization to form cyclic CPPs (cCPPs) with better cellular uptake, as shown for example by Cardoso *et al.* for the Tat peptide.[43] cCPPs have found countless applications by appending them on a cargo of choice, with some of the most efficient cytosolic delivery reported.[44] Alternatively, secondary structures such as α-helices can be stabilized by stapling to enforce the desired conformation and precise presentation of specific residues on one face. Pentelute *et al.*, for example, showed that stapling of peptides with a "superhydrophobic" perfluorobiphenyl linker greatly enhanced their cell-penetrating ability,[45] even through the highly impermeable blood-brain barrier.[46]

1.2.3. CPP Mimics with Better Activity and Lower Toxicity

The popularity of CPPs is in part due to the ease of synthesis of peptides by solid-phase synthesis, making it easy to study their structure-activity relationships. Stereochemistry in oligoarginines **2** and **3** was showed to influence the uptake properties and the proteolysis degradation.[35] Varying the scaffold and replacing the peptidic backbone with other chemistries also bears the potential to yield better uptake and toxicity profiles. As early as 2000, Wender *et al.* investigated different backbones equipped with guanidinium side chains as mimics of oligoarginine peptides.[35] Switching from peptides to peptoids **4**, on top of giving more protease-resistant transporters, increased the uptake efficiency of such compounds (Figure 8).

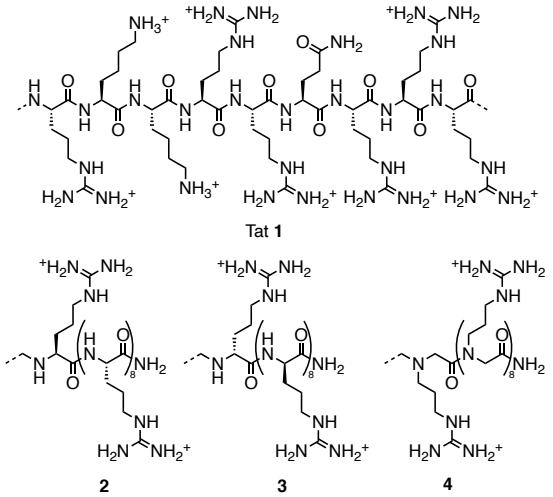

Figure 8. Cell-penetrating peptides based on the Tat sequence and oligoarginine peptides and peptoids.

Going from polyamides to polycarbamates **5**,[47] with the same number of guanidinium moieties, even more efficient transporters could be obtained (Figure 9). A few years later, Wender, Waymouth and coworkers introduced oligocarbonate transporters **6**,[48] based on novel oligomerization strategies. These exhibited lower toxicity, possibly thanks to rapid degradation of the transporter after cellular uptake. Going from hydrolysable carbonates to more robust and water-soluble phosphoesters **7** further improved the cellular uptake profile of oligoguanidinium transporters.[49] With guanidinium and histidine-type side chains, foldamers based on oligoureas **8** were reported by Guichard *et al.* to have excellent gene transfection efficiency.[50] The same group later reported post-elongation strategies to transform oligoureas into oligoguanidiniums **9** directly in the backbone, without consideration for cellular uptake so far.[51] Ribbon-like foldamers based on α-amino- γ-lactams **10** also achieve good cytosolic delivery.[52]

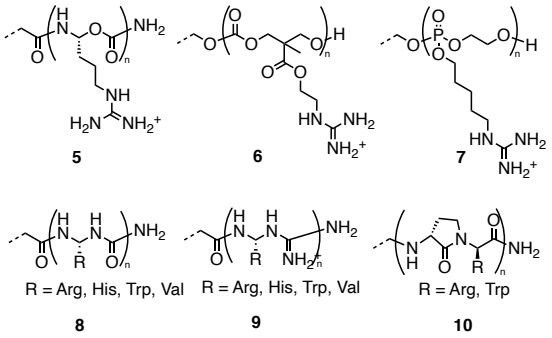

5 6 7

8 9 10

Figure 9. Different backbones used to install guanidinium on linear oligomers and foldamers.

In 2013, our group reported the synthesis of guanidinium-rich cell-penetrating poly(disulfide)s (CPDs), which showed excellent cellular uptake without entrapment in endosomes, and low toxicity thanks to intracellular depolymerization.[53,54] CPDs and their specificity will be developed further in section 1.3.3.3.

1.2.4. Dynamic Covalent Chemistry for Cellular Uptake

In the context of cellular uptake, dynamic covalent chemistry has been widely used.[55,56] Many dynamic covalent polymers have been used for biomedical applications, and can be segregated in two main categories: those which use dynamic covalent bonds for degradation of the transporter after cellular uptake, and those which use dynamic bonds to promote uptake.

For the first class, various reversible reactions have been used to created polymers responsive to certain biological cues, mostly for gene delivery. Ulrich *et al*., for example, used hydrazone chemistry to create pH-responsive polymers able to deliver siRNA in live cells.[57,58] Aida and coworkers synthesized disulfide-bridged molecular glues *via* templated polymerization on a siRNA strand that achieved excellent cytosolic delivery.[59–61] Montenegro *et al.* synthesized several dynamic covalent polymers where reversible linkages are

used to install side chains. Using polymer scaffolds bearing hydrazides, they installed cationic and lipophilic side chains to screen for efficient gene delivery agents.[62,63]

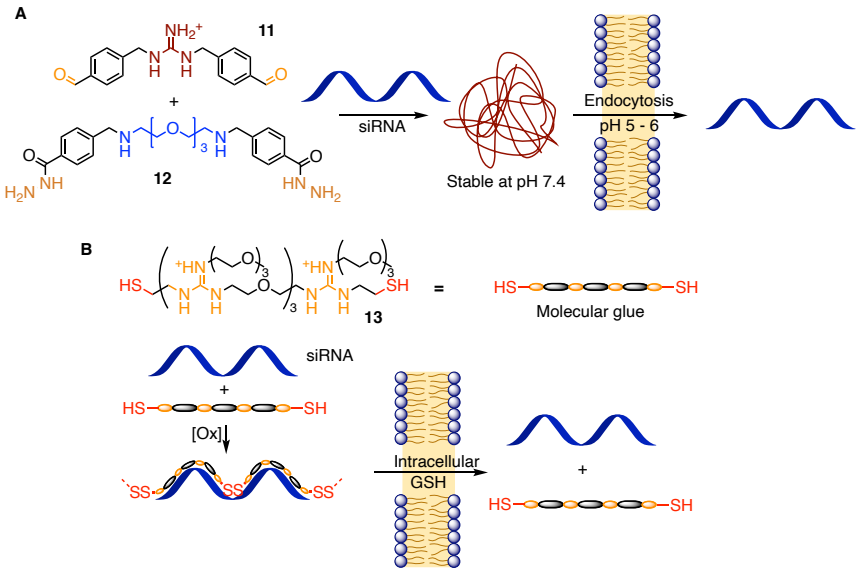

Figure 10. A) pH-responsive polyplexes for intracellular DNA delivery.[57] B) Reduction-sensitive molecular glue for siRNA delivery.[59]

Examples of dynamic covalent chemistry used to interact with the cell membrane to trigger uptake are scarcer. Boronates[64] and iminoboronates [65] have been used by Raines and Gao to deliver proteins in cells and target bacterial membranes, respectively. These target diols present at the surface of cells, in the various glycans and peptidoglycans. Apart from these two examples, most dynamic covalent systems targeting the cell membrane are based on thiol-disulfide exchanges and fall under the definition of thiol-mediated uptake.[66]

1.3. Thiol-Mediated Uptake in Nature and Cellular Delivery

1.3.1. Thiol-Mediated Uptake in Nature: Viruses and Toxins

Whereas the term "thiol-mediated uptake" was only coined a decade ago, its occurrence in nature has been observed as early as 1990. Studying the cellular uptake of a radiolabeled polylysine-tyramine conjugated, connected through a disulfide bridge, Ryser *et al.* first highlighted the importance of cell-surface thiols.[67] Pre-treatment of the cells with Ellman's reagent (5,5'-dithiobis-(2-nitrobenzoic acid) DTNB **14** resulted in inhibition of the cellular uptake, which led to the conclusion that thiols present at the cell membrane were involved.

This observation was quickly transposed to study the mode of uptake of viruses and toxins. The activity of the diphtheria toxin was shown to depend on disulfide cleavage at the cell surface, and could be inhibited both by DTNB and inhibitors of the protein disulfide isomerase (PDI).[68] On the contrary, ricin, another toxin activated by disulfide cleavage, was insensitive to DTNB inhibition and depended on glutathione-mediated cleavage after endocytosis. Similarly, infection by the HIV virus could be inhibited by DTNB and PDI inhibitors (Figure 11).[69] After recognition by a cell-surface receptor (CD4) of the gp120 unit on the HIV membrane, PDI cleaves a disulfide in this subunit, inducing conformational changes that eventually leads to membrane fusion.

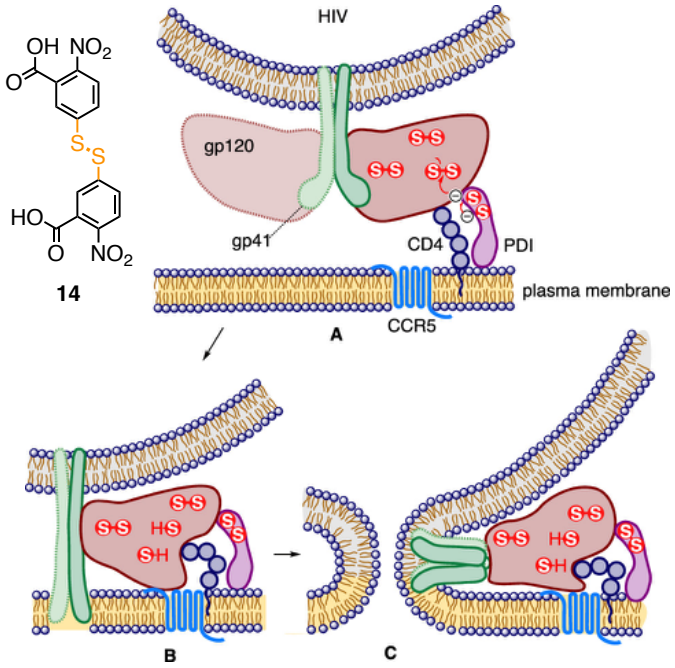

Figure 11. Thiol-mediated uptake of HIV: DTNB-inhibitable dynamic covalent disulfide exchange between PDI and gp120 (A, B) prepares for fusion (C). Image from reference.[66]

1.3.2. First Artificial Systems Found by Serendipity

The first example of artificial systems taking advantage of thiol-mediated uptake for delivery was reported by Behr *et al*. in 1995.[70] When decorating liposomes **15** with various thiol-reactive moieties (Figure 12, A), the transfection efficiency increased up to 100-fold. Whilst covalent anchoring to cell-surface thiols followed by endocytosis is discussed, no inhibition data is reported. This was a serendipitous discovery, the most active compound being a control experiment on the way to the synthesis of glycosylated lipids.

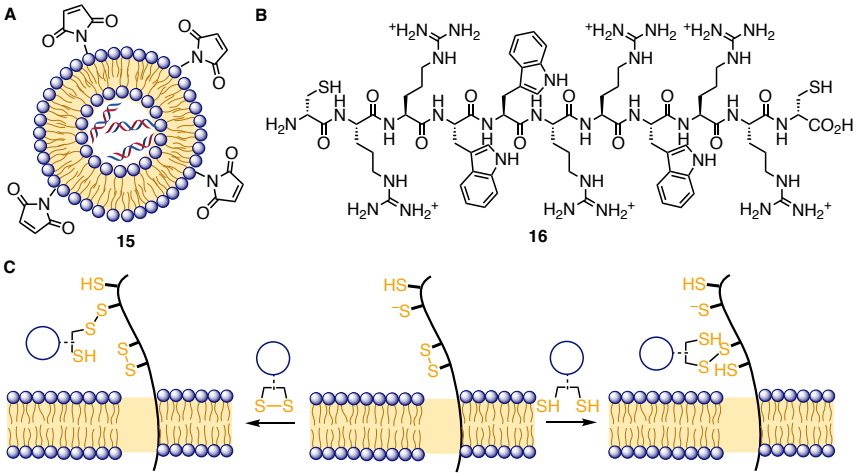

Figure 12. A) Maleimide-decorated liposomes; B) Thiol-decorated CPP with high cell-surface binding; C) Proposed mechanism for binding to cell-surface thiols and disulfides. Adapted from reference.[66]

In 2009, Sagan *et al.* reported a systematic investigation of disulfide-containing cell-penetrating peptides like **16**.[71] Using MALDI-TOF mass spectrometry after cell-lysis, the amount of membrane-associated lipid was quantified and found to be much higher for disulfide-containing CPPs (Figure 12, B). The membrane anchoring of these compounds was completely inhibited by preincubation with DTNB. Interestingly, both the oxidized disulfide and reduced dithiols had similar cellular uptake properties, hinting towards disulfides present at the cell surface also playing a role.

In 2012, Torres and Gait reviewed the exploitation of cell-surface thiols to enhance cellular uptake scattered throughout literature.[72] Oligonucleotides, peptides, nanoparticles and other systems, appended with thiols or disulfides, usually show better uptake than their non-functionalized controls. Both disulfides reacting with exofacial thiols and thiols reacting with exofacial disulfides are mentioned as possible mechanisms (Figure 12, C). The examples

reported are however mostly empirical, without rational design of the sulfur-based transporter, and often without consideration for the mechanisms responsible for the increased cellular uptake. Nonetheless, the generality, ease of installation, and efficiency of cellular uptake using such transporters is appealing. The authors concluded that their article "aimed at raising awareness of the potential for the use of exofacial thiols to enhance cellular delivery", a goal achieved with the rational design and applications of thiol-mediate uptake transporters later on.

1.3.3. Poly(disulfide)s for Materials and Cellular Uptake

1.3.3.1. Lipoic Acid for Ring-Opening Polymerization

Lipoic acid **17**, also known as thioctic acid, is a small natural molecule used as an intermediate in the biosynthesis of acetyl-CoA.[73] The 1,2-dithiolane moiety in **17** has been exploited to perform ring-opening polymerization and synthesize polymers with interesting degradability and self-healing properties. In 2010, Endo *et al*. reported the first self-polymerization of lipoic acid induced by heat.[74] Cyclic, catenated polymers **18** were obtained as shown by NMR spectroscopy and GPC (Figure 13, A). When the polymerization was carried out with a catalytic amount of dihydrolipoic acid **19**, open chain thiol-terminated polymers **20** were obtained.

Later on, the ring-opening polymerization of lipoic acid was widely studied by Tian, Feringa *et al*. to produce "green plastics" (Figure 13, A).[75] Unlike what was reported by Endo *et al.*, linear poly(disulfide)s **21** were obtained and the properties of the materials obtained were characterized. Covalent cross-linking and metal binding through the carboxylate groups yielded moldable, stretchable and self-healing polymers with excellent adhesive properties.[76] By simply diluting the polymers, the process was highly reversible and lipoic acid was obtained again. Starting from sodium lipoate, polymer films alternating

hydrophobic and hydrophilic layers were observed, highly deformable and with similar recyclability.[77]

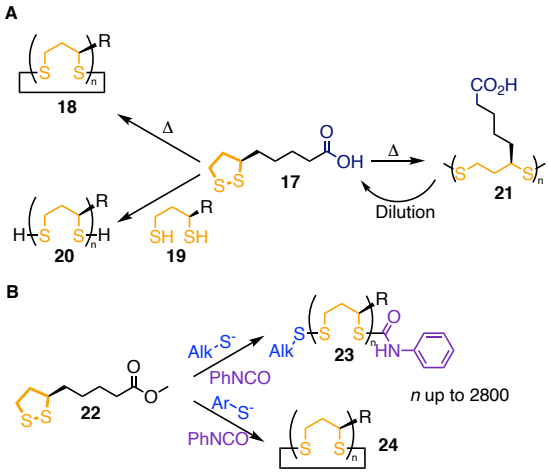

Figure 13. Ring-opening polymerization of lipoic acid under thermal conditions (A) and initiated by thiols (B).

Recently, Moore *et al.* studied in detail the polymerization of methyl lipoate **22** in organic solvent, screening for a wide variety of bases and initiators.[78] They found that strong bases were needed for the ring-opening polymerization to occur in THF. Furthermore, aliphatic thiols were found to result in linear polymers **23**, whereas aromatic thiophenol derivatives provided cyclic poly(disulfide)s **24** (Figure 13, B). Both architectures could be readily degraded back to the starting material with up to 95% purity by simply heating in the presence of a thiolate catalyst.

1.3.3.2. Templated Polymerization of 1,2-Dithiolanes

Because of the reversibility of the polymerization reaction, the ring-opening polymerization of 1,2-dithiolanes is usually performed at high concentration (200 mM – 1 M range).[53,78] This results in a relatively high polydispersity of the

obtained polymers. To avoid this, templated polymerization is usually the way to go.

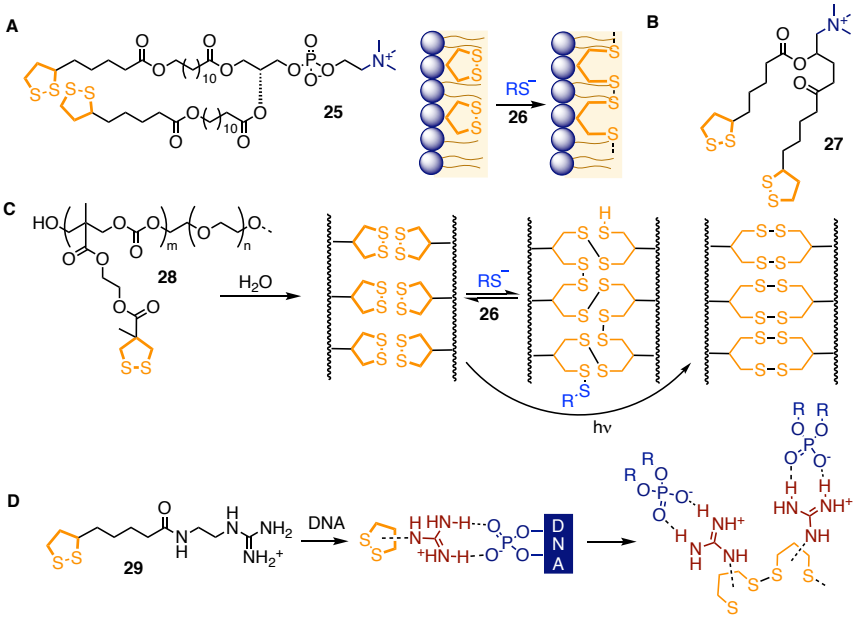

Figure 14. Templated polymerization of 1,2-dithiolanes. A) Lipoic-acid containing lipids for polymerized liposomes. B) Amphiphile for polymerized micelles. C) Block copolymers for dynamic hydrogels. D) Guanidinium-containing lipoic acid for polymerized oligonucleotide nanoparticles.

As early as 1986, Regen *et al*. polymerized lipoic acid-containing lipids in vesicles. First forming liposomes from lipid **25** containing 1,2-dithiolane moieties in its hydrophobic tail, the system was then polymerized using catalytic amounts of thiol **26** (Figure 14, A).[79] The local concentration of disulfides in the vesicles being high, the disulfides readily polymerized to afford more robust liposomes, resisting surfactant denaturation conditions and stable for months at room temperature.

In a similar fashion, lipoic acid was used as a building block for ring-opening polymerization of micelles. Positively charged lipoic acid derivatives **27** formed

micelles in water, and polymerized due to high local concentrations, yielding strengthened materials (Figure 14, B).[80] Ring-opening polymerization of esterified lipoic acid followed by nucleophilic substitution with viologen, a popular non-covalent π-stacking binder of aromatic pollutants often found in water, afforded functional polymers.[81] In water, these formed coacervates that efficiently captured pollutants by simple sonication.

In recent studies, Waymouth *et al*. reported the behavior of hydrogels derived from 1,2-dithiolanes.[82] Block copolymers containing asparagusic derivatives **28** were found to assemble into flower micelles above the critical micellar concentration (Figure 14, C). Upon reaction with thiols, the properties of the hydrogels changed, giving materials with better flow properties. When quenching with maleimide to cap free thiols, irreversible crosslinks were formed, giving gels with much lower deformation properties. Photocrosslinking also led to similar behavior, with interesting three-dimensional arrangements upon crystallization.[83]

Based on similar amphiphilic behavior, polymers were grown inside oligonucleotide nanoparticles. Yang *et al.* showed that the guanidinium-containing lipoic acid derivative **29** could self-assemble with oligonucleotide DNA strands into stable nanoparticles (Figure 14, D).[84] This process depended on the size of the DNA strand, and produced nanoparticles that were responsive to reducing conditions, and disassembled upon incubation with GSH. The polymerization process was not initiated by thiols and occurred spontaneously, hinting toward a very high local concentration by the self-assembly, most likely through the formation of supramolecular spherical nucleic acids (SNA). These nanoparticles exhibited excellent transfection efficiency, as will be discussed in the following subsection.

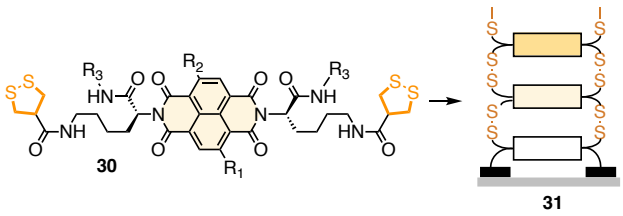

Figure 15. Self-organizing surface-initiated polymerization to create double channel photosystems.

Finally, templated polymerization of 1,2-dithiolanes has also been the method of choice to synthesize oriented double-channel photosystems **31**.[85] Using naphthalene diimide (NDI) functionalized with asparagusic acid on both sides **30**, π-stacking of the aromatic units could align the dithiolanes and trigger the templated polymerization (Figure 15).

1.3.3.3. Cell-Penetrating Poly(Disulfide)s

After studying the surface-induced polymerization of 1,2-dithiolanes, our group gained interest in substrate-initiated ring-opening polymerization in 2013.[53] Starting from readily accessible monomers based on lipoic (**32**, **33**) and asparagusic acids (**34**, **35**) and cysteine-derived initiators, various CPDs were synthesized and their transport activity in fluorogenic vesicles assessed (Figure 16). Substrate-initiated polymerization and DTT-induced depolymerization correlated with the appearance and disappearance of transport activity. Lipoic acid **32** appeared as the substrate of choice for CPDs, as asparagusic acid **34** readily polymerized in the absence of initiator. Using derivatives of NDI on both initiator and terminator, FRET was used as a method to assess incorporation of the terminator and time-dependence of polymer length. This first study of CPDs paved the way for backbone and sidechain modifications to modulate their properties,[86] as well as human cell experiments and applications to the delivery of biologically relevant substrates.

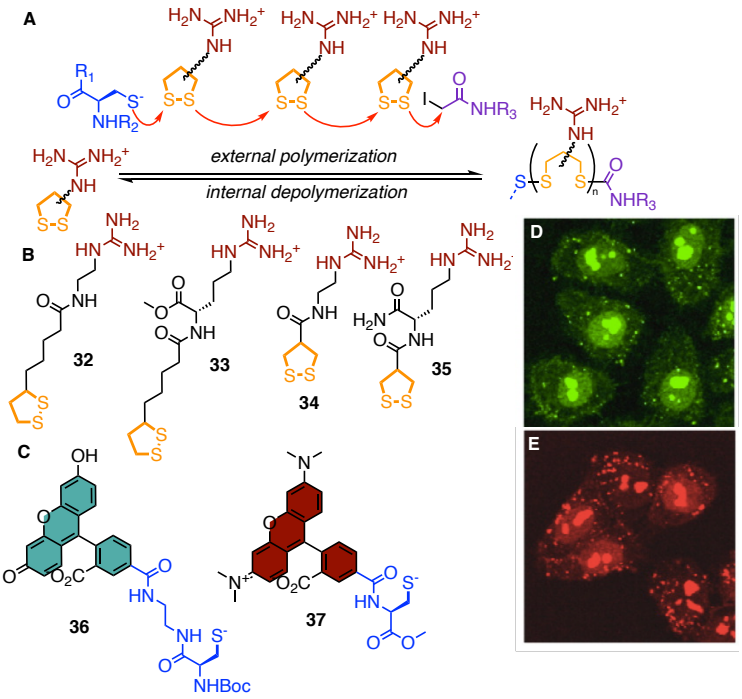

Figure 16. A) Substrate-initiated synthesis of cell-penetrating poly(disulfide)s with representative monomers (B) and initiators (C) used for ring-opening polymerization. D, E) Representative CLSM images of HeLa Kyoto cells incubated with CPDs grown from **36** and **37**, respectively. Adapted from reference.[54]

CPDs labelled with fluorophores were synthesized from lipoic acid **32**/**33** or asparagusic acid **34**/**35** monomers based on the previously developed methodology.[54] HeLa cells were incubated with these polymers and their uptake ability was assessed using confocal laser scanning microscopy (CLSM, Figure 16, D, E) and flow cytometry. Whereas the initiators **31** and **32** were not uptaken, polymers grown on these showed high level of intracellular fluorescence, with different subcellular localization depending on length, branching, hydrophobicity and disulfide-exchange kinetics.[87–89] Significant decrease of uptake was observed when cells were preincubated with Ellman's reagent

(DTNB, **14**), which inactivates thiols on the surface of cellular membranes. This proved thiol-mediated uptake took a crucial role, as shown previously by Sagan *et al.* and other seminal work.[68,71] Depolymerization kinetics was the crucial parameter to allow CPDs to navigate through the cytosol all the way to the nucleus and accumulate there, but were found to be an empirical parameter for each monomer.[87] The introduction of functional terminators and side-chain engineering improved the uptake ability, the targeting, and the applicability of CPDs to biological challenges.[88–90]

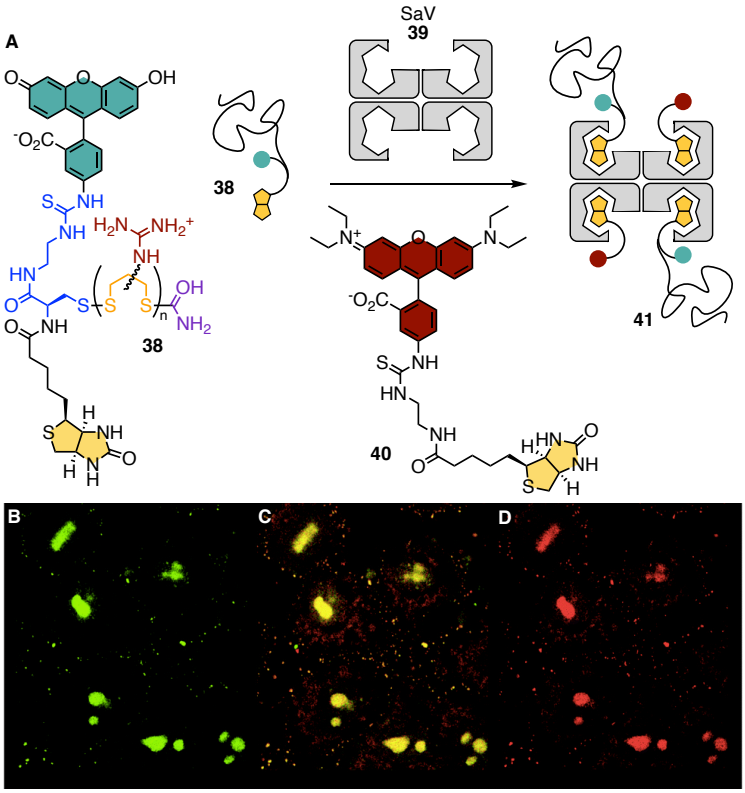

Figure 17. A) Fluorescein-tagged biotinylated CPD **38** used to form complexes with SaV and biotinylated fluorophore **40**; CLSM images of HeLa Kyoto cells incubated with **41** seen in the green (B) and red channel (D), and merged (C). Adapted from reference.[91]

Until this point, only small-molecule fluorophores were delivered in cells by CPDs, which is of interest for fundamental development, but not so much for biologically-relevant applications. To study the delivery of larger substrates such as proteins or quantum dots, the attention turned to the biotin-streptavidin biotechnology.[91] Streptavidin (SaV, **39**) is a tetrameric protein with four binding sites to biotin. With an exceptionally high binding affinity ($K_d \sim 10^{-14}$) to streptavidin, biotin has been employed as a supramolecular way to interface various systems with proteins. To take advantage of this technology with CPDs, biotin-containing initiators were introduced to grow CPDs that could bind SaV (**38**, Figure 17).[91] These CPDs efficiently delivered SaV in a non-linear fashion: the uptake ability of SaV with four polymers increased beyond additivity, showing a synergetic effect. With two SaV pockets filled with biotinylated polymers and two filled with a biotinylated rhodamine derivative (**40**, Figure 17), both green and red fluorescence could be observed with nearly perfect colocalization in the nucleoli, the same subcellular localization than the polymer alone (Figure 17, B – D). This proved that the mode of action of CPDs is not hindered by the presence of large macromolecules, highlighting the power of this method to deliver intact proteins, antibodies or other large entities.

The same strategy was used to deliver a wide variety of large substrates into cells.[92] Streptavidin-coated quantum dots (QDs) uptake was greatly improved by the presence of CPD **42** (Figure 18, A), with around 70 QDs per cells uptaken, 90% of which are freely diffusing inside the cytosol. Both biotinylated GFP and anti-GFP nanobodies (GBP) were efficiently co-delivered with the QDs using this method and colocalized in the cells after incubation. With 15 nm diameters, QDs were the biggest substrate uptaken by CPDs. Later on, biotinylated CPD **42** was used in combination with ruthenium complex **43** to create a cell-penetrating artificial metalloenzyme **44** (ArM) that could activate a prodrug **45** in the cytosol of human cells to eventually turn on the expression of a specific gene by the action of thyroxine **46** (Figure 19).[93] Uptake of the ArM was followed by

fluorescence microscopy thanks to the TAMRA moiety in **42**, and efficient activation of the prodrug monitored by enzymatic activity assays indicated cytosolic delivery of the intact and functional ArM.

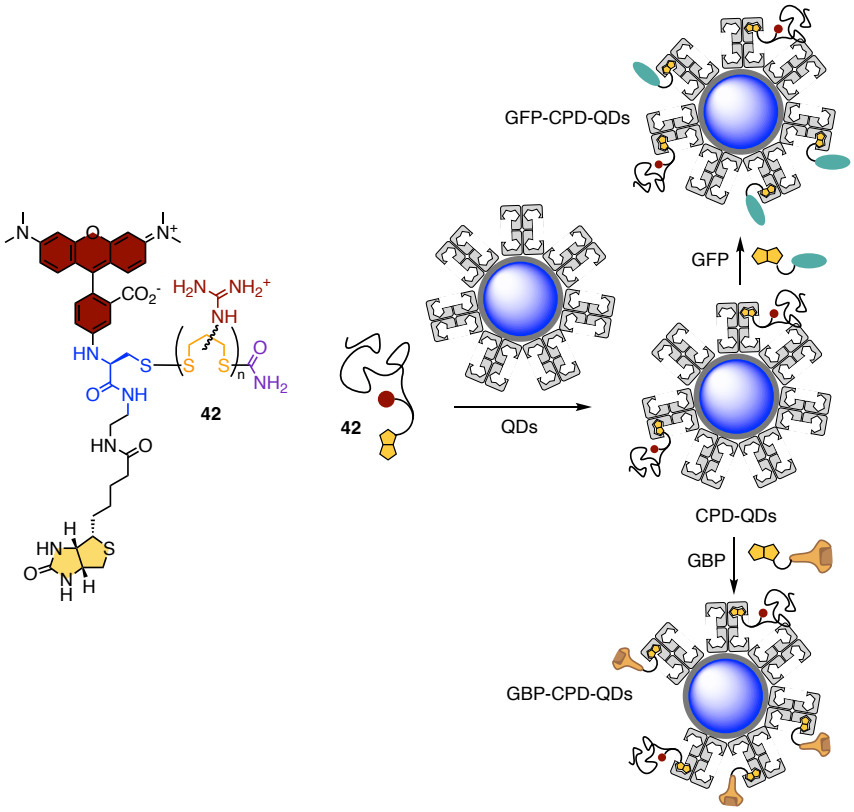

Figure 18. Fluorescently-labelled CPD for the delivery of QD coated or not with biotinylated GFP or GBP. Adapted from reference.[92]

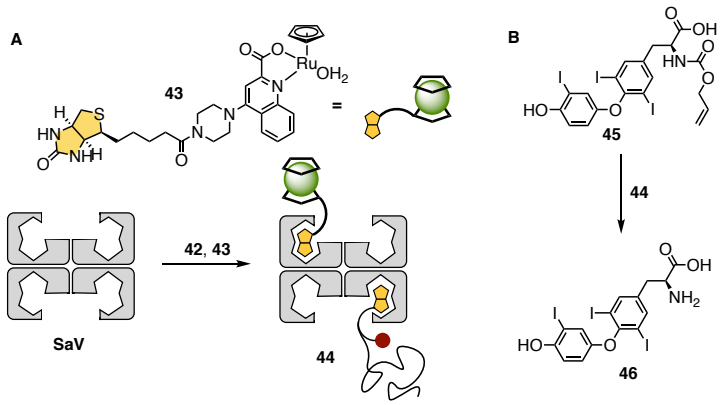

Figure 19. A) Artificial metalloenzyme delivered by CPDs activating a prodrug in the cytosol (B). Adapted from reference.[93]

The group of Yao *et al.* has been highly active in the field of CPD applications over the past seven years.[94–96] Interfacing either with biotin-streptavidin biotechnology (**I**$_{\mathbf{biotin}}$), *click* chemistry (**I**$_{\mathbf{Tz}}$), His$_6$-NTA (**I**$_{\mathbf{NTA}}$), oxime ligation (**I**$_{\mathbf{AO}}$) or simple supramolecular charge attraction, they studied the cytosolic delivery of native or non-native proteins and antibodies (Figure 20, A). For example, using post-translational protein modifications with self-immolative linkers between the CPD and the protein (**48**), native proteins **49** could be delivered into the cytosol (Figure 20, B).[95] Fluorescently-labeled human IgG and bovine serum albumin (BSA) were both delivered with this traceless ligation method. Two enzymes, Horseradish peroxidase and RNAse A, were also successfully delivered in their native form with high enzymatic activity in the cytosol.

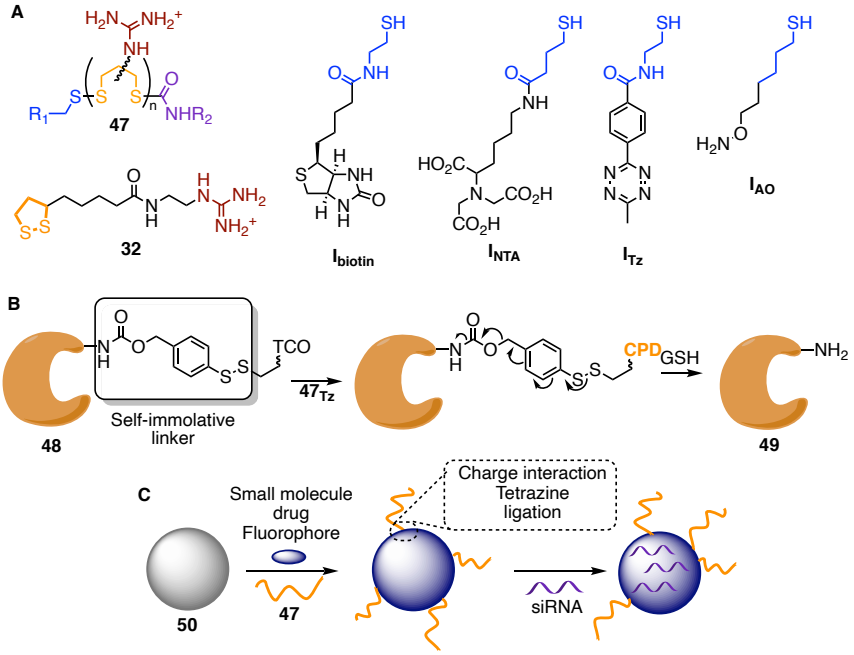

Figure 20. A) Different initiators and propagators used by Yao *et al.* to synthesize CPDs with different interfacing technologies. B) Post-translational modifications to introduce CPDs in proteins for delivery of native protein. TCO = *trans*-cyclooctene for "click" chemistry with tetrazine. C) Mesoporous silica nanoparticles decorated with CPDs, small molecule drugs and macromolecules. Adapted from references.[94–98]

The same group extensively used mesoporous silica nanoparticles (MSNs, **50**), interfaced by various means with CPDs **47**, to deliver biologically relevant cargos such as oligonucleotides, antibodies and proteins (Figure 20, C).[97–99] For example, high anticancer activity could be achieved with a combination of a small-molecule drug and an antisense oligonucleotide targeted against micro-RNA mir-21.[98] Using the high versatility of the nanoparticle platform, it can be used as both delivery and detection system, allowing the real-time monitoring of the release of the drug inside the cytosol. Biodegradable MSNs were introduced

to deliver native antibodies without the need for functionalization, and could even be targeted to specific organelles such as mitochondria.[100,101]

As mentioned in section 1.3.3.2, mixing of oligonucleotides with guanidinium-containing lipoic acid derivative **32**, proximity-induced ring-opening polymerization took place and nanoparticles were obtained (Figure 14, D).[84] Upon incubation of cells with these nanoparticles labelled with a fluorophore, a time-dependent uptake was observed by confocal microscopy, in an endocytosis-independent manner. The uptake was inhibited by Ellman's reagent, an indication of thiol-mediated uptake taking place. Uptake of antisense oligonucleotides for the survivin gene and GFP plasmid DNA nanoparticles was also performed, resulting in lowered levels of survivin expression, correlating with cell death, and expression of GFP monitored by confocal microscopy, respectively. In a similar fashion, Ping *et al.* recently reported that poly(disulfide)s could be used to simultaneously deliver the whole genome editing toolbox necessary (Cas9 plasmid, mRNA and ribonucleoprotein) for CRISPR-Cas9 function.[102] This allowed *in vitro* and *in vivo* editing, highlighting the power and increasing attention received by CPDs for therapeutic applications.

Recently, Lu *et al.* reported a mild new grafting-from synthesis of poly(disulfide)s.[103] Cryo-ring-opening polymerization (CryoROP) enabled the growth of poly(disulfide)s directly on the reactive cysteine residues of proteins of interest. CryoROP was not hindered by native disulfides, and proceeded with high efficiency on various substrates (genetically modified and native proteins) and with various 1,2-dithiolane propagators, as confirmed by SDS-page and ESI-MS studies. When grown on enzymes, the polymers inactivated the enzyme if the cysteine was part of its active site, but activity could be fully restored by DTT-induced depolymerization (Figure 21, A). If the active site does not contain any cysteine residues, the enzymatic activity was retained. Fluorescent or fluorescently-labelled proteins were used as initiators to polymerize a lipoic acid

derivative containing a positively charged tertiary amine **51**, to yield cell-penetrating protein conjugates **52**. These were uptaken by cells as assessed by confocal microscopy, without being trapped in endosomes, and remained functional once in the cytosol (Figure 21, B).

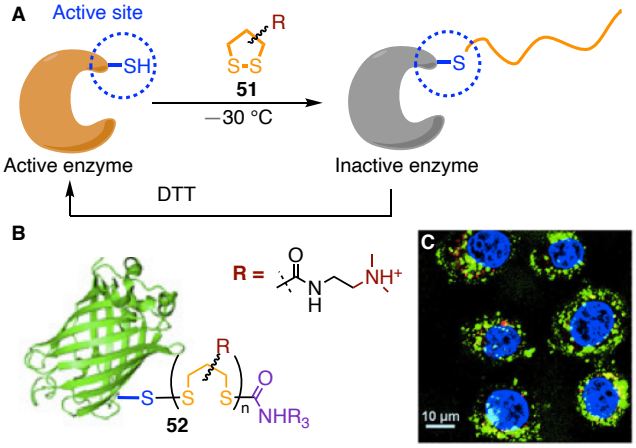

Figure 21. A) Cryo-polymerization method to grow poly(disulfide)s on native cysteine residues in proteins. B) CPDs grown on cysteine-modified GFP with C) CLSM image of HeLa cells incubated with **52**. Adapted from reference.[103]

Still relatively recent, the cell-penetrating poly(disulfide)s introduced in this section hold great promises for future applications. Over the past few years, countless cargos have been delivered in an endocytosis-independent fashion using CPDs, *in vitro* and recently even *in vivo*. Despite these excellent results, applicability is still limited by somewhat complicated syntheses and the need to introduce post-translational modifications on the cargo to interface it with the CPD. Shifting from polymers to small molecules, while maintaining excellent cellular uptake efficiencies, was therefore of interest.

1.3.4. Cyclic Oligochalcogenides: Ring Tension and Dynamic Covalent Chemistry

1.3.4.1. Ring Tension in Cyclic Disulfides for Efficient Uptake

Rooting from previous work on CPDs, thiolate-disulfide exchange chemistry at the cell surface was studied by our group in combination with ring tension. In CPDs, linear disulfides have no ring tension, making them poorly reactive towards thiolates at the surface, hence the need of polymers and combination with counterion-mediated attraction towards cells to increase local concentration. In 2015, ring tension was introduced to create highly reactive disulfides.[104] It was found that higher ring tension in asparagusic acid (AspA) **54** as compared to lipoic acid (LipA) **55** and dithiothreitol (DTT) **56** correlated with higher cellular uptake of fluorescently-labelled transporters, and more than linear disulfides **57** and **58** (Figure 22, A). Similarly to CPDs, uptake of strained disulfides was insensitive to endocytosis inhibitors, inhibited by Ellman's reagent DTNB **14** and by low temperature, indicating an endocytosis-independent but energy-dependent uptake pathway relying on thiols. Interestingly, treatment with DTNB favored the uptake of thiolated compound **59**, hinting towards the mechanism shown in Figure 12, with thiol-based transporters reacting with exofacial disulfides. Treatment with DTT to reduce all disulfides at the cell surface increased disulfide-mediated uptake.

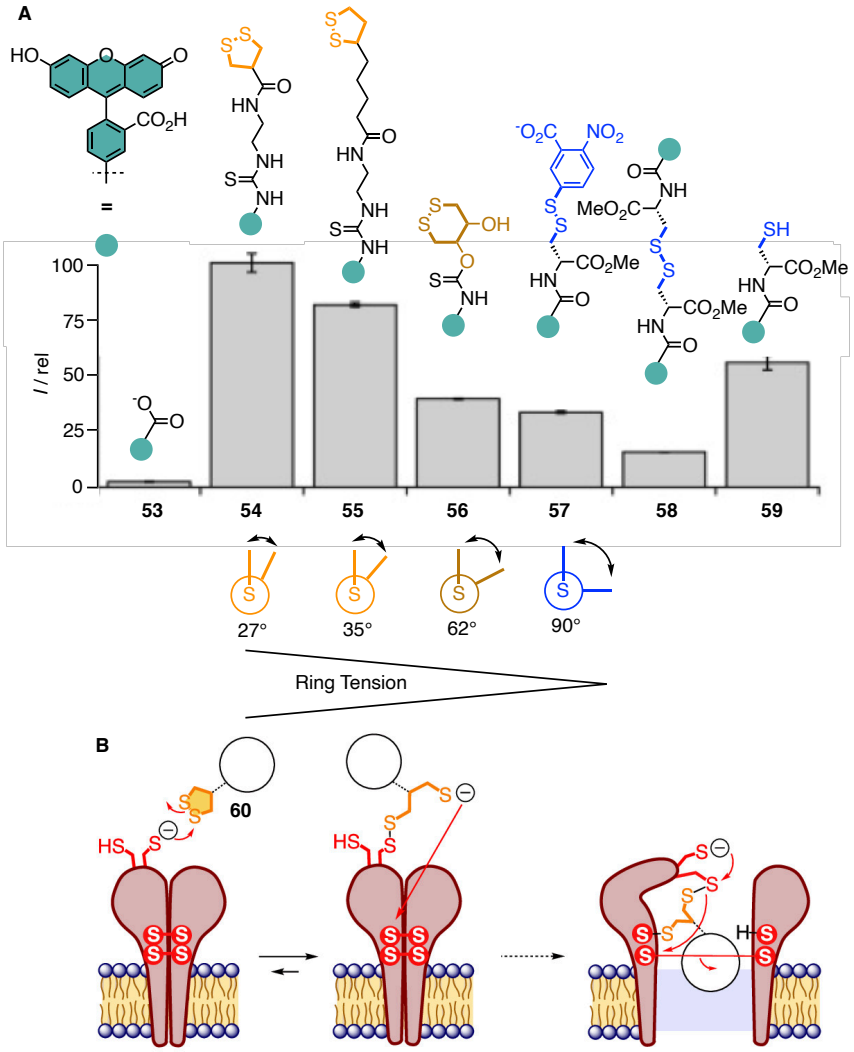

Figure 22. A) Normalized cellular uptake of ring-strained and linear disulfides measured by flow cytometry and representative CSSC dihedral angles. Adapted from reference.[104] B) Proposed mechanism for the transferrin-receptor mediated uptake of AspA. Adapted from reference.[66]

To further understand the mechanisms by which AspA-tagged cargos are uptaken, mechanistic studies were performed in a collaboration between our

group and the Adibekian group.[105] A fluorescently labelled random heptapeptide was efficiently uptaken in HeLa Kyoto cells and evenly distributed throughout the cytosol, as observed by confocal microscopy. Then, to prove that functional peptides could be delivered via this method, the pro-apoptotic peptide Bak-BH3 was tagged with AspA. Cellular death followed a clear concentration dependence with EC_{50} values in the µM range only for AspA-tagged peptide **60**, not for untagged negative controls. Proteomic studies then revealed several protein targets of AspA. The prime target of AspA was found to be the transferrin receptor TfR, explaining its possible uptake by endocytosis. However, secondary targets include several cytosolic proteins, such as cytoskeleton-associated protein 4 and chloride intracellular channel 1, indicating endocytosis-independent uptake and subsequent cytosolic availability of the cargo. Two cysteine residues of TfR were found to be the exact targets of AspA. Upon mutating both these residues to serine, endocytosis-dependent uptake of AspA was shut down, as can be seen by disappearance of punctate fluorescence. However, cells were still fluorescent, with a weaker, diffuse signal throughout the cytosol, indicating TfR-independent and cytosolic uptake still takes place.

Building on the ease of synthesis and derivatization of AspA, several applications have been published. Rivera-Fuentes *et al.* showed that AspA could be incorporated on lysine side chains and undergo solid-phase peptide synthesis.[106] This was applied to the delivery of a small peptide probe to study trafficking between the endoplasmic reticulum and the Golgi apparatus.[107] Using amphiphiles containing strained disulfides, liposomes and polymersomes loaded with sulforhodamine B were decorated with AspA.[108] Efficient uptake of these structures was observed by confocal microscopy and flow cytometry experiment, and was efficiently inhibited by DTNB, a clear proof of thiol-mediated uptake. During the course of this PhD, our group could also show that multivalency was important for AspA-induced cellular uptake.[109] The number and positioning of AspA units along a peptide backbone were shown to be

detrimental for its uptake in both 2D and 3D cell cultures, as measured by the newly introduced CAPA assay.[110]

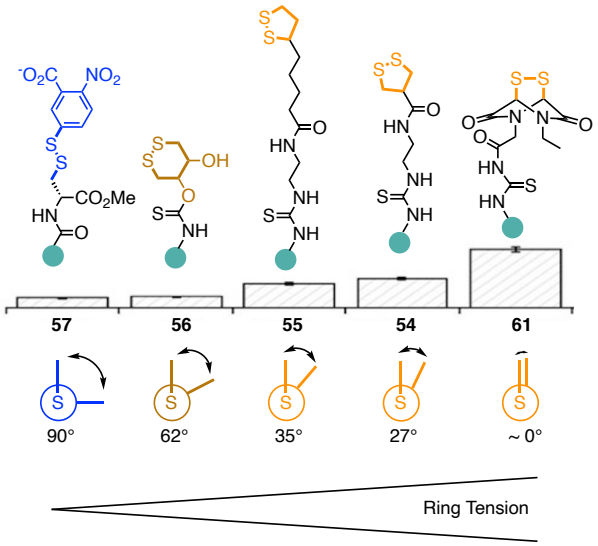

Figure 23. Normalized cellular uptake of ring-strained and linear disulfides measured by flow cytometry and representative CSSC dihedral angles. Adapted from reference.[111]

In 2018, epidithiodiketopiperazine (ETP) **61** was introduced as the most strained cyclic disulfide, with CSSC dihedral angle approaching 0°, as compared to 27° in AspA **54** or 90° in relaxed disulfides (Figure 23).[111] As previously proven, higher ring tension correlated with higher cellular uptake of the fluorophore-labelled compound because of higher reactivity towards exofacial thiols, as observed by flow cytometry and confocal microscopy. ETP was found to be insensitive to DTNB preincubation of cells, and fluorescent signal was fully diffuse in the cytosol and nucleus, not suffering from endosomal capture like AspA. Thiol-disulfide exchanges in solution were studied to explain this uptake behavior. Whilst AspA required strong reaction conditions to be reduced and re-oxidized, ETP was extremely reactive to even poor reducing agents such as GSH,

and could be rapidly re-oxidized with mild oxidants such as GSSG, but no to the cyclic form. This highly dynamic behavior of ETP can be explained by lower pK_a of the corresponding thiol, and might account for insensitivity to DTNB inhibition, with traces of cell surface thiols being enough to induce cellular uptake. This is unprecedented in thiol-mediated uptake, as DTNB pretreatment usually prevents internalization. This inactivity of DTNB for inhibition was the basis for the search of new thiol-mediated uptake inhibitors, as will be described in section 1.3.5.

1.3.4.2. More Dynamic Systems with Higher Efficiency

A simple shift from disulfides to diselenides was introduced to investigate its importance on thiol-mediated uptake.[112] Even cyclic diselenides such as **63** show no ring tension because of longer C-Se and Se-Se bonds as compared to C-S and S-S. Nonetheless, a large increase of uptake ability was observed for acyclic diselenides, and even greater for cyclic 1,2-diselenolanes **63** and **64** (DSL, Figure 24, A). Interactions between DSL **63** and thiols was proven by an acceleration of DTT oxidation in the presence of air, going through a mixed selenosulfide species, producing a diselenol which rapidly oxidizes to the diselenide in the presence of oxygen. Because of the absence of ring tension, this ring closing oxidation is highly favored, and could explain results of thiol-affinity column experiments. Whereas AspA **54** and acyclic diselenide **62** were retained by thiols on the column, diselenolanes **63** and **64**, as well as ETP **61** were not retained, in spite of their proven fast exchange with thiols (Figure 24, B). These results could be explained by the highly dynamic character of compounds **61** and **63**: after reacting with thiols, they produce a highly reactive species (a thiol with low pK_a and a selenol, respectively), which is likely to react with neighboring disulfides or to go back to the ring-closed form. AspA **54** and linear diselenides **62** were found to mainly undergo endocytosis, consistently with the formation of stable mixed disulfide and selenosulfide with surface thiols. On the other hand, ETP **61** and DSL **63**, because of their dynamic character, do not remain

immobilized and can be regenerated after reaction with thiol, giving a hopping mechanism until they freely reach the cytosol. This mechanism will be refined in follow-up studies in section 3.1.3.2.

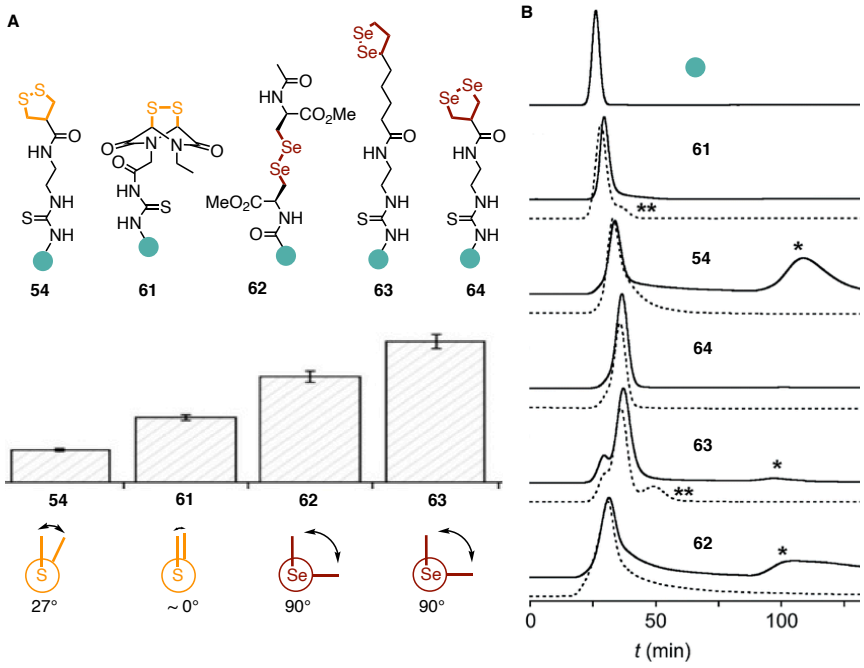

Figure 24. A) Normalized cellular uptake of ring-strained and linear disulfides measured by flow cytometry and representative CXXC dihedral angles (X = S, Se). B) Thiol-affinity column chromatograms of **61**-**64** with a 0–50 mM DTT gradient at t = 60–70 min (solid) and constant 50 mM DTT from t = 0 (dashed). Adapted from reference.[112]

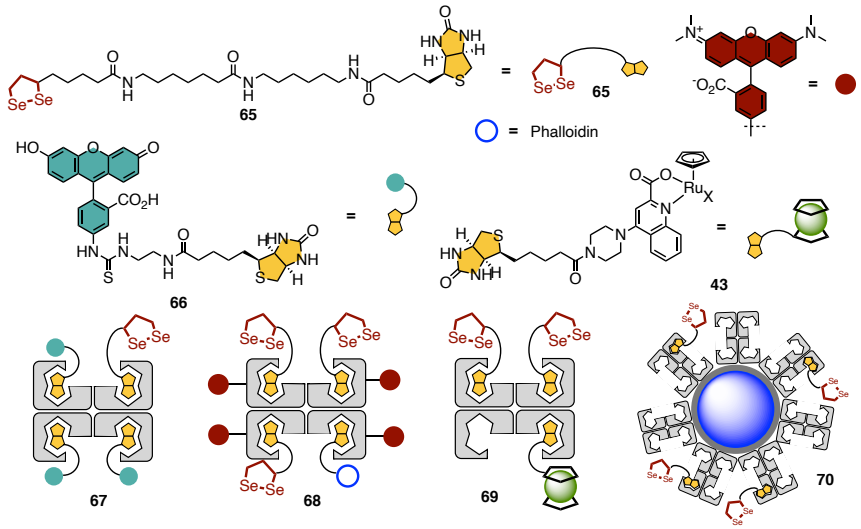

Figure 25. Application of biotin-streptavidin biotechnology. Cell-penetrating SaV complexes **67**-**69** bearing fluorophores (**67**, **68**), targeting peptide (**68**), or artificial metalloenzyme (**69**) and SaV-coated quantum dots are uptaken thanks to biotinylated DSL **65**. Adapted from reference.[113]

In 2019, we applied biotin-streptavidin biotechnology to cellular uptake thanks to biotinylated DSL **65**.[113] Forming supramolecular complexes with SaV and other biotinylated compounds (**66**, **43**), the delivery of proteins **67**, targeting peptides **68**, artificial metalloenzymes **69** and quantum dots **70** was achieved, bypassing endocytosis to deliver the cargo directly to the cytosol (Figure 25). A hypothetical mechanism was proposed, based on the walker hypothesis, where DSL is considered as a bipedal molecular walker, walking through disulfide tracks in transmembrane proteins all the way to the cytosol. This will be further developed in section 3.1.3.2.

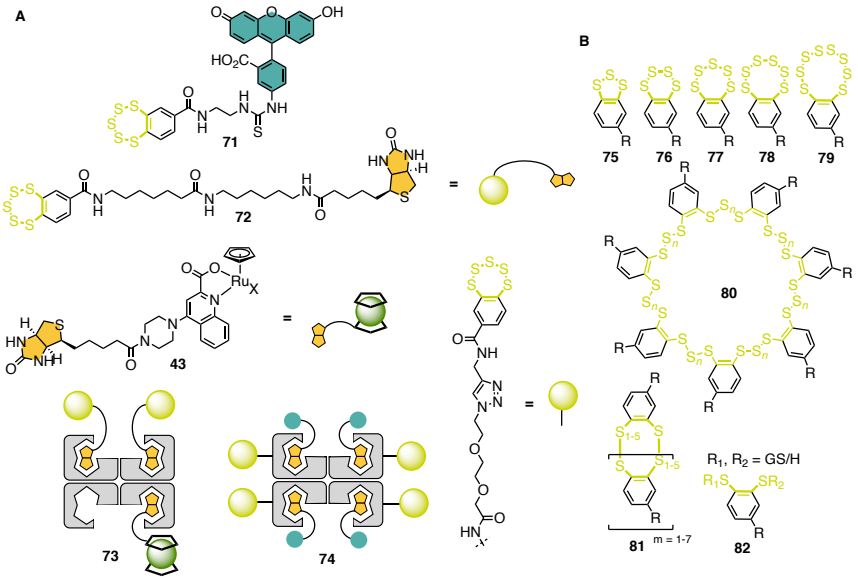

Figure 26. A) FITC-tagged BPS **71** and biotin-streptavidin biotechnology used in combination with BPS **72** to deliver fluorophores (**74**) and artificial metalloenzymes (**73**). B) Dynamic covalent character of BPS as observed by HPLC-MS. Adapted from reference.[114]

Benzopolysulfane (BPS) **71** was then found to outperform every transporter reported so far when attached to fluorescein.[114] Using biotin-streptavidin biotechnology, **72** could also efficiently deliver fluorophores, proteins **69** and artificial metalloenzymes **73** (Figure 26, A). Mechanistic studies performed on the BPS system found that it behaves as a dynamic combinatorial library upon initiation with thiols or disulfides (Figure 26, B). Ring expansion and contraction from BPS_5 to $BPS_{3\text{-}9}$ **75** – **79** could be observed, as well as cyclic oligomers **81** up to heptameters with 19 sulfur atoms (**80**). As a result from this chemistry, BPS was highly retained on thiol-affinity column, highlighting special properties of the dynamic covalent chemistry involved. Uptake of **71**, contrary to ETP or DSL, was impaired by DTNB inhibition. It is believed that, from such adaptive network, the system is able to "select" the best transporter from the library,

uptake it thanks to its highly dynamic character with thiols and disulfides, and that uptake induces a shift in equilibrium in the library, which in response creates more of the best transporter.

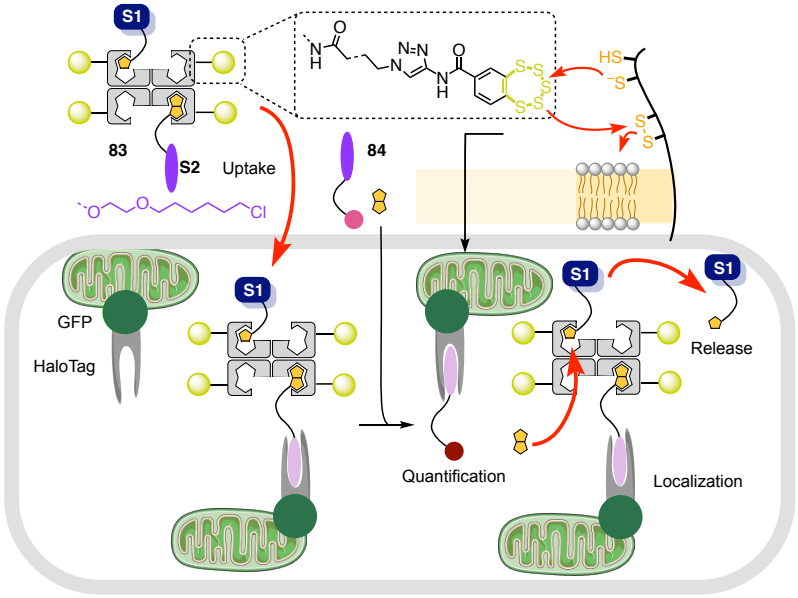

Figure 27. Cell-penetrating streptavidin (CPS) for precise localization, quantification, and spatio-temporal release of substrates of choice in the cytosol. SaV **83** decorated with BPS, loaded with a cargo S1 and a targeting agent S2, is uptaken by thiol-mediated uptake. Uptake is quantified by chloroalkane penetration assay. S1 can be release by incubation with biotin. Adapted from reference.[115]

Cell-penetrating streptavidin **83** (CPS) was introduced in 2020 as a general delivery platform of biotinylated cargos (Figure 27).[115] As showed previously, SaV could be labelled by BPS and other transporters (AspA, DSL) or controls ($C_{13}H_{27}$) through click chemistry after functionalization of lysine side-chains. The CPS formed was rapidly uptaken by cells in an endocytosis-independent manner. The four binding pockets of SaV can be filled with two different ligands: a cargo S1 (fluorescent probes, PNA) and a targeting agent S2 (chloroalkane,

anti-GFP nanobody). All substrates could be delivered to cells, and targeted to the desired sub-cellular compartment. Efficient delivery could be assessed by a novel high-content chloroalkane penetration assay (HC-CAPA), thanks to chloroalkane rhodamine **84**, adapting the previously developed method to automated confocal microscopy.[116] Taking advantage of desthiobiotin-biotin exchange, S1 could be released from the CPS in a controlled fashion upon incubation with biotin. For example, PNA could be uptaken, targeted to mitochondria, subsequently released and diffused into the cytosol. The CPS introduced here are taking full advantage of biotin-streptavidin biotechnology for cellular uptake and appear as a general platform for the controlled delivery of almost native cargos bearing minimal modifications.

1.3.5. Dynamic and Irreversible Inhibitors of Thiol-Mediated Uptake

As mentioned earlier, the proof of transporters operating through thiol-mediated uptake came from the study of their reaction with thiols and disulfides, and, more importantly, inhibition by Ellman's reagent DTNB **14**. However, some of the best transporters, namely ETP **61** and DSL **63** were insensitive to DTNB inhibition. This is in part attributed to the high reactivity of the disulfides produced by the reaction between exofacial thiols and **14**, and the poor reactivity of DTNB. Considering the high potential of thiol-mediated uptake for the cytosolic delivery of large biomolecules, it was of interest to develop more reliable tools to inhibit it.

Our group synthesized and tested a wide range of analogs of cyclic oligochalcogenides (COCs) and irreversible thiol-reactive molecules for their ability to block the uptake of fluorescently labelled ETP **61** and BPS **71**.[117]

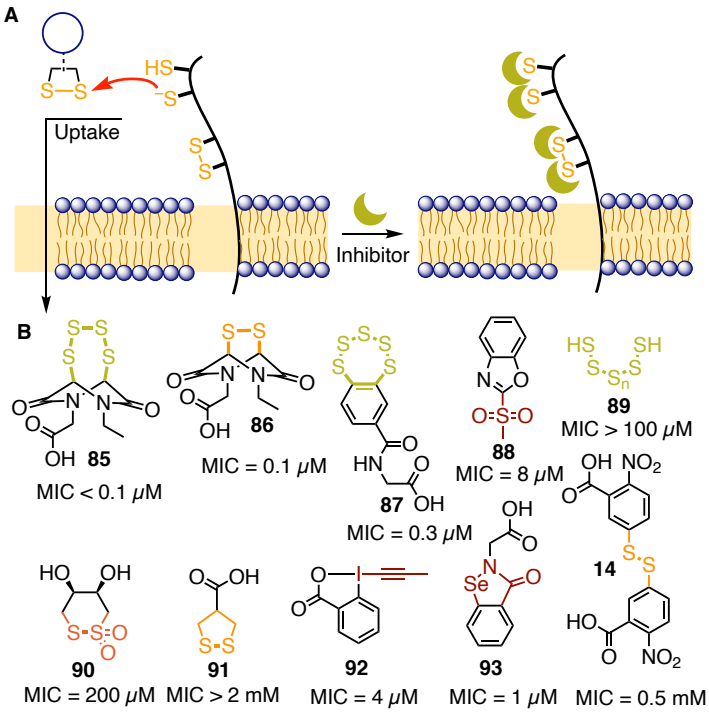

Figure 28. A) Inhibition of thiol-mediated uptake by reversible and non-reversible thiol- and disulfide-reactive agents. B) Structure of selected inhibitor candidates **85** – **93** with their concentrations needed to inhibit by ~15% (MIC) the uptake of ETP **61** (1 h preincubation with inhibitors, 30 min incubation with **61**). Adapted from references.[117,118]

Two recently published studies, and others ongoing, yielded a library of about a hundred inhibitors with activities up to 5000-fold better than DTNB **14**.[117,118] It is important to note that different inhibitors gave different selectivity for one transporter or another. This supported that thiol-mediated uptake, as a general concept, covers several internalization pathways with multiple targets involved, highlighting the importance of precise mechanistic studies to better understand this process. When ETP **61** was used as a transporter, the best inhibitors identified were also cyclic oligochalcogenides, hinting towards the fact that the reversibility provided by COCs is crucial.[117] On the other hand, irreversible

covalent inhibitors, although less active, were still up to 250 times more efficient than DTNB and showed good correlation between reactivity and inhibition.[118]

1.3.6. Perspectives: What Remains Unknown

Thiol-mediated uptake is increasingly gaining interest as an unusual way to penetrate cells for cytosolic delivery. Many directions can still be explored to make the field mature, starting from a better understanding of the precise mechanism of action of transporters. Proteomics studies have been performed using an asparagusic acid derivative, identifying several proteins involved in its uptake, starting with the transferrin receptor TfR.[105] With knockdown and overexpression of this protein in cells, the uptake of AspA could be regulated. However, already the next transporter introduced, ETP **61**, was insensitive to TfR knockdown, highlighting other proteins must be at play.[111] With the wide variety of transporters and inhibitors of thiol-mediated uptake available today, in depth characterization of the protein partners will be crucial for the understanding of thiol-mediated uptake mechanism.

Regarding poly(disulfide)s, CPDs are the most widely used thiol-mediated uptake transporters, recently even for *in vivo* applications.[102,119] Their mechanism of action has been supposed to be similar to CPPs, forming transient micellar pores in the cell membrane, allowing the cargo to freely enter the cytosol, without causing damages to the membrane.[40] Investigating the occurrence of such pores during thiol-mediated uptake would give valuable mechanistic information.

The quest for new, more efficient thiol-mediated uptake transporters is a never-ending one. Going away from classical thiol-disulfide exchange towards extreme chalcogen chemistry, such as polysulfanes[114] or diselenides,[112] already excellent transport activities have been achieved. A rich untapped potential of diverse reactivities exist for dynamic covalent bonds based on chalcogenides, *e.g.* with thiosulfonates and thiosulfinates,[117] phosphorothioates and

selenolates,[120] … Fully synthetic transporters can be synthesized from scratch, and inspiration can also come from nature. Several viruses and toxins use dynamic covalent thiol-disulfide exchanges,[68,69] and other sulfur-based compounds, *e.g.* oligonucleotide phosphorothioates,[121] have good cellular uptake properties. Studying more in depth such systems could give inspiration to design new transporters.

Most existing applications of thiol-mediated uptake have been focused on mammalian cells, most of the time HeLa cells. The uptake of CPDs and COCs is more or less constant in different mammalian cell lines, highlighting the generality of the method. Non-eukaryotic cells have nonetheless not been probed for their propension to uptake chalcogen-based transporters. Applying thiol-mediated uptake to bacteria, for example, would be of interest to overcome permeability issues in Gram– bacteria.

Last but not least, *in vivo* applications are so far limited to a few scarce examples.[102,119] A recent study showed that poly(disulfide)s could be rationally designed to complex all the components needed for CRISPR-Cas9 gene editing, and deliver them into the cytosol.[102] In mice, excellent prevention of hepatic failure was observed using this gene editing method. Small molecule transporters have not been studied *in vivo* yet, but hold much promises for more efficient gene therapies.

Chapter 2

OBJECTIVES

Thiol-mediated uptake, although widely applicable *in vitro*, is still a young field, and a lot of unknowns remain. The main objective of this thesis is to better understand the mechanisms that are at play in thiol-mediated uptake, both for small molecule and polymeric transporters. New applications of thiol-mediated uptake, especially in non-mammalian cells, can also be envisioned.

In a first part, the ring opening of 1,2-dithiolanes and diselenolanes will be developed. This project started with a curiosity question, to figure out whether the ring-opening polymerization of lipoic acid derivatives is regioselective. This clarification is important for the structure of cell-penetrating poly(disulfide)s (CPDs), thiol-mediated uptake transporters developed in our group. Studying the dynamic covalent exchanges between thiols and dithiolanes or diselenolanes could also give valuable information concerning their mode of action.

Then, the lessons learned from the ring opening of cyclic disulfides and diselenides can be applied to perform their precise oligomerization. Poly(disulfide)s are most of the time synthesized by ring-opening polymerization at high concentrations, with large distribution of sizes. Using a peptide foldamer as a template, we aim at aligning a precise number of disulfide-containing monomers in a define three-dimensional structure. Using orthogonal dynamic covalent chemistries, loading of monomers, oligomerization, and release of the oligomer will be described. With the same system, the first partial ring-opening oligomerization of 1,2-diselenolane will also be mentioned.

In a third section, the application of thiol-mediated uptake to non-mammalian cells, namely bacteria, will be described. Whereas many applications of thiol-mediated uptake to human cells have been described over the years, no trials in

bacteria have been reported. Attaching cyclic oligochalcogenides (COCs) to Gram+ antibiotics, we will study their possible activation against Gram– bacteria. Using antibiotics with various modes of action, with either intracellular or extracellular targets, conclusions will be drawn regarding the mechanism of thiol-mediated uptake.

Finally, in the last section, the study of the cellular uptake of oligonucleotide phosphorothioates will be reported. Known to have up to 200-fold higher cellular uptake than non-modified DNA oligonucleotides thanks to interactions with transmembrane proteins, their precise mechanism of uptake is unknown. Studies of the dynamic covalent chemistry of the phosphorothioate moiety will be reported, drawing important implications concerning the molecular mechanisms at play during their cellular uptake.

Chapter 3

RESULTS AND DISCUSSION

3.1. Ring Opening of 1,2-Dithiolanes and 1,2-Diselenolanes

The results presented in this section have been published.[122]

3.1.1. Design: A Regioselectivity Question

First project carried out during my PhD, this section will describe the study of the thiolate-mediated ring-opening reaction of 1,2-dithiolanes and 1,2-diselenolanes.[122] Acyclic disulfides and diselenides adopt a conformation to maximize hyperconjugation and minimize lone pair repulsion where the CXXC dihedral angle is 90° (X = S or Se).[123,124] However, in cyclic dichalcogenides, ring strain arises from this dihedral angle being much lower (e.g. 35° in lipoic acid derivatives, up to 0° in epidithiodiketopiperazines (ETP)).[111,125] This strain favorizes the thiol-mediated opening of 1,2-dithiolanes, to release the ring tension.[104]

This project started with a curiosity question: is the attack of a thiolate on such molecules regioselective? As mentioned in section 1.3.3.3, our group introduced cell-penetrating poly(disulfide)s (CPDs) as cell-penetrating peptide (CPP) mimics with excellent cellular uptake properties, thanks to a combination of counterion- and thiol-mediated uptake.[54] CPDs are synthesized by the ring-opening polymerization of 1,2-dithiolanes, namely lipoic acid derivatives, and often drawn in literature as regio-regular polymers for easier representation.[53,78,126] Nonetheless, studies on the regioselectivity of this cascade ring-opening were lacking. Clarification of this selectivity is not only relevant to the tacticity of poly(disulfide)s, but also to the biosynthesis of acetyl-

CoA, which goes through a similar ring opening of a lipoic acid derivative.[73,127,128] We therefore sought to investigate the thiol-mediated opening of 3-alkyl-1,2-dithiolane **22** and diselenolanes **96** (Figure 29).

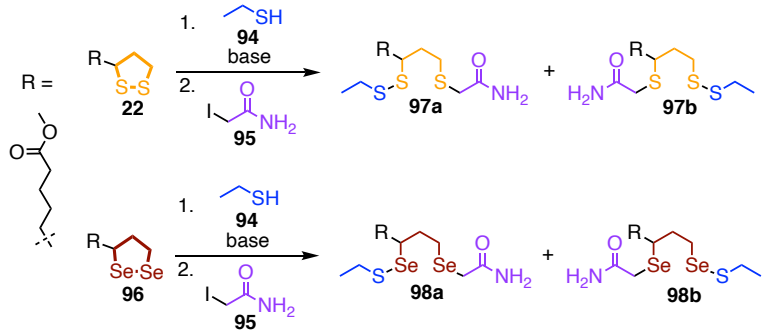

Figure 29. Thiol-mediated opening of 3-alkyl-1,2-dithiolane **22** and diselenolane **96** can produce two regioisomers **97a**/**b** and **98a**/**b** respectively.

Varying the reaction conditions, different ratio of the different regioisomers **97a/b** and **98a/b** should be obtained, thus determining the regioselectivity of the attack. Both starting materials were synthesized from their carboxylic acid counterpart *via* Fischer esterification following or adapting literature procedures.[129] The ring-opening reactions were performed in organic solvent (namely, dichloromethane) to study the processes involved at low temperature, and to allow the trapping of otherwise elusive short-lived intermediates. In the following, the study of 1,2-dithiolane **22** will be described first, with the consequences for polymerization and acetyl-CoA biosynthesis. In the next subsection, it will be shown that shifting from sulfur to selenium in 1,2-diselenolane **96** is not a simple extension, and that the results may account for the high cellular uptake performance of COCs such as **63**.

3.1.2. Ring Opening of 1,2-Dithiolanes and Consequences for Poly(Disulfide)s

3.1.2.1. Thiolate-Mediated Ring Opening at Equilibrium

To prevent polymerization of lipoic acid methyl ester **22** and study only the ring opening of one monomer, the reactions were carried out at lower concentration of **22** as compared to poly(disulfide) synthesis (40 mM *vs* 1 M).[78] Despite the ring tension, at such concentrations, the reaction is not quantitative: the ring opening was initiated by the addition, at –78 °C, of five equivalents of thiol **94** and diisopropylethylamine (DIPEA). Ten seconds to one minute after this addition, the reaction was quenched with five equivalents of iodoacetamide **95**, still at –78 °C, to trap the highly reactive ring-open intermediate **99a** and **99b** (Figure 30, A). To improve the conversion, these two additions were repeated four times. With this procedure, LCMS studies showed good conversion to the expected trapped mixed disulfides **100a** and **100b** (Figure 30, B).

The observed low conversion can be attributed to a lower acidity of thiols in organic solvents as compared to aqueous media. For example, to study the polymerization of lipoic acid methyl ester **22** in tetrahydrofuran (THF), Moore *et al.* screened various organic bases, and showed that very strong base such as tetramethylguanidine or phosphazenes were needed.[78] On the other hand, the system used here, with the relatively weak DIPEA as a base, made the exchange reactions slower, making it possible to trap highly reactive intermediates and study extremely fast processes.

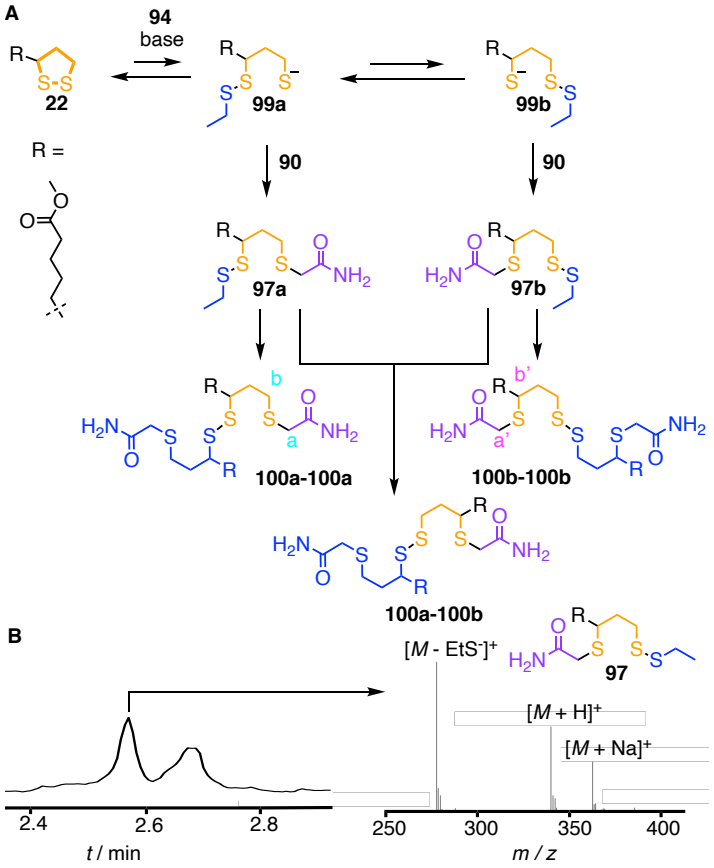

Figure 30. A) Reaction of dithiolane **22** with thiol **94** under basic conditions in CH_2Cl_2 at –78 °C followed by quenching with **95** at –78 °C and workup afford dimers of regioisomers **97a** and **97b**. B) LCMS trace of the reaction mixture of **22** reacted with **84** followed by **95**, with MS of **97a**/**b**.

97a and **97b** being two regioisomers with highly similar structures, they were undistinguishable by LCMS. In the process of isolating **97a**/**b**, the two regioisomers were converted into dimers **100a-100a**, **100a-100b** and **100b-100b**. This conversion can be explained by the fact that exchange reactions still take place in the dynamic **97a** and **97b**, and the formation of dimers is driven by the evaporation of the highly volatile ethanethiol **94**. Whereas this would

theoretically overcomplicate the system, the ratios **100a**/**b** reflect the ratios of **97a**/**b** thanks to the irreversible sulfide bond formed by trapping with iodoacetamide. Additionally, in the NMR spectra, the heterodimer **100a**-**100b** was undistinguishable from homodimers **100a**-**100a** and **100b**-**100b** (Figure 31, A). In other words, the ratios observed by NMR is a measure of the overall proportion of the **100a** and **100b** parts, regardless of what is connected through the central disulfide.

In the ^{1}H NMR spectra of the purified mixture after complete reaction, two sets of signals could be observed, corresponding to the two regioisomers **100a**/**b**, although most signals were overlapping due to the high similarity between both isomers. Two singlets at 3.21 and 3.23 ppm were well resolved, and could be assigned to the acetamide protons attached either to the primary (in **100a**) or secondary sulfide (in **100b**) thanks to the HMBC spectra (Figure 31, A). The correlation found between the larger peak at 3.23 ppm and the CH_2 carbon (assigned by DEPT-135) showed that these peaks belonged to the **100a** part of the dimers. Similarly, the cross peak between the smaller, more upfield acetamide proton signal and the CH carbon corresponded to the secondary sulfide in **100b**. Integration of the proton signals yielded a 3:2 ratio in favor of the primary sulfide **100a**, as expected: the primary thiolate in **99a** is more acidic, and therefore a better leaving group than the secondary thiolate in **99b**, which ultimately resulted in the same preference for **100a** as compared to **100b**.

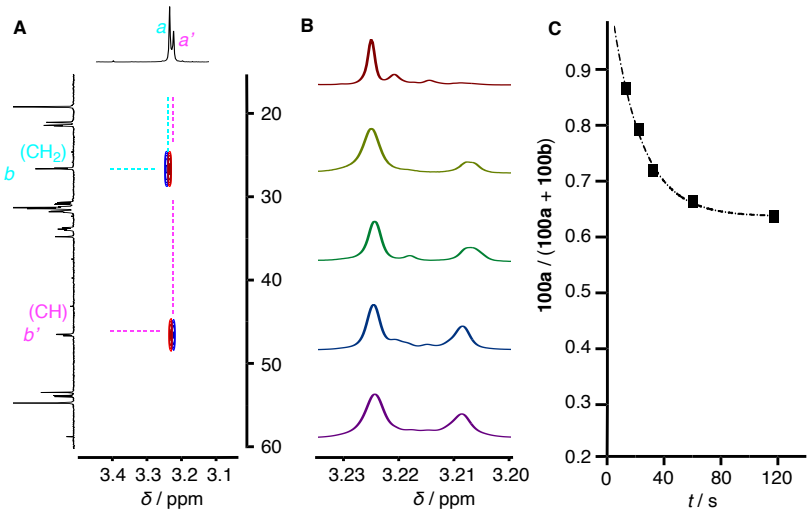

Figure 31. A) Diagnostic region of the HMBC NMR spectrum in $CDCl_3$ to assign regioisomers **100a** (cyan) and **100b** (pink) in the product mixture. B) ^1H NMR spectra in $CDCl_3$ with 10, 20, 30 and 60 s between the addition of thiolate **94** and iodoacetamide **95** at –78 °C in CH_2Cl_2 (from top to bottom), and with 10 s between additions at 0 °C (bottom). C) Ratio of **100a**/(**100a**+**100b**) as a function of reaction time at –78 °C in CH_2Cl_2 before quenching with **95**.

3.1.2.2. Varying Time Before Quenching: Trapping Reactive Intermediates

To study the processes that yield the observed 3:2 ratio, the time between the addition of thiolate **94** and terminator **95** at –78 °C was then varied. At first, with short reaction times, the primary sulfide **100a** was almost the only product observed (Figure 31, B), suggesting that the initiator attacked selectively the secondary sulfur atom to release the primary thiolate in **99a**. Although, as stated earlier, a primary thiolate is a better leaving group, this selectivity goes against sterics: the secondary sulfur atom in **22** is more hindered than the primary one. However, the same experiment using *tert*-butyl mercaptan **101** instead of ethanethiol **94** gave the same distribution (Figure 78, Figure 79, see experimental section), indicating that leaving group ability was predominant as compared to sterics.

When increasing the reaction time from 10 to 60 s, the upfield peak corresponding to **100b** increased, the **100a**/**b** ratio going from 9:1 to the ~ 3:2 observed at higher temperature and with high reaction time (Figure 31, C). This evolution arises from a rapid isomerization of **99a** into **99b** *via* intramolecular thiolate migration, from the secondary to the primary sulfur atom. Under these conditions, this intramolecular migration occurred up to a maximum of 37% of conversion, corresponding to an equilibrium constant $K = 0.61$ (Table 1).

Table 1. Ratios of **100a**/**b** at –78 °C as a function of time.

t / s	Ratio **100a**/**b**
10	88/12
20	80/20
30	72/28
60	66/34
Equilibrium	63/37

The data obtained in Table 1 was fitted to a single exponential decay using Equation 1 where r is the ratio of both isomers, k_1 the forward rate constant and k_{-1} the reverse rate constant.

$$r(t) = r_{eq} + (r_0 - r_{eq})\exp(-k_1+k_{-1})t) \qquad \text{(Eq. 1)}$$

This gave a rate constant $k_1 = 1.7 \times 10^{-2}$ s^{-1}, corresponding to a half lifetime at –78 °C of $t_{50} = 15$ s. Whereas the rate constant at a different temperature would be needed to extrapolate t_{50} at room temperature, this could not be achieved because the equilibrium was already too fast at –40 °C. A rough approximation, considering rate constants of reactions happening at room temperature double for every 10 °C rise in temperature, gave an estimation of t_{50} ~ 7 ms at 25 °C. What is important to note is that the intramolecular thiolate migration is in any case extremely fast at room temperature.

Further variations of parameters did not lead to drastic changes in the obtained equilibrium, and the **100a**/**b** ratio was independent of stereochemistry, solvent and initiator (Figure 79, see experimental section).

3.1.2.3. Consequences for Poly(Disulfide)s and Biosynthesis of Acetyl-CoA

In the biosynthesis pathway of acetyl-CoA **102** from pyruvate **104**, a key step is the nucleophilic ring opening of a lipoyl amide **106** in one of the enzyme subunits, initiated by a so-called "Breslow intermediate", acetyl thiamine **105** (Scheme 1). Initial studies by Ronald Breslow proposed that the attack occurred on the secondary sulfur atom, yielding **107a**, as observed here.[73] However, further studies supported a kinetic and thermodynamic preference for the less hindered primary sulfur (**107b**).[127,130] Although the two systems differ quite a lot, with a thiolate instead of a carbon-based nucleophile, and a study in solution and not in an enzyme, our findings go in favor of the initially proposed attack on the secondary sulfur, with leaving group ability dominating sterics.

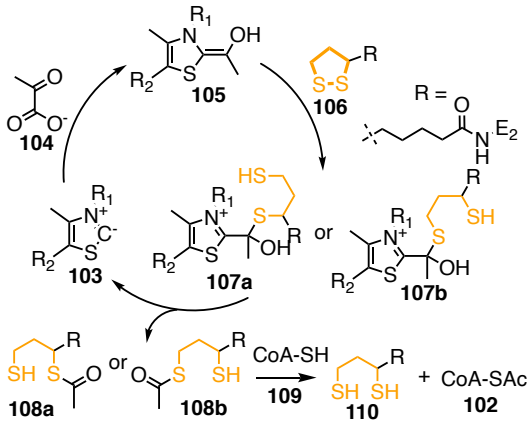

Scheme 1. Biosynthesis of acetyl-CoA **102** from pyruvate **104**. Addition of **104** on thiamine pyrophosphate (TPP) **103** followed by a decarboxylation gives "Breslow intermediate" acetyl thiamine **105**. Nucleophilic attack of **105** on enzyme-bound lipoyl amide **106** can give two regioisomers **107a**/**b**. TPP elimination regenerates **103** and acetyl dihydrolipoyl derivatives **108a**/**b**, which acetylates CoA-SH **109**.

The observation that the thermodynamic equilibrium gives a 3:2 ratio between **100a** and **100b**, and that the thiolate migration from the secondary to the primary sulfur atom is fast at room temperature, have clear consequences on the structure of poly(disulfide)s made from lipoic acid derivatives (see Figure 16).[75,77,78,103] Regio-regular *head-tail* polymers **112** would be formed only if the polymerization is faster than the intramolecular rearrangement, which is possible at high concentrations, but rather unlikely (Figure 32).[131] From the preferential attack on the secondary sulfur atom, regio-regular polymer **113** cannot be obtained in any case. Instead, considering that thiolate migration is fast enough to reach equilibrium before a second monomer is added, the structure of poly(disulfide)s should be the regio-irregular **111**, with the ratio of *head-tail*, *head-head* and *tail-tail* fusions reflecting the 3:2 ratio observed between **100a** and **100b**.

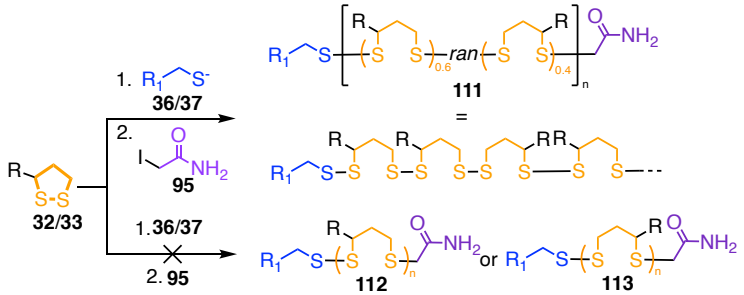

Figure 32. Ring opening polymerization of lipoic acid derivatives **32**/**33** produces the regio-irregular polymer **111** rather than regio-regular **112** or **113**.

The structural information of the trapped ring-open monomers presented here is important, because such precise NMR assignments cannot be obtained from the study of the polymers themselves where broad peaks are observed in the NMR spectra.

3.1.3. Ring Opening of 1,2-Diselenolanes and Consequences for Cellular Uptake

3.1.3.1. Thermodynamics and Kinetics of Thiolate-Mediated Ring Opening

A simple shift from sulfur to selenium is not as trivial as it seems. First, because of the longer Se-Se and Se-C bonds and of the selenophilicity of selenium, the ring tension in **96** is minimal, despite a CSeSeC dihedral angle close to 0°.[112,132] Then, thiol/selenol exchanges have been shown to be much faster with selenium than with sulfur, up to seven orders of magnitude, because of both selenophilicity and higher acidity of selenols (pK_a ~ 5, as compared to ~ 8 for thiols).[133] This highly dynamic character is best exemplified by the oxygen-mediated oxidation of dithiothreitol (DTT) catalyzed by diselenolipoic acid, which greatly increases the reaction rate without being able to detect the ring-open selenosulfide or selenol intermediates.[112] Consequently, 1,2-diselenolanes have a strong preference for their closed form, make it challenging to trap selenosulfide and selenolate intermediates.[134–136]

For these reasons, the ring opening of 3-alkyl-1,2-diselenolanes **96** was then studied (Figure 29, Figure 33) following the same procedure as described above (section 3.1.2). Under these conditions, the ring opening took place in a similar fashion than with 1,2-dithiolanes. Under inert atmosphere, the produced selenolates in **114a**/**b** were long-lived enough to be trapped by iodoacetamide **95**, and the quenched selenosulfides **98a**/**b** were observed by LCMS (Figure 33, B).

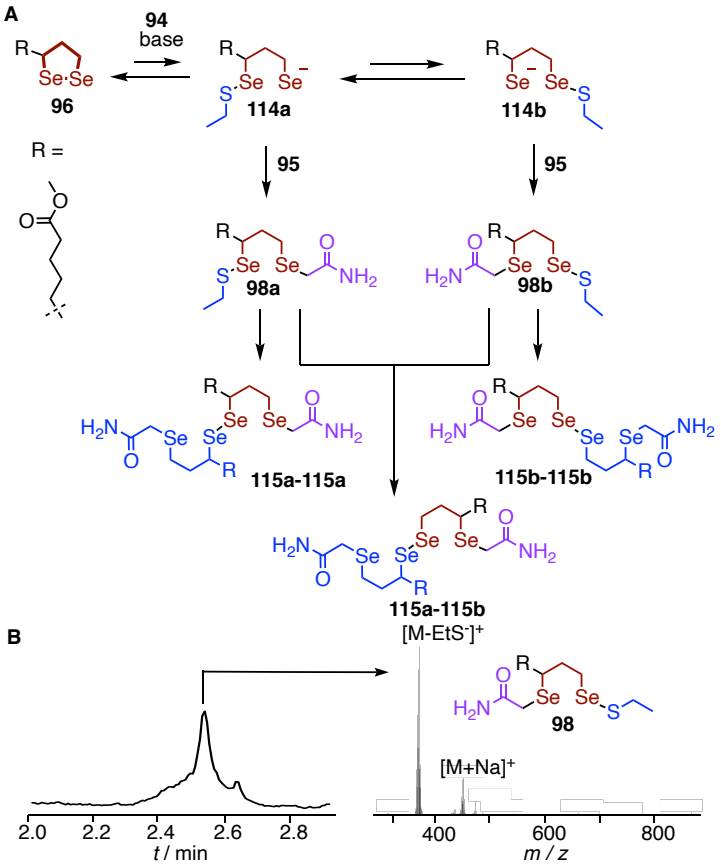

Figure 33. A) Reaction of diselenolane **96** with thiol **94** under basic conditions in CH_2Cl_2 at –78 °C followed by quenching with **95** at –78 °C and workup afford dimers of regioisomers **98a** and **98b**. B) LCMS trace of the reaction mixture of **96** reacted with **94** followed by **95**, with MS of **98a**/**b**.

Unsurprisingly, the mixed selenosulfides in **98a**/**b** were rapidly converted into the diselenides dimers **115** during workup because of the volatility of ethanethiol and the relative higher stability of diselenides as compared to selenosulfides.[134] Similarly to what was presented above for dithiolanes, the ^{1}H and HMBC NMR spectra were used to assign the peaks in **115a**/**b** corresponding to the primary or secondary selenolate leaving group in **109a**/**b**. When the

thermodynamic equilibrium was reached, a ratio of **115a**/**b** of 3:2 similar to the one observed for dithiolanes was obtained.

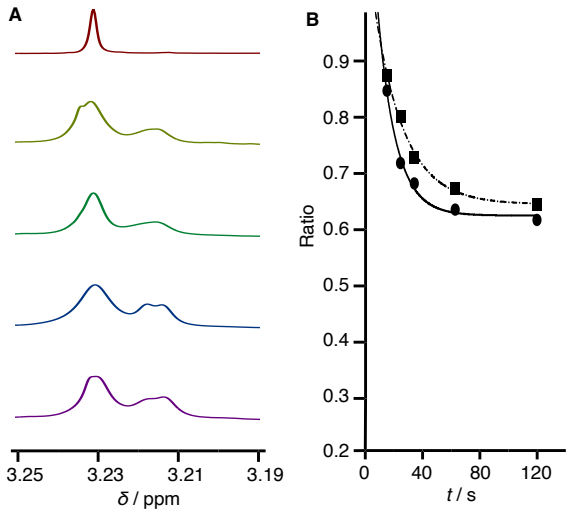

Figure 34. A) ^{1}H NMR spectra in $CDCl_3$ with 10, 20, 30 and 60 s between the addition of thiolate **94** and iodoacetamide **95** at –78 °C in CH_2Cl_2 (from top to bottom), and with 10 s between additions at 0 °C (bottom). B) Comparison of ratios of **100a**/(**100a**+**100b**) (■) and **115a**/(**115a**+**115b**) (●) as a function of reaction time at –78 °C in CH_2Cl_2 before quenching with **95**.

Studying the events that lead to this distribution, there was once again a high similarity in the behaviors of diselenolanes and dithiolanes (Figure 34, Table 2). Initiator **94** also almost exclusively attacked the secondary selenium atom in **2** to release the primary selenolate in **114a**. With time, thiolate migration occurred to equilibrate between **114a** and **114b**, with a rate constant $k_1 = 3.03 \times 10^{-2}$ s^{-1}, only 1.7-fold faster than for dithiolane **22** (Figure 34, B). Compared to $t_{50} \sim 7$ ms at 25 °C for **22**, this corresponds to $t_{50} \sim 4$ ms for diselenolane **96**, slightly faster as expected from the higher exchange kinetics reported in literature for selenium as compared to sulfur.[133] However, the relatively small difference of migration rate between S and Se suggested that this equilibrium is not governed by the nature

of the chalcogen atom, but rather by the electrophile and by proximity effects, which are similar in both systems.

Table 2. Ratios of **115a**/**b** at −78 °C as a function of time.

t / s	Ratio **115a**/**b**
10	85/15
20	71/29
30	67/33
60	62/38
Equilibrium	60/40

3.1.3.2. Consequences on the Cellular Uptake Mechanism of 1,2-Diselenolanes

As mentioned in the introduction, our group has shown in two recent studies that diselenolipoic acid derivatives are efficient at transporting into cells not only fluorophores, but also cargos as big as artificial metalloenzymes and fluorescent quantum dots, more efficiently than with their disulfide counterparts.[112,113] However, contrary to cyclic disulfides, these results cannot be rationalized by an increase of ring tension, as 1,2-diselenolanes are mostly not strained.

Before this study, direct proofs of interaction of 1,2-diselenolanes with thiolates remained lacking. For example, in thiol-affinity column chromatography, these compounds were not retained, which was attributed to the fast ring closing after ring opening, but this remains speculative (see section 1.3.4.2).[112] The results presented here provided a direct proof that 1,2-diselenolanes can react with thiolates, with the otherwise elusive selenosulfide intermediates **98** observed by LCMS. Taken together with the absence of retention on thiol-affinity columns, and the fact that acyclic diselenides, although uptaken into cells, remain trapped in endosomes, we proposed that diselenolanes

could function as molecular walkers,[137–140] moving along disulfides in transmembrane proteins (Figure 35).

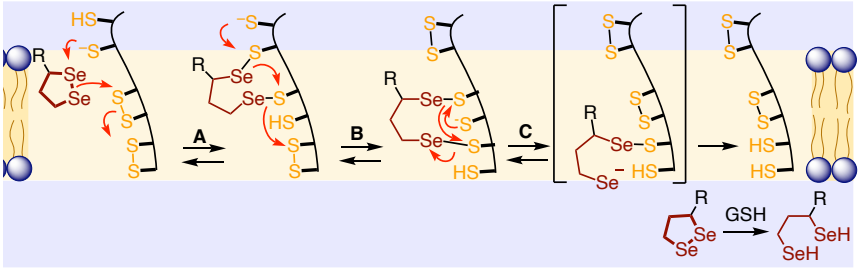

Figure 35. A hypothetical model to account for the cell-penetrating ability of 1,2-diselenolanes. A) 1,2-diselenolane is open by a thiolate in a transmembrane protein, producing a short-lived selenol, that is quenched with a neighboring disulfide. B) A proximal thiol releases the first "foot" and triggers isomerization as observed in **114a**, producing a new selenol that is quenched with another disulfide. C) Multiple iterations of this "walking" steps move the diselenolane across the membrane to reach the cytosol.

In this hypothetical model, each step is based on the series of events reported in this study. First, an exofacial thiolate on a membrane-bound protein attacks the 1,2-diselenolane to give a ring-open product reminiscent to **114a**/**b**. Due to its low pK_a, the produced selenol remains deprotonated and highly reactive, reacting quickly with a neighboring disulfide, creating a bridged species (Figure 35, A). With the help of a proximal thiol, the first "foot" of the walker is then released, triggering an isomerization similar to the fast transformation of **114a** into **114b** observed in our study (Figure 35, B). A series of such isomerizations can move the walker along "disulfide tracks" in transmembrane proteins, all the way to the cytosol (Figure 35, C). Finally, the proteins that got denatured after walking should be refolded to their initial state, which can also be catalyzed by diselenides.[135] All of these reactions being reversible, a driving force has to account for the directionality of this motion across the lipid bilayer. With a concentration of glutathione (GSH) of about 10 mM, the cytosol is a highly reductive environment. Under these conditions, the diselenolane can be reduced,

producing a diselenol that either cannot take a step back, either gets scavenged by intracellular electrophiles.

Although hypothetical, this mechanism is also supported by the nature of the few known targets of thiol-mediated uptake transporters. In collaboration with the Adibekian group, our group showed that asparagusic acid reacts with proteins that match the description of the potential "walker" targets.[105] For example, it was shown to first react with Cys 556/558 of the transferrin receptor (TfR), two cysteines that are in close proximity, essential for the release of the first "foot" (Figure 35, A). TfR is a dimeric protein, held together by two disulfide bonds in close proximity to the membrane, that could be a target for the subsequent exchange (Figure 35, B).[141,142] Other potential targets include the chloride intracellular channel protein 1 (CLIC1),[143,144] epidermal growth factor receptor (EGFR),[145] cysteine-rich ion channels[146] and scramblases,[147,148] disulfide-rich stabilins,[149] …

According to the results showed in section 3.1.2, thiolate migration after ring opening also happens in 1,2-dithiolanes, with a rate constant in the same order of magnitude as compared to 1,2-diselenolane. The same mechanism could therefore be responsible for the uptake of cyclic disulfides as well. However, because of the large differences in pK_a values, thiol-disulfide exchange should be much slower than selenol/selenosulfide exchange at physiological pH,[133] thus explaining the difference of uptake efficiency of cyclic disulfides as compared to cyclic diselenides. Although the high ring tension in AspA **54** and ETP **61**[111] can account for their reactivity in the first walking step (the ring opening reaction), further steps depend solely on the rate of these exchanges. In addition to ring tension, the lower pK_a of the thiol produced by ring opening of ETP (pK_a < 7 as compared to ~ 8 in AspA) could account for ETP's higher cellular uptake *via* a similar molecular walker mechanism.[111,150]

3.1.4. Conclusions

In this section, experimental evidence for the ring opening of 1,2-dithiolanes and diselenolanes were provided. This ring opening was showed to happen for both species, preferentially on the secondary chalcogen atom, followed by a fast intramolecular rearrangement by thiolate migration. These observations on dithiolanes allowed the assignment of the structure of poly(disulfide)s as being regio-irregular polymers, and clarified the regioselectivity of the nucleophilic attack, relevant for instance in acetyl-CoA biosynthesis.

Similar results were observed for 1,2-diselenolanes, resulting in a hypothetical molecular walker mechanism to explain the exceptional cellular uptake ability of such compounds. In addition, the trapping of ring-open selenosulfide/selenolate species **114a**/**b** provided proof that diselenolanes like **96** should be polymerizable, a nice perspective considering the high activity and growing interest in cell-penetrating poly(disulfide)s.

The results presented from this first project represent a first step in our quest to better understand the mechanisms by which thiol-mediated uptake operates. Although hypothetical, the walker mechanism is in accordance with the observation that more dynamic systems such as diselenolanes or benzopolysulfanes lead to better cellular uptake. A gallery of potential targets starts to appear, with structural aspects like thiol- and disulfide-rich regions, and playing a role in the cellular uptake of other systems like viruses and modified oligonucleotide. As will be shown in the following sections, this appears not to be a coincidence.

3.2. Templated Cascade Oligomerization of Cyclic Dichalcogenides on a 3_{10}-Helix Template

3.2.1. Design: A 3_{10}-Helix Template for 3D Template-Directed Ring-Opening Oligomerization

3.2.1.1. Covalent Template-Directed Synthesis of Linear Oligomers

Apart from the polymerization of dithiolanes (see section 1.3.3.2), throughout literature, virtually all polymerization processes have been adapted on a template.[151,152] The monomers are usually loaded on a template of choice by non-covalent interactions, often H-bonding.[153] While the templates are usually oligomers similar to the ones formed by the polymerization reaction, they can also be structurally different. Vesicle-templated polymerization has for example been largely exploited over the past decades.[154] A very efficient way to perform templated polymerization is the use of Watson-Crick-Franklin base pairing to mimic what is done by nature.

Oligomers and polymers are the basis of the storage of genetic information, with nucleic acids encoding the information and the cell machinery translating it into polymers of amino acids with defined sequences. To ensure the fidelity of the information storage, nature uses template-directed synthesis to facilitate the precise polymerization process.[155] Fully synthetic processes have been reported, mimicking DNA replication using mostly non-natural backbone modifications, but still based on the nucleic acid language and H-bonding to transfer sequence information.[156]

Recently, Hunter *et al.* have introduced a method based on covalent template-directed synthesis capable of transferring information from one oligomer to a "daughter" strand.[157] Using ester linkers, the monomers can be covalently loaded on the template, reacted together *via* "click" chemistry and detached, thus avoiding the limitations of non-covalent templates: incomplete monomer

binding, intramolecular folding of the template and product inhibition. With minor modifications, this system enabled quantitative yields of the copy strands,[158,159] exact strand replication[160] and controlled mutations.[161]

For the cascade ring-opening polymerization of cyclic disulfides, covalent template-directed oligomerization is appealing because of the reversibility of the polymerization reactions. In Hunter's system, the monomers are reacted together *via* irreversible CuAAC, which drives the reaction to completion. With reversible disulfide exchange, a high preorganization is needed that a non-covalent template would not achieve.

3.2.1.2. Peptide Foldamers for Template-Directed Cascade Ring Opening

In nature, proteins and peptides adopt a wide range of three-dimensional conformations depending on their sequence, based on non-covalent interactions such as H-bonding interactions and hydrophobicity effects. Decades of studies have made it clear that these 3D conformations regulate most biological processes involving proteins. α-helices and β-sheets are the most common secondary structures found in proteins, followed by β- and γ-turns. Inspired by such folding, chemists have developed over the past few decades smaller mimics of these, called "foldamers", a term coined by Samuel H. Gellman.[162] From the twenty natural amino acids, or from unnatural oligoureas,[163] azapeptides,[164] or β-, γ-[165] and δ- peptides,[166] as well as aromatic polyamides,[167] countless examples have been reported, covering an extremely wide space of conformations. Applications range from pure structural studies[168] to molecular recognition,[169] cellular uptake,[52] gene transfection,[50] antibacterial activity,[170] signal transduction,[171] and many others.

Among all peptide foldamers in literature, helical ones are arguably the most widely studied. Enforcing constrained helical structures by stapling short peptides is a well-established strategy[172] to screen for peptide binders of challenging targets, for example.[173] For cell-penetrating peptides, amphiphilic

helices with a precise presentation of polar and apolar groups along different faces were showed to balance well toxicity and cell-penetrating abilities (see section 1.2.2).[174] Among the different possible helical structures, α-helices, with their connectivity between the *i* and *i*+4 amino acids and the 3.6 residue per turn, do not have the most aligned faces possible. On the contrary, 3_{10}-helices are made from a H-bonding between the *i* and *i*+3 residues, and possess 3 well-aligned faces (see Figure 36).

This regular structure has been taken advantage of to align precisely some motives along one axis with a precise distance between them, one turn of the helix being ~ 6 Å. Aligning naphthalene units along a 3_{10}-helix, Kimura *et al.* obtained a structure capable of generating a photocurrent upon light irradiation.[175] 3_{10}-helices were widely studied by Clayden, Webb *et al.* as regard to their helicity[176] and its inversion,[168] and their use in molecular recognition.[177] For example, a tetramer of aminoisobutyric acid (Aib, helix promoter) equipped with a boronic acid on its N-terminus could change helicity from a 1:1 *M*/*P* ratio to a chiral purely *M* or purely *P* helix, as sensed on the C-terminus.[178] Longer, membrane-spanning foldamers were later used by the same groups to perform signal transduction through a lipid bilayer using photoswitchable chiral inducers.[171] Starting from $(Aib)_8$, such peptide foldamers were also shown to span through a lipid bilayer, dimerizing to form transmembrane pores.[179]

Although α-helices have been widely used in literature to induce proximity between coupling partners and perform reactions,[180] 3_{10}-helices are less popular, probably because of their more challenging synthesis as compared to the ease of production of α-helices from natural amino acids by solid-phase peptide synthesis (SPPS).

3.2.1.3. 3_{10}-Helix Template for 3D Template-Directed Ring-Opening Oligomerization

For this project, we aimed at creating a versatile platform for the template-directed ring-opening oligomerization of cyclic dichalcogenides. As stated above, because of the reversibility of the ring-opening reactions, we sought to have the best preorganization possible on the template. 3_{10}-helices were therefore selected as the template of choice to enforce the alignment of the monomers along a defined axis (Figure 36, A-C). Such almost perfect alignment should favor the formation of longer oligomers as compared to monomers and short oligomers.

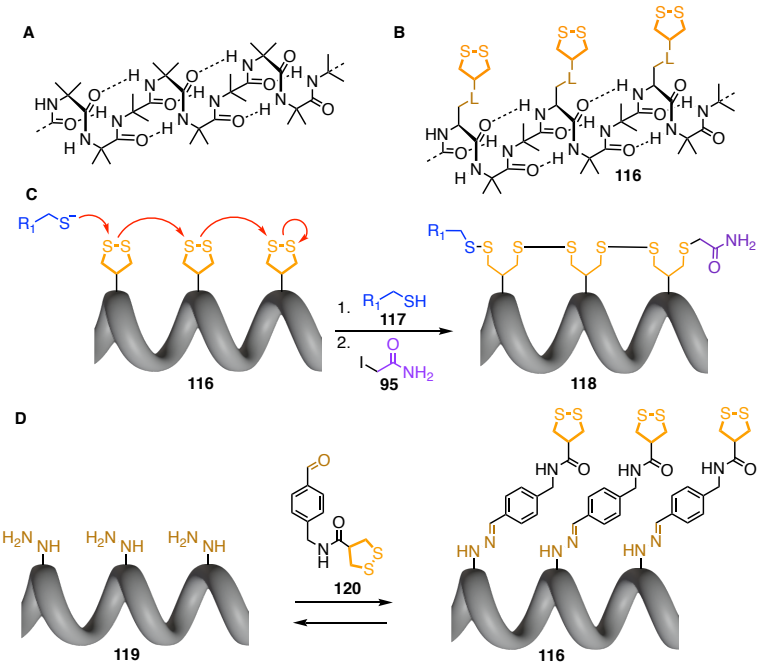

Figure 36. A) Structure of a pure 3_{10}-helix from Aib repeats. B) Replacing 1 out of 3 Aib with functionalized amino acids, COCs are aligned along one face of the helix, attached through a linker L. C) Schematic representation of the cascade ring-opening oligomerization along a 3_{10}-helix template. D) Hydrazine-hydrazone dynamic covalent chemistry used to attach and detach the monomers.

Ideally, the two COCs on the outer parts should be more accessible to the thiol initiator because of the steric bulk in the middle of the helix. However, should the initiator react on the middle COCs, the reactions being reversible, an error correction mechanism should take place, eventually yielding only the most thermodynamically stable desired oligomer, where all the cyclic dichalcogenides have been opened.

To attach the monomers to the template, the linker chemistry should be stable upon thiol-disulfide exchange, while keeping it possible to detach the oligomer after the reaction. Following Hunter's example, esters could be used, but might lack stability in slightly basic aqueous conditions needed for thiol-disulfide exchange. Instead, our choice laid on hydrazine-hydrazone dynamic covalent chemistry (DCC), which is orthogonal to disulfide exchange and fully reversible (Figure 36, D).[137]

With these orthogonal dynamic covalent chemistries, a molecular factory can be built (Figure 37). The loading of the COC-bearing aldehyde **120** on the peptide template carrying a hydrazine moiety **119** can be performed at acidic pH, catalyzed by an amine buffer catalyst if need be.[181] Increasing the pH from 5 to 8 should lock the hydrazone bond in **116** while making thiol-disulfide exchanges possible, to perform the cascade ring-opening oligomerization on the template, giving **118**. Decreasing again the pH to reactivate the hydrazine-hydrazone dynamic covalent chemistry, the oligomer can be detached by the formation of the more thermodynamically stable oxime in **122**.[182,183] The inspiration for this system came for Leigh *et al*. small molecule molecular walker which operate with the same dynamic covalent chemistries.[137]

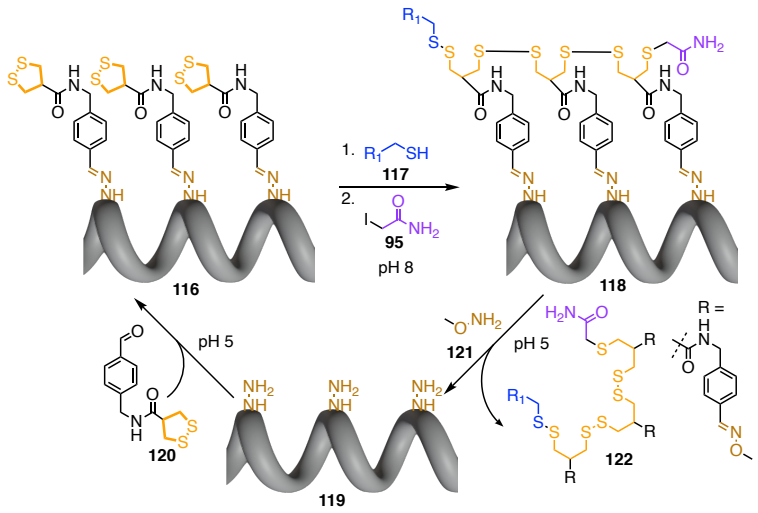

Figure 37. Schematic representation of a molecular factory to build oligo(disulfide)s on a 3_{10}-helix template.

3.2.2. Synthesis of the Peptide Templates

To synthesize the desired peptides, solution-phase peptide synthesis was used, starting from Dap-Aib-Aib tripeptides. Diaminopropionic acid (Dap) is used to introduce an amine group to be functionalized, while maintaining as short as possible distance from the peptide backbone for better templation. Whereas solid-phase peptide synthesis (SPPS) is used extensively to synthesize peptides derived of the 20 natural amino acids, couplings of several Aib residues gives low yields in classical SPPS because of the steric bulk of the *gem*-dimethyl group in the α carbons. Clayden *et al.* recently developed a microwave-assisted automated SPPS allowing the coupling of up to 14 consecutive Aib residues,[184] but the equipment necessary to perform such reactions was unavailable in our lab. Instead, a method developed by Demizu *et al.* was used, assembling tripeptide fragment together through an Aib residue, to prevent epimerization during fragment couplings.[185] This allows the use of relatively mild conditions,

whereas harsh reaction conditions are needed to assemble fragments through two Aib residues.[179]

3.2.2.1. Synthesis of the Peptide Backbones

The tripeptide building blocks were first synthesized, using classical solution-phase peptide synthesis and deprotection conditions (Scheme 2).

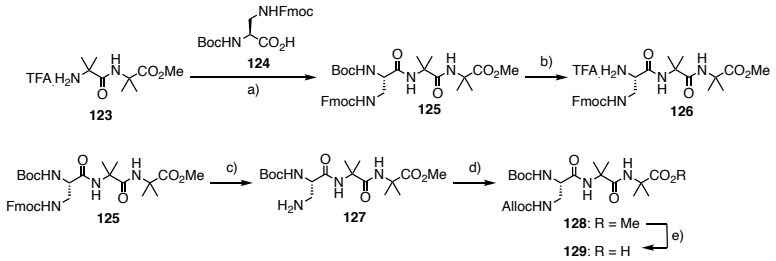

Scheme 2. Synthesis of the tripeptide building blocks. a) **124**, HBTU, DIPEA, DMF, rt, 1 h, 79%; b) CH_2Cl_2/TFA (1:1), rt, 30 min, quant.; c) Me_2NH, THF, rt, 20 min, 96%; d) AllocCl, Et_3N, H_2O/1,4-dioxane, rt, 1 h, 93%; e) 1 M LiOH, MeOH, rt, 1 h, 89%.

The deprotected Aib dimer **123** was synthesized following a reported procedure, before being coupled with orthogonally protected Dap derivative **124**. Tripeptide **125** served as the basis for further derivatization and was synthesized on the multigram scale. The Boc group was removed in acidic conditions to give **126** for further peptide couplings (see below). Alternatively, the Fmoc group was cleaved by treatment with a dimethylamine solution in THF, to exchange it for an Alloc protecting group in **128**, stable in both acidic and basic conditions, and selectively deprotected by palladium(0) catalysis. The methyl ester in **128** could be saponified to afford **129**, tripeptide deprotected on the C-terminus that can then be coupled with N-terminus deprotected peptides.

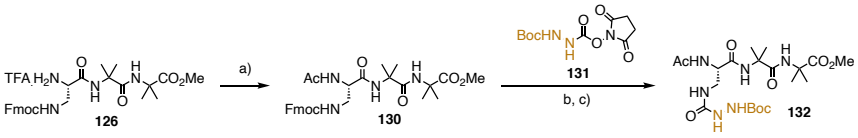

Scheme 3. Synthesis of semicarbazide-containing model tripeptide. a) Ac_2O, DIPEA, DMF, rt, 1 h, 94%; b) Me_2NH, THF, rt, 20 min; c) **131**, DIPEA, DMF, rt, 1 h, 54% (2 steps).

Before assembling the different tripeptides together, **126** was further derivatized on the tripeptide level to synthesize model compound **132** (Scheme 3). The N-terminus of the tripeptide was first acetylated to yield **130**, before a Fmoc deprotection followed by semicarbazide formation with the Boc-protected, NHS-activated carbazate **131**. Tripeptide **132** can then serve as a model compounds to optimize deprotection, semicarbazone formation and ring opening on the monomer level.

Because the C-terminus residue in **129** is achiral, no epimerization can take place during saponification or further peptide coupling, despite the formation of oxazolone **133**, confirmed by LCMS (Scheme 4).

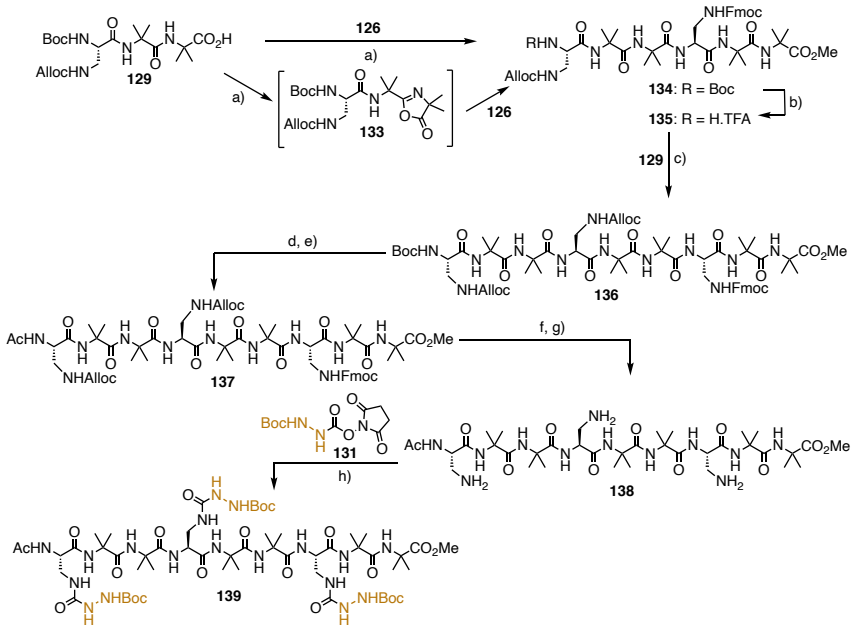

Scheme 4. Synthesis of nonapeptides. a) HBTU, DIPEA, DMF, then **126**, rt, 2 h, 77%; b) CH_2Cl_2/TFA (1:1), rt, 30 min, quant.; c) **129**, HBTU, DIPEA, DMF, rt, 72 h, 59%; d) CH_2Cl_2/TFA (1:1), rt, 30 min, quant.; e) Ac_2O, DIPEA, DMF, rt, 1 h, 82%; f) $Pd(PPh_3)_4$, $PhSiH_3$, CH_2Cl_2, rt, 2 h; g) Me_2NH, THF, rt, 20 min, 62% (2 steps); h) **131**, DIPEA, DMF, rt, 1 h, 43%.

The nonapeptides were synthesized by iterations of coupling-deprotection-coupling steps. Hexapeptide **134** was first obtained from **129** and **126**, before being deprotected and coupled again with **129** to afford **136**. A series of protecting group exchange gave the N-terminus acetylated nonapeptide **137**, which was then deprotected to free the Dap amines in **138**. Finally, a 5-fold excess of the activated carbazate **131** reacted on these amines to yield the desired functionalized peptide **139**. Upon acidic deprotection of the Boc-protected semicarbazides in **139**, degradation was observed when trying to isolate the product, which was therefore only deprotected and used *in situ* for further derivatization.

With two Aib residues in between two Dap, the semicarbazides in **139** were placed to be well aligned on the 3_{10}-helix template (Figure 36, B). To prove that the alignment on the three-dimensional template is responsible for the proper oligomerization of the cyclic disulfides, we sought to synthesize the shifted template **152**, where one Dap residue has been shifted by one position. First, dipeptide and tetrapeptide building blocks were synthesized using the same strategy described in Scheme 2 (Scheme 5).

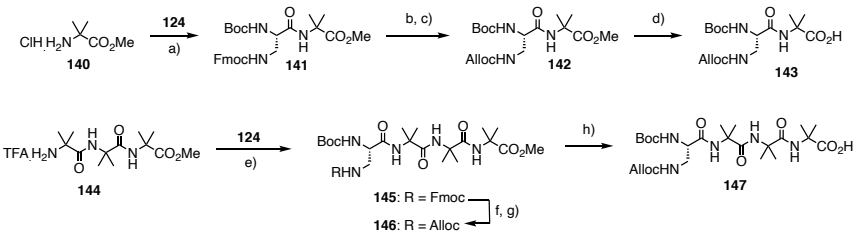

Scheme 5. Synthesis of dipeptide and tetrapeptide building blocks. a) **124**, HBTU, DIPEA, DMF, rt, 1 h, 95%; b) Me_2NH, THF, rt, 20 min; c) AllocCl, Et_3N, H_2O/1,4-dioxane, rt, 1 h, 69% (2 steps); d) 1 M LiOH, MeOH/THF, rt, 1 h, 95%; e) **124**, HATU, DIPEA, DMF, rt, 1 h, 84%; f) Me_2NH, THF, rt, 20 min; g) AllocCl, Et_3N, H_2O/1,4-dioxane, rt, 1 h, 71% (2 steps); h) 1 M LiOH, MeOH, rt, 1 h, 98%.

The dipeptide, tripeptide and tetrapeptide fragments were then assembled together in a similar fashion as in Scheme 4 to afford the shifted nonapeptide **152**. First, dipeptide **143** and tripeptide **126** were assembled to make pentapeptide **148** where the two Dap residues are separated only by one Aib. Then tetrapeptide **147** was then coupled to afford the nonapeptide **149**. After protecting group exchange and final coupling, semicarbazide-functionalized **152** is obtained (Scheme 6).

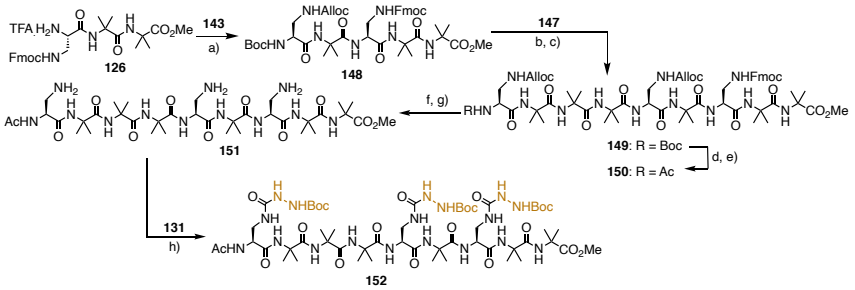

Scheme 6. Synthesis of shifted nonapeptide. a) **143**, HATU, DIPEA, DMF, rt, 1 h, 65%; b) CH_2Cl_2/TFA (1:1), rt, 30 min, quant.; c) **147**, HATU, DIPEA, DMF, rt, 16 h, 54%; d) CH_2Cl_2/TFA (1:1), rt, 30 min, quant.; e) Ac_2O, DIPEA, DMF, rt, 1 h, 97%; f) $Pd(PPh_3)_4$, $PhSiH_3$, CH_2Cl_2, rt, 2 h; g) Me_2NH, THF, rt, 20 min, 71% (2 steps); h) **131**, DIPEA, DMF, rt, 1 h, 54%.

The helical structure of the nonapeptides was assessed by circular dichroism (CD). In trifluoroethanol (TFE), the CD spectra of the peptides shorter than nine amino acids showed no significant features apart from these of a random coil peptide (Figure 38). On the contrary, all nonapeptide intermediates and, more importantly, final compounds **139** and **152** showed a positive Cotton effect around 195 nm, and a double negative Cotton effect at 208 and 220 nm, characteristic of a helical structure. In an α-helix, the two negative peaks have the same intensity, whereas a 3_{10}-helix shows a deeper signal at 208 nm, which is what is observed in the case of our peptides, confirming the predominant 3_{10}-helix structure. In the NMR spectra of the peptides, the chemical shifts of the Dap residues are characteristic of a helical structure: one of α protons is deshielded and shifted downfield, whereas the corresponding carbon is shifted upfield (see the experimental section, e.g. NMR of **138**).

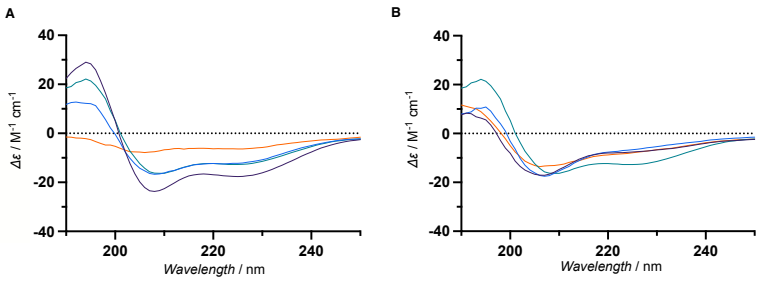

Figure 38. CD spectra of the intermediates to access nonapeptides measured at 200 µM in TFE. A) CD spectrum of **134** (orange), **136** (blue), **137** (green) and **139** (purple). B) CD spectrum of **148** (orange), **149** (blue), **150** (green) and **151** (purple).

3.2.2.2. Synthesis of COC-Containing Aldehydes

With the peptide backbones synthesized, COC-containing aldehydes then had to be made (Scheme 7), to then be attached on the semicarbazide in **132**, **139** and **152** to yield the final semicarbazone products.

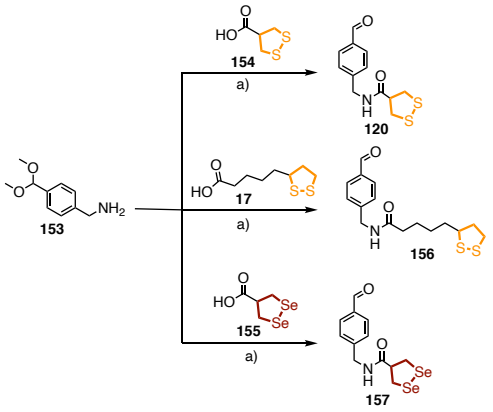

Scheme 7. Synthesis of COC-containing aldehydes. a) HATU, DIPEA, DMF, rt, 1 h, then H_3O^+, 96% (**120**); 99% (**156**); 55% (**157**).

Starting from the acetal-protected amino aldehyde **153**, HATU peptide coupling conditions followed by an acidic workup hydrolyzing the acetal back to aldehyde afforded three aldehydes containing AspA, LipA and diseleno-AspA **120**, **156** and **157**, respectively.

3.2.2.3. Formation of Semicarbazones

All building blocks for the formation of the final semicarbazone products being ready, this reaction was then optimized. As mentioned above, the deprotected semicarbazides were found to be unstable upon attempted purification, and were therefore deprotected using 4 M HCl in 1,4-dioxane. After reaction completion, the solvent was removed and the crude deprotected products were used *in situ* (Scheme 8).

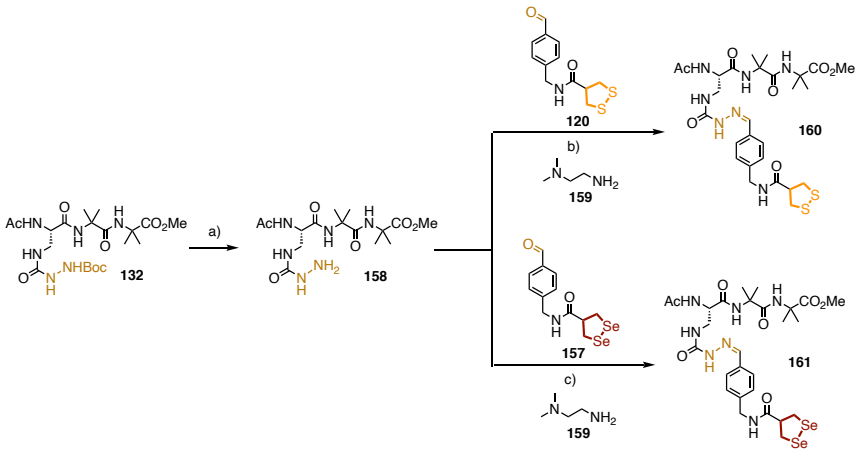

Scheme 8. Synthesis of model semicarbazone tripeptides. a) 4 M HCl, 1,4-dioxane, rt, 1 h, 88%; b) **120**, 50 mM **159**, 150 mM NaCl, rt, 1 h, 79%; c) **157**, 50 mM **159**, 150 mM NaCl, rt, 1 h, 75%.

Although hydrazones and related compounds can form in water at slightly acidic pH, the reaction is often slow. Extensive work has been done by Dawson,[186] Kool[181] and others to develop catalysts to speed up this process. The use of amine buffer-catalyst (ABC), described by Kool *et al.*, is one of the

latest developments in this field. The best amine buffer/catalyst described, *unsym*-dimethylethylenediamine **159**, at 50 mM with 150 mM NaCl, was therefore used as the buffer to perform the semicarbazone formation (Scheme 8).[181] Using stoichiometric amounts of aldehydes **120** and **157**, full conversion was observed in one hour at room temperature, with minimal side-products observed by LCMS (Figure 39, A). Model tripeptides **160** and **161** could therefore be used *in situ*, but were nonetheless purified and characterized.

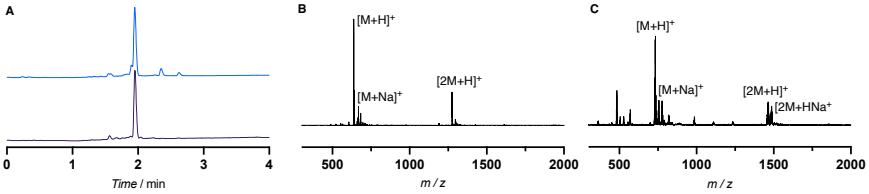

Figure 39. A) HPLC trace of the reaction mixtures between **158** and **120** (purple) or **157** (blue). B) ESI-MS spectrum of **160**. C) ESI-MS spectrum of **161**.

The same procedure was then applied to nonapeptide **139**: after acidic deprotection of the three Boc protecting groups, it was submitted to the semicarbazone formation conditions with aldehydes **120**, **156** and **157** to afford the final products **116**, **162** and **163** (Scheme 9, A). Because three semicarbazones have to be formed, full conversion was not reached as clean as on the tripeptide, and an excess of aldehyde had to be added (5 equiv. instead of 3). Nonetheless, the three desired products could be obtained in good yields, their helical structure being confirmed again by circular dichroism (see experimental section). The shifted nonapeptide **152** was also submitted to the same reaction conditions, first Boc-deprotected, then coupled with AspA-bearing aldehyde **120**. This compound being synthesized as a control to assess the efficiency of the three-dimensional preorganization of the template, it was not coupled with the other two COC-bearing aldehydes **156** and **157**.

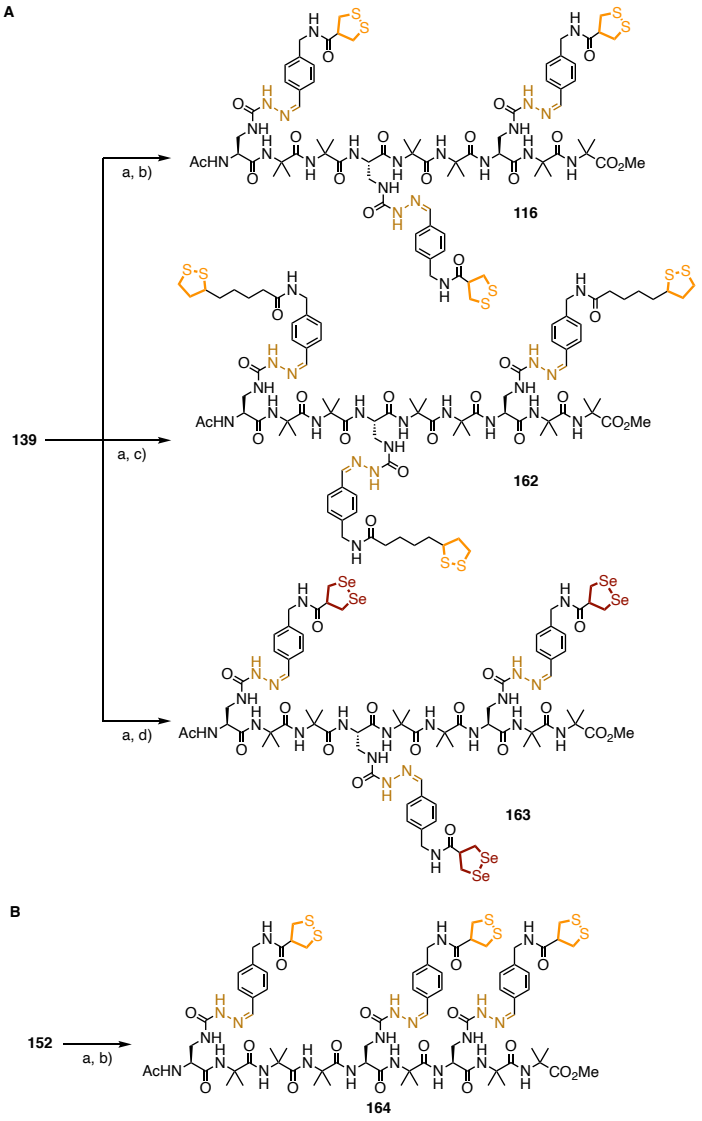

Scheme 9. A) Synthesis of aligned nonapeptide tris-semicarbazones bearing the COCs. a) 4 M HCl, 1,4-dioxane, rt, 1 h, quant.; b) **120**, 50 mM **159**, 150 mM NaCl, rt, 16 h, 62%; c) **156**, 50 mM **159**, 150 mM NaCl, rt, 1 h, 75%, d) **157**, 50 mM **159**, 150 mM NaCl, rt, 1 h, 53%. B) Synthesis of shifted nonapeptide tris-semicarbazone **164** bearing the COC. a) 4 M HCl, 1,4-dioxane, rt, 1 h, quant.; b) **120**, 50 mM **159**, 150 mM NaCl, rt, 16 h, 72%.

With two tripeptides and four different nonapeptides synthesized, isolated and characterized, the ring-opening reaction then had to be performed. It was first optimized on the monomer level, either with tripeptides **160** and **161** or with smaller derivatives of **120**.

3.2.3. Optimization of the Ring Opening on the Monomer Level

3.2.3.1. Optimization of the Reaction with Thiolates

The ring opening reaction was first studied on the monomer level with tripeptides **160** and **161**, starting with primary thiols to mimic the results described in section 3.1. To prevent troubles arising from the lower acidity of thiols in organic solvents, we moved from dichloromethane to aqueous solutions.

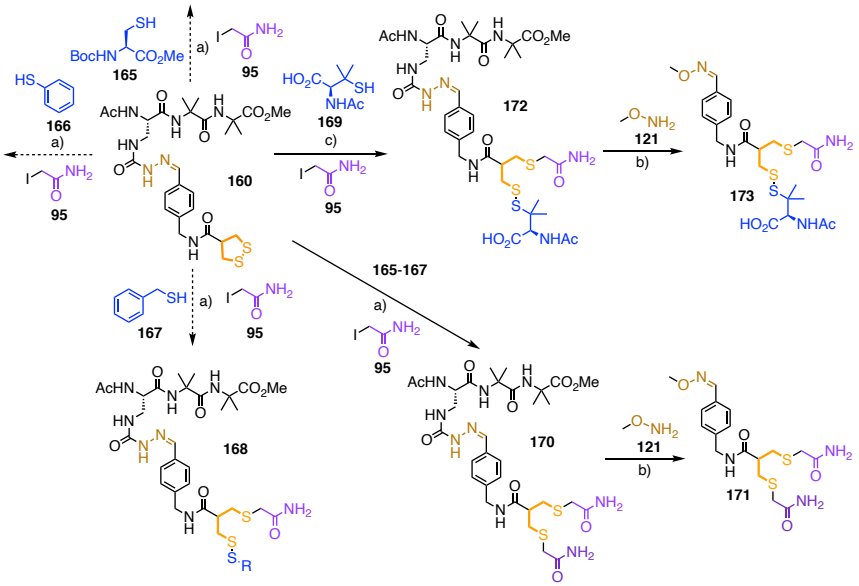

Scheme 10. Ring opening of monomer **160** with primary and tertiary thiols. a) 10 mM **160**, 50 – 500 mM **165-167**, 10 mM Tris pH 8.7, rt, 1 h then addition of **95**; b) 100 mM **121**, 50 mM **159**, 150 mM NaCl, pH 5.0, rt, 16 h; c) 100 µM **160**, 2 mM **169**, 10 mM Tris pH 9.0, rt, 30 min then addition of **95**.

First, **160** was reacted with several primary thiols to test its reactivity. 10 mM of **160** was reacted with various amounts of protected cysteine **165**, thiophenol **166** and benzylmercaptan **167** (Scheme 10). The results are summarized in Table 3.

Table 3. Outcome of the ring opening reaction in buffer with primary thiols.

Thiol	Equiv.	Temperature	Outcome
165	5	rt	No conversion
165	50	rt	Reduction to dithiol
165	5	40 °C	Low conversion
166	10	rt	No conversion
167	10	rt	Reduction to dithiol
169	20	rt	Good conversion

With thiophenol **166**, no reaction was observed, probably because the reverse ring-closing reaction is favored by the good leaving group ability of **166**.[78] With **165** and **167**, a high number of equivalents was needed to push the otherwise low conversion. Under these conditions, the ring open products **168** were observed only in very low amounts, and the quenched reduced dithiol **170**, and then **171** after oxime formation, were obtained. This can be explained by the fact that, with high number of equivalents, the open mixed disulfide is rapidly attacked by another thiol, forming the initiator's disulfide and the reduced dithiol of AspA.

With the tertiary thiol in N-acetyl-penicillamine **169**, this secondary reaction is unfavored, because it would form a highly hindered hexa-substituted disulfide. The use of this thiol allowed a decrease of the concentration of **160** to 100 µM, which reacted with **169** to give good conversion toward the ring-open product **172**, without traces of the dithiol side-product. Higher number of equivalents, up to 10 equivalents of **169,** were optimal under these conditions to get the ring open product in ~ 50% conversion.

Applying the same reaction conditions to 1,2-diselenolane tripeptide **161**, the selenolate produced by the ring opening was not stable enough under aerobic conditions to be trapped as the selenide in **174**. Instead, after ring opening, the produced selenolate is rapidly oxidized together with a second equivalent of initiator **169** to yield the double selenosulfide **175** (Scheme 11).

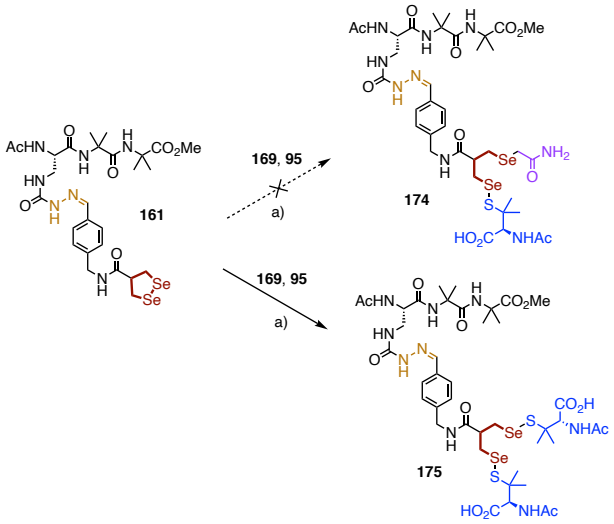

Scheme 11. Ring opening of 1,2-diselenolane with tertiary thiol. a) 100 µM **161**, 200 µM – 2 mM **169**, 10 mM Tris pH 9.0, rt, 1 to 30 min then addition of **95**.

The same results were obtained under inert atmosphere with degassed buffer, and with short reaction times before addition of iodoacetamide. This observation is consistent with the reduction potential of selenols in water reported in literature, which are much higher than that of the corresponding thiol.[187]

3.2.3.2. Absence of Oligomerization on the Monomer Level

To test for the possible uncontrolled polymerization of AspA monomers under these conditions, tripeptide **160** was not the best model compounds, the AspA units being hindered by the peptide backbone. Instead, the aldehyde **120** was converted to the oxime **176** with methoxylamine **121** prior to the ring

opening (Scheme 12). Then, using a fixed 2 mM concentration of the thiol initiator **169**, the concentration of **176** was increased up to its solubility limit in a 1 to 1 mixture of buffer and trifluoroethanol at pH 9 (Scheme 12).

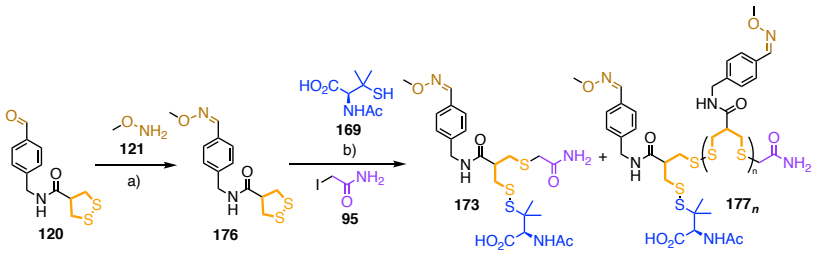

Scheme 12. Synthesis of oxime and screening of monomer concentration. a) **121**, 50 mM **159**, 150 mM NaCl, pH 5.0, rt, 30 min; b) 100 µM – 30 mM **176**, 2 mM **169**, 10 mM Tris pH 9.0, rt, 30 min, then addition of **95**.

Up to 30 mM, no oligomers **177** were observed: only starting material **176** and ring-open product **173** were present in solution (Figure 40). This absence of oligomers was desirable, as it shows that non-templated polymerization does not occur. If oligomers are obtained by reaction on the template, this will give an estimation of the effective molarity of the AspA monomers on the template being higher than 30 mM and of the efficiency of our approach.[158]

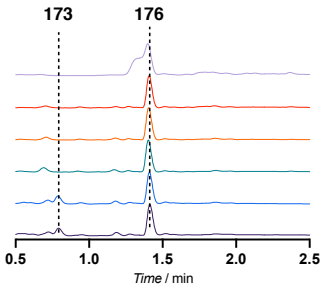

Figure 40. Normalized HPLC chromatograms of the reaction mixture of 2 mM **169** with 100 µM, 300 µM, 1 mM, 3 mM, 10 mM and 30 mM **176** (bottom to top) in 1:1 Tris buffer/TFE at pH 9.0.

3.2.4. Templated Cascade Ring-Opening Oligomerization of Cyclic Disulfides

3.2.4.1. Reaction with Primary Thiolates: Reduction of the COC

Despite the observation that the ring opening of AspA monomer was unfavored with primary thiolates, resulting rather in the full reduction of AspA to its dithiol counterpart, the same might not be true for the nonapeptide template **116**, and the presence of the template could affect the outcome of the reaction (Scheme 13).

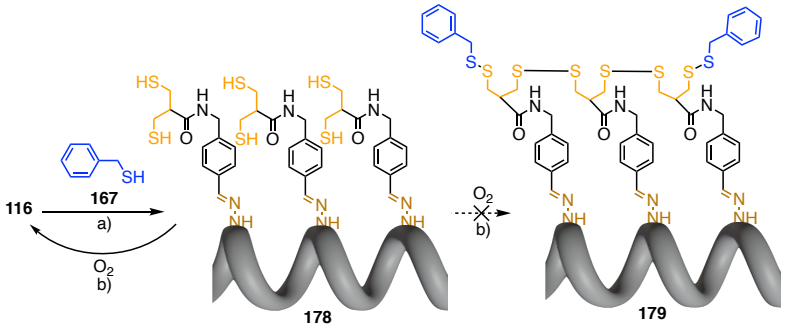

Scheme 13. Reaction of template **116** with benzyl mercaptan **167**. a) 100 µM **116**, 1 – 10 mM **167**, 10 mM Tris pH 9.0, 2 h, rt; b) Air, 10 mM Tris pH 9.0, 24 h, rt.

Unsurprisingly, under these conditions, the three AspA units of **116** were reduced to the dithiol, giving the fully reduced peptide **178**. Upon oxidation overnight with air, **178** was converted back to the starting material **116** instead of the ring-open oligomer **179**. This can be explained by the amounts of thiol **167** in solution being too low to form the mixed disulfides in **179**, thus favoring the ring-closing oxidation of the dithiols back to the cyclic AspA, despite the ring tension.

The same results were observed with the LipA-containing nonapeptide **162**, the only difference being a lower conversion as compared to AspA, as expected from the difference of ring tension in these two compounds.

With DSL-containing template **163**, no conversion was observed under these conditions, with the initiator **167** rapidly being oxidized to its disulfide, as was observed previously for 1,2-diselenolanes.[112]

Considering the promising results obtained with tertiary thiols on the monomer level, such initiators were then used to promote the cascade ring-opening oligomerization and avoid full reduction of the disulfides.

3.2.4.2. Cascade Ring Opening with Tertiary Thiolates

Applying the optimized conditions developed in section 3.2.3.1 to the nonapeptide **116**, the ring opening did take place (Scheme 14). Several isomers of mono-addition product **118** and double-addition product **180** were observed, with mostly mono-addition with low number of equivalents of the initiator **169** (Figure 41).

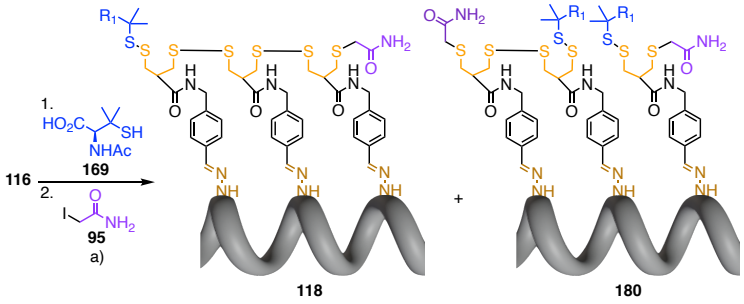

Scheme 14. Cascade ring-opening oligomerization on nonapeptide **116**. a) 100 µM **116**, 1 – 5 mM **169**, 10 mM Tris, 1 mM EDTA, 1:1 TFE/H_2O, pH 9, rt, 30 min, then addition of **95**.

When looking at the product distribution with different numbers of equivalents of **169**, about 70% conversion could be obtained using twenty

equivalents. The different products observed could be assigned using LCMS (Figure 41). Four peaks corresponding to the molecular mass of **118** were found, as well as some peaks for double-addition product **180**. This was expected as up to 9 constitutional isomers can be obtained for the mono-addition of **169** onto the AspA trimer **116** (Figure 80). In addition, a chiral center is created in α position to the amide upon ring opening, multiplying the number of possible isomers. However, because these isomers all have very similar structures, they cannot be distinguished one from another in the HPLC traces. Under the same conditions, LipA-containing peptide **162** was found to be unreactive, because of the lower ring tension as compared to AspA.

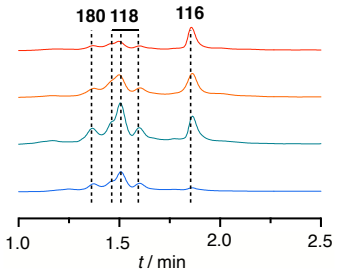

Figure 41. HPLC chromatograms of the reaction mixtures of **116** with 50 (red), 25 (orange), and 20 (green) equiv. of **169** in buffer without or with (blue) 80% of trifluoroethanol (TFE, see below).

To facilitate the identification of the different products observed, the reaction mixture was diluted with Kool's ABC buffer to reactivate the semicarbazone exchange and detach the formed oligomers from the peptide template (Scheme 15). Although they are dynamic under these conditions, the semicarbazones would not dissociate without a driving force. To drive the detachment, a strategy developed by Ulrich *et al.* was used: using a 1000-fold excess of methoxylamine **121**, the semicarbazones exchanged to the oxime, thus releasing the tris-semicarbazide template **119** and the oximes of monomer **173**, oligomers **181**-**182**, as well as the one of the unreacted AspA units **176**.[183]

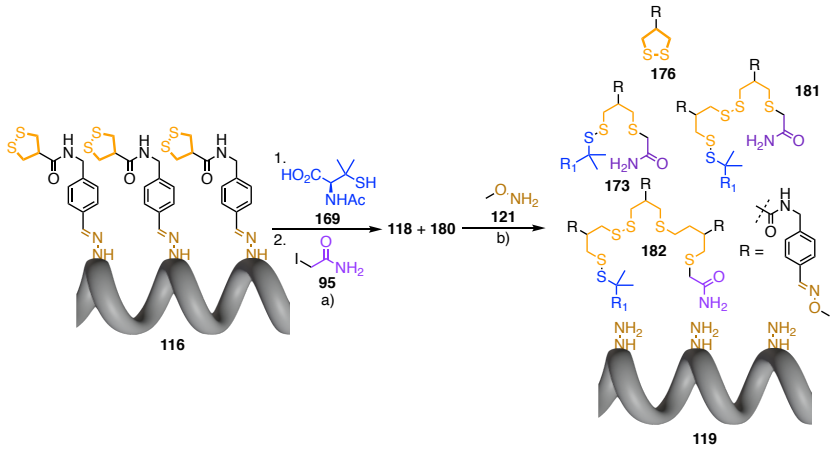

Scheme 15. Detachment from the template by oxime formation. a) 100 µM **116**, 1 – 5 mM **169**, 10 mM Tris, 1 mM EDTA, 1:1 TFE/H_2O, pH 9.0, rt, 30 min, then addition of **95**; b) 20 µM **118**/**180**, 100 mM **121**, 50 mM **159**, 150 mM NaCl, pH 5.0, rt, 16 h.

Upon this detachment, the product distribution observed was simplified and only four products were observed: the ring-open monomer **173**, dimer **181** and trimer **182** and the unreacted AspA **176** (Figure 42). Maximum conversion of the AspA units was observed using 20 equivalents of initiator **169**, and this ratio was used in all the subsequent optimizations.

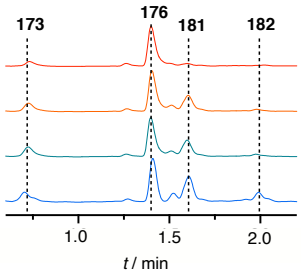

Figure 42. HPLC chromatograms of the reaction mixtures of **116** with with 50 (red), 25 (orange), and 20 (green) equiv. of **169** in buffer without or with (blue) 80% of trifluoroethanol (TFE, see below) after detachment from the peptide template.

Under these conditions, the main product observed was the AspA dimer **181**, with some monomer **173** and trimer **182**. To quantify the efficiency of the templation, the "templation factor" was introduced. It is defined as the ratio of the percentages of templated products (dimer **181** and trimer **182**) and of non-templated monomer **173**: $T_f = \log[(\eta_{181}+\eta_{182})/\eta_{173}]$. Central addition as in **180** limits templation to $\eta_{177}^{max} = 66\%$ but still gives maximum templation with this definition of T_f. Minimal acceptable templation was limited arbitrarily to $\eta_{181} + \eta_{182} = 20\%$ yield of templated products, that is $T_f^{min} = -0.60$. The effective templation was thus defined as $T_{eff} = T_f - T_f^{min}$. Based on the integration of the HPLC chromatograms in Figure 42, the distributions reported in Figure 43, A were obtained for the screening of the number of equivalents. As can be expected, with lower number of equivalents, the templation was better: the double-addition product **180**, that can only lead to monomer **173** and dimer **181**, is disfavored. However, this better templation took place at the expense of conversion, with only 35% of the AspA units being open. The efficiency of ring opening was defined as RO = 100% - η_{176}, where η_{176} is the yield of ring-closed monomer **176**.

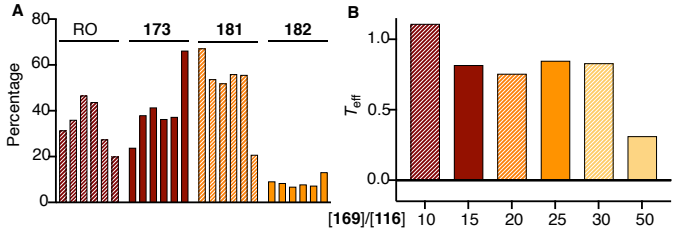

Figure 43. A) Percentage of conversion and product distribution extracted from HPLC chromatograms. Left to right: 10, 15, 20, 25, 30 and 50 equiv. **169**. B) Effective templation under the different reaction conditions.

The presence of templated products in the reaction mixture is promising and shows that the approach to template the cascade ring-opening oligomerization of

cyclic disulfides works. Further optimizations of the reaction parameters have then been performed, to try and push for the formation of the desired trimer **182**.

3.2.4.3. Optimization of the Reaction Parameters

First, the reaction time allowed for the system to equilibrate after addition of the thiol was investigated. The equilibrium was in any case reached rapidly, and the reaction time did not have any influence on the product distribution after quenching. This is in accordance to the results in organic solvents reported in section 3.1.2, where half-times for thiolate migrations of the ring-open products were in the ms range at room temperature.

Changing the pH of the reaction mixture in a range from 8.7 to 11.0 improved ring opening up to RO = 65% at pH 10.0, without significant impact on the templation (Figure 44). However, at pH > 9, degradation products started to be observed, and the pH was kept at 9.0 for the following experiments.

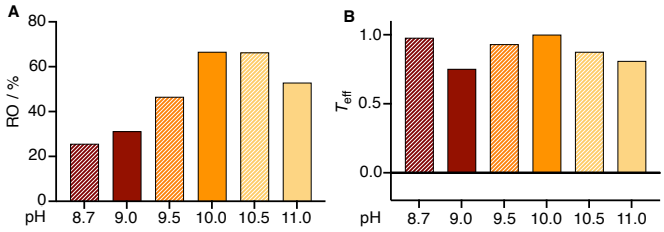

Figure 44. A) Percentage of conversion RO of AspA units to ring-open products at different pH. B) Effective templation at different pH.

One of the factors which had the most influence on the outcome of the reaction was the percentage of TFE used as solvent (Figure 45). Because of its large dipolar moment, TFE is well-known to stabilize helical structures, which possess a large macrodipole.[188] Going from a buffer containing 1 M of urea, used to disrupt intramolecular H-bonding and break the helix, to one containing up to 80% of TFE, the conversion remained around RO = 55%, whereas the effective templation gradually increased from 0.44 to 1.22.

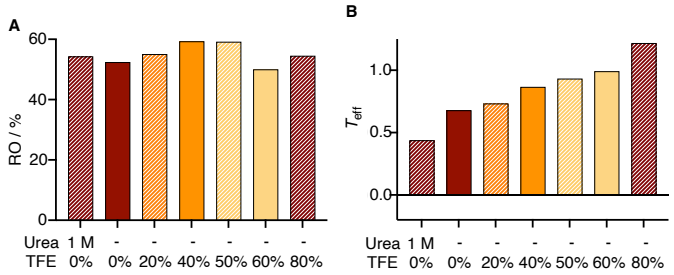

Figure 45. A) Percentage of conversion of AspA units to ring-open products at different buffer compositions. B) Effective templation at different buffer compositions.

Studying the helicity of peptide **116** by circular dichroism in the different buffers used here showed that increasing the percentage of TFE favored the 3_{10}-helix nature of the peptide (Figure 46). In literature, the ratio of CD signal at 220 and 208 nm $R = \Delta\varepsilon_{220}/\ \Delta\varepsilon_{208}$ has been introduced as a way to discriminate between an α- and a 3_{10}-helix.[189] If R = 1, the peptide adopts an α-helix conformation; if $R < 1$, it adopts a 3_{10}-helix conformation. Going from pure water to pure TFE, R went from 1 to 0.6, indicating that the peptide goes from an α- to a 3_{10}-helix, thus giving a better alignment of the AspA units, which explains the higher effective templation. The lower hydrophilicity of the reaction mixture when going from water to TFE could also play a role in the outcome of the thiol-disulfide exchange reaction, although mostly kinetics should be influenced.[190]

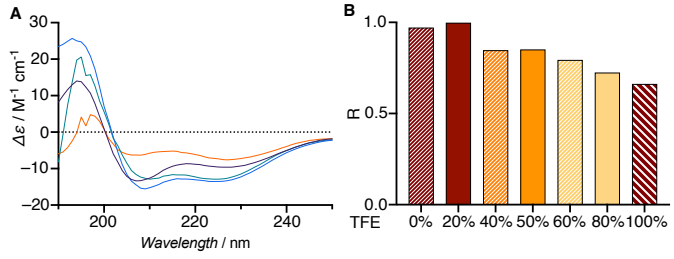

Figure 46. A) CD spectra of **116** in pure buffer (orange), 20 (green), 50 (blue) and 100% TFE (purple). B) $R = \Delta\varepsilon_{220}/\ \Delta\varepsilon_{208}$ at different percentages of TFE.

A similar trend was observed when the reaction was performed at different temperatures in 1:1 TFE/buffer at pH 9.0 (Figure 47, A). At high temperatures, almost no templated products were obtained. On the other hand, the lower the temperature, the better the templation, from a combination of better helicity and entropically-favored oligomerization. When studying the CD spectra of **116** at different temperature, a deeper negative Cotton effect at 208 nm for the 3_{10}-helix was found at low temperature (Figure 47, B), but the differences are too small to justify alone the large variations in templation efficiency.

In the thermodynamics of a polymerization process, ΔS is always negative, because degrees of freedom are lost. Even on the template, several degrees of freedom are frozen upon oligomerization, mostly from the lost flexibility of the side chains containing the AspA. Therefore, the entropy factor becomes unfavorable at high temperatures, from the side chains of the peptide being more flexible and less aligned, which can also account for the better templation at low temperatures.

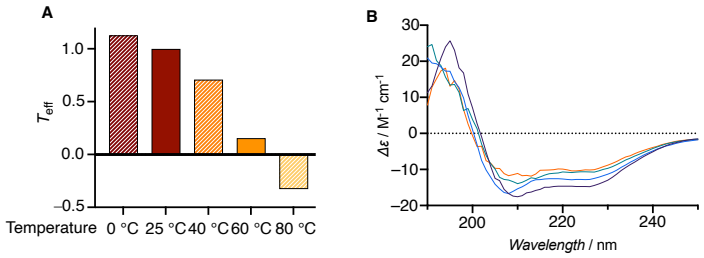

Figure 47. A) Effective templation at different temperatures in 1:1 TFE/buffer at pH 9.0. B) CD spectra of **116** in 80% TFE in buffer at 10 (purple), 20 (blue), 40 (green) and 60 °C (orange).

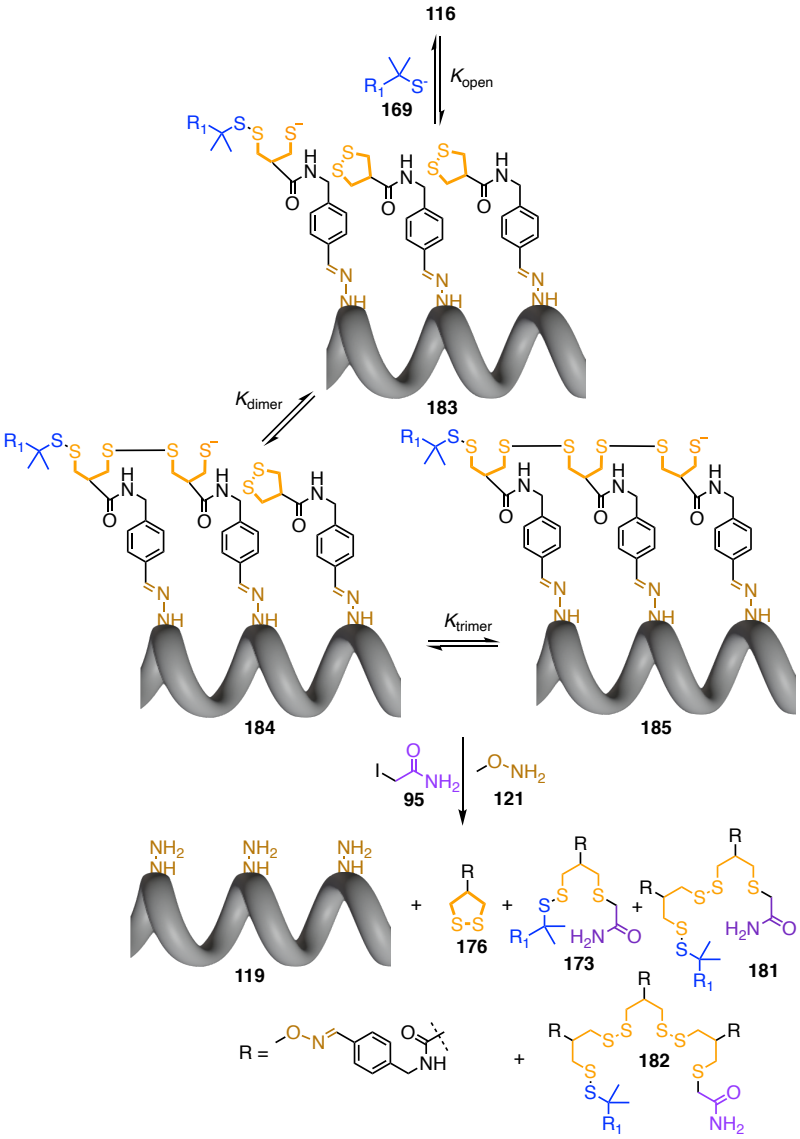

Scheme 16. Schematic representation of the reactions involved in the cascade ring-opening oligomerization.

Under fully optimized conditions, the effective templation reached a maximum of T_{eff} = 1.22, but with a large preference for dimer **181** over trimer

182. This is a direct consequence of all the reactions involved in the oligomerization process being reversible (Scheme 16). First, the ring opening of one AspA unit occurs by the attack of the thiolate, in a similar fashion to what has been described in section 3.1.2. This first process is reversible, but favored because of the ring strain (ΔH^0 ~ 15 kJ/mol for LipA, slightly higher for AspA),[126] hence $K_{open} > 1$. Then, the ring-open thiolate can react on a neighboring AspA monomer, in cascade, to get to the dimer and trimer. This is still favored by enthalpy, but entropically disfavored. With the optimized conditions described above, the final distribution of products gives $K_{dimer} > 1$ and $K_{trimer} < 1$. However, this is an oversimplification considering that the initial thiolate attack takes place on one of the AspA units at the extremities of the template. Considering that the attack can take place indifferently on any of the monomers, the maximum yield of trimer is 66%, and not 100%.

Nonetheless, the system does not produce exclusively products where all the AspA units have been open, despite the excellent preorganization on the three-dimensional template. From this distribution, the gain of enthalpy upon ring opening and release of the ring strain is compensated by unfavored entropic factors during the cascade macrocyclization. What, then, could be done to produce almost quantitatively the desired longer oligomers?

First, applying the system described here to non-reversible reactions, similar to the "click" chemistry used by Hunter *et al.*,[157] only trimers would be obtained, the reaction having a real driving force. Then, focusing on cascade ring-opening oligomerization, one could consider changing the COC used: the ring tension in AspA is higher than the one in LipA, but far from being the highest. Using ETP monomers, where ring tension is at its extreme, would probably result in mostly trimer being formed, still in a 2:1 ratio with dimers because of the possible attack of the initiator on the monomer in the middle. To prevent this issue and provide directionality to the system, the thiolate could be attached on the N- or C-terminus of the peptide and perform the first ring opening intramolecularly.

Alternatively, a vesicle-based artificial signal transduction through a lipid bilayer was used to provide directionality, as will be described in section 3.2.6.

3.2.4.4. Shifted Template: Anti-Templation Effect

The results described so far showed that the approach is promising to preorganize monomers on a peptide foldamer template. However, there is so far no way to distinguish between the three-dimensional preorganization introduced here and the previously described two-dimensional approach developed by Hunter *et al.*[157] The shifted template peptide **159** was synthesized for this purpose. In a 3_{10}-helix, each turn represents precisely three amino acids, meaning that the side chains of two consecutive amino acids are shifted by a 120° angle (Figure 48). In **159**, two consecutive monomers are therefore shifted by 120° in the 3_{10}-helix, which should prevent their reaction one with another and therefore result in mostly monomers and possibly dimers under the cascade ring-opening oligomerization conditions (Scheme 17).

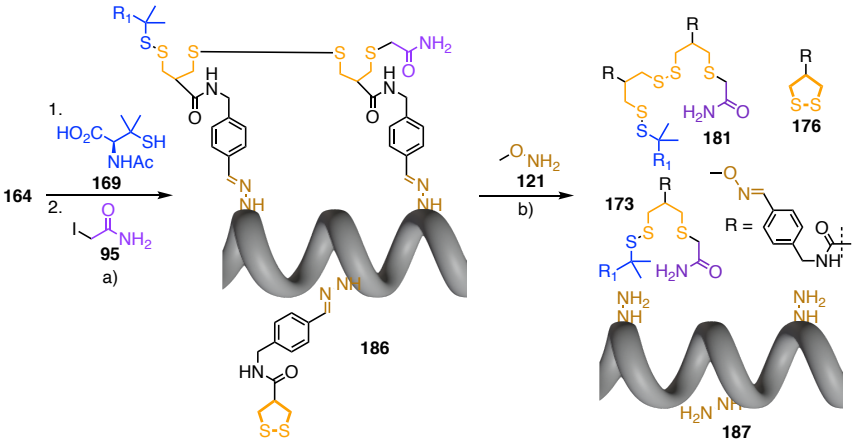

Scheme 17. Cascade ring-opening oligomerization on shifted nonapeptide **164**. a) 100 µM **162**, 2 mM **169**, 10 mM Tris, 1 mM EDTA, 0:1 to 4:1 TFE/H_2O, pH 9, 30 min, rt, then addition of **95**; b) 100 mM **121**, 50 mM **159**, 150 mM NaCl, pH 5, 16 h, rt.

With such a shift in the alignment, dimers can theoretically still be obtained from the reaction between monomers at positions *i* and *i+6*, but the trimers should be inaccessible. Varying the percentage of TFE in the buffer, the shifted peptide **164** followed an exactly opposite trend as compared to aligned peptide **116** (Figure 49).

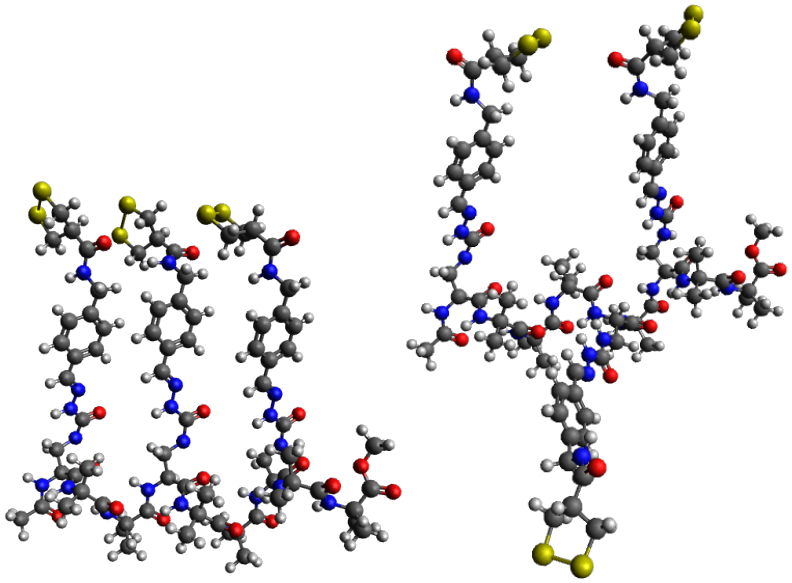

Figure 48. Ball and stick models of aligned peptide **116** (left) and shifted peptide **164** (right). Obtained with Avogadro with a MMFF94 force field optimization.

In the presence of 1 M of urea to disrupt the H-bonding network and destroy the helix, both **116** and **164** gave the same distribution of products, because the peptides are both in a random coil conformation. This corresponds to a two-dimensional templation, similar to what was reported by Hunter *et al.* When removing the urea and increasing the proportion of TFE to 50%, the peptides adopted a helical conformation in between an α- and a 3_{10}-helix, with the monomers getting aligned in **116**. On the contrary, in **164**, such a conformation placed the monomers further to each other, thus giving a still low effective

templation. Going to 80% of TFE, this effect was even more pronounced: whereas the templation was the most efficient with **116** (T_{eff} = 1.22), it got even lower with the shifted template **164** (T_{eff} = –0.15), which can therefore be described as an "anti-template", putting the monomers away from each other to avoid their reaction together.

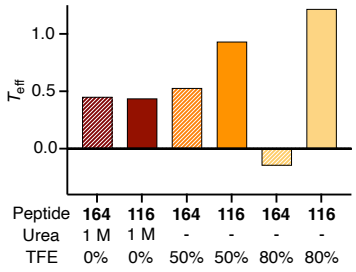

Figure 49. Comparison of the effective templation on aligned (**116**) and shifted template (**164**) in different helicity conditions.

These results prove that the peptide template acts as envisioned, with the three-dimensional structure of the foldamer being the most important parameter. As compared to the covalent templates introduced by Hunter *et al.*, the proximity of the monomers in the two-dimensional sequence does not provide efficient templation here, as exemplified by the results with urea in the reaction mixture. An interesting comparison would be to use the foldamer template for "click" reactions similar to the ones used in literature to compare the effective molarities on the template and have a direct readout of the template's efficiency.[158,159]

3.2.5. Application to 1,2-Diselenolanes

3.2.5.1. Short-Lived Ring-Open Selenolates in Buffer

Contrary to what was described in section 3.1.3, the ring-open selenols and selenolates produced by the ring opening of 1,2-diselenolanes are too reactive species to be trapped in water (see section 3.2.3.1). This was not surprising

considering the extensive literature describing the use of diselenides to catalyze the oxidation of thiols to disulfides without the possibility to isolate selenosulfide and selenolate intermediates.[112,135]

As described in Scheme 11, on tripeptide **161**, no matter the timing of addition of iodoacetamide **95**, the trapped selenide could not be observed, and the selenolate produced after ring opening was immediately oxidized to a selenosulfide with a second equivalent of thiol initiator. However, on the nonapeptide template **163**, this selenolate could react faster on a neighboring diselenide rather than being oxidized, therefore still performing the cascade ring-opening oligomerization before being quenched as selenosulfides (Scheme 18). This would yield, after detachment, ring-open monomer, dimer and trimer **189** – **191**, terminated as selenosulfides on both ends.

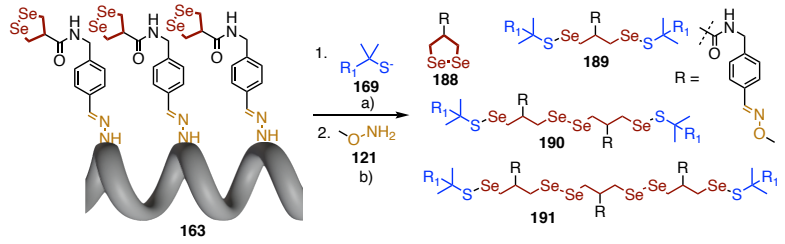

Scheme 18. Cascade ring-opening oligomerization of 1,2-diselenolanes. a) 100 µM **163**, 2 mM **169**, 10 mM Tris, 1 mM EDTA, 4:1 TFE/H_2O, pH 9, 30 min, rt; b) 100 mM **121**, 50 mM **159**, 150 mM NaCl, pH 5, 16 h, rt.

3.2.5.2. Cascade Ring Opening

Under the optimized reaction conditions developed for the cascade ring-opening oligomerization of 1,2-dithiolanes, diselenolane-containing **163** also gave a mixture of singly- and doubly-open peptides **192** and **193**. Several constitutional isomers in various ratios were obtained depending on the number of equivalents used (Scheme 19), similarly to what was observed for dithiolanes (Scheme 14).

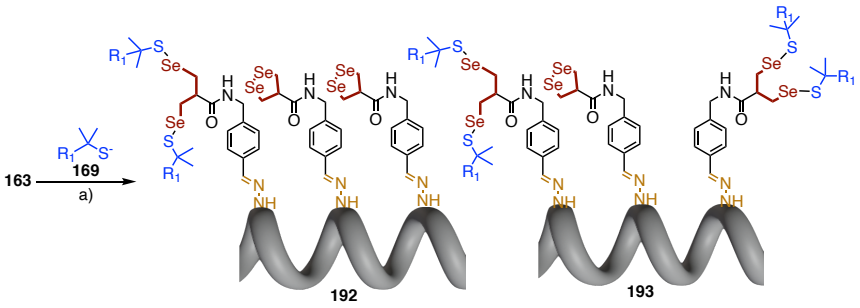

Scheme 19. On-peptide ring opening of the 1,2-diselenolane trimer **163**. a) 100 µM **163**, 200 µM – 2 mM **169**, 10 mM Tris, 1 mM EDTA, 4:1 TFE/H_2O, pH 9, 30 min, rt.

Upon detachment from the peptide template by oxime formation, mostly the ring-closed and ring-open monomers **188** and **189** were observed, with a small proportion of dimer **190**, but no trimer **191**. With varying numbers of equivalents of initiator **169**, different distributions were observed together with increasing conversion (Figure 50), similar to what was observed for disulfides (Figure 43).

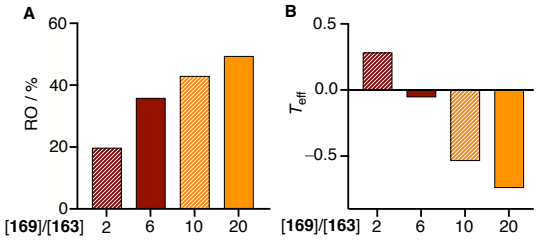

Figure 50. A) Percentage of conversion of each DSL unit in **163** with various numbers of equivalents of **169**; B) Effective templation with various number of equivalents of **169**.

However, with 1,2-diselenolanes, the effective templation was low in any case (T_{eff} = 0.28 at best), with only dimer **190** observed, in minority as compared to monomer **189**. The reaction mechanism shown in Scheme 20 could rationalize these results. After the first ring opening of **163**, the ring-open **194** is rapidly

quenched as a double selenosulfide to yield **192** before the equilibrium with the dimer in **195** can be reached. Only a small proportion of **195** is therefore formed, which is in turn also rapidly oxidized to **192'** without the possibility to reach **196**. Performing the reaction in degassed buffer and under inert atmosphere did not improve the formation of oligomers, which would require the reaction to be performed in organic solvents under strictly inert atmosphere.

Nonetheless, the existence of dimer **190**, and its stability in HPLC conditions is encouraging, as it shows the polymerization of 1,2-diselenolanes would be possible. Considering their high cellular uptake ability, the perspective of synthesizing cell-penetrating poly(diselenides)s similar to CPDs is attractive.

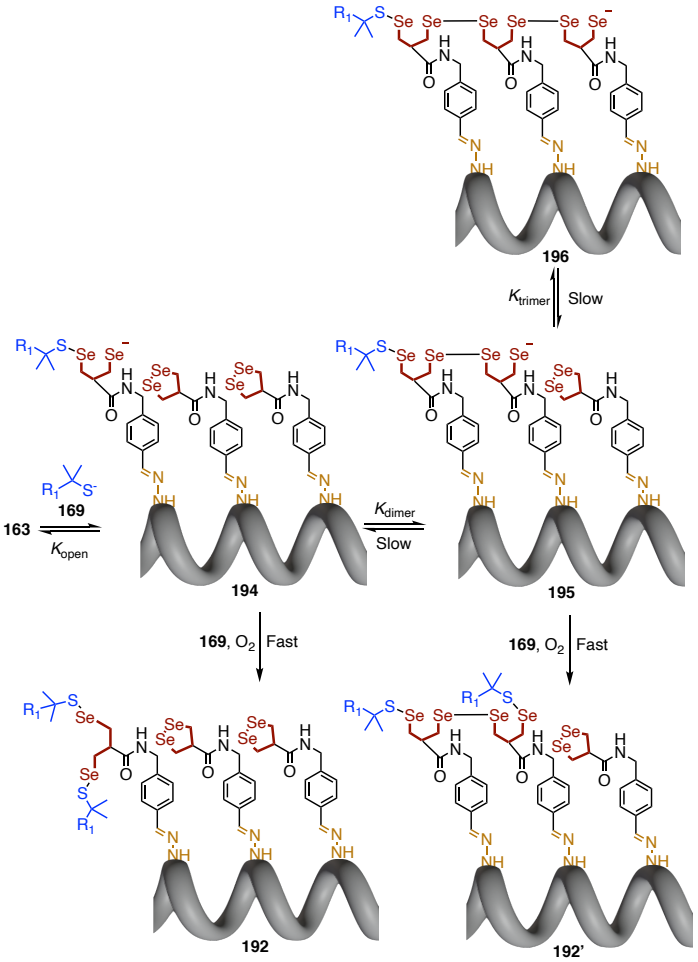

Scheme 20. Proposed mechanism for the low conversion to oligomers of 1,2-diselenolanes by selenol oxidation.

3.2.6. Artificial Redox Signal Transduction Through a Lipid Bilayer

3.2.6.1. 3_{10}-Helices for Artificial Signal Transduction

As mentioned in section 3.2.1.2, 3_{10}-helices as the ones synthesized for this project are able to insert well in lipid membranes.[179,191] If long enough, they can span the entire membrane, creating ion pores. They were also shown to perform artificial signal transduction from the outer side of the bilayer to the inside.[171]

To prevent the attack of the initiator on the middle disulfide of the template, and therefore give directionality to the system, a vesicle-based assay was envisioned to perform artificial redox signal transduction through the membrane (Figure 51).[192]

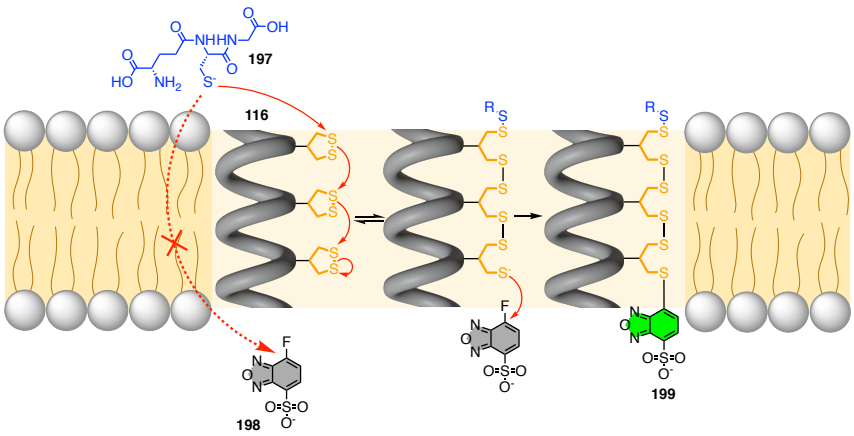

Figure 51. A vesicle-based assay to perform cascade ring-opening oligomerization through a membrane bilayer.

With nonapeptide **116** embedded in the DPPC lipid bilayer of large unilamellar vesicles (LUVs), the hydrophobic environment should favor intramolecular H-bonding and enforce the 3_{10}-helix conformation. Inside the vesicle is entrapped a fluorogenic molecule, SBD-F **198**, which becomes fluorescent only after nucleophilic aromatic substitution (S_NAr) of a thiolate on

the fluoride. Thanks to its sulfonate group, **198** should not be membrane permeable and remain entrapped in the vesicles. On the outer part of the LUVs would be added glutathione (GSH, **197**), also membrane impermeable thanks to its two carboxylates. The direct reaction of GSH and SBD-F would therefore be prohibited: an observed increase of fluorescence signal could only come from the cascade ring-opening oligomerization of **116**, creating a thiolate in the inner leaflet of the lipid bilayer to react with SBD-F and create fluorescent adduct **199**.

3.2.6.2. Redox Signal Transduction with a Disulfide Track

The reaction conditions were first optimized to make sure an increase of fluorescence upon reaction of a thiolate with SBD-F could be observed. LUVs were made from 1,2-dipalmitoylphosphatidylcholine (DPPC) with an inner solution containing 1 mM SBD-F in 10 mM Tris, 100 mM NaCl buffer at pH 8.0. Higher pH and lower ionic strength yielded leaky vesicles. Under these conditions, the stability of the vesicles was investigated in the presence of GSH in the outer solution, as well as the kinetics of the reaction with SBD-F at 50 °C (Figure 52), a temperature above the phase transition of DPPC (T_m = 42 °C), the vesicles being in a liquid disordered phase.

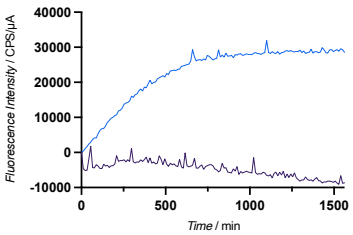

Figure 52. Fluorescence intensity as a function of time for LUVs in the presence (blue) or the absence (purple) of 0.1% Triton-X. Inner solution: 1 mM SBD-F, 10 mM Tris, 100 mM NaCl, pH 8.0; outer solution: 1 mM GSH, 10 mM Tris, 100 mM NaCl, pH 8.0; 50 °C. λ_{exc} = 385 nm, λ_{em} = 535 nm, slits 5:5.

In the presence of the vesicles alone with 1 mM of GSH in the outer solution, the fluorescence signal remained constant (Figure 52, purple line), indicating that the vesicles were stable under these conditions. When 0.1% of Triton-X was added to destroy the vesicles, a large increase of fluorescence was found over the first ten hours followed by a plateau, indicating that the reaction of the thiol of GSH with SBD-F is complete after this time (Figure 52, blue line). The relatively slow kinetics of the S_NAr were expected, the optimal conditions recommended by the supplier of SBD-F (Sigma-Aldrich) being 1 h at 60 °C and pH 9.5, conditions that were not compatible with the use of vesicles. Despite this slow kinetics, the vesicles appeared stable over the time needed, the conditions used here were ideal to follow the cascade ring opening.

As mentioned previously, 3_{10}-helices are known to create ion pores in membranes if long enough, which could make the vesicles permeable to GSH **197** or SBD-F **198**. To make sure that this was not the case, two assays were setup in parallel, one with the template **116** and one with control helix **139** (Figure 53). If the helical peptide in **116** was responsible for an increase of fluorescence by making the LUVs permeable to GSH or SBD-F, the same would be true for **139**.

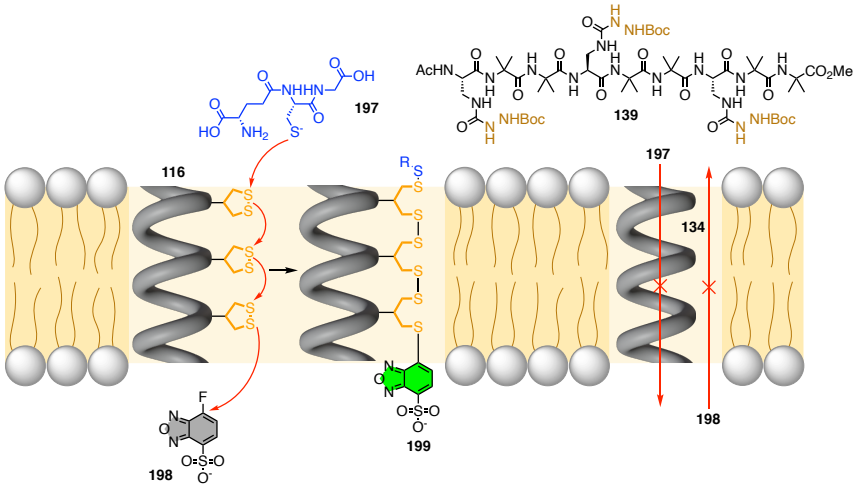

Figure 53. Cascade ring-opening oligomerization through the lipid bilayer and control experiment with helix **139**.

With helix **139**, only a small increase of fluorescence was observed over the first 300 min, which can be attributed to leakage of the vesicle (Figure 54, A, orange line). However, after this period of time, the fluorescence remained low and far from the level obtained with LUVs destroyed with Triton-X, indicating that the helix did not make the membrane highly permeable to either GSH **197** or SBD-F **198** (Figure 54, orange line).

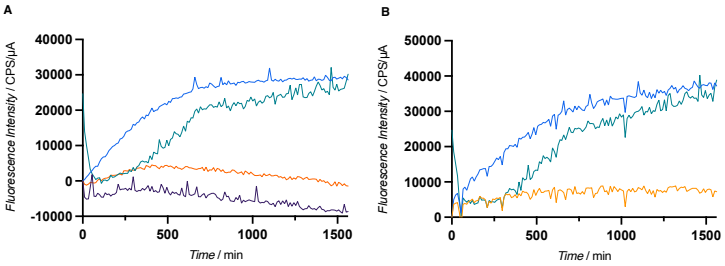

Figure 54. A) Fluorescence intensity as a function of time for LUVs alone (purple), in the presence of 0.1% Triton-X (blue), 10 mol% **139** (orange) or 10 mol% **116** (green); B) Same as A with background subtraction from vesicles alone. Inner solution: 1 mM SBD-F, 10 mM Tris, 100 mM NaCl, pH 8; outer solution: 1 mM GSH, 10 mM Tris, 100 mM NaCl, pH 8; 50 °C. λ_{exc} = 385 nm, λ_{em} = 535 nm, slits 5:5.

In the presence of 10 mol% of **116** as compared to lipids, the curve was first almost superimposable with the one obtained with **139**, indicating that the same leakage is first taking place (Figure 54, green line). This first phase was also observed when only the vesicles were present, and can therefore be attributed to leftover, non-encapsulated SBD-F as can be seen from background-subtracted curves (Figure 54, B). However, after this first phase, a large increase of fluorescence can be observed only with **116**, reaching a plateau after about ten hours, and to similar levels as for destroyed vesicles, indicating that almost all of the SBD-F has been substituted by a thiol. With passive diffusion ruled out from control experiments, this increase of fluorescence could only come from the cascade ring-opening oligomerization through the lipid bilayer.

The results presented in this section remain highly preliminary and a more in-depth characterization would be needed, *e.g.* isolating the trimer **199** after the reaction, repeating the experiment with shifted template **164**, with different loadings of peptides, … Nonetheless, with the controls performed here, the cascade ring-opening oligomerization seems to take place through the

membrane, performing artificial redox signal transduction through a lipid bilayer.

3.2.7. Conclusions and Perspectives

With this project, we sought to go one step further in the study of the ring opening of 1,2-dithiolanes and diselenolanes, performing this reaction in cascade in a controlled fashion on a 3_{10}-helix peptide template. A large number of peptides were synthesized and equipped with various COCs, both on the monomer and on the trimer level. The ring opening was first re-optimized to move from organic solvents to aqueous media, and the optimized conditions were applied to the templated oligomerization. For 1,2-dithiolanes, an excellent templation efficiency was obtained, forming oligomers up to trimers depending on the helicity of the peptide. The application to 1,2-diselenolanes was complicated by the short lifespan of the ring-open selenols, which were too rapidly oxidized into selenosulfides to perform the cascade efficiently. The perspective of synthesizing cell-penetrating poly(diselenides)s is nonetheless exciting. Finally, the peptide templates could serve as an artificial redox signal transduction system through a lipid bilayer, although these results are still preliminary.

Thanks to the versatility of the chemistry employed to attach the COCs to the peptide, much more can be done with relatively little adjustments. First, the peptide template could be used as a platform to screen for possible new CPD mimics and determine whether or not newly introduced COCs, such as thiosulfinates, thiosulfonates or other derivatives could be polymerized (Figure 55, A). Alternatively, using a third orthogonal dynamic covalent bond, namely boronic acid/ester chemistry,[193] one could envision transforming our system to introduce a control of the sequence, creating alternating oligomers in a controlled fashion (Figure 55, B). Playing around with sequences, introducing selenosulfides or thiosulfonates in a CPD backbone, for example, could have interesting effects on their cell-penetrating properties.

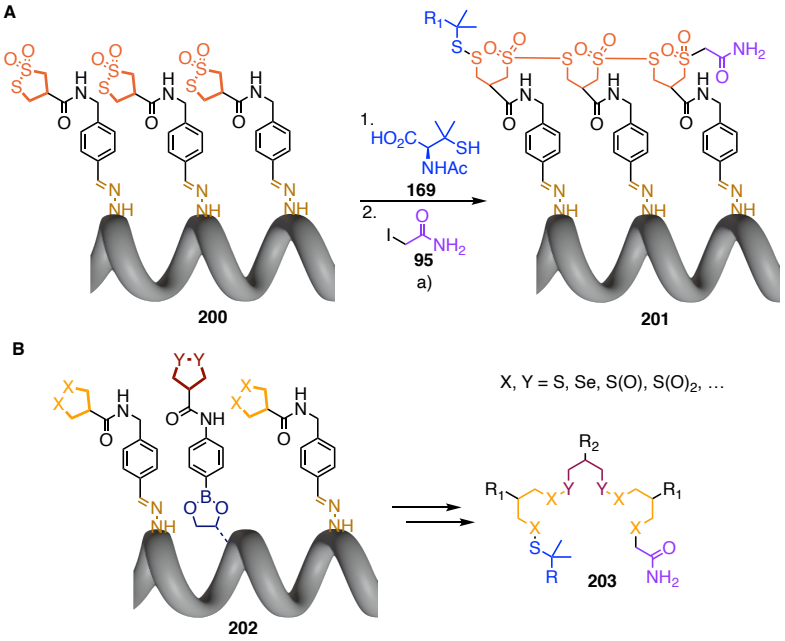

Figure 55. A) Using the same template to probe for possible polymerization of new COCs such as thiosulfonates; B) Introducing a third orthogonal dynamic covalent bond for sequence control. X, Y = S, Se, S(O), $S(O)_2$, …

Longer oligomers can also be envisioned, although the solution-phase peptide synthesis reaches its limits with yields dropping drastically for the coupling of tripeptide fragments over a certain length. With the newly introduced microwave assisted SPPS designed by Clayden *et al.*, this limitation could be overcome.[184]

When it comes to the directionality of the system, more in-depth characterization of the artificial signal transduction system has to be performed. Another alternative is to tweak the synthesis to introduce either the initiator or the terminator, or both, directly on the N- or C-terminus of the peptide. The issue would then become the detachment of the oligomers from the template, which could once again take place using a third orthogonal dynamic covalent bond to attach the initiator/terminator.

Finally, even if the cascade ring-opening oligomerization was herein performed on purified products, the system could be adapted to work *in situ* as a molecular factory as described in Figure 37. The uncomplete formation of semicarbazones in stoichiometric amounts of semicarbazide and aldehyde could be overcome by immobilizing the peptide template on a solid support through the N- or C-terminus. Then, an excess of aldehyde could be loaded and washed away, the reaction mixture exchanged for thiol-disulfide exchange to take place, followed by further washings and detachment to recover the oligomers and the recycled template ready to be reused.

Although this project does not provide direct information on the mechanism by which thiol-mediated uptake operates, the potential applications described in these perspectives could help completing the mapping of structure-activity relationship of transporters based on different scaffolds, different sequences, and make another step forward in the understanding of thiol-mediated uptake.

3.3. Probing for Thiol-Mediated Uptake into Bacteria

The results presented in this section have been published.[194]

3.3.1. Design: Making Gram+ Antibiotics Active in Gram– Bacteria

3.3.1.1. Antimicrobial Resistance

Antibiotic resistance has been coined by the WHO as a major public health issue in the upcoming years.[195] However, since the discovery of penicillin in 1928 and a "golden age" of novel antibiotics until the 1960s, the discovery of new antibiotics slowed down, resulting in a life-threatening problem.[196] For example, the key *ESKAPE* pathogens, such as *S. aureus* or *P. aeruginosa*, are becoming resistant to first-line antibiotics (e.g. β-lactams), and even to last resort antibiotics like vancomycin.[197]

In Gram– bacteria, the presence of two lipid bilayers in the cell envelope, with an outer membrane (OM) and an inner membrane (IM) surrounding a layer of peptidoglycans in the periplasm, hinders the delivery of potential antibiotics to the cytoplasm. This lack of penetration is for example responsible for the lack of activity of vancomycin or erythromycin against Gram– pathogens.[198]

Tremendous efforts from academics and pharmaceutical companies are made to discover new scaffolds with antibacterial activity. On the other hand, overcoming the permeability barrier in Gram– bacteria to make Gram+-only antibiotics active against them is also attractive, as it relies on already established scaffolds. Although this goal can be achieved from structure-activity relationships,[199] efficient strategies mostly rely on conjugation with large delivery systems: carbon nanotubes, dendrimers, nanoparticles, vesicles, etc…[200] A well-established strategy employs siderophores, bacteria-secreted iron chelators, as a way of entry into the bacteria, as will be developed in the following subsection.

3.3.1.2. The "Trojan Horse" Strategy: Hijacking Bacterial Siderophores

Several bacterial biosynthetic pathways rely on iron ions, be it electron transport, metabolic processes or DNA synthesis.[201] Whereas animals can source iron from food, bacteria need to scavenge it from their surroundings. To do so, they secrete iron chelators called siderophores (from the Greek "iron carrier"),[202] small molecules with high affinity for the Fe(III) ion, usually forming hexadentate complexes through catecholates, hydroxamates or α-hydroxy carboxylates.[203] They are then internalized through specific receptors with relatively low selectivity, resulting in the good internalization of modified siderophores.

Hijacking this bacteria iron internalization pathway has been coined the *Trojan Horse* strategy. The group of Marvin J. Miller, as well as others, have shown that this approach is successful to bring Gram+-only antibiotics to their potential targets in Gram– bacteria, conferring them high activity against these more challenging targets.[204–208] Both natural, semi-synthetic and fully synthetic siderophores have been conjugated, through cleavable or non-cleavable linkers, to a wide range of antibiotics (β-lactams, cyclosporine, daptomycin, …) with good success.

Inspired by this strategy, we sought to apply thiol-mediated uptake, highly efficient in eukaryotic cells, to the delivery of Gram+ antibiotics into Gram– bacteria as a conceptually new way to penetrate these. Thiol-mediated uptake shares similarities with the internalization of siderophores, namely a low selectivity for different cell lines[115] and the ease of conjugation of transporters to antibiotics. Additionally, both Gram+ and Gram– were shown to present thiols at their surface,[209,210] making thiol-mediated uptake a conceivable option.

3.3.1.3. Choice of Transporters and Antibiotics to Derivatize

To probe for thiol-mediated uptake in bacteria, three transporters with different activities were selected: lipoic acid (LipA), asparagusic acid (AspA)

and diselenolipoic acid (DSL). While the ring tension in LipA is relatively small, AspA is more reactive towards exofacial thiols, and a better transporter.[104] With DSL, a different mode of action was investigated: whereas strained disulfides rely at least partially on endocytosis, diselenolanes are believed to operate *via* a molecular walker mechanism through the lipid bilayer (see section 3.1.3.2).[112,113,122]

As stated above, the goal of this project was to make Gram+-only antibiotics active in Gram– bacteria. Five antibiotics active against the Gram+ strains available, *B. subtilis*, were chosen: erythromycin **204**, eperezolid **205**, ampicillin **206**, vancomycin **207** and daptomycin **208**.

Erythromycin **204** is a broad-spectrum antibiotic, amongst the most prescribed worldwide, mostly to patients allergic to penicillin. With an intracellular mode of action, by binding to the exit tunnel in the 50S ribosomal subunit, it interferes with protein synthesis by preventing elongation of the growing protein. Derivatives of **204** bearing oximes instead of the macrolide ketone were shown to maintain antimicrobial activity,[211] this modification was therefore chosen to attach the transporters.

Eperezolid **205** also interacts with bacterial protein synthesis, by preventing the assembly of the two ribosome subunits. Derivatives bearing an amine instead of the alcohol in **205**, subsequently functionalized by amide bond formation, have been reported to have good Gram+ antibiotic activity.[207]

Ampicillin **206** is a β-lactam, a penicillin derivative bearing an amino group next in α position to the exocyclic amide. This class of antibiotics inhibits cell wall synthesis by interaction with membrane-bound or cytosolic penicillin-binding proteins. The presence of this primary amine also gives ampicillin a mild activity against Gram– bacteria, by passage of the OM through counterion-gated porins.[198] Removal of this group in penicillin makes it inactive against Gram– bacteria, while remaining active against Gram+.

Vancomycin **207** is a last resort antibiotic, mostly used to treat infections by methicillin-resistant *S. aureus* (MRSA), amongst the most common resistant bacterial strain.[212] By binding to a D-Ala-D-Ala moiety during the synthesis of peptidoglycans, vancomycin inhibits cell wall biosynthesis. Many derivatives have been reported, containing variations either on the amine of the sugar or on the core carboxylic acid. The sugar amine was chosen for the incorporation of the transporters.

Finally, daptomycin **208** is a lipopeptide antibiotic that aggregates in the cell membrane of Gram+ bacteria in a phosphatidylglycerol-dependent manner, thus creating pores and inducing depolarization of the membrane.[213] Several derivatives on the ornithine residue have been reported to be well tolerated, and this site was therefore chosen for conjugation of the COCs.

3.3.2. Synthesis of Antibiotic-Transporter Conjugates

3.3.2.1. Synthesis via Amide Bond Formation

Taking advantage of the amine functional group present in **205**, **206** and **208**, peptide coupling conditions from the NHS-activated esters of the COCs were used. After purification by RP-HPLC or flash column chromatography, the antibiotic-COC conjugates were obtained in moderate to good yields (Scheme 21 – Scheme 23). The synthesis of daptomycin derivatives **208a**-**208c** was performed by Dr. Mathéo Berthet in the group of Prof. Nicolas Winssinger.

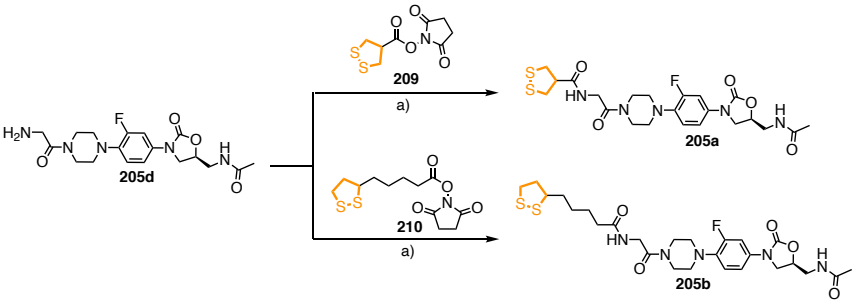

Scheme 21. Synthesis of eperezolid-COC conjugates. a) DIPEA, DMF, rt, 1 h, 49% (**205a**), 33% (**205b**).

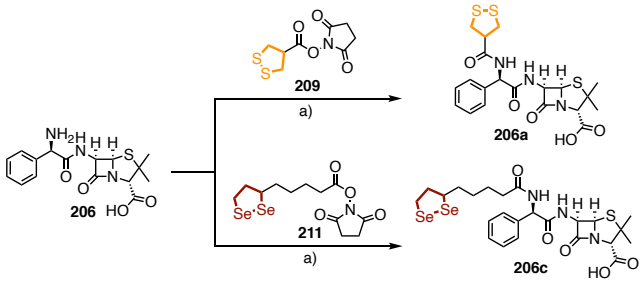

Scheme 22. Synthesis of ampicillin-COC conjugates. a) DIPEA, DMF, rt, 1.5 h, 61% (**206a**), 78% (**206c**).

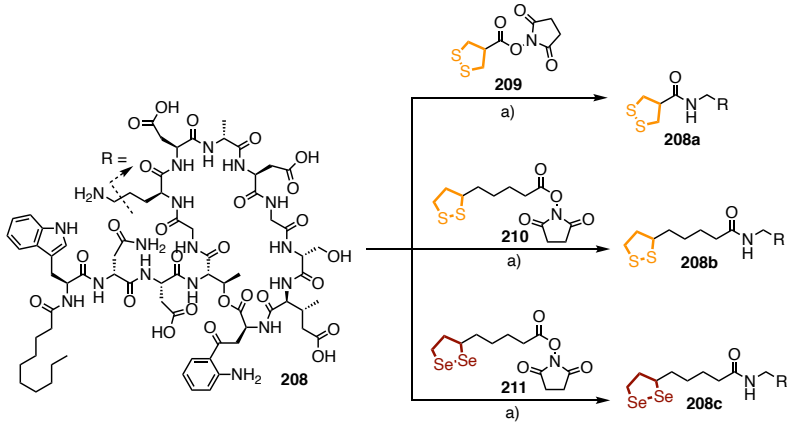

Scheme 23. Synthesis of daptomycin-COC conjugates. a) $NaHCO_3$, DMAP, THF/H_2O, rt, 16 h, 62% (**208a**), 48% (**208b**), 62% (**208c**). Synthesis performed by Dr. Mathéo Berthet.

3.3.2.2. Synthesis via "Click" Chemistry

Contrary to **205**, **206** and **208**, erythromycin **204** and vancomycin **207** were first derivatized to install a "click" chemistry handle, on which the COCs were installed *via* CuAAC.

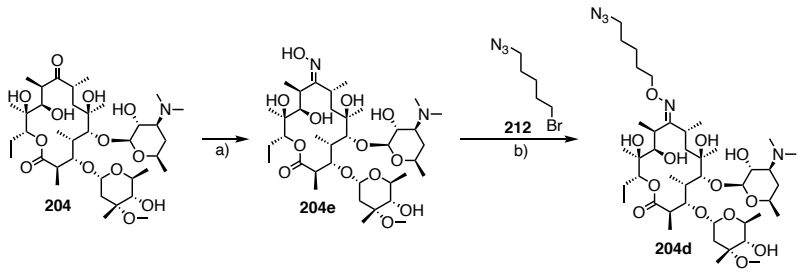

Scheme 24. Synthesis of azide-functionalized erythromycin. a) Hydroxylamine hydrochloride, Et_3N, MeOH, reflux, 16 h, 41%; b) KOH, CH_3CN, rt, 16 h, 36%.

First, erythromycin **204** was converted to its oxime, following a reported procedure.[214] Nucleophilic substitution on 1-azido-5-bromopentane **212** then afforded the azide-functionalized erythromycin **204d** (Scheme 24).

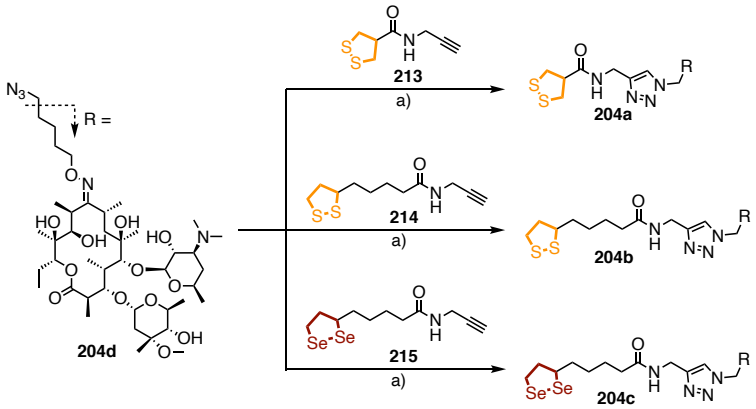

Scheme 25. Synthesis of erythromycin-COC conjugates. a) Sodium ascorbate, $CuSO_4 \cdot 5H_2O$, TBTA, H_2O/THF 1:1, rt, 1.5 h, 35% (**204a**), 29% (**204b**), 33% (**204c**).

Then, *via* classical CuAAC "click" chemistry conditions, **204d** was derivatized with the 3 different COC alkynes **213-215** to afford COC-derived erythromycins **204a-c** in moderate yields (Scheme 25).

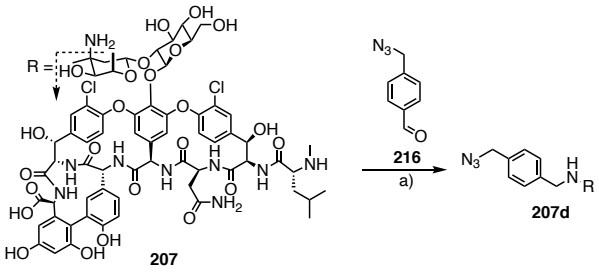

Scheme 26. Synthesis of azide-functionalized vancomycin **207d**. a) DIPEA, DMF, 70 °C, 6 h then $NaBH_3CN$, DMF, 70 °C, 16 h, 46%. Synthesis performed by Dr. Mathéo Berthet.

Vancomycin **207** was derivatized by Dr. Mathéo Berthet *via* reductive amination with 4-azidoemethylbenzaldehyde **216** to install the "click" handle in **207d** (Scheme 26), which was further functionalized by CuAAC to install the COCs (Scheme 27).

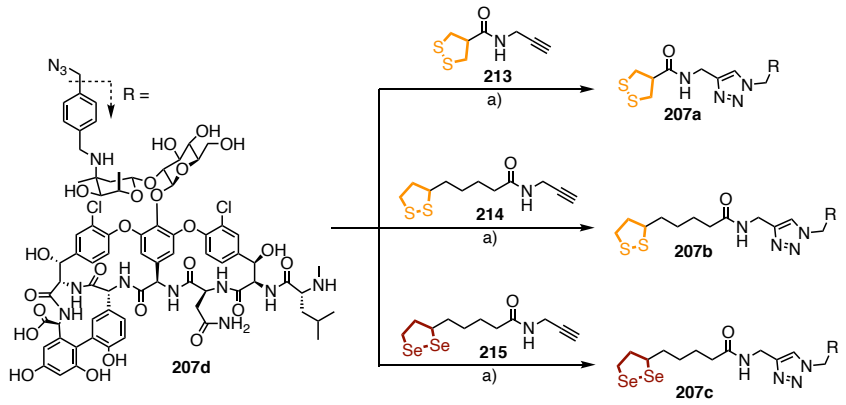

Scheme 27. Synthesis of vancomycin-COC conjugates. a) Sodium ascorbate, $CuSO_4 \cdot 5H_2O$, TBTA, H_2O/THF 1:1, rt, 1.5 h, 31% (**207a**), 43% (**207b**), 45% (**207c**). Synthesis performed by Dr. Mathéo Berthet.

With this library of 13 antibiotic-COC conjugates in hands, their antibiotic activities had to be tested in a growth inhibition assay.

3.3.3. Antibacterial Activity and Proposed Mechanism of Inactivation

All the antibacterial activities reported here were measured by Dr. Mathéo Berthet and Dr. Sofia Barluenga using growth inhibition assays to determine the minimum inhibitory concentrations (MIC) by measurement of the optical density at 600 nm (OD_{600}) of bacterial suspensions. *B. subtilis* was chosen as a Gram+ bacterial strain and *E. coli* as Gram–. Ciprofloxacin (CF) and kanamycin (KM) were used as positive controls with low μM efficiencies against both these strains.

3.3.3.1. Antibacterial Activity of Antibiotics with Extracellular Targets

Out of the five antibiotics selected for this study, the modes of action differ, as mentioned in section 3.3.1.3. Vancomycin **207** and daptomycin **208** both have extracellular targets, binding to D-Ala-D-Ala in growing peptidoglycans or forming pores in the bacterial cell membrane, respectively. First the activity of both antibiotics against the Gram+ bacterial strains used in this study, *B. subtilis*, was confirmed, although activity of **208** was relatively low (Table 4).

Table 4. Minimum inhibitory concentrations (MICs, μM) of vancomycin- and daptomycin-COC conjugates against *B. subtilis* and *E. coli.*

Vancomycin	*MIC* / μM		Daptomycin	*MIC* / μM	
	B. subtilis	*E. coli*		*B. subtilis*	*E. coli*
207	< 0.28	> 50	**208**	50	> 100
207a	0.46	> 50	**208a**	100	> 100
207b	< 0.28	> 50	**208b**	> 100	> 100
207c	1.3	> 50	**208c**	100	> 100
207d	< 0.28	> 50			

Upon conjugation with COCs, both vancomycin and daptomycin retained similar levels of activity against *B. subtilis*, with only a 2 to 5-fold increase of the MIC values, if any, **207b** maintaining the same MIC < 0.28 µM for example. In both cases, no activity was observed against Gram– *E. coli*. Whereas this could have been foreseen for vancomycin, for which the siderophore-based *Trojan Horse* strategy proved ineffective,[215] this was surprising for daptomycin **208**. Indeed, when conjugated to siderophores on the same ornithine residue, Miller *et al.* showed that **208** gained a high potency against Gram– *A. baumanii*.[207] One possible explanation for this lack of activity is that only specific bacterial strains could be sensitive to the *Trojan Horse* strategy, and the appropriate strains were not screened for here.

Despite the lack of activation in Gram– bacteria, the retained activity of the antibiotics-COC conjugates presented here is of interest, as it shows that disulfide-containing modifications are well tolerated by these antibiotics. Gademann *et al*. later showed that similar modifications on vancomycin could confer potent activity against vancomycin-resistant strains, as well as some Gram– bacteria.[216] This confirmed the potential of this approach, and that testing a wider range of bacterial strains might bring more positive results (see section 3.3.3.3).

3.3.3.2. Antibacterial Activity of Antibiotics with Intracellular Targets

Erythromycin **204**, eperezolid **205** and ampicillin **206** all have intracellular targets (the ribosomal complex for **204** and **205**, and penicillin-binding proteins for **206**), thus relying on their cellular uptake to function. Mostly passive diffusion is responsible for the cellular uptake of such small molecule drugs. The results of antibacterial activity of antibiotic-COC conjugates with **204**-**206** are summarized in Table 5.

Table 5. Minimum inhibitory concentrations (MICs, μM) of erythromycin-, eperezolid- and ampicillin-COC conjugates against *B. subtilis* and *E. coli.*

Erythromycin	*MIC* / μM		Eperezolid	*MIC* / μM	
	B. subtilis	*E. coli*		*B. subtilis*	*E. coli*
204	2.2	> 50	**205**	2.2	> 50
204a	> 10	> 50	**205a**	> 10	> 50
204b	> 10	> 50	**205b**	> 10	> 50
204c	> 10	> 50	**205d**	> 10	> 50
204d	10	> 50	Ampicillin	*MIC* / μM	
204e	6	> 50	**206**	10	11
			206a	> 10	> 50
			206c	> 10	> 50

Whereas the replacement of the hydroxyl group of eperezolid **205** by an amine (**205d**) was reported to maintain activity in Gram+ bacterial strains,[207] **205d** was inactive in the *B. subtilis* strain used in this study. Unsurprisingly, COC conjugates **205a-b** were also inactive, and this antibiotic was not further studied.

For erythromycin **204**, modification of the ketone into oximes in **204d** and **204e** was well tolerated, resulting only in a mild increase of the MIC against *B. subtilis* (from 2.2 to 10 and 6 μM, respectively), as reported in literature.[211] The ketone pointing outside of the ribosome exit tunnel,[217] many modifications of erythromycin rely on such oxime formation. However, upon conjugation with COCs, activity was lost with all MIC > 10 μM. In Gram– bacteria, all the erythromycin derivatives were inactive with MIC > 50 μM.

Because of its primary amine, ampicillin **206** is mildly active against Gram– bacteria such as *E. coli* (MIC = 11 μM), as mentioned previously.[198] When conjugated to COCs, the activity was once again lost in both Gram+ and Gram– bacteria.

Taken together, these results indicate that not only is thiol-mediated uptake unable to deliver the antibiotics through the OM better than a positively charged ammonium cation, but also that it inhibits passive diffusion. A probable mechanism for this inactivation is proposed in the following subsection.

3.3.3.3. Proposed Mechanism of Action

With thiols being present at the surface of both Gram+ and Gram– bacteria, thiol-mediated uptake into bacterial cells was conceivable to activate Gram+-only antibiotics into Gram–. However, according to the results presented above, the conjugation of antibiotics with COCs inhibited rather than activated the five antibiotics tested in this study. We proposed that, after reaction of COC with exofacial thiols, cellular uptake *via* either endocytosis[105] or a molecular walker mechanism[113] cannot take place.

For vancomycin **207** and daptomycin **208**, this inactivation was only mild, if any. These two antibiotics have extracellular targets, and this limited loss of activity could be explained by a competition binding between the thiols and the drug's target (Figure 56).

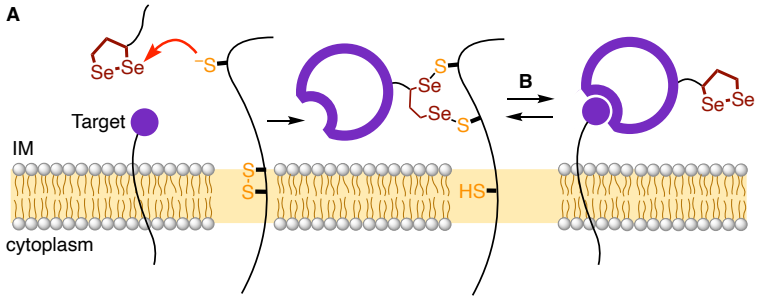

Figure 56. Proposed mechanism for the retained activity of Gram+ antibiotics with extracellular targets. After ring opening of the COC with exofacial thiol (A), competitive binding to thiols and the antibiotic's target takes place (B).

For erythromycin **204**, eperezolid **205** and ampicillin **206**, however, conjugation with the COCs led to a complete loss of activity in Gram+ bacteria.

Instead of competitive binding, the reaction with exofacial thiols prevents passive diffusion, which is needed for the drug to reach its target (Figure 57). As a result, the antibiotics are most likely immobilized at the bacterial cell surface.

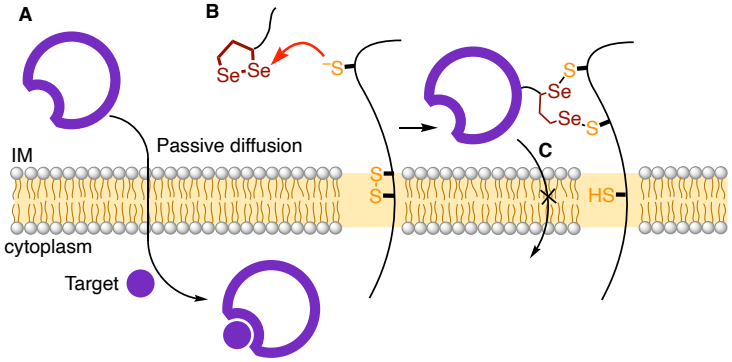

Figure 57. Proposed mechanism for the inactivation of antibiotics with intracellular targets. Without COCs, passive diffusion allows the antibiotics to reach its target (A). Upon reaction with exofacial thiols (B), passive diffusion is prohibited and the drug is immobilized at the cell surface (C).

Such inactivation could of course also be explained by a loss of target engagement when the drug is modified. However, the generality of the results over several antibiotics with different modes of action, as well as extensive derivatizations of the same drugs found throughout literature discarded this hypothesis.

In Gram– bacteria, the thiol-mediated uptake based *Trojan Horse* strategy did not proceed as envisioned. Whereas hijacking the siderophore uptake pathway proved successful in literature for similar antibiotics,[206,207] no activity was observed for the antibiotics-COC conjugates. Most likely, after reaction with exofacial thiols, the conjugates once again remain stuck at the outer membrane, unable to reach their targets, similar to Gram+ bacteria (Figure 57). This proposed mechanism is best exemplified by the case of ampicillin **206**, which

alone is active against *E. coli* thanks to its protonated primary amine, but loses activity upon the conjugation of COCs (Figure 58).

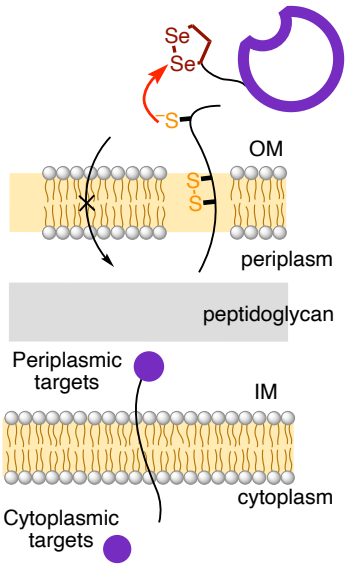

Figure 58. Proposed mechanism for the absence of activity in Gram– bacteria.

In literature, the siderophore-based *Trojan Horse* strategy showed the best results when the antibiotics and the transporter were linked through a cleavable linker.[205,207,218,219] The lack of activity observed here could be linked to the absence of release for the thiol- and disulfide-containing protein targets. A similar approach could therefore be employed in this system to further probe for thiol-mediated uptake in bacteria. However, since not even mild activities were observed in Gram– bacteria within the scope of this study, this route was not pursued.

It is important to note that recently, Gademann *et al.* reported that disulfide-containing derivatives of antibiotics such as vancomycin **207**[216] and cephalosporin[220] could have activity against some Gram– strains, as well as an

improved ability to disrupt biofilms. Among the features of thiol-mediated uptake, its most appreciated is its lack of specificity: COCs can be attacked by non-specific thiols,[221,222] resulting in a broad spectrum of eukaryotic cells being able to uptake them.[115] This does not appear to be the case in bacteria, where only specific strains respond positively. The reasons behind this observation remain elusive, as the detailed mechanism of thiol-mediated uptake remains unknown. One possible explanation could be the difference of composition of the lipid bilayer membranes of eukaryotic and bacterial cells. Bacteria being much smaller, their membranes are much less fluid than those of mammalian cells,[223,224] which could result in the impossibility to create micellar pores which are believed to be needed for cargo translocation during thiol-mediated uptake. This would also explain the limited success of antibiotic-CPP conjugates in literature,[225–228] as they rely on similar micellar pore formation.[39,40]

3.3.4. Conclusions

In this section, the synthesis and antibacterial activity of antibiotic-COC conjugates was introduced. With a library of 13 conjugates bearing different COCs and antibiotics with several modes of action, thiol-mediated uptake into bacteria was probed. Antibiotics with extracellular targets retained activity in Gram+ bacteria, and Gademann *et al.* later showed that similar structures could disrupt biofilm formation and have activity against some Gram– strains. On the other hand, antibiotics with intracellular targets lost all antibacterial activity, and none of the conjugates gained activity against Gram– *E. coli*.

These results led to a proposed mechanism for this inactivation: after reaction with thiol- and disulfide-containing protein targets, the COCs remain immobilized at the bacterial cell surface, without the possibility to get internalized. This interaction prevents the passive diffusion that was needed for the drug's activity.

This study showed that, while thiol-mediated uptake has a broad spectrum of activity in eukaryotic cells, it does not appear to take place in bacteria, thus highlighting that non-trivial mechanisms are at play. Although disappointing from an application point of view, the absence of thiol-mediated uptake in bacteria hints towards specific proteins or membrane properties of eukaryotic cells playing an important role, which is of importance to better understand the mechanisms occurring during thiol-mediated uptake.

3.4. Oligonucleotide Phosphorothioates Enter Cells *via* Thiol-Mediated Uptake

The results presented in this section have been published.[229]

3.4.1. Molecular Targets of Phosphorothioates: Disulfide-Rich Membrane Proteins

3.4.1.1. Oligonucleotide Phosphorothioates

In this chapter, the dynamic covalent chemistry of the phosphorothioate (PS) moiety will be described, in connection with its cellular uptake. Introduced several decades ago, the phosphorothioate modification of the DNA backbone has been a game changer.[230] Simply replacing one of the oxygen atoms of the phosphodiester (PO) linkage in DNA by a sulfur (Figure 59) has drastic repercussions on the physical and biological properties of oligonucleotides.[231] The stability in physiological media of oligonucleotide phosphorothioates (OPS) is much higher than that of non-modified DNA, from a combination of higher nuclease resistance and hydrophobicity. Their most important feature for this project is the higher cellular-uptake ability of OPS as compared to DNA, which can be up to several orders of magnitude, resulting in much higher therapeutic benefits without the need for transfection agents.[121] Before 2018, the only antisense oligonucleotide drugs approved by the FDA all relied on this PS modification,[232] hinting toward their importance for therapies.

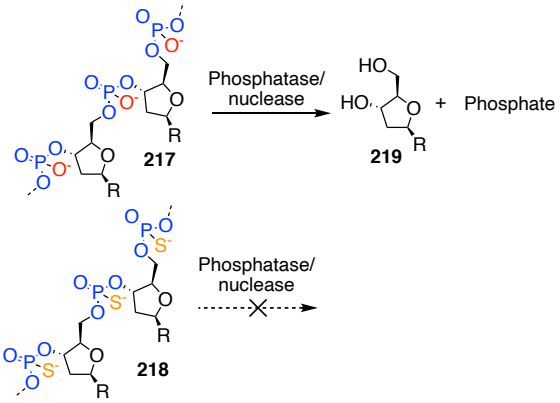

Figure 59. Non-modified (**217**) and PS-modified (**218**) DNA strands and phosphatase/nuclease degradation.

With a pK_a lower than that of phosphodiesters, OPS are highly charged at physiological pH, with the negative charge localized on the sulfur.[233] Passive diffusion through the lipid bilayer can therefore be excluded as a way for OPS to enter cells, despite their higher hydrophobicity as compared to non-modified DNA. Instead, extensive work by Crooke *et al.* showed that OPS are uptaken mostly by endocytosis, mediated by the binding to transmembrane proteins, followed by subsequent endosomal escape.[232,234] However, the precise molecular mechanisms by which this occurs remain elusive, despite several proteins being identified as OPS targets.

3.4.1.2. Disulfide-Rich Membrane Proteins Targets

Among the identified proteins shown to be involved in OPS uptake, many are disulfide-rich transmembrane proteins: Stabilin-1 and 2,[149] EGFR,[235] SCARB1[232] and others. This suggested that dynamic covalent chemistry between protein disulfides and phosphorothioates could take place, and that thiol-mediated uptake could be responsible for the entry of OPS into cells.[66]

In literature, little is known about the post-synthetic chemistry of the phosphorothioate moiety. The efforts have mostly been focused on improving the synthesis of OPS, developing enantioselective approaches,[236] or mixing PS, PO and other linkages in a single DNA strand to optimize the pharmacological properties.[237] Nonetheless, several studies report the existence of pseudo-disulfides made from the reaction of phosphorothioates with activated disulfides (Scheme 28),[238] templated or not by DNA preassembly.[239–242] The low pK_a of phosphorothioate making it a good leaving group, such pseudo-disulfides are however unfavored and can readily react with thiols to form disulfides and release the PS moiety. Notably, this approach has been used to synthesize disulfide-bridged DNA-protein conjugates.[242]

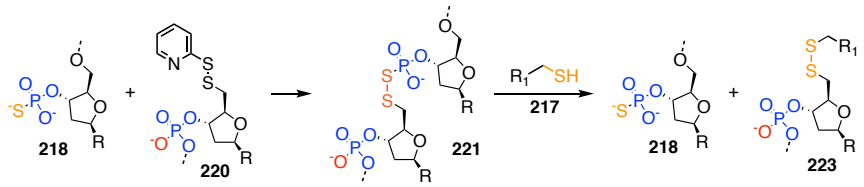

Scheme 28. Pseudo-disulfide formation with phosphorothioate reported in literature.

In the following, the results of inhibition of OPS entry by thiol-mediated uptake inhibitors[117] will be described (Figure 60), together with studies of the dynamic covalent chemistry of the PS moiety, proving that OPS enter cells *via* thiol-mediated uptake.

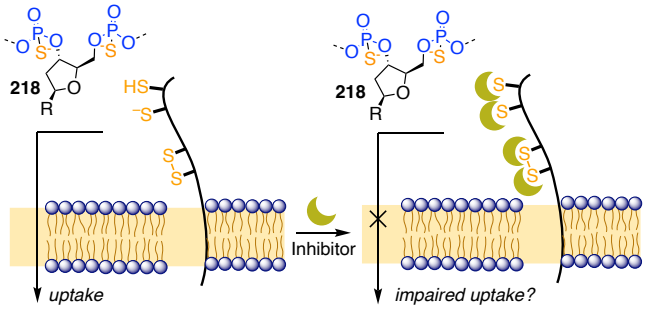

Figure 60. Possible inhibition of OPS uptake by thiol-mediated inhibitors.

3.4.2. Inhibition of OPS Uptake by Thiol-Mediated Uptake Inhibitors

The occurrence of thiol-mediated uptake has generally been proven by its inhibition by Ellman's reagent, DTNB **14**.[71] Recently, our group has introduced much more potent inhibitors of the dynamic covalent exchange taking place during the cellular uptake, with activities up to 5000-fold higher than DTNB.[117] This library covers a wide range of reactivities and at least some of the different, still elusive, uptake pathways involved.

3.4.2.1. Study of Cellular Uptake Without Inhibitors and Data Analysis

Before studying the inhibition of OPS uptake by thiol-mediated uptake inhibitors, we sought to reproduce what is known in literature, for OPS uptake being much higher than non-modified DNA.[121] Using Cy_5-labelled random 18-mers of DNA **217** and OPS **218**, their unaided cellular uptake was first assessed by confocal microscopy (Figure 61).

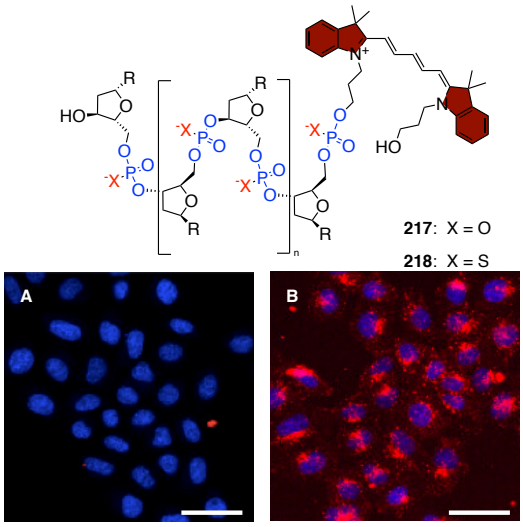

Figure 61. CLSM images of HeLa Kyoto cells after 2 h incubation with 500 nM DNA **217** (A) and OPS **218** (B); red = **217**, **218**; blue = Hoechst 33342; scale bar = 50 µm. R = nucleobases, sequence AGGTCCCCATACACCGAC.

Unsurprisingly, OPS **218** showed intense red fluorescence inside HeLa Kyoto cells after two hours of incubation at 500 nM, whereas non-modified DNA **217** was poorly uptaken. Fluorescence from OPS **218** being rather punctate, it most likely came from endosomes, as expected from literature.[121] From these images, data analysis was performed with the help of Dr. Dimitri Moreau to extract the average fluorescence intensity values of the whole cell, the punctate structures and the background (see experimental section).

3.4.2.2. Inhibition with Thiol-Mediated Uptake Inhibitors

From the collection of inhibitors mentioned previously, ten candidates were selected to study how their preincubation with HeLa cells affected the uptake of OPS **1** (Figure 62). If not commercially available, the inhibitors were prepared following reported procedures, or readily available in our lab.[117] To study inhibition, we used a recently developed high-content high-throughput (HCHT)

screening assay, resulting in data from multiwell plates with thousands of HeLa Kyoto cells analyzed.[116]

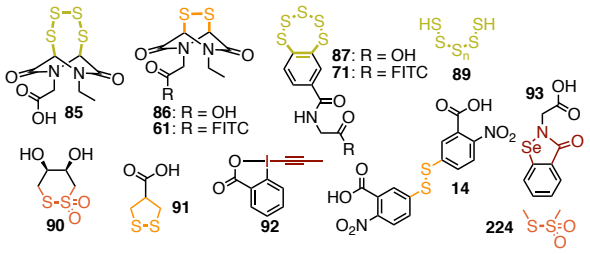

Figure 62. Structure of the inhibitors used in this study.

The cells were first preincubated with the inhibitors for one hour at various concentrations below their previously reported toxicity limit.[117] Then, after thorough washings to remove unreacted inhibitors, the cells were incubated for two hours with **218** as in Figure 61. During data analysis, the average fluorescence intensity per cell I was calculated by subtracting the average background intensity from the average intensity of the whole cell. Average intensities I for each condition were then normalized against that obtained without the addition of inhibitors I_0 giving $I_T = I / I_0$. The dependence of I_T to the concentration on inhibitor $c_{inhibitor}$ was plotted and fitted to a Hill equation to retrieve the half-maximal inhibitory concentration IC_{50} and the Hill coefficient n using Equation 2.

$$I_T = 1 / (1 + (IC_{50} / c_{inhibitor})^{-n}) \quad \text{(Eq. 2)}$$

Minimum inhibitory concentrations (MIC) were estimated from the fit curve as the concentration at which 15% of uptake was inhibited. The results are summarized in Table 6 and the dose-response curves can be found in Figure 63, A and Figure 89 (see experimental section).

Table 6. MIC and IC_{50} data for inhibitors. [a]Concentration of OPS **218**. [b]Minimum inhibitory concentration. [c]Half maximum inhibitory concentration. [d]Hill coefficient.

Compound	*c* / nM[a]	*MIC* / µM[b]	IC_{50} / µM[c]	*n*[d]
85	1000	2	29	1.0
86	500	15	31	1.9
87	1000	3	32	1.0
89	500	24	165	0.6
90	500	250	550	4.0
91	500	450	550	5.4
92	500	0.3	14	1.2
93	500	> 100	> 100	-
224	500	> 33	> 33	-
14	250	870	3600	1.5

Several of the tested inhibitors were found to inhibit the uptake of OPS **218**, the best being hypervalent iodine reagent **92** with a sub-micromolar MIC of 0.3 µM and an IC_{50} of 14 µM. **92** being an irreversible inhibitor of thiols,[118] its good activity hints towards a redox regulation in disulfide-containing proteins, with disulfides being in equilibrium with vicinal dithiols and this equilibrium being shifted by trapping of the thiols (see Figure 64). Substantial inhibition was also obtained with highly reactive COCs like BPS pentasulfide **87**, ETP tetrasulfide **85** and ETP disulfide **86**, as well as inorganic polysulfide **89**. Other, less reactive disulfides like AspA **91** and DTNB **14** still inhibited OPS uptake, but to a lesser extent. Cyclic thiosulfonates like **90** were rather poor inhibitors, and ebselen analog **93** and linear thiosulfonate MMTS **224** were inactive.

It is important to note that comparing the inhibition of OPS uptake with that of fluorescent ETP **61** revealed an overall positive correlation of MICs, with some outliers (Figure 63, B).[111,117] Similar results were previously obtained comparing the inhibition of uptake of **61** and **71**, with some inhibitors performing

better against one or the other. Whilst correlations can be made from the reactivity of the different inhibitors, the presence of outliers supports the existence of multiple targets for different transporters, which operate *via* similar mechanisms. For example, proteomics analysis previously revealed the transferrin receptor TfR as a target for AspA,[104,105] but not for ETP.[111] Overall, the correlation observed here for OPS **218** and ETP **61** might imply that the proteins known to account for OPS uptake may also be responsible for that of COCs. SCARB1, for example, was identified as one of the targets of AspA, and is also involved in OPS uptake.[232] Similarly, proteins such as TfR, EGFR, integrins or CLIC are involved in both uptake processes, hinting towards thiol-mediated uptake taking place in all the cases and being a unifying mechanism responsible for cell entry of such compounds.

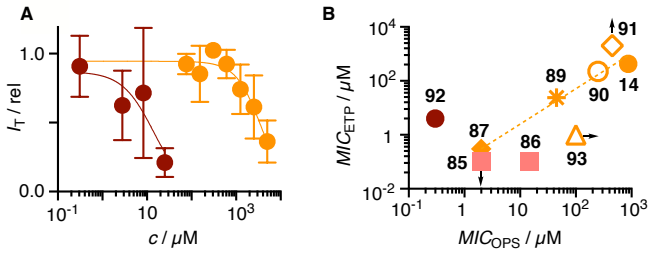

Figure 63. A) Dose-response curves for **92** (brown) and **14** (orange) fitted to the Hill equation; B) Comparison of MICs against OPS **218** and ETP **61** (upward and rightward arrows: MIC > c_{max}; downward arrow: MIC < c_{min}) with trend line.

The good inhibition of OPS **218** uptake with thiol-mediated uptake inhibitors is a first indication that thiol-mediated uptake plays a role in the cell entry of **218**. We then sought to investigate the dynamic covalent chemistry of phosphorothioates to further understand the uptake process on the molecular level.

3.4.3. Dynamic Covalent Chemistry of the Phosphorothioate Moiety

3.4.3.1. Interaction Between a Model Phosphorothioate and Cysteine Disulfides

From the significant inhibition with thiol-mediated uptake inhibitors and the existence of disulfide-rich membrane proteins as targets for the uptake of OPS, the mechanism in Figure 64 was proposed.

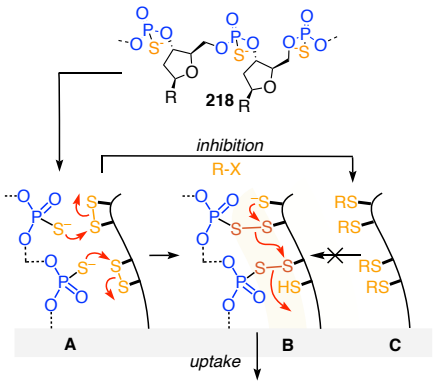

Figure 64. Proposed mechanism of the dynamic covalent exchanges taking place for the thiol-mediated uptake of OPS. A) OPS **218** reacts with cysteine disulfides in transmembrane proteins to form B) a pseudo-disulfide network responsible for the interaction with the targets. C) The process is inhibited by thiol-mediated uptake inhibitors.

To account for the interaction between OPS and disulfide-rich protein targets, pseudo-disulfide exchanges were hypothesized to take place between phosphorothioates and cysteine disulfides (Figure 64, A, B). To study the occurrence of such dynamic covalent chemistry, the system was simplified by the use of 5'-AMPS **225**, a monomer of nucleoside bearing a single phosphorothioate moiety. Whereas the formation of pseudo-disulfide has been described with activated disulfides,[238,241] the reaction with cysteine-based disulfides was not, and was investigated by HPLC-MS (Figure 65).

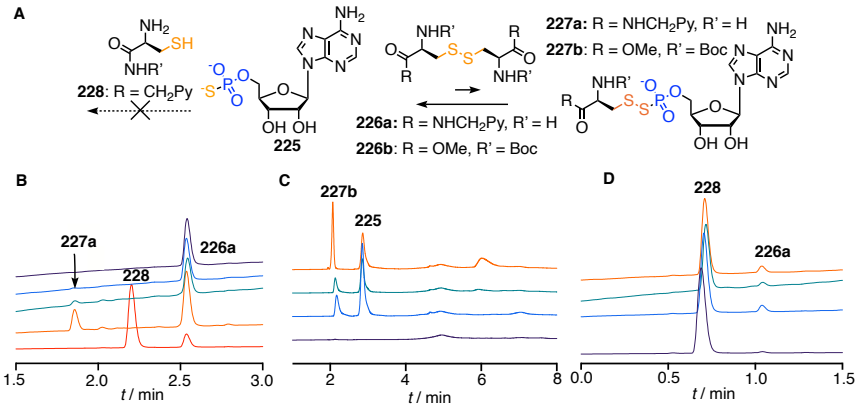

Figure 65. A) Reaction of 5'-AMPS **225** with two cystine derivatives **226a**/**b** and reduced cysteine **228**; B) Normalized HPLC chromatograms of **226a** (purple) and of **226a** with 1.0 (blue), 10 (green) and 100 (orange) equiv. of **225**, and of 100 equiv. of **225** on **226a** after addition of 100 equiv. of TCEP (red); C) Normalized HPLC chromatograms of **226b** (purple) and of **225** with 1.0 (blue), 10 (green) and 100 (orange) equiv. of **226b**; D) Normalized HPLC chromatograms of **228** (purple) and of **228** with 1.0 (blue), 10 (green) and 100 (orange) equiv. of **225**.

Following the UV signal of the pyrene-containing cystine derivative **226a** (synthesized by Dr. Naomi Sakai) with increasing amounts of **225**, a new peak corresponding to a more polar compound was observed, with an ESI-MS signal matching the mass of the pseudo-disulfide **227a** (Figure 65, B). Upon incubation of **227a** with 100 equiv. of TCEP, it got converted into the reduced cysteine **228**, confirming the formation of a redox sensitive bond. The same was true for another cystine derivative, **226b**, where the titration was performed in the opposite way, with increasing amounts of **226b** added to **225** (Figure 65, C). However, when reacting **225** with reduced cysteine **228**, no reaction was observed, confirming the preferential exchange of phosphorothioates with disulfides, and not with thiols (Figure 65, D).

The formation of pseudo-disulfides with inactivated cysteine disulfides similar to the ones found in transmembrane proteins goes in favor of the

mechanism proposed in Figure 64. Despite the equilibria being greatly shifted towards the phosphorothioate side, multivalency in OPS can account for the good binding of OPS to their target by multiple pseudo-disulfide bridge formations, as shown for other systems.[109,110,115]

3.4.3.2. Pseudo-Disulfide Formation with Activated Disulfides and Analogs

To further study the dynamic covalent chemistry of the phosphorothioate moiety and how it could influence cellular uptake, we investigated the dynamic exchange of **225** with several activated disulfides and analogs.

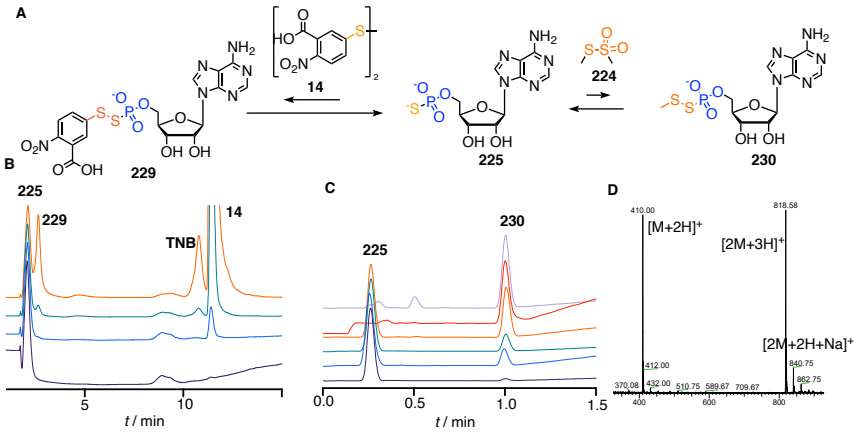

Figure 66. A) Reaction of 5'-AMPS **225** with activated disulfide **14** and MMTS **224**; B) Normalized HPLC chromatograms of **225** with 0.1 (purple), 1.0 (blue), 10 (green) and 100 (orange) equiv. of **14**; C) Normalized HPLC chromatograms of **225** with 0.1 (purple), 0.2 (blue), 0.5 (green), 1.0 (orange), 4.0 (red) and 10 (lavender) equiv. of **224**; D) ESI-MS spectrum of exchange product **230**.

The exchange of **225** with DTNB **14** was reported in literature and could be reproduced, following the appearance of exchange product **229** by HPLC-MS rather than UV spectroscopy (Figure 66, A, B).[238] Similarly, **225** reacted with MMTS **224**, which is known to transfer thiomethyl groups on thiols efficiently, and the reaction was complete with only four equivalents of MMTS (Figure 66,

A, C, D). This equilibrium was much more favorable than with non-activated cystine derivatives. The formation of the pseudo-disulfide products was confirmed by HRMS.

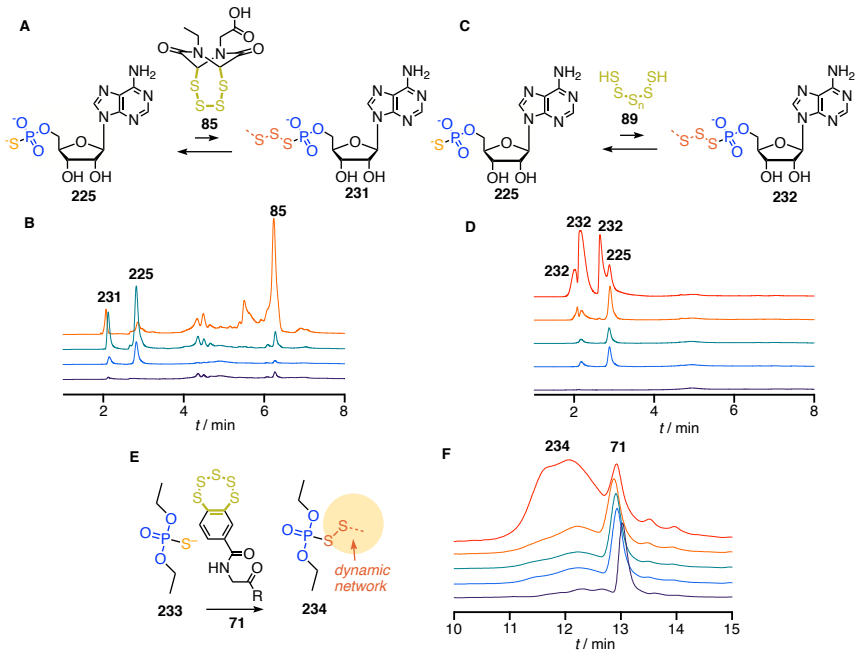

Figure 67. A) Reaction of 5'-AMPS **225** with ETP tetrasulfide **85**; B) HPLC chromatograms of **85** (purple) and of **225** with 1.0 (blue), 10 (green) and 100 (orange) equiv. of **85**; C) Reaction of 5'-AMPS **225** with inorganic polysulfides **89**; D) HPLC chromatograms of **89** (purple) and of **225** with 1.0 (blue), 10 (green), 100 (orange) and 1000 (red) equiv. of **89**; E) Reaction of O,O'-diethylthiophosphate **233** with fluorescent BPS **71**; F) Normalized HPLC chromatograms of **71** (purple) and of **71** with 0.5 (blue), 1.0 (green), 10 (orange) and 100 (red) equiv. of **233**.

225 was also found to exchange with polysulfides like ETP tetrasulfide **85** and inorganic polysulfides **89** (Figure 67, A – D) to form a dynamic library of pseudo-polysulfides **231**-**232**.[114] However, such pseudo-polysulfides could only be observed by HPLC but were not identified by ESI-MS, most likely because

the species formed are too transient to be isolated due to the high reactivity of polysulfide networks. Similarly, O,O-diethylthiophosphate **233** was found to trigger the emergence of a dynamic polysulfide network from BPS **71**, described previously only with thiols.[114]

3.4.3.3. Activation of Uptake and Apparent Endosomal Escape

Having determined that pseudo-disulfides can be formed on phosphorothioates, their effect on the cellular uptake process was investigated. By preactivating OPS **218** with potential activators, more protein targets could possibly be reached, including thiol- rather than disulfide-containing proteins, thus improving the cell penetration abilities of OPS (Figure 68, D – E).

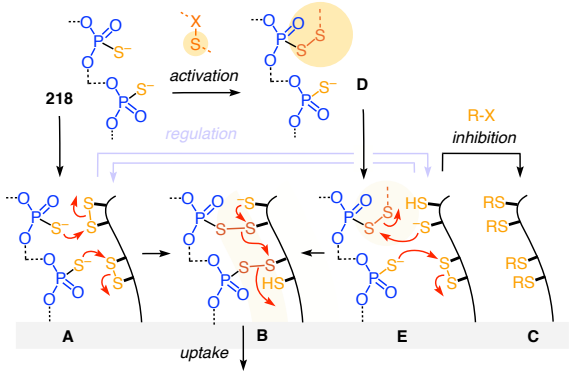

Figure 68. A proposed mechanism for the cellular uptake of inactivated (A – C) and pseudo-disulfide activated OPS **218** (D – E).

To activate the uptake *in situ*, OPS **218** was incubated for 30 min with various concentrations of potential activators **85**, **87**, **89**, **90**, **93**, **14** and **224**, followed or not by purification by centrifugal filtration through membrane filters with the appropriate molecular weight cut-off. In all cases, an increase of fluorescence was observed with the tested activators (Figure 69), as compared to the non-modified OPS **218**, with up to 1.7-fold increase with **85**, **89** and **93**.

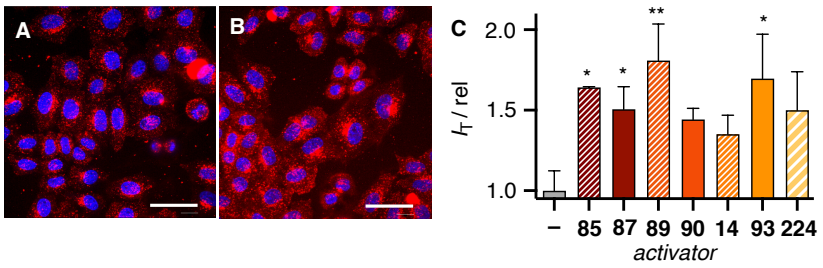

Figure 69. CLSM images of HeLa Kyoto cells after 2 h incubation at 37 °C with A) 500 nM non-modified OPS **218** and B) 500 nM **218** activated with 500 µM **85**, PBS pH 7.4, 30 min, 25 °C, followed by centrifugal filtration, scale bar = 50 µm. C) HCHT data showing normalized average fluorescence intensity in the whole cell I_T for OPS **218** activated with **85** (500 µM with purification after activation), **87** (500 µM with purification), **89** (25 µM), **90** (20 µM), **14** (500 µM), **93** (50 µM) and **224** (50 µM), divided by fluorescence intensity per cell I_0 of non-activated OPS **218**. Data are average values from > 2 sets of experiments ± SEM and analyzed by one-way ANOVA compared to that without activation (* $P < 0.033$; ** $P < 0.0021$).

Added as mixtures without purification, the uptake of OPS increased with increasing concentrations of activators up to a concentration close to the MIC. Over this threshold, leftover activator started to inhibit uptake, creating a competition between activation and inhibition. In most cases, the removal of excess activators was beneficial because it prevented this competition (Figure 70). As observed by HPLC-MS, with most of these activators, relatively stable pseudo-disulfide phosphorothioates derivatives could be observed and isolated, except with **85** and **89**. It therefore makes sense that purification by centrifugal membrane filtration is not detrimental to the activation, the preactivated OPS mixtures being stable enough.

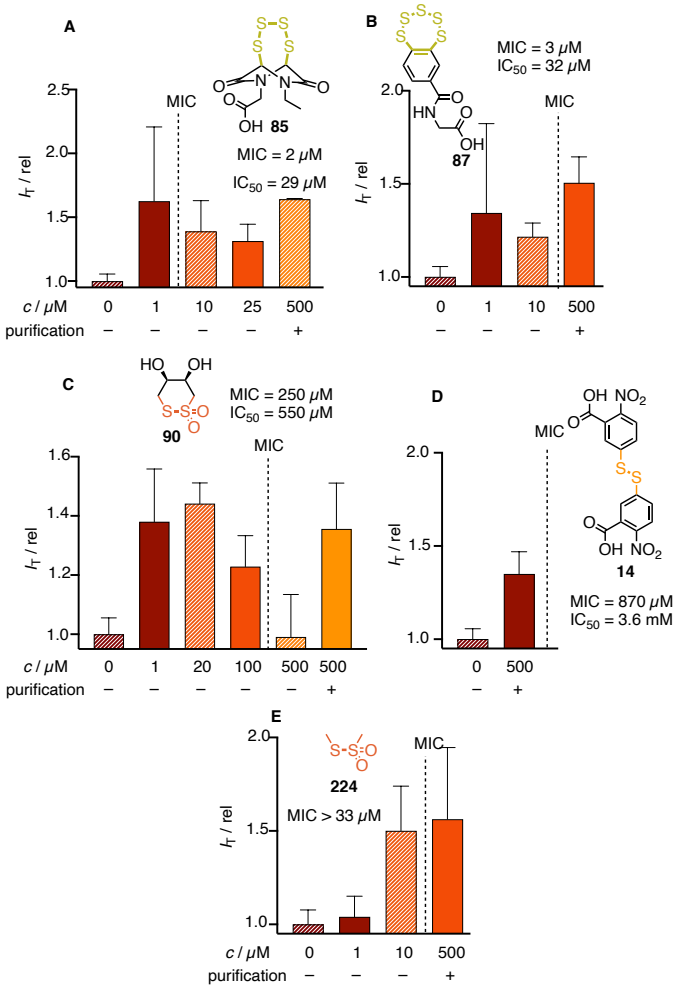

Figure 70. Automatically analyzed HCHT data showing the relative fluorescence intensity I_T in HeLa Kyoto cells after 2 h incubation at 37 °C with OPS **1** (500 nM) activated with different concentrations of **85** (A), **87** (B), **90** (C), **14** (D) and **224** (E) with or without purification.

On the other hand, with activators **89** and **93**, activation was partially lost upon purification (Figure 71). In accordance with what was observed by HPLC for the reaction of 5'-AMPS with **89** (Figure 67, C, D), the transient nature of the

activated OPS makes it too unstable to be purified, and only transient activation can be performed. The same was true with ebselen **93** which should form a highly reactive pseudo-selenosulfide when reacted with OPS **218**.

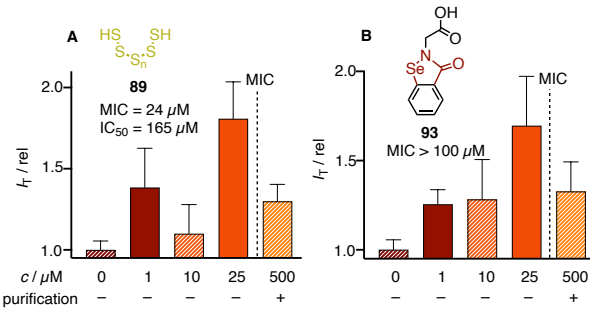

Figure 71. Automatically analyzed HCHT data showing the activation of OPS **218** (500 nM) activated with different concentrations of **89** (A) and **93** (B) with or without purification.

When looking at the sub-cellular localization of OPS after cellular uptake, they are usually in early and late endosomes within 10 to 50 min and in lysosomes afterwards, their activity starting to be observable only after several hours, indicating that endosomal escape is relatively slow.[121] Upon OPS activation, a more diffuse fluorescence was observed in CLSM images (Figure 69, A, B). To confirm this, more precise image analysis was performed by Dr. Dimitri Moreau, to segment the punctate structure that should correspond to endosomes. First, a *top-hat* transformation was performed on the red channel image to facilitate the segmentation of the dotted structures (Figure 72, A, B). Then a mask based on the detected dots was applied to extract the integrated and average fluorescence intensities within the mask (Figure 72, C, D). The data extracted from the "dots" mask was then treated as described above for the whole cell, and both were compared. All data showed in Figure 70 and Figure 71 were I_T, average fluorescence intensity extracted from the "whole cell" mask.

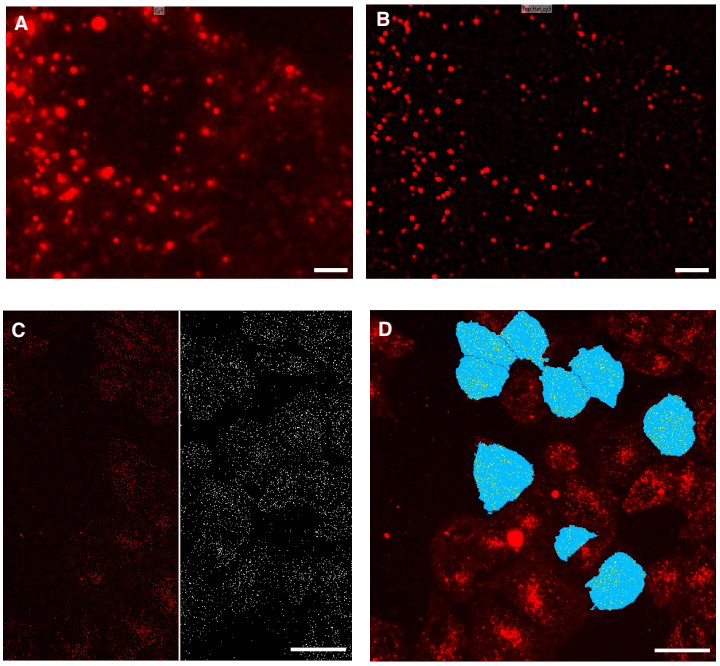

Figure 72. *Top-hat* transform (B) of the red channel image (A), zoomed in, scale bar = 3.5 µm; C) Segmentation of the dotted structures based on the *top-hat* transformation, scale bar = 30 µm; D) Final mask applied on the cells, blue = whole cell, yellow = dots, scale bar = 30 µm.

When using this segmentation to plot the average fluorescence intensity within the "dots" mask, I_M, upon preincubation with **85** almost no difference in I_M was found as compared to I_T (Figure 73, A). The same was true for all other activators for which this analysis was performed (Figure 73, B). Such differences of intensity within the different masks indicated that the increase of fluorescence observed with the different activators is correlated with a more diffuse, cytosolic localization.

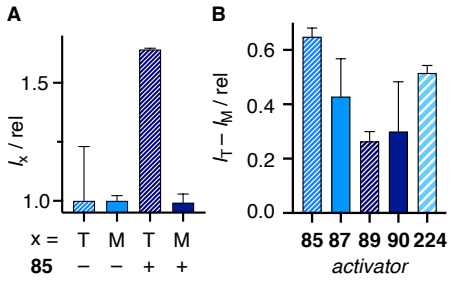

Figure 73. A) Normalized fluorescence intensity in whole cells I_T vs. in punctate dots I_M of OPS **218** (500 nM) activated with **85** (500 µM with purification, dark blue) as compared to non-activated **218** (500 nM, light blue). B) Difference I_T–I_M for OPS **218** activated with **85**, **87**, **89**, **90** and **224**.

It can therefore be concluded that the activation of OPS **218** as pseudo-disulfides does induce a shift of reactivity towards transmembrane proteins responsible for their uptake, including also thiol-containing proteins. This activation leading to more cytosolic uptake, it implies that either direct translocation, either endosomal escape happens, in both cases resulting in an increasing amount OPS in the cytosol. To further confirm that this would correlate with activity, a functional assay reporting on oligonucleotide uptake and availability should be used, which was beyond the scope of this study.

3.4.4. Conclusions and Perspectives

To summarize this final chapter, it was showed herein that oligonucleotide phosphorothioates (OPS) enter cells *via* thiol-mediated uptake. Despite a good understanding of the biology of OPS, with several protein targets being identified as responsible for their uptake, the precise molecular mechanisms by which this uptake occurs remained elusive. Using a combination of HPLC and high-content high-throughput microscopy, it was showed that dynamic covalent chemistry taking place on the phosphorothioate moiety was key to the uptake, by the formation of pseudo-disulfide in membrane proteins. Taking advantage of this

chemistry to preactivate OPS, their uptake increased by about 70%, seemingly bypassing entrapment in endosomes, which should lead to better activities.

In terms of perspectives, the findings of this project can be developed in two main directions. First, knowing that OPS enter cells by thiol-mediated uptake, and several protein targets of OPS being known, it would be of interest to study if the same proteins are involved in the thiol-mediated uptake of the synthetic transporters developed in our group, whether it is COCs or CPDs. Such experiments are ongoing in our lab, first looking at Stabilin-1 and -2, two of the targets of OPS. Then, because the post-synthetic chemistry, especially the dynamic covalent character of the phosphorothioate moiety, were so far underexplored, synthesizing small-molecule mimics of OPS is also of interest. The synthesis of monomers and dimers of phosphorothioates, as well as cyclic pseudo-disulfides based on phosphorothioate, is ongoing and their uptake ability will be measured and compared to other COC transporters.

In the general outline of this thesis, the identification of thiol-mediated uptake as being responsible for OPS entry in cells is of great importance. Whereas some natural systems like the diphtheria toxin or the HIV virus have been shown to enter cells in a thiol-dependent manner, little attention has been given to these by the scientific community. On the contrary, phosphorothioates are among the most popular DNA modifications, from fundamental research to clinics. We hope the results presented here highlight the need for understanding molecular principles responsible for desirable biological properties, and shine a new light on thiol-mediated uptake as a practical way to enter cells.

Chapter 4

CONCLUSIONS AND PERSPECTIVES

In this thesis, the efforts were focused on improving the understanding of thiol-mediated uptake mechanism.

In the first section, the dynamic covalent exchanges between thiolates and cyclic disulfides and diselenides was reported. Started to answer a curiosity question on the structure of poly(disulfide)s obtained by ring-opening polymerization of lipoic acid derivatives, this project gave valuable information about the mechanism of uptake of cyclic dichalcogenides. It was observed that the ring opening reaction was initially regioselective, followed by a fast isomerization to equilibrate between the primary and secondary chalcogen atoms. This observation led to the conclusion that poly(disulfide)s obtained by ring-opening polymerization were regio-irregular, the rearrangement being faster than the addition of another monomer. More importantly, it led to the hypothesis that cyclic dichalcogenides could penetrate cells *via* a molecular walker mechanism, performing cascade dynamic covalent exchanges with neighboring vicinal dithiols and disulfides in cysteine-rich membrane proteins. This model being just a hypothesis so far, one could envision several ways to prove that it does occur. For example, disulfide tracks mimicking those present in possible targets could be synthesized, with a dithiol initiator and a thermodynamic trap on both ends (Figure 74, A). Alternatively, a vesicle-based thiol-mediated uptake model was envisioned, with thiols embedded at the surface, and disulfide-containing lipids in the membrane, with a streptavidin-based detection system encapsulated (Figure 74, B).

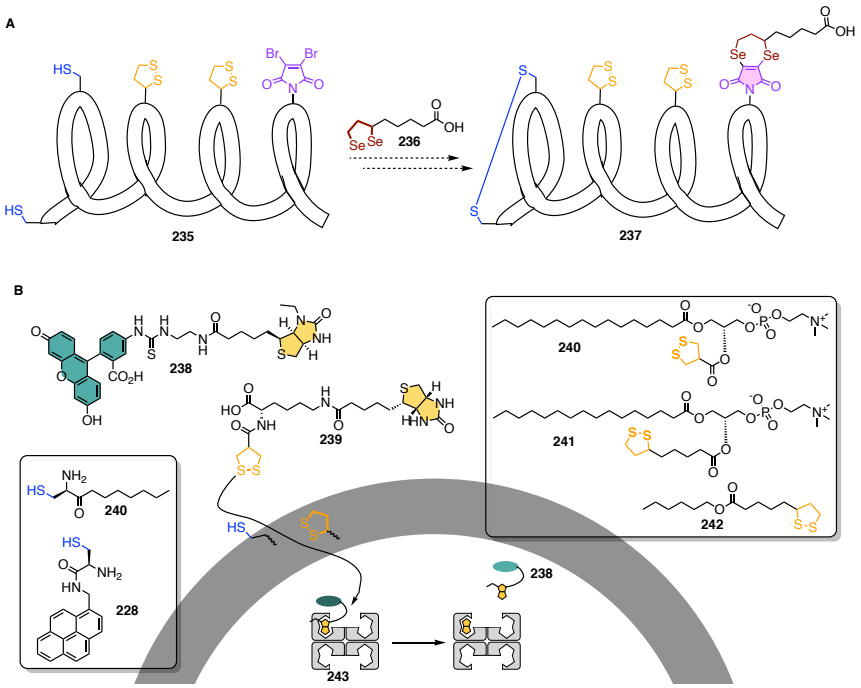

Figure 74. A) A possible disulfide track **235** to prove the 1,2-diselenolane walker hypothesis. B) A vesicle-based thiol-mediated uptake model. Cysteine derivatives **240**/**228** at the vesicle surface initiate the opening of a biotinylated AspA **239**, which then "walks" on disulfide-containing lipids **240**-**242**. Detection is achieved with a complex of ethyl-biotin FITC **238** and streptavidin **243**, showing increase of fluorescence upon uptake by dequenching of FITC.

Then, the lessons learned from this first project were applied to the cascade ring-opening oligomerization of 1,2-dithiolanes and 1,2-diselenolanes. Using orthogonal dynamic covalent chemistries on a helical peptide template, disulfide- and diselenide-containing monomers were loaded, polymerized, and released from the template sequentially. The templation efficiency depended highly on the reaction parameters, especially the helicity of the peptide template, with the three-dimensional structure being the most important. This proof-of-concept can be developed in multiple directions. First, because the monomers are loaded and the polymers detached by hydrazide/hydrazone/oxime dynamic covalent

chemistry, many other monomers can be envisioned without changing the template. For example, thiosulfonates are emerging as interesting dynamic covalent exchangers for transport and inhibition of thiol-mediated uptake, and could be of interest (Figure 55, A). Because up to four dynamic covalent bonds can be exchanged in an orthogonal fashion,[243] sequence-controlled oligomers could be envisioned (Figure 55, B). The 3_{10}-helix peptide templates used for this project have been shown to insert well in lipid membranes. Preliminary results showed that cascade ring-opening polymerization could take place through a lipid bilayer, performing artificial signal transduction, and need to be confirmed and further studied.

Thiol-mediated uptake was then applied to deliver Gram+ only antibiotics into Gram– bacteria. Although no activation of antibiotic activity was observed in Gram– bacteria, the observation that conjugation with cyclic oligochalcogenides inhibited antibacterial action was of interest. It showed that thiol-mediated uptake is anything but trivial, although applicable to various mammalian cell lines. This encourages to look for potential protein targets of various transporters in a systematic way, to better understand the mechanisms by which thiol-mediated uptake operates. This can be envisioned performing proteomics studies similar to the one performed for asparagusic acid, but not only. Systematic knockdown of a large variety of proteins, for example screening siRNA libraries, and measuring the impact of these knockdown on the uptake of fluorescently-labelled transporters using HCHT microscopy assays could be the best way to proceed.

Finally, the last chapter of this thesis introduced the study of oligonucleotide phosphorothioates for thiol-mediated uptake. Using a combination of fluorescent microscopy and HPLC-MS studies on a model compound, it was showed that OPS enter cells by thiol-mediated uptake, performing dynamic covalent exchanges with disulfide-rich membrane proteins. Taking advantage of this chemistry, the cytosolic delivery of OPS could be improved, seemingly

bypassing endocytosis. Several targets of OPS are known, for example stabilins, but have not been considered as targets for other thiol-mediated uptake transporters. Our group is currently investigating the influence of stabilin overexpression on the uptake of fluorescently-labelled thiol-mediated uptake transporters. Similar studies could be envisioned with other known targets of OPS to continue mapping the different pathways by which thiol-mediated uptake operates. Alternatively, small-molecule mimics of OPS could be synthesized and evaluated for their possible thiol-mediated uptake or inhibition (Figure 75, A). Biotinylated OPS could also be envisioned to couple their uptake with biotin-streptavidin biotechnology, using the OPS as both the transporter and, eventually, a targeting agent to bring streptavidin in desired subcellular localizations (Figure 75, B).

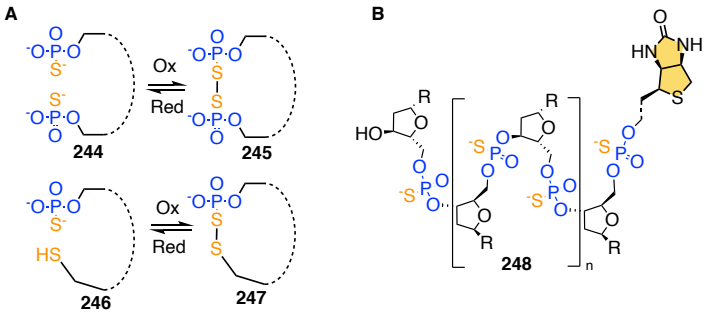

Figure 75. A) Small-molecular phosphorothioates for thiol-mediated uptake or inhibition. B) Biotinylated OPS to use with biotin-streptavidin biotechnology.

When it comes to perspectives of thiol-mediated uptake in general, two axes can be pursued to develop it as a more widely used technique. First, because of the somewhat lengthy syntheses of both poly(disulfide)s as well as the best cyclic oligochalcogenides, it remains a niche field and is not readily available for cell biologists to use. Developing straightforward bioconjugation methods, preferably bioreversible to release the native cargo inside the cells, compatible with the chemistry of thiol-mediated uptake transporters would be a large step

forward to democratize it. Then, with easier-to-use thiol-mediated uptake systems, following studies could focus on their *in vivo* applications, to confirm their usefulness in clinically-relevant settings. So far, very limited results have been reported in animal models, but bear promises. Thiol-mediated uptake is still a young field, and future developments will be of great interest to bring it to a new dimension.

Chapter 5

EXPERIMENTAL SECTION

5.1. General

5.1.1. Reagents, Solvents, and Equipment

As in references, reagents for synthesis and analysis were purchased from Fluka, Sigma-Aldrich, TCI, Acros, Alfa Aesar, Apollo Scientific, Iris Biotech or Life Technologies. Amino acid derivatives were purchased from Novabiochem and Bachem. Buffers and salts of the best grade available from Fluka or Sigma-Aldrich were used as received. Phosphate buffered saline (PBS, pH = 7.4), DMEM (GlutaMAX, 4.5 g/L D-glucose, with phenol red) medium, FluoroBrite DMEM (high D-Glucose) medium, Penicillin-Streptomycin, Fetal Bovine Serum, TrypLE Express Enzyme were obtained from Thermo Fisher Scientific. μμ-Plate 96-Well were obtained from Ibidi. Hoechst 33342 (10 mg/mL solution in water) was obtained from Invitrogen by Thermo Fisher Scientific.

Organic solvents used for synthesis and experiments were of HPLC or reagent grade purity. Organic solvents such as acetonitrile, dichloromethane, diethyl ether or tetrahydrofuran were purified using a solvent purification system from Solv-tek. Buffer solutions were prepared using bidistilled water.

All reactions were carried out with magnetic stirring and, if specified, under nitrogen atmosphere. Solvents were evaporated using rotavapor R-210 from Büchi equipped with a vacuum controller V-850, a pump V-700 and a heating bath B-491 from Büchi.

Glassware used for synthesis or experiments was washed with soap solution, demineralized water and acetone and dried in an oven. Bidistilled water was used for cell culture, experiments and cleaning.

5.1.2. Compound Purification and Characterization

As in references. Normal phase column chromatography was carried out on Biotage Isolera™ Dalton 2000 with APCI detector using Biotage® SNAP, Claricep® or BGB Scorpius® columns, or on silica gel (SilicaFlash® P60, SILICYCLE, 230–400 mesh). Reverse phase chromatography was performed using Biotage® SNAP, Claricep® or BGB Scorpius® C_{18} columns. Semi-preparative HPLC was performed using JASCO LC-2000 Plus system equipped with a quaternary pump (JASCO PU-2089), a Jupiter 4 μm Proteo 90 A 250 x 10.0 mm column, and a UV/Vis detector (JASCO UV-2077 Plus) with an elution gradient CH_3CN/H_2O with 0.01% TFA indicated for each purification, at a flow rate of 3.0 mL/min. Gradients are reported as [percentage of CH_3CN, time]. Retention times R_t are reported in minutes. Analytical thin-layer chromatography (TLC) was performed on silica gel 60 F_{254} (Merck).

All ^1H and ^{13}C spectra were recorded (as indicated) on Bruker 300 MHz, 400 MHz or 500 MHz spectrometers and are reported as chemical shifts (δ) in ppm relative to TMS ($\delta = 0$). Spin multiplicities are reported as a singlet (s), doublet (d), triplet (t) and quartet (q) with coupling constants (J) given in Hz, or multiplet (m). Broad peaks are marked as br. ^1H and ^{13}C resonances were assigned with the aid of additional information from 1D and 2D NMR spectra (H,H-COSY, DEPT-135, HSQC and HMBC).

LCMS were recorded using a Thermo Scientific Accela HPLC equipped with a Thermo C_{18} Hypersil GOLD column (50 × 2.1 mm, 1.9 μm particles size) coupled with a LCQ Fleet three-dimensional ion trap mass spectrometer (ESI, Thermo Scientific) with a linear elution gradient from 95% H_2O / 5% CH_3CN + 0.1% TFA to 10% H_2O / 90% CH_3CN + 0.1% TFA in 4.0 minutes at a flow rate

of 0.75 mL/min (method B5) or 70% H_2O / 30% CH_3CN + 0.1% TFA to 10% H_2O / 90% CH_3CN + 0.1% TFA in 4.0 minutes at a flow rate of 0.75 mL/min (method B30) or 40% H_2O / 60% CH_3CN + 0.1% TFA to 10% H_2O / 90% CH_3CN + 0.1% TFA in 4.0 minutes at a flow rate of 0.75 mL/min (method B60). Retention times are reported in minutes and ESI-MS are reported as mass-per-charge ratio *m*/*z* (intensity in %, [assignment]).

ESI-HRMS was measured on Xevo G2-S Tof (Waters). All mass data are reported as mass-per-charge ratio *m/z* calculated and observed. MALDI-TOF analysis was performed on Axima CFR$^+$ (Shimadzu) in reflectron mode and is reported as mass-per-charge ratio *m*/*z* calculated and observed.

$[\alpha]_D^{20}$ values were recorded on a Jasco P-1030 Polarimeter using a sodium lamp (λ = 587 nm) in a quartz cell of 10 cm length at 20 °C.

Melting points (Mp) were measured on a Melting Point M-565 (Büchi).

IR spectra were recorded on a Perkin Elmer Spectrum 100 FT-IR spectrometer (ATR, Golden Gate) and are reported as wavenumbers υ in cm^{-1} with band intensities indicated as s (strong), m (medium), w (weak), br (broad).

Circular dichroism spectra were measured on a JASCO J-815 spectropolarimeter and are reported as extremum wavelengths λ in nm ($\Delta\varepsilon$ in $M^{-1}.cm^{-1}$).

5.1.3. Equipment in Experiments

Micropipettes Vaudoux-Eppendorf (Switzerland) calibrated for volumes 0-10 µL, 20-200 µL and 100-1000 µL were used to prepare aqueous solutions. Volatile solvents were dosed with glass syringes from Hamilton (Bonaduz, Switzerland) equipped with steel needles or with graduated pipettes.

Fluorescence cellular imaging was performed using an IXM-C automated microscope from ImageXpress equipped with a Lumencor Aura III with 5 independently selectable solid-state light sources, bandpass filters and 5

objectives (4x to 60x). Sample preparation and washing on 96-well plates was performed using a Plate washer Biotek EL406®.

5.1.4. Cell Culture

Human cervical cancer-derived HeLa Kyoto cells were cultured in DMEM (GlutaMAX, 4.5 g/L D-glucose, with phenol red) medium containing 10% fetal bovine serum (FBS) and 1% Penicillin/Streptomycin (Pen/Strep). The cells were grown at 37 °C under 5% CO_2 on a 25 cm^3 tissue culture flask (TPD Corporation). Cells were detached by treatment with 1.5 mL of TrypLE Express at 37 °C for 5 min, followed by the addition of 6 mL of DMEM (GlutaMAX, 4.5 g/L D-glucose, with phenol red) medium at 37 °C. The cells were resuspended in DMEM (GlutaMAX, 4.5 g/L D-glucose, with phenol red) medium and plated according to the concentration needed.

5.1.5. Bacterial Cell Culture

Bacterial strains used in the present study (Gram-positive: *B. subtilis* (BS), Gram-negative: *E. coli* DH5a (EC)) were grown at 37°C in lysogeny broth medium (sterilized by autoclaving at 121 °C for 15 min). MIC values were determined by using the twofold serial dilution technique in 96-well plates. The concentration of the initial dilution was 10 or 50 μM for Gram-positive bacteria and 50 or 100 μM for Gram-negative bacteria, a total of 6 two-fold dilutions were performed and all experiments were conducted in triplicate. Bacteria growth was followed in a kinetic mode by measuring optical density at 600 nm using a Spectra Max i3. The MIC value was taken to be the lowest concentration that inhibited visible growth of the microorganism after 24 h at 37 °C.

5.2. Synthesis

5.2.1. Synthesis of 1,2-Dithiolane and Diselenolane

Compound 22 was synthesized according to a procedure described in reference.[129]

Compound 96. Diselenolipoic acid (150 mg, 0.50 mmol) was dissolved in dry MeOH (80 mL) under nitrogen. Concentrated sulfuric acid (0.20 mL, 3.7 mmol) was added and the reaction mixture was stirred at rt for 16 h. The reaction mixture was concentrated to ~ 5 mL, diluted with EtOAc (50 mL) and washed with water (2 x 50 mL), then brine (50 mL). The organic layer was dried over Na_2SO_4, filtered and concentrated under reduced pressure to yield **96** as a dark orange oil (155 mg, 99%). R_f (CH_2Cl_2): 0.67; IR (neat): 3289 (br), 2925 (m), 2853 (m), 1734 (s), 1659 (m), 1545 (s), 1435 (m), 1362 (s), 1195 (m), 1171 (m), 1007 (s); ^{1}H NMR (400 MHz, $CDCl_3$): 3.97 – 3.83 (m, 1H), 3.66 (s, 3H), 3.31 (t, $^3J_{H\text{-}H}$ = 6.2 Hz, 2H), 2.99 – 2.93 (m, 1H), 2.55 – 2.46 (m, 1H), 2.32 (t, $^3J_{H\text{-}H}$ = 7.4 Hz, 2H), 1.88 – 1.61 (m, 4H), 1.52 – 1.38 (m, 2H); ^{13}C NMR (101 MHz, $CDCl_3$): 174.0 (C), 52.7 (CH), 51.7 (CH_3), 45.8 (CH_2), 35.5 (CH_2), 33.9 (CH_2), 29.9 (CH_2), 29.5 (CH_2), 24.7 (CH_2); HRMS (MALDI-TOF, HCCA 10 mg/mL, +ve) calc. for $C_9H_{16}O_2Se_2$: 315.9478, found: 315.9502.

5.2.2. Synthesis of Peptide Backbones

Compound 123 was prepared following a reported procedure.[244]

Compound 125. To a solution of **124** (1.51 g, 3.50 mmol), HBTU (2.01 g, 5.30 mmol) and DIPEA (1.23 mL, 7.10 mmol) in DMF (20 mL) was added **123** (1.10 g, 3.50 mmol) and the reaction mixture was stirred at rt for 1 h. The crude reaction mixture was diluted with EtOAc (150 mL), washed with aq. $NaHCO_3$ (sat. 3 x 150 mL) and brine (3 x 150 mL), dried over Na_2SO_4 and concentrated *in vacuo*. The crude product was purified by flash column chromatography (Biotage® SNAP Ultra 20 g, 40 mL/min, linear gradient 0 – 10% MeOH in

CH_2Cl_2) to yield **125** as a colorless solid (1.80 g, 83%). R_f (CH_2Cl_2 + 10% MeOH): 0.61; IR (neat): 3321 (br), 2981 (w), 2941 (w), 1693 (s), 1520 (s), 1450 (m), 1388 (w), 1366 (w), 1251 (s), 1157 (s), 1024 (w), 760 (w), 742 (w); $[\alpha]_D^{20}$ –1.24 (*c* 1.00, EtOH); ^{1}H NMR (300 MHz, $CDCl_3$): 7.73 (d, $^3J_{H\text{-}H}$ = 7.5 Hz, 2H), 7.56 (d, $^3J_{H\text{-}H}$ = 7.4 Hz, 2H), 7.36 (t, $^3J_{H\text{-}H}$ = 7.4 Hz, 2H), 7.30 – 7.23 (m, 2H), 6.96 (s, 1H), 6.32 – 6.17 (m, 2H), 4.34 (d, $^3J_{H\text{-}H}$ = 7.3 Hz, 2H), 4.20 – 4.08 (m, 2H), 3.68 (s, 3H), 3.62 – 3.51 (m, 2H), 1.52 (s, 9H), 1.48 (s, 3H), 1.43 (s, 9H); ^{13}C NMR (75 MHz, $CDCl_3$): 175.4 (C), 173.5 (C), 170.4 (C), 157.8 (C), 156.3 (C), 143.8 (C), 143.7 (C), 141.2 (C), 127.7 (CH), 127.1 (CH), 125.1 (CH), 120.0 (CH), 80.6 (C), 67.2 (CH_2), 57.1 (C), 56.7 (CH), 56.3 (C), 52.5 (CH_3), 47.0 (CH), 42.4 (CH_2), 28.3 (CH_3), 25.7 (CH_3), 24.9 (CH_3), 24.7 (CH_3), 24.6 (CH_3).

Compound 126. To a solution of **125** (245 mg, 0.400 mmol) in CH_2Cl_2 (1.5 mL) was added TFA (1.5 mL), and the reaction mixture was stirred at rt for 20 min. The crude reaction mixture was precipitated with Et_2O/pentane (1:1, 50 mL), the precipitate was recovered, washed with Et_2O/pentane (1:1, 3 x 50 mL) and dried *in vacuo* to yield **126** as a colorless solid (239 mg, 97%). R_f (CH_2Cl_2 + 10% MeOH): 0.26; IR (neat): 3329 (br), 2850 (br), 1709 (m), 1667 (s), 1526 (s), 1446 (m), 1387 (w), 1367 (w), 1264 (m), 1181 (s), 1137 (s), 991 (w), 837 (w), 800 (w), 758 (m), 734 (s); $[\alpha]_D^{20}$ +8.90 (*c* 1.00, EtOH); ^{1}H NMR (300 MHz, $CDCl_3$): 8.40 (br, 2H), 8.27 (s, 1H), 7.70 (d, $^3J_{H\text{-}H}$ = 7.5 Hz, 2H), 7.53 (d, $^3J_{H\text{-}H}$ = 7.4 Hz, 2H), 7.34 (t, $^3J_{H\text{-}H}$ = 7.4 Hz, 2H), 7.34 (s, 1H), 7.23 (t, $^3J_{H\text{-}H}$ = 6.5 Hz, 2H), 6.81 (s, 1H), 4.39 (s, 1H), 4.33 – 4.16 (m, 2H), 4.09 (t, $^3J_{H\text{-}H}$ = 7.2 Hz, 1H), 3.75 (br, 2H), 3.64 (s, 3H), 1.46 (s, 3H), 1.44 (s, 6H), 1.39 (s, 3H); ^{13}C NMR (75 MHz, $CDCl_3$): 175.7 (C), 174.1 (C), 167.3 (C), 161.6 (q, $^2J_{C\text{-}F}$ = 37 Hz, C TFA), 158.0 (C), 143.5 (C), 143.5 (C), 141.2 (C), 127.8 (CH), 127.1 (CH), 125.1 (CH), 120.0 (CH), 116.0 (q, $^1J_{C\text{-}F}$ = 291 Hz, CF_3 TFA), 67.7 (CH_2), 57.4 (C), 56.6 (C), 53.8 (CH), 52.7 (CH_3), 46.8 (CH), 41.7 (CH_2), 24.7 (CH_3), 24.5 (CH_3), 24.2 (CH_3).

Compound 127. 125 (1.50 g, 2.46 mmol) was dissolved in a solution of Me_2NH in THF (2 M, 10 mL) and the reaction mixture was stirred at rt for 20 min. The solvent was removed *in vacuo* and the residue was dissolved in CH_2Cl_2 (1 mL) and precipitated with pentane (50 mL). The precipitate was recovered, washed with pentane (3 x 50 mL) and dried *in vacuo* to yield to yield **127** as a colorless solid (0.91 g, 96%). R_f (CH_2Cl_2 + 10% MeOH): 0.31; IR (neat): 3305 (br), 2983 (w), 2937 (w), 1665 (s), 1527 (s), 1455 (m), 1387 (m), 1302 (w), 1250 (m), 1162 (s), 1050 (w), 1025 (w), 870 (w), 760 (w); $[\alpha]_D^{20}$ –1.75 (*c* 1.00, EtOH); ^{1}H NMR (300 MHz, $CDCl_3$): 7.38 – 7.28 (m, 2H), 5.79 (d, $^3J_{H\text{-}H}$= 6.1 Hz, 1H), 3.97 (m, 1H), 3.67 (s, 3H), 3.16 (dd, $^3J_{H\text{-}H}$ = 12.4, 4.5 Hz, 1H), 2.85 (dd, $^3J_{H\text{-}H}$ = 12.4, 6.6 Hz, 1H), 2.01 (br, 2H), 1.50 (s, 3H), 1.48 (s, 3H), 1.46 (s, 6H), 1.41 (s, 9H); ^{13}C NMR (75 MHz, $CDCl_3$): 175.2 (C), 173.4 (C), 170.9 (C), 156.0 (C), 80.2 (C), 57.3 (C), 56.3 (C), 55.8 (CH), 53.4 (CH_2), 52.4 (CH_3), 43.5 (CH_2), 28.3 (CH_3), 25.9 (CH_3), 24.8 (CH_3), 24.5 (CH_3).

Compound 128. To a solution of **127** (389 mg, 1.00 mmol) and Et_3N (280 µL, 2.90 mmol) in H_2O/1,4-dioxane (1:1; 6 mL) at 0 °C was added AllocCl (160 µL, 1.50 mmol) dropwise. The reaction mixture was stirred at rt for 1 h, then diluted with H_2O (60 mL) and extracted with EtOAc (3 x 60 mL). The organic layer was washed with brine (100 mL), dried over Na_2SO_4 and concentrated *in vacuo* to yield **128** as a colorless solid (440 mg, 93%). R_f (CH_2Cl_2 + 1% MeOH): 0.21; IR (neat): 3330 (br), 2984 (w), 2942 (w), 1683 (s), 1512 (s), 1456 (m), 1386 (w), 1366 (m),1249 (s), 1153 (s), 1101 (w), 1047 (w), 993 (m), 929 (w), 850 (w), 734 (m); $[\alpha]_D^{20}$ –1.44 (*c* 1.00, EtOH); ^{1}H NMR (300 MHz, $CDCl_3$): 7.18 (s, 1H), 6.89 (s, 1H), 6.10 (s, 1H), 6.03 (s, 1H), 5.83 (ddt, $^3J_{H\text{-}H}$ = 16.9, 10.4, 5.6 Hz, 1H), 5.23 (d, $^3J_{H\text{-}H}$ = 16.9 Hz, 1H), 5.14 (d, $^3J_{H\text{-}H}$ = 10.4 Hz, 1H), 4.50 (d, $^3J_{H\text{-}H}$ = 5.6 Hz, 2H), 4.03 (q, $^3J_{H\text{-}H}$ = 5.6 Hz, 1H), 3.64 (s, 3H), 3.56 – 3.39 (m, 2H), 1.47 – 1.43 (m, 9H), 1.42 (s, 3H), 1.38 (s, 9H); ^{13}C NMR (75 MHz, $CDCl_3$): 175.2 (C), 173.4 (C), 170.2 (C), 157.6 (C), 156.2 (C), 132.6 (CH), 117.7 (CH_2), 80.5 (C),

65.8 (CH_2), 57.1 (C), 56.6 (CH), 56.2 (C), 52.4 (CH_3), 42.3 (CH_2), 28.2 (CH_3), 25.6 (CH_3), 24.8 (CH_3), 24.7 (CH_3), 24.5 (CH_3).

Compound 129. To a solution of **128** (80 mg, 0.17 mmol) in MeOH (1 mL) was added aq. LiOH (1 M, 1 mL). The reaction mixture was stirred at rt for 2 h, then concentrated *in vacuo*. The residue was dissolved in H_2O (20 mL), acidified to pH ~ 1 with aq. 1 M HCl and extracted with EtOAc (3 x 20 mL). The organic layer was washed with brine (60 mL), dried over Na_2SO_4 and concentrated *in vacuo* to yield **129** as a colorless solid (69 mg, 89%). R_f (CH_2Cl_2 + 10% MeOH): 0.15; IR (neat): 3331 (br), 2983 (w), 2937 (w), 1684 (s), 1526 (s), 1462 (w), 1392 (w), 1367 (w), 1255 (s), 1164 (s), 1086 (w), 1017 (w), 929 (w), 853 (w), 804 (w), 774 (w); $[\alpha]_D^{20}$ –1.49 (*c* 1.00, EtOH); ^{1}H NMR (300 MHz, $CDCl_3$ + 5% CD_3OD): 5.88 (ddt, $^3J_{H\text{-}H}$ = 17.2, 10.5, 5.6 Hz, 1H), 5.28 (d, $^3J_{H\text{-}H}$ = 17.2 Hz, 1H), 5.19 (d, $^3J_{H\text{-}H}$ = 10.5 Hz, 1H), 4.54 (d, $^3J_{H\text{-}H}$ = 5.6 Hz, 2H), 4.03 (t, $^3J_{H\text{-}H}$ = 5.4 Hz, 1H), 3.49 (dd, $^2J_{H\text{-}H}$ = 14.5, $^3J_{H\text{-}H}$ = 5.4 Hz, 1H), 3.35 (dd, $^2J_{H\text{-}H}$ = 14.5, $^3J_{H\text{-}H}$ = 5.4 Hz, 1H), 1.51 (s, 6H), 1.46 (s, 3H), 1.44 (s, 3H), 1.42 (s, 9H); ^{13}C NMR (75 MHz, $CDCl_3$ + 5% CD_3OD): 178.0 (C), 176.5 (C), 174.8 (C), 161.7 (C), 160.4 (C), 136.5 (CH), 121.0 (CH_2), 84.1 (C), 69.6 (CH_2), 61.6 (C), 60.9 (CH), 59.5 (C), 45.8 (CH_2), 31.8 (CH_3), 28.6 (CH_3), 28.3 (CH_3), 27.7 (CH_3), 27.5 (CH_3).

Compound 130. To a solution of **126** (562 mg, 1.10 mmol) in DMF (5 mL) was added DIPEA (211 µL, 1.21 mmol) and acetic anhydride (114 µL, 1.21 mmol). The reaction mixture was stirred at room temperature for 30 min before being diluted with ethyl acetate (50 mL). The organic layer was washed with 10% citric acid (3 x 50 mL), aq. $NaHCO_3$ (sat., 3 x 50 mL) and brine (3 x 50 mL), dried over Na_2SO_4 and concentrated *in vacuo* to yield **130** (571 mg, 94 %) as a colorless solid. R_f (CH_2Cl_2 + 10% MeOH): 0.57; IR (neat): 3313 (br), 2991 (br), 1729 (s), 1660 (s), 1532 (s), 1450 (m), 1366 (m), 1260 (s), 1230 (m), 1154 (m), 1008 (w), 911 (w), 760 (w), 735 (m); $[\alpha]_D^{20}$ –1.39 (*c* 1.00, EtOH); ^{1}H NMR (400 MHz, $CDCl_3$): 7.77 (d, $^3J_{H\text{-}H}$ = 7.6 Hz, 2H), 7.59 (d, $^3J_{H\text{-}H}$ = 7.5 Hz, 2H), 7.41 (t, $^3J_{H\text{-}H}$ = 7.6 Hz, 2H), 7.31 (t, $^3J_{H\text{-}H}$ = 7.5, 2H), 7.14 (s, 1H), 7.00 (d, $^3J_{H\text{-}H}$ = 5.8

Hz, 1H), 6.96 (s, 1H), 6.00 (s, 1H), 4.47 – 4.33 (m, 3H), 4.21 (t, $^{3}J_{H\text{-}H}$ = 7.1 Hz, 1H), 3.72 (s, 3H), 3.66 – 3.52 (m, 2H), 2.03 (s, 3H), 1.56 (s, 6H), 1.53 (s, 3H), 1.51 (s, 3H). ^{13}C NMR (101 MHz, $CDCl_3$): 175.5 (C), 173.1 (C), 171.4 (C), 169.8 (C), 158.1 (C), 143.6 (C), 141.3 (C), 127.8 (CH), 127.1 (CH), 125.1 (CH), 125.0 (CH), 120.1 (CH), 67.3 (CH_2), 57.5 (C), 56.6 (C), 55.5 (CH), 52.7 (CH_3), 47.1 (CH), 42.8 (CH_2), 25.4 (CH_3), 25.1 (CH_3), 24.5 (CH_3), 23.2 (CH_3).

Compound 131. To a suspension of *N,N'*-disuccinimidyl carbonate (2.05 g, 8.00 mmol) at 0 °C in acetonitrile (15 mL) was added tert-butyl carbazate (264 mg, 2.00 mmol) in acetonitrile (5 mL) dropwise. The reaction mixture was stirred at rt for 1 h. Unreacted *N,N'*-disuccinimidyl carbonate was filtered off, the solvent was concentrated *in vacuo* and the crude mixture was purified by flash column chromatography (BGB Scorpius® Silica 12 g, 45 mL/min, linear gradient 0 – 100% EtOAc in CH_2Cl_2) to yield **131** (430 mg, 79%) as a colorless solid. R_f (EtOAc): 0.78; IR (neat): 3325 (br), 2984 (m), 2910 (w), 1714 (s), 1507 (m), 1389 (m), 1366 (m), 1249 (s), 1163 (s), 1082 (s), 964 (w), 856 (w), 651 (m); ^{1}H NMR (400 MHz, $CDCl_3$): 2.85 (s, 4H), 1.50 (s, 9H); ^{13}C NMR (75 MHz, DMSO-d_6) δ 171.0 (C), 155.5 (C), 153.1 (C), 80.3 (C), 28.5 (CH_2), 25.8 (CH_3).

Compound 132. 130 (571 mg, 1.03 mmol) was dissolved in Me_2NH in THF (2 M, 5.2 mL) and the reaction mixture was stirred at room temperature for 20 min. The solvent was removed *in vacuo*, the residue was dissolved in a minimal amount of CH_2Cl_2 and precipitated with pentane. The precipitate was filtered, washed twice with pentane, and the crude product was used without further purification.

To a solution of deprotected **130** (34 mg, 10 µmol) and DIPEA (18 µL, 10 µmol) in DMF (1 mL) was added **131** (28 mg, 10 µmol), and the reaction mixture was stirred at rt for 1 h. The crude mixture was purified by RP flash column chromatography (BGB Scorpius® C_{18} 20 g, 25 mL/min, linear gradient 5 – 50% MeCN + 0.1% TFA in H_2O + 0.1% TFA) to afford **132** (25 mg, 50 %) as a colorless solid. IR (neat): 3291 (br), 2947 (br), 1738 (m), 1642 (s), 1528 (s), 1438

(m), 1384 (m), 1365 (m), 1304 (m), 1272 (m), 1220 (m), 1194 (m), 1151 (s), 916 (m), 884 (w), 728 (s); $[\alpha]_D^{20}$ –1.41 (*c* 1.00, EtOH); ^{1}H NMR (400 MHz, $CDCl_3$): 7.58 (s, 1H), 7.39 (s, 1H), 7.14 (s, 1H), 6.84 (s, 1H), 6.61 (s, 1H), 6.36 (s, 1H), 4.33 (q, $^3J_{H\text{-}H}$ = 5.2 Hz, 1H), 3.81 – 3.75 (m, 1H), 3.75 (s, 3H), 3.49 (d, $^2J_{H\text{-}H}$ = 14.1 Hz, 1H), 2.04 (s, 3H), 1.55 (s, 3H), 1.54 (s, 3H), 1.47 (s, 9H), 1.46 (s, 3H); ^{13}C NMR (101 MHz, $CDCl_3$): 175.9 (C), 174.0 (C), 171.1 (C), 170.7 (C), 161.0 (C), 156.1 (C), 81.9 (C), 57.4 (C), 56.9 (CH), 56.6 (C), 52.8 (CH_3), 41.9 (CH_2), 29.7 (C), 28.2 (CH_3), 25.3 (CH_3), 24.8 (CH_3), 24.5 (CH_3), 23.2 (CH_3).

Compound 134. To a solution of **129** (310 mg, 0.560 mmol) in DMF (5 mL) were added HBTU (350 mg, 0.670 mmol) and DIPEA (146 µL, 0.840 mmol). After stirring at rt for 2 min, **126** (254 mg, 0.560 mmol) was added and the reaction mixture was stirred at rt for 2 h. The crude reaction mixture was diluted with EtOAc (50 mL), washed with aq. $NaHCO_3$ (sat., 3 x 50 mL) and brine (3 x 50 mL), dried over Na_2SO_4 and concentrated *in vacuo*. The crude product was purified by flash column chromatography (Claricep® 12 g, 36 mL/min, linear gradient 0 – 10% MeOH in CH_2Cl_2) to yield **134** as a colorless solid (410 mg, 77%). R_f (CH_2Cl_2 + 10% MeOH): 0.50; IR (neat): 3325 (br), 2972 (w), 2934 (w), 1736 (s), 1661 (s), 1528 (s), 1445 (m),1366 (m), 1229 (s), 1216 (s), 1158 (m), 993 (w), 933 (w), 739 (w); CD (TFE, 0.2 mM): 226 (–6.4), 206 (–7.8), 190 (–1.5); ^{1}H NMR (400 MHz, $CDCl_3$ + 5% CD_3OD): 7.73 (d, $^3J_{H\text{-}H}$ = 7.5 Hz, 2H), 7.55 (d, $^3J_{H\text{-}H}$ = 7.7 Hz, 2H), 7.39 – 7.30 (m, 4H), 7.30 – 7.25 (m, 2H), 5.92 – 5.76 (m, 1H), 5.34 – 5.15 (m, 2H), 4.62 – 4.46 (m, 2H), 4.38 – 4.20 (m, 3H), 4.17 (t, $^3J_{H\text{-}H}$ = 7.1 Hz, 1H), 4.02 (t, $^3J_{H\text{-}H}$ = 5.8 Hz, 1H), 3.78 – 3.70 (m, 1H), 3.68 (s, 3H), 3.65 – 3.52 (m, 2H), 3.50 – 3.43 (m, 1H), 3.37 – 3.29 (m, 1H), 1.49 (s, 10H), 1.48 (s, 6H), 1.45 (s, 3H), 1.42 (s, 3H), 1.40 (s, 9H), 1.39 (s, 3H); ^{13}C NMR (101 MHz, $CDCl_3$ + 5% CD_3OD): 175.0 (C), 174.4 (C), 173.2 (C), 173.1 (C), 170.5 (C), 169.0 (C), 157.1 (C), 156.0 (C), 155.7 (C), 142.9 (C), 140.2 (C), 131.2 (CH), 126.7 (CH), 126.1 (CH), 124.0 (CH), 119.0 (CH), 117.3 (CH_2), 80.1 (C), 65.9 (CH_2), 65.2 (CH_2), 56.2 (C), 56.1 (C), 56.0 (C), 55.9 (C), 55.8 (C), 55.8 (C), 54.9

(CH), 54.8 (CH), 51.2 (CH_3), 46.1 (CH), 41.0 (CH_2), 40.6 (CH_2), 27.2 (CH_3), 25.5 (CH_3), 25.3 (CH_3), 24.9 (CH_3), 24.0 (CH_3), 23.4 (CH_3), 23.4 (CH_3), 22.9 (CH_3), 22.6 (CH_3).

Compound 135. To a solution of **134** (410 mg, 0.430 mmol) in CH_2Cl_2 (1.5 mL) was added TFA (1.5 mL), and the reaction mixture was stirred at rt for 20 min. The crude reaction mixture was precipitated with Et_2O/pentane (1:1, 50 mL), the precipitate was recovered, washed with Et_2O/pentane (1:1, 3 x 50 mL) and dried *in vacuo* to yield **135** as a colorless solid (415 mg, quant.). The product was used directly without further purification.

Compound 136. To a solution of **129** (1.08 g, 1.58 mmol) in DMF (8 mL) were added HBTU (1.02 g, 2.68 mmol) and DIPEA (549 µL, 3.15 mmol). After stirring at rt for 2 min, crude **135** (1.50 g, 1.58 mmol) was added and the reaction mixture was stirred at rt for 24 h. The crude reaction mixture was diluted with EtOAc (80 mL), washed with 10% citric acid (3 x 80 mL), aq. $NaHCO_3$ (sat., 3 x 80 mL) and brine (3 x 80 mL), dried over Na_2SO_4 and concentrated *in vacuo*. The crude product was purified by flash column chromatography (Claricep® 25 g, 45 mL/min, linear gradient 0 – 10% MeOH in CH_2Cl_2) to yield **136** as a colorless solid (1.20 g, 59%). R_f (CH_2Cl_2 + 10% MeOH): 0.55; IR (neat): 3323 (br), 2986 (w), 2944 (w), 1727 (m), 1657 (s), 1524 (s), 1449 (m), 1385 (m), 1366 (m), 1252 (s), 1156 (s), 995 (w), 931 (w), 760 (w), 739 (m); CD (TFE, 0.2 mM): 226 (–12.2), 208 (–16.7), 192 (+12.6); ^{1}H NMR (500 MHz, DMSO-d_6): 8.58 (s, 1H), 7.85 (d, $^3J_{H\text{-}H}$ = 7.7 Hz, 2H), 7.82 (s, 1H), 7.68 (br, 1H), 7.61 (dd, $^3J_{H\text{-}H}$ = 7.5, $^4J_{H\text{-}H}$ = 3.4 Hz, 2H), 7.39 (t, $^3J_{H\text{-}H}$ = 7.5 Hz, 2H), 7.27 (t, $^3J_{H\text{-}H}$ = 7.7 Hz, 2H), 5.91 – 5.77 (m, 2H), 5.29 – 5.07 (m, 4H), 4.48 – 4.36 (m, 4H), 4.23 (d, $^3J_{H\text{-}H}$ = 7.0 Hz, 2H), 4.15 (t, $^3J_{H\text{-}H}$ = 7.0 Hz, 1H), 4.09 – 4.04 (m, 1H), 4.02 (t, $^3J_{H\text{-}H}$ = 6.5 Hz, 1H), 3.98 – 3.94 (m, 1H), 3.49 – 3.21 (m, 6H), 1.39 – 1.29 (m, 42H), 1.28 (s, 3H), 1.24 (s, 3H); ^{13}C NMR (126 MHz, DMSO-d_6): 176.4 (C), 175.8 (C), 175.3 (C), 175.1 (C), 174.9 (C), 173.9 (C), 172.1 (C), 171.7 (C), 169.4 (C), 156.8 (C), 156.8 (C), 156.5 (C), 156.2 (C), 144.1 (C), 141.1 (C), 133.8 (CH), 128.1 (CH),

127.5 (CH), 125.5 (CH), 120.6 (CH), 117.6 (CH_2), 117.5 (CH_2), 79.2 (C), 66.3 (CH_2), 65.1 (CH_2), 56.8 (CH), 56.6 (C), 56.5 (C), 56.4 (C), 56.3 (C), 56.3 (C), 56.2 (C), 55.4 (CH), 55.3 (CH), 52.2 (CH), 47.0 (CH_3), 41.9 (CH_2), 41.2 (CH_2), 40.8 (CH_2), 28.5 (CH_3), 26.5 (CH_3), 26.5 (CH_3), 26.0 (CH_3), 25.6 (CH_3), 25.5 (CH_3), 25.2 (CH_3), 25.0 (CH_3), 24.9 (CH_3), 24.5 (CH_3), 23.8 (CH_3), 23.6 (CH_3), 23.4 (CH_3).

Compound 137. To a solution of **136** (760 mg, 0.580 mmol) in CH_2Cl_2 (3 mL) was added TFA (3 mL), and the reaction mixture was stirred at rt for 20 min. The crude reaction mixture was precipitated with Et_2O/pentane (1:1, 50 mL), the precipitate was recovered, washed with Et_2O/pentane (1:1, 3 x 50 mL) and dried *in vacuo*. The crude deprotected product was dissolved in DMF (2 mL), DIPEA (114 µL, 0.65 mmol) and Ac_2O (62 µL, 0.65 mmol) were added and the reaction mixture was stirred at rt for 1 h. The crude reaction mixture was diluted with EtOAc (50 mL), washed with 10% citric acid (3 x 50 mL), aq. $NaHCO_3$ (sat., 3 x 50 mL) and brine (3 x 50 mL), dried over Na_2SO_4 and concentrated *in vacuo* to yield **137** as a colorless solid (580 mg, 82%). R_f (CH_2Cl_2 + 10% MeOH): 0.50; IR (neat): 3338 (br), 3030 (br), 1740 (s), 1440 (w), 1367 (m), 1229 (m), 1216 (m), 1045 (w), 907 (w), 756 (w); CD (TFE, 0.2 mM): 226 (–12.7), 208 (–16.3), 194 (+22.1); ^{1}H NMR (500 MHz, $CDCl_3$ + 5% CD_3OD): 8.00 (s, 1H), 7.98 (s, 1H), 7.84 (br, 1H), 7.72 (s, 1H), 7.67 (d, $^3J_{H\text{-}H}$ = 8.0 Hz, 2H), 7.81 (d, $^3J_{H\text{-}H}$ = 7.8 Hz, 2H), 7.30 (d, $^3J_{H\text{-}H}$ = 8.0 Hz, 2H), 7.20 (d, $^3J_{H\text{-}H}$ = 7.8 Hz, 2H), 5.83 (ddt, $^3J_{H\text{-}H}$ = 16.3, 10.8, 5.6 Hz, 1H), 5.72 (ddt, $^3J_{H\text{-}H}$ = 16.3, 10.7, 5.5 Hz, 1H), 5.29 – 5.04 (m, 4H), 4.49 (d, $^3J_{H\text{-}H}$ = 5.6 Hz, 2H), 4.41 (m, 1H), 4.39 (d, $^3J_{H\text{-}H}$ = 5.5 Hz, 2H), 4.31 – 4.07 (m, 8H), 3.77 – 3.66 (m, 3H), 3.61 (s, 3H), 3.59 – 3.43 (m, 3H), 1.96 (s, 3H), 1.47 (s, 3H), 1.46 (s, 3H), 1.45 – 1.43 (m, 9H), 1.42 (s, 9H), 1.41 (s, 3H), 1.40 (s, 3H), 1.37 (s, 3H), 1.33 (s, 3H); ^{13}C NMR (126 MHz, $CDCl_3$ + 5% CD_3OD): 176.3 (C), 175.8 (C), 174.6 (C), 174.4 (C), 173.7 (C), 173.6 (C), 171.0 (C), 169.9 (C), 169.2 (C), 156.8 (C), 156.1 (C), 155.9 (C), 143.0 (C), 142.9 (C), 140.3 (C), 131.6 (CH), 131.3 (CH), 126.7 (CH), 126.1 (CH), 124.1 (CH),

118.9 (CH), 117.3 (CH), 116.6 (CH), 67.0 (CH_2), 66.0 (CH_2), 65.2 (CH_2), 64.6 (CH_2), 56.3 (C), 56.2 (C), 56.0 (CH), 55.8 (C), 55.3 (C), 54.9 (C), 54.8 (CH), 54.2 (C), 53.3 (CH), 51.2 (CH), 46.1 (CH_3), 41.6 (CH_2), 40.3 (CH_2), 40.1 (CH_2), 26.3 (CH_3), 26.1 (CH_3), 25.8 (CH_3), 25.7 (CH_3), 25.6 (CH_3), 25.3 (CH_3), 25.2 (CH_3), 25.0 (CH_3), 24.6 (CH_3), 24.1 (CH_3), 23.3 (CH_3), 23.0 (CH_3), 22.7 (CH_3), 22.4 (CH_3), 22.0 (CH_3), 21.9 (CH_3), 21.7 (CH_3).

Compound 138. To a solution of **137** (520 mg, 0.420 mmol) in CH_2Cl_2 (7 mL) was added $Pd(PPh_3)_4$ (48 mg, 42 μmol) and phenylsilane (1.0 mL, 8.4 mmol) and the reaction mixture was stirred at rt for 1 h. The crude reaction mixture was precipitated with Et_2O (50 mL), the precipitate was recovered, washed with Et_2O (3 x 50 mL) and dried *in vacuo*. The crude deprotected product was dissolved in Me_2NH in THF (2 M, 5 mL) and the reaction mixture was stirred at rt for 20 min. The crude reaction mixture was precipitated with pentane (50 mL), the precipitate was recovered, washed with pentane (3 x 50 mL) and dried *in vacuo*, before being purified by RP flash column chromatography (Claricep® C_{18} 20 g, 20 mL/min, linear gradient 5 – 50% MeCN + 0.1% TFA in H_2O + 0.1% TFA) to yield **138** as a colorless solid (TFA salt, 307 mg, 62%). IR (neat): 3296 (br), 2970 (br), 1740 (s), 1443 (w), 1367 (m), 1229 (m), 1216 (m), 1094 (w), 903 (w), 758 (w); CD (TFE, 0.2 mM): 226 (–27.1), 209 (–28.8), 196 (+32.7); ^{1}H NMR (500 MHz, CD_3OD): 4.75 (dd, $^3J_{H\text{-}H}$ = 8.9, 4.9 Hz, 1H), 4.45 (dd, $^3J_{H\text{-}H}$ = 8.5, 5.0 Hz, 1H), 4.32 (dd, $^3J_{H\text{-}H}$ = 7.3, 5.6 Hz, 1H), 3.70 (s, 3H), 3.73 – 3.60 (m, 2H), 3.51 (dd, $^2J_{H\text{-}H}$ = 13.2, $^3J_{H\text{-}H}$ = 5.0 Hz, 1H), 3.48 (dd, $^2J_{H\text{-}H}$ = 14.1, $^3J_{H\text{-}H}$ = 4.9 Hz, 1H), 3.37 – 3.23 (m, 2H), 2.10 (s, 3H), 1.55 (s, 3H), 1.53 (s, 3H), 1.52 (s, 3H), 1.51 (s, 3H), 1.50 – 1.48 (m, 15H), 1.48 (s, 3H), 1.47 (s, 3H), 1.46 (s, 3H); ^{13}C NMR (126 MHz, CD_3OD): 177.7 (C), 176.3 (C), 176.2 (C), 175.4 (C), 175.2 (C), 174.9 (C), 173.3 (C), 171.4 (C), 170.2 (C), 168.3 (C), 161.6 (q, $^2J_{C\text{-}F}$ = 34.8 Hz, TFA), 116.4 (q, $^1J_{C\text{-}F}$ = 292.4 Hz, TFA), 56.8 (C), 56.8 (C), 56.7 (C), 56.6 (C), 56.5 (C), 56.0 (C), 51.6 (CH), 51.5 (CH_3), 51.0 (CH), 50.6 (CH), 41.0 (CH_2), 39.7 (CH_2), 39.4 (CH_2), 25.4 (CH_3), 25.3 (CH_3), 24.8 (CH_3), 24.5 (CH_3), 24.2

(CH_3), 23.9 (CH_3), 23.6 (CH_3), 23.4 (CH_3), 22.8 (CH_3), 22.4 (CH_3), 22.1 (CH_3), 21.5 (CH_3).

Compound 139. To a solution of **138** (30 mg, 36 µmol) in DMF (2 mL) was added DIPEA (25 µL, 0.14 mmol) and **131** (32 mg, 0.12 mmol) and the reaction mixture was stirred at rt for 1 h. The crude mixture was directly purified by RP flash column chromatography (BGB Scorpius® C_{18} 5.4 g, 10 mL/min, linear gradient 20 – 95% MeCN + 0.1% TFA in H_2O + 0.1% TFA) to yield **139** as a colorless solid (20 mg, 43%). IR (neat): 3300 (br), 2985 (w), 2946 (w), 1767 (m), 1659 (s), 1549 (s), 1461 (w), 1440 (w), 1274 (m), 1250 (m), 1226 (m), 1166 (s), 1063 (w); CD (TFE, 0.2 mM): 226 (–17.6), 208 (–23.7), 194 (+29.0); ^{1}H NMR (500 MHz, CD_3OD): 4.34 (s, 1H), 4.27 (t, $^3J_{H\text{-}H}$ = 6.7 Hz, 1H), 4.12 (dd, $^3J_{H\text{-}H}$ = 9.3, 4.1 Hz, 1H), 3.85 – 3.70 (m, 4H), 3.68 (s, 3H), 3.65 – 3.51 (m, 2H), 2.04 (s, 3H), 1.55 (s, 3H), 1.53 (s, 9H), 1.52 (s, 3H), 1.51 (s, 6H), 1.51 – 1.50 (m, 18H), 1.50 (s, 3H), 1.49 (s, 3H), 1.47 (s, 3H), 1.47 (s, 18H); ^{13}C NMR (126 MHz, CD_3OD): 178.8 (C), 178.4 (C), 177.0 (C), 176.8 (C), 176.5 (C), 176.5 (C), 173.7 (C), 173.6 (C), 172.9 (C), 172.1 (C), 161.5 (C), 161.4 (C), 161.0 (C), 158.6 (C), 158.4 (C), 158.3 (C), 82.3 (C), 82.0 (C), 58.6 (CH), 58.3 (C), 58.2 (C), 58.1 (C), 58.1 (C), 58.0 (C), 57.9 (CH), 57.2 (C), 56.2 (CH), 52.6 (CH_3), 42.0 (CH_2), 41.4 (CH_2), 41.3 (CH_2), 28.7 (CH_3), 27.4 (CH_3), 27.3 (CH_3), 26.8 (CH_3), 26.8 (CH_3), 26.6 (CH_3), 25.7 (CH_3), 24.8 (CH_3), 24.7 (CH_3), 24.5 (CH_3), 24.2 (CH_3), 23.8 (CH_3), 23.4 (CH_3), 22.7 (CH_3).

Compound 141. To a solution of **124** (1.90 g, 4.45 mmol), HBTU (3.40 g, 9.90 mmol), HOBt (1.30 g, 9.90 mmol) and DIPEA (1.70 mL, 9.90 mmol) was added **140** (785 mg, 6.68 mmol), and the reaction mixture was stirred at rt for 1h. The solvent was removed *in vacuo* and the crude residue was dissolved in CH_2Cl_2 (100 mL), washed with water (3 x 100 mL), aq. $NaHCO_3$ (sat., 3 x 100 mL) and brine (3 x 100 mL). The combined organic layers were dried over Na_2SO_4, filtered, and concentrated *in vacuo*. The crude product was purified by flash column chromatography (Biotage® SNAP Ultra 50 g, 50 mL/min, linear gradient

0 – 10% MeOH in CH_2Cl_2) to yield **141** as a colorless solid (2.20 g, 95%). R_f (CH_2Cl_2 + 10% MeOH): 0.81; IR (neat): 3338 (br), 3027 (br), 1674 (s), 1531 (s), 1450 (m), 1368 (w), 1262 (m), 1202 (m), 1139 (m), 1028 (w), 865 (w), 760 (w), 741 (w); $[\alpha]_D^{20}$ –7.50 (*c* 1.00, EtOH); ^{1}H NMR (400 MHz, $CDCl_3$): 7.76 (d, $^3J_{H-H}$ = 7.5 Hz, 2H), 7.59 (d, $^3J_{H-H}$ = 7.2 Hz, 2H), 7.40 (t, $^3J_{H-H}$ = 7.5 Hz, 2H), 7.31 (m, 2H), 7.07 (br, 1H), 5.66 – 5.56 (m, 1H), 4.45 – 4.35 (m, 2H), 4.27 – 4.10 (m, 2H), 3.72 (s, 3H), 3.68 – 3.57 (m, 1H), 3.57 – 3.45 (m, 1H), 1.54 (s, 3H), 1.52 (s, 3H), 1.45 (s, 9H); ^{13}C NMR (101 MHz, $CDCl_3$): 174.7 (C), 170.0 (C), 157.5 (C), 143.8 (C), 143.7 (C), 141.3 (CH), 127.8 (CH), 127.1 (CH), 125.1 (CH), 120.0 (CH), 80.6 (C), 67.2 (CH_2), 56.6 (C), 55.1 (CH), 52.7 (CH_3), 47.1 (CH), 43.0 (CH_2), 28.3 (CH_3), 25.1 (CH_3), 24.8 (CH_3).

Compound 142. 141 (2.00 g, 3.81 mmol) was dissolved in Me_2NH in THF (2 M, 15 mL) and the reaction mixture was stirred at rt for 20 min. The solvent was removed in vacuo, the residue redissolved in CH_2Cl_2 (2 mL) and precipitated with pentane (200 mL). The precipitate was filtered, washed with pentane (3 x 200 mL) and dried *in vacuo*. Crude deprotected product was dissolved in H_2O/1,4-dioxane (1:1, 20 mL), and allyl chloroformate (284 µL, 2.67 mmol) and triethylamine (496 µL, 3.56 mmol) were added. The reaction mixture was stirred at rt for 1 h before being diluted with H_2O (100 mL) and acidified to pH ~ 2 with 1 M HCl, extracted with EtOAc (3 x 150 mL), washed with brine (150 mL), and dried over Na_2SO_4. The solvent was then removed *in vacuo* to afford **142** (626 mg, 69%, 2 steps) as a colorless solid. R_f (CH_2Cl_2 + 10% MeOH): 0.77; IR (neat): 3328 (br), 2980 (br), 1719 (s), 1536 (s), 1466 (w), 1388 (m), 1364 (m), 1250 (s), 1159 (s), 1060 (w), 999 (w), 853 (w), 785 (m); $[\alpha]_D^{20}$ –8.88 (*c* 1.00, EtOH); ^{1}H NMR (400 MHz, $CDCl_3$): 7.05 (s, 1H), 6.01 – 5.85 (m, 1H), 5.60 (s, 1H), 5.49 (s, 1H), 5.31 (dq, $^4J_{H-H}$ = 1.6, $^3J_{H-H}$ = 17.2, $^2J_{H-H}$ = 1.6 Hz, 1H), 5.22 (dq, $^4J_{H-H}$ = 1.6, $^3J_{H-H}$ = 10.5, $^2J_{H-H}$ = 1.6 Hz, 1H), 4.64 – 4.54 (m, 2H), 4.18 (s, 1H), 3.74 (s, 3H), 3.61 (m, 1H), 3.52 (m, 1H), 1.55 (s, 3H), 1.53 (s, 3H), 1.46 (s, 9H); ^{13}C NMR (101 MHz, $CDCl_3$): 174.6 (C), 169.9 (C), 157.4 (C), 156.1 (C), 132.6 (CH),

117.8 (CH_2), 80.6 (C), 65.9 (CH_2), 56.6 (C), 55.1 (CH), 52.7 (CH_3), 42.9 (CH_2), 28.3 (CH_3), 25.0 (CH_3), 24.7 (CH_3).

Compound 143. 142 (620 mg, 1.60 mmol) was dissolved in MeOH/THF/1 M LiOH (1:1:1, 15 mL) and the reaction mixture was stirred at rt for 1 h. The reaction mixture was diluted with 1 M HCl (20 mL) and extracted with EtOAc (3 x 50 mL). The organic layer was washed with brine (150 mL), dried over Na_2SO_4 and the solvent was removed in vacuo to afford **143** (566 mg, 95 %) as a colorless solid. R_f (CH_2Cl_2 + 10% MeOH): 0.22; IR (neat): 3325 (br), 2980 (w), 2945 (w), 1680 (s), 1541 (s), 1460 (m), 1388 (m), 1366 (m), 1272 (w), 1250 (w), 1221 (w), 1164 (s), 849 (m); $[\alpha]_D^{20}$ –4.71 (*c* 1.00, EtOH); ^{1}H NMR (400 MHz, $CDCl_3$): 7.22 (s, 1H), 6.00 – 5.85 (m, 2H), 5.72 (s, 1H), 5.30 (dd, $^3J_{H\text{-}H}$ = 17.4, $^2J_{H\text{-}H}$ =1.8 Hz, 1H), 5.21 (d, ^3J = 10.4 Hz, 1H), 4.57 (d, ^3J = 5.6 Hz, 2H), 4.26 (s, 1H), 3.60 – 3.50 (m, 2H), 1.56 (s, 3H), 1.54 (s, 3H), 1.45 (s, 9H); ^{13}C NMR (101 MHz, $CDCl_3$): 176.0 (C), 171.2 (C), 157.6 (C), 156.3 (C), 132.6 (CH), 117.8 (CH_2), 80.8 (C), 66.0 (CH_2), 56.6 (C), 55.3 (CH), 42.6 (CH_2), 29.7 (CH_3), 28.3 (CH_3), 25.0 (CH_3), 24.6 (CH_3).

Compound 144 was prepared according to a reported procedure.[244]

Compound 145. To a solution of **124** (1.32 g, 3.09 mmol), HATU (1.29 g, 3.40 mmol) and DIPEA (1.08 mL, 6.18 mmol) in DMF (15 mL) was added **144** (1.24 g, 3.09 mmol) and the reaction mixture was stirred at rt for 1 h. The reaction mixture was diluted with EtOAc (150 mL) and the organic layer was washed with 10% citric acid (3 x 150 mL), aq. $NaHCO_3$ (sat., 3 x 150 mL) and brine (3 x 150 mL) and dried over Na_2SO_4. The solvent was removed *in vacuo* to afford **145** (1.80 g, 84 %) as a colorless solid. R_f (CH_2Cl_2 + 10% MeOH): 0.78; IR (neat): 3680 (w), 2974 (S), 2895 (s), 1680 (br), 1402 (m), 1388 (m), 1366 (m), 1268 (m), 1241 (m), 1054 (s); $[\alpha]_D^{20}$ –8.10 (*c* 1.00, EtOH); ^{1}H NMR (400 MHz, $CDCl_3$): 7.77 (d, $^3J_{H\text{-}H}$ = 7.6 Hz, 2H), 7.59 (d, $^3J_{H\text{-}H}$ = 7.5 Hz, 2H), 7.41 (t, $^3J_{H\text{-}H}$ = 7.6 Hz, 2H), 7.32 (td, $^3J_{H\text{-}H}$ = 7.5 Hz, $^4J_{H\text{-}H}$ = 3.0 Hz, 2H), 7.20 (s, 1H), 6.97 (s, 1H), 6.71 (s, 1H), 6.10 (s, 1H), 5.67 (s, 1H), 4.48 – 4.38 (m, 2H), 4.22 (t, $^3J_{H\text{-}H}$ =

6.9 Hz, 1H), 4.02 (q, $^{3}J_{H\text{-}H}$ = 5.0 Hz, 1H), 3.71 (s, 3H), 3.65 – 3.50 (m, 2H), 1.53 (s, 3H), 1.52 (s, 3H), 1.49 (s, 3H), 1.49 (s, 3H), 1.48 (s, 3H), 1.47 (s, 12H); ^{13}C NMR (101 MHz, $CDCl_3$): 175.5 (C), 174.0 (C), 172.7 (C), 170.6 (C), 158.1 (C), 149.7 (C), 143.7 (C), 141.3 (C), 127.9 (CH), 127.1 (CH), 125.0 (CH), 120.1 (CH), 81.2 (C), 67.4 (CH_2), 57.5 (CH), 57.1 (C), 57.0 (C), 56.1 (C), 52.3 (CH), 47.1 (CH_3), 42.1 (CH_2), 28.2 (CH_3), 25.9 (CH_3), 24.9 (CH_3), 24.6 (CH_3).

Compound 146. 145 (1.70 g, 2.44 mmol) was dissolved in Me_2NH in THF (2 M, 15 mL) and the reaction mixture was stirred at rt for 20 min. The solvent was removed *in vacuo*, the residue redissolved in CH_2Cl_2 (2 mL) and precipitated with pentane (200 mL). The precipitate was filtered, washed with pentane (3 x 200 mL) and dried to afford a colorless solid (990 mg) that was used directly without further purification. To a solution of deprotected **145** (900 mg, 1.90 mmol) in H_2O/1,4-dioxane (1:1, 20 mL) was added allyl chloroformate (303 µL, 2.85 mmol) and triethylamine (530 µL, 3.80 mmol), and the reaction mixture was stirred at rt for 1 h. The reaction mixture was diluted with H_2O (100 mL) and acidified to pH ~ 2 with 1 M HCl, extracted with EtOAc (3 x 150 mL), washed with brine (150 mL), and dried over Na_2SO_4. The solvent was then removed *in vacuo* to afford **146** (875 mg, 71%, 2 steps) as a colorless solid. R_f (CH_2Cl_2 + 10% MeOH): 0.74; IR (neat): 3320 (br), 2990 (w), 2971 (w), 1680 (s), 1584 (s), 1459 (m), 1388 (m), 1366 (m), 1251 (s), 1154 (s), 1081 (w), 1052 (w), 1000 (m), 923 (w), 852 (w), 787 (w); $[\alpha]_D^{20}$ –7.73 (*c* 1.00, EtOH); ^{1}H NMR (400 MHz, $CDCl_3$): 7.43 (s, 1H), 7.16 (s, 1H), 7.03 (s, 1H), 6.37 (s, 1H), 6.12 (s, 1H), 5.91 – 5.77 (m, 1H), 5.24 (d, $^{3}J_{H\text{-}H}$ = 15.3 Hz, 2H), 5.15 (d, $^{3}J_{H\text{-}H}$ = 10.5 Hz, 1H), 4.57 – 4.46 (m, 2H), 3.96 (q, $^{3}J_{H\text{-}H}$ = 6.3 Hz, 1H), 3.63 (s, 3H), 3.59 – 3.41 (m, 2H), 1.47 (s, 6H), 1.45 – 1.42 (m, 9H), 1.42 – 1.38 (m, 12H); ^{13}C NMR (101 MHz, $CDCl_3$): 175.6 (C), 174.8 (C), 174.7 (C), 172.9 (C), 171.0 (C), 157.4 (C), 156.4 (C), 132.6 (CH), 117.6 (CH_2), 80.6 (C), 65.8 (CH_2), 57.0 (CH), 56.9 (C), 56.7 (C), 55.8 (C), 52.1 (CH_3), 41.6 (CH_2), 28.3 (CH_3), 25.4 (CH_3), 25.3 (CH_3), 25.2 (CH_3), 24.8 (CH_3), 24.8 (CH_3).

Compound 147. 146 (586 mg, 1.05 mmol) was dissolved in MeOH/THF/1 M LiOH (1:1:1, 15 mL) and the reaction mixture was stirred at rt for 1 h. The reaction mixture was diluted with 1 M HCl (20 mL) and extracted with EtOAc (3 x 50 mL). The organic layer was washed with brine (150 mL), dried over Na_2SO_4 and the solvent was removed in vacuo to afford **147** (562 mg, 98%) as a colorless solid. R_f (CH_2Cl_2 + 10% MeOH): 0.23; IR (neat): 3312 (br), 2989 (m), 2971 (w), 1657 (s), 1543 (s), 1454 (w), 1388 (m), 1366 (m), 1250 (s), 1164 (s), 997 (w), 929 (w), 850 (w), 781 (w); $[\alpha]_D^{20}$ –9.92 (*c* 1.00, EtOH); ^{1}H NMR (400 MHz, $CDCl_3$): 7.82 (s, 1H), 7.72 (s, 1H), 7.66 (s, 1H), 6.25 (s, 1H), 6.06 (t, $^3J_{H-H}$ = 6.3 Hz, 1H), 5.90 (ddt, $^3J_{H-H}$ = 16.3, 10.8, 5.6 Hz, 1H), 5.39 – 5.13 (m, 2H), 4.63 – 4.50 (m, 2H), 4.15 – 3.99 (m, 1H), 3.64 – 3.42 (m, 2H), 1.57 (s, 6H), 1.47 (s, 3H), 1.45 (s, 12H); ^{13}C NMR (101 MHz, $CDCl_3$): 176.6 (C), 175.5 (C), 175.2 (C), 171.2 (C), 157.3 (C), 156.8 (C), 132.7 (CH), 117.7 (CH_2), 80.8 (C), 65.8 (C), 56.9 (C), 56.8 (C), 56.6 (CH), 41.7 (CH_2), 29.7 (CH_3), 28.3 (CH_3), 25.1 (CH_3), 25.0 (CH_3), 24.9 (CH_3), 24.9 (CH_3), 24.8 (CH_3).

Compound 148. To a solution of **143** (429 mg, 1.15 mmol), DIPEA (220 µL, 1.26 mmol) and HATU (481 mg, 1.26 mmol) in DMF (5.75 mL) was added **126** (717 mg, 1.15 mmol) and the reaction mixture was stirred at rt for 1 h, before being diluted with EtOAc (240 mL). The organic layer was washed with 10% citric acid (3 x 250 mL), aq. $NaHCO_3$ (sat., 3 x 250 mL) and brine (3 x 250 mL), dried over Na_2SO_4, filtered and concentrated in vacuo. The crude mixture was purified by flash column chromatography (BGB Scorpius® Silica 25 g, 45 mL/min, linear gradient 0 – 10% MeOH in CH_2Cl_2) to yield **148** (652 mg, 65 %) as a colorless solid. R_f (CH_2Cl_2 + 10% MeOH): 0.49; IR (neat): 3315 (br), 1726 (s), 1677 (s), 1541 (s), 1451 (m), 1388 (m), 1366 (m), 1254 (s), 1155 (s), 1000 (w), 852 (w), 744 (w); CD (TFE, 0.2 mM): 206 (–13.5), 190 (+11.6); ^{1}H NMR (400 MHz, $CDCl_3$): 7.96 (d, $^3J_{H-H}$ = 5.6 Hz, 1H), 7.75 (d, $^3J_{H-H}$ = 7.5 Hz, 2H), 7.57 (d, $^3J_{H-H}$ = 7.5 Hz, 2H), 7.46 – 7.34 (m, 4H), 7.33 – 7.24 (m, 3H), 7.19 (s, 1H), 6.22 (t, $^3J_{H-H}$ = 6.3 Hz, 1H), 5.86 (ddt, $^3J_{H-H}$ = 16.3, 10.8, 5.6 Hz, 1H), 5.32

– 5.13 (m, 2H), 4.60 – 4.47 (m, 2H), 4.43 – 4.27 (m, 2H), 4.18 (t, $^{3}J_{H\text{-}H}$ = 7.2 Hz, 1H), 4.12 (p, $^{3}J_{H\text{-}H}$ = 5.6 Hz, 2H), 3.68 (s, 3H), 3.70 – 3.61 (m, 1H), 3.60 – 3.45 (m, 2H), 3.41 – 3.31 (m, 1H), 1.52 (s, 3H), 1.51 (s, 3H), 1.50 (s, 3H), 1.48 (s, 3H), 1.46 (s, 3H), 1.44 (s, 3H), 1.41 (s, 9H); ^{13}C NMR (101 MHz, $CDCl_3$): 175.5 (C), 175.1 (C), 174.1 (C), 171.1 (C), 171.0 (C), 169.6 (C), 158.0 (C), 157.6 (C), 156.6 (C), 143.7 (C), 143.6 (C), 141.3 (C), 141.2 (C), 132.4 (CH), 127.8 (CH), 127.1 (CH), 125.1 (CH), 125.0 (CH), 120.0 (CH), 118.0 (CH_2), 81.0 (C), 67.3 (CH_2), 66.0 (CH_2), 57.2 (C), 56.9 (CH), 56.8 (C), 56.0 (C), 55.9 (CH), 52.3 (CH_3), 47.0 (CH), 42.0 (CH_2), 41.8 (CH_2), 28.2 (CH_3), 26.0 (CH_3), 25.8 (CH_3), 25.1 (CH_3), 24.6 (CH_3), 24.4 (CH_3).

Compound 149. 148 (395 mg, 0.456 mmol) was dissolved in CH_2Cl_2/TFA (1:1, 5 mL) and the reaction mixture was stirred at rt for 30 min before being precipitate with Et_2O (100 mL). The precipitate was filtered, washed with Et_2O (3 x 100 mL), dried and used directly without further purification.

To a solution of **147** (248 mg, 0.460 mmol), HATU (191 mg, 0.500 mmol) and DIPEA (159 µL, 0.910 mmol) in DMF (2 mL) was added crude deprotected **148**, and the solution was stirred at rt for 16 h before being diluted with EtOAc (240 mL). The organic layer was washed with 10% citric acid (3 x 250 mL), aq. $NaHCO_3$ (sat., 3 x 250 mL) and brine (3 x 250 mL), dried over Na_2SO_4, filtered and concentrated in vacuo. The crude mixture was purified by flash column chromatography (BGB Scorpius® Silica 25 g, 45 mL/min, linear gradient 0 – 10% MeOH in CH_2Cl_2) to yield **149** (321 mg, 54 %) as a colorless solid. R_f (CH_2Cl_2 + 10% MeOH): 0.49; IR (neat): 3341 (br), 3000 (br), 1749 (m), 1681 (s), 1563 (s), 1456 (w), 1401 (m), 1369 (m), 1252 (s), 1179 (m), 1170 (m), 1076 (s), 948 (w), 903 (w), 853 (w), 798 (w), 745 (w); CD (TFE, 0.2 mM): 207 (–17.5), 195 (+10.8); ^{1}H NMR (400 MHz, $CDCl_3$ + 5% CD_3OD): 8.14 (s, 1H), 7.82 (s, 1H), 7.70 (d, $^{3}J_{H\text{-}H}$ = 7.2 Hz, 4H), 7.58 (s, 1H), 7.54 (t, $^{3}J_{H\text{-}H}$ = 7.3 Hz, 3H), 7.38 – 7.29 (m, 3H), 7.27 – 7.20 (m, 3H), 6.84 (q, $^{3}J_{H\text{-}H}$ = 6.6 Hz, 1H), 6.77 – 6.64 (m, 1H), 5.91 – 5.74 (m, 2H), 5.33 – 5.07 (m, 4H), 4.58 – 4.42 (m, 4H), 4.27

(d, $^{3}J_{H\text{-}H}$ = 7.2 Hz, 2H), 4.15 (t, $^{3}J_{H\text{-}H}$ = 7.2 Hz, 2H), 4.14 – 4.05 (m, 2H), 4.00 – 3.88 (m, 1H), 3.82 – 3.68 (m, 2H), 3.64 – 3.62 (m, 1H), 3.63 (s, 3H), 3.61 – 3.28 (m, 5H), 1.51 (s, 3H), 1.49 (s, 6H), 1.48 (s, 3H), 1.46 (s, 12H), 1.43 (s, 6H), 1.41 (s, 12H), 1.38 (s, 3H); ^{13}C NMR (101 MHz, $CDCl_3$ + 5% CD_3OD): 177.3 (C), 177.2 (C), 175.5 (C), 174.6 (C), 174.4 (C), 173.9 (C), 170.4 (C), 169.92, 169.0 (C), 155.8 (C), 155.6 (C), 155.5 (C), 155.3 (C), 142.9 (C), 142.8 (C), 140.3 (C), 140.2 (C), 131.8 (CH), 131.7 (CH), 131.4 (CH), 126.8 (CH), 126.7 (CH), 126.1 (CH), 124.1 (CH), 118.9 (CH), 117.0 (CH_2), 116.2 (CH_2), 80.1 (C), 66.0 (CH_2), 65.0 (CH_2), 64.8 (CH_2), 64.4 (CH_2), 56.6 (CH), 56.5 (CH), 56.2 (CH), 56.1 (CH), 56.0 (C), 56.0 (C), 55.9 (C), 55.7 (C), 55.6 (CH), 54.9 (CH), 51.1 (CH_3), 46.1 (CH), 40.6 (CH_2), 40.4 (CH_2), 40.0 (CH_2), 27.2 (CH_3), 26.1 (CH_3), 26.0 (CH_3), 25.9 (CH_3), 25.8 (CH_3), 24.4 (CH_3), 23.3 (CH_3), 22.6 (CH_3), 22.4 (CH_3), 22.3 (CH_3), 22.0 (CH_3), 21.9 (CH_3), 21.8 (CH_3).

Compound 150. 149 (300 mg, 0.23 mmol) was dissolved in CH_2Cl_2/TFA (1:1, 5 mL) and the reaction mixture was stirred at rt for 30 min before being precipitated with Et_2O. The precipitate was filtered off, washed with Et_2O, and used directly without further purification.

To a solution of crude deprotected product in DMF (1.5 mL) was added acetic anhydride (26 µL, 0.28 mmol) and DIPEA (49 µL, 0.28 mmol), and the reaction mixture was stirred at rt for 1 h before being diluted with EtOAc (15 mL), washed with 10% citric acid (3 x 15 mL), aq. $NaHCO_3$ (sat., 3 x 15 mL) and brine (3 x 15 mL). The organic layer was dried over Na_2SO_4, filtered, and concentrated in vacuo to afford **150** (270 mg, 94 %) as a colorless solid. R_f (CH_2Cl_2 + 10% MeOH): 0.48; IR (neat): 3325 (br), 2970 (br), 2489 (br), 1780 (m), 1651 (s), 1548 (m), 1447 (s), 1388 (m), 1366 (m), 1249 (s), 1154 (m), 1000 (w), 937 (w), 812 (w), 757 (w), 744 (w); CD (TFE, 0.2 mM): 208 (–18.2), 195 (+12.9); ^{1}H NMR (400 MHz, $CDCl_3$): 7.77 (d, $^{3}J_{H\text{-}H}$ = 7.8 Hz, 2H), 7.61 (d, $^{3}J_{H\text{-}H}$ = 7.4 Hz, 2H), 7.36 (t, $^{3}J_{H\text{-}H}$ = 7.5 Hz, 2H), 7.28 (t, $^{3}J_{H\text{-}H}$ = 6.7 Hz, 2H), 5.98 – 5.79 (m, 2H), 5.34 – 5.08 (m, 4H), 4.54 (t, $^{3}J_{H\text{-}H}$ = 5.1 Hz, 2H), 4.46 (t, $^{3}J_{H\text{-}H}$ = 4.7 Hz, 2H),

4.34 – 4.30 (m, 2H), 4.26 (t, $^{3}J_{H\text{-}H}$ = 6.4 Hz, 1H), 4.18 (q, $^{3}J_{H\text{-}H}$ = 6.5 Hz, 1H), 4.15 – 4.05 (m, 2H), 3.64 (s, 3H), 3.77 – 3.35 (m, 6H), 1.99 (s, 3H), 1.49 (s, 6H), 1.48 (s, 6H), 1.46 (s, 6H), 1.45 (s, 3H), 1.46 – 1.41 (m, 21H), 1.42 (s, 3H); ^{13}C NMR (101 MHz, $CDCl_3$): 177.8 (C), 176.5 (C), 176.2 (C), 176.0 (C), 175.9 (C), 175.8 (C), 175.3 (C), 175.0 (C), 172.3 (C), 172.3 (C), 171.4 (C), 171.2 (C), 170.3 (C), 157.7 (C), 157.5 (C), 157.2 (C), 157.1 (C), 156.9 (C), 156.8 (C), 143.9 (C), 143.8 (C), 141.2 (C), 132.8 (CH), 127.4 (CH), 126.8 (CH), 124.8 (CH), 124.7 (CH), 119.6 (CH), 116.4 (CH_2), 116.2 (CH_2), 66.5 (CH_2), 65.4 (CH_2), 65.3 (CH_2), 65.1 (CH_2), 56.8 (C), 56.7 (C), 56.6 (CH), 56.6 (C), 56.6 (C), 56.5 (C), 56.5 (CH), 56.4 (C), 56.0 (CH), 55.7 (C), 54.8 (CH), 54.5 (CH), 51.2 (CH_3), 41.4 (CH_2), 41.1 (CH_2), 40.6 (CH_2), 25.6 (CH_3), 25.2 (CH_3), 25.0 (CH_3), 24.3 (CH_3), 24.2 (CH_3), 24.1 (CH_3), 23.6 (CH_3), 23.5 (CH_3), 23.3 (CH_3), 23.2 (CH_3), 23.0 (CH_3), 22.9 (CH_3), 22.6 (CH_3), 22.5 (CH_3), 22.3 (CH_3), 21.2 (CH_3).

Compound 151. To a solution of **150** (250 mg, 0.200 mmol) in CH_2Cl_2 (3 mL) was added tetrakis(triphenylphosphine)palladium (2.3 mg, 2.0 μmol) and phenylsilane (500 μL, 4.05 mmol), and the reaction mixture was stirred at rt for 2 h. The reaction mixture was precipitated with Et_2O and the precipitate was filtered, washed twice with Et_2O and dried *in vacuo*. The crude deprotected product was dissolved in Me_2NH in THF (2 M, 5 mL) and stirred at rt for 20 min. The solvent was removed *in vacuo*, the product was dissolved in a minimum amount of CH_2Cl_2, precipitated with pentane, filtered, washed twice with pentane and dried *in vacuo*. The crude product was purified by RP column chromatography (BGB Scorpius® C_{18} 5.4 g, linear gradient 5 – 30% MeCN + 0.1% TFA in H_2O + 0.1% TFA) to afford **151** (170 mg, 71 %) as a colorless solid. IR (neat): 2991 (br), 1677 (s), 1546 (s), 1471 (w), 1388 (m), 1367 (w), 1203 (s), 1187 (s), 1146 (s), 1073 (s), 841 (w), 725 (w); CD (TFE, 0.2 mM): 240 (–2.4), 213 (–3.5), 193 (–4.6); ^{1}H NMR (500 MHz, CD_3OD): 4.46 – 4.28 (m, 3H), 3.66 (s, 3H), 3.65 – 3.45 (m, 4H), 3.28 – 3.21 (m, 2H), 2.07 (s, 3H), 1.56 – 1.52 (m, 6H), 1.51 – 1.48 (m, 12H), 1.48 – 1.45 (m, 6H), 1.45 (s, 3H), 1.44 – 1.43 (m, 3H),

1.42 (s, 3H); ^{13}C NMR (126 MHz, CD_3OD): 177.7 (C), 176.5 (C), 176.3 (C), 175.8 (C), 175.3 (C), 174.7 (C), 173.2 (C), 173.1 (C), 170.3 (C), 170.2 (C), 169.7 (C), 168.7 (C), 161.6 (q, $^2J_{C\text{-}F}$ = 34.8 Hz, TFA), 116.4 (q, $^1J_{C\text{-}F}$ = 292.4 Hz, TFA), 57.0 (C), 56.9 (C), 56.8 (C), 56.6 (C), 56.5 (C), 55.9 (C), 51.8 (CH), 51.6 (CH), 51.3 (CH_3), 50.9 (CH), 40.0 (CH_2), 39.3 (CH_2), 39.0 (CH_2), 25.0 (CH_3), 24.9 (CH_3), 24.8 (CH_3), 24.7 (CH_3), 24.5 (CH_3), 24.4 (CH_3), 24.3 (CH_3), 24.1 (CH_3), 23.6 (CH_3), 23.5 (CH_3), 23.4 (CH_3), 23.2 (CH_3), 23.1 (CH_3), 23.0 (CH_3), 22.9 (CH_3), 22.8 (CH_3), 22.7 (CH_3), 21.5 (CH_3).

Compound 152. To a solution of **151** (85 mg, 70 μmol) and DIPEA (50 μL, 0.29 mmol) in DMF (3 mL) was added **131** (78 mg, 0.29 mmol), and the reaction mixture was stirred at rt for 1 h. The crude mixture was purified by RP flash column chromatography (BGB Scorpius® C_{18} 20 g, 25 mL/min, linear gradient 5 – 50% MeCN + 0.1% TFA in H_2O + 0.1% TFA) to afford **152** (51 mg, 54 %) as a colorless solid. IR (neat): 3310 (br), 2980 (br), 1730 (m), 1664 (s), 1541 (s), 1459 (m), 1390 (m), 1367 (m), 1251 (m), 1229 (m), 1162 (m), 1074 (s), 1050 (s), 872 (w), 861 (w), 822 (w), 749 (w), 723 (w); CD (TFE, 0.2 mM): 224 (–7.7), 207 (–17.1), 191 (+8.3); ^{1}H NMR (500 MHz, CD_3OD): 4.25 – 4.17 (m, 2H), 4.07 – 3.99 (m, 1H), 3.75 – 3.52 (m, 6H), 3.65 (s, 1H) 3.48 – 3.33 (m, 1H), 2.01 (s, 3H), 1.51 (s, 3H), 1.49 (s, 9H), 1.49 – 1.47 (m, 12H), 1.47 – 1.46 (m, 9H), 1.46 – 1.43 (m, 30H); ^{13}C NMR (126 MHz, CD_3OD): 177.2 (C), 176.5 (C), 175.9 (C), 175.6 (C), 175.4 (C), 175.2 (C), 172.3 (C), 171.6 (C), 171.3 (C), 170.5 (C), 160.2 (C), 160.1 (C), 160.0 (C), 157.2 (C), 157.0 (C), 156.8 (C), 80.8 (C), 80.7 (C), 80.6 (C), 56.8 (C), 56.7 (C), 56.6 (C), 56.5 (C), 56.5 (C), 56.4 (CH), 55.7 (C), 55.4 (CH), 55.2 (CH), 51.2 (CH_3), 40.3 (CH_2), 39.9 (CH^{+}), 39.7 (CH_2), 27.3 (CH_3), 24.8 (CH_3), 24.7 (CH_3), 24.2 (CH_3), 24.0 (CH_3), 23.8 (CH_3), 23.7 (CH_3), 23.5 (CH_3), 23.4 (CH_3), 21.3 (CH_3).

5.2.3. Synthesis of Dichalcogenide-Containing Aldehydes

Compound 153 was synthesized according to a procedure described in reference.[245]

Compound 154 was synthesized according to a procedure described in reference.[125]

Compound 155 was synthesized according to a procedure described in reference.[112]

Compound 120. To a solution of **154** (300 mg, 2.00 mmol), HATU (837 mg, 2.20 mmol) and DIPEA (383 µL, 2.20 mmol) in DMF (10 mL) was added **153** (362 mg, 2.00 mmol). The reaction mixture was stirred at room temperature for 30 min before being diluted with EtOAc (100 mL). The organic layer was washed with 10% citric acid (3 x 100 mL), aq. $NaHCO_3$ (sat., 3 x 100 mL) and brine (3 x 100 mL), dried over Na_2SO_4, filtered, and concentrated *in vacuo* to yield **120** (480 mg, 96%) as a light-yellow solid without further purification. R_f (CH_2Cl_2 + 10% MeOH): 0.63; IR (neat): 3310 (br), 1704 (s), 1656 (s), 1609 (s), 1551 (s), 1442 (w), 1211 (m), 600 (s); ^{1}H NMR (400 MHz, $CDCl_3$): 10.02 (s, 1H), 7.87 (d, $^3J_{H\text{-}H}$ = 8.1 Hz, 2H), 7.45 (d, $^3J_{H\text{-}H}$ = 8.1 Hz, 2H), 6.25 (s, 1H), 4.56 (d, $^3J_{H\text{-}H}$ = 5.9 Hz, 2H), 3.58 – 3.26 (m, 5H); ^{13}C NMR (101 MHz, $CDCl_3$): 191.7 (C), 171.9 (C), 144.8 (C), 135.8 (C), 130.2 (CH), 128.1 (CH), 52.3 (CH), 43.5 (CH_2), 42.8 (CH_2).

Compound 156. To a solution of lipoic acid **17** (1.03 g, 5.00 mmol), HATU (2.09 g, 5.50 mmol) and DIPEA (958 µL, 5.50 mmol) in DMF (25 mL) was added **153** (906 mg, 5.00 mmol). The reaction mixture was stirred at room temperature for 30 min before being diluted with EtOAc (250 mL). The organic layer was washed with 10% citric acid (3 x 250 mL), aq. $NaHCO_3$ (sat., 3 x 250 mL) and brine (3 x 250 mL), dried over Na_2SO_4, filtered, and concentrated in vacuo to yield **156** (1.60 g, 99 %) as a yellow solid without further purification. R_f (CH_2Cl_2 + 10% MeOH): 0.76; IR (neat): 3283 (s), 2931 (m), 2850 (m), 1694

(s), 1634 (s), 1607 (m), 1563 (s), 1461 (w), 1416 (m), 1384 (w), 1300 (w), 1251 (m), 1202 (m), 1166 (m), 828 (m), 787 (m), 694 (m); ^{1}H NMR (400 MHz, $CDCl_3$): 10.01 (s, 1H), 7.86 (d, $^{3}J_{H\text{-}H}$ = 8.2 Hz, 2H), 7.45 (d, $^{3}J_{H\text{-}H}$ = 8.2 Hz, 2H), 5.87 (s, 1H), 4.54 (d, $^{3}J_{H\text{-}H}$ = 6.0 Hz, 2H), 3.68 – 3.50 (m, 1H), 3.24 – 3.06 (m, 2H), 2.57 – 2.38 (m, 1H), 2.28 (t, $^{3}J_{H\text{-}H}$ = 7.4 Hz, 2H), 2.00 – 1.83 (m, 2H), 1.82 – 1.62 (m, 4H), 1.56 – 1.42 (m, 2H); ^{13}C NMR (101 MHz, $CDCl_3$): 191.9 (C), 172.9 (C), 145.5 (C), 135.8 (C), 130.3 (CH), 128.3 (CH), 56.6 (CH), 43.4 (CH_2), 40.4 (CH_2), 38.6 (CH_2), 36.5 (CH_2), 34.7 (CH_2), 29.0 (CH_2), 25.5 (CH_2).

Compound 157. To a solution of **155** (156 mg, 0.640 mmol), HATU (267 mg, 0.700 mmol) and DIPEA (122 µL, 0.700 mmol) in DMF (3 mL) was added **153** (116 mg, 0.640 mmol). The reaction mixture was stirred at room temperature for 30 min before being diluted with EtOAc (100 mL). The organic layer was washed with 10% citric acid (3 x 100 mL), aq. $NaHCO_3$ (sat., 3 x 100 mL) and brine (3 x 100 mL), dried over Na_2SO_4, filtered, and concentrated in vacuo to yield **157** (127 mg, 55%) as a red solid without further purification. R_f (CH_2Cl_2 + 10% MeOH): 0.63; IR (neat): 3301 (br), 2980 (s), 2927 (s), 2853 (s), 1661 (s), 1603 (m), 1548 (m), 1452 (m), 1381 (m), 1304 (w), 1240 (m), 1167 (w), 1061 (s), 1049 (s), 1012 (m), 823 (m); ^{1}H NMR (400 MHz, $CDCl_3$): 10.01 (s, 1H), 7.86 (d, $^{3}J_{H\text{-}H}$ = 8.1 Hz, 2H), 7.47 (d, $^{3}J_{H\text{-}H}$ = 8.1 Hz, 2H), 6.53 (s, 1H), 4.57 (d, $^{3}J_{H\text{-}H}$ = 5.8 Hz, 2H), 3.79 – 3.69 (m, 1H), 3.63 (dd, $^{2}J_{H\text{-}H}$ = 10.6, $^{3}J_{H\text{-}H}$ = 6.6 Hz, 2H), 3.54 – 3.46 (m, 2H); ^{13}C NMR (101 MHz, $CDCl_3$): 190.6 (C), 170.8 (C), 143.7 (C), 134.9 (C), 129.2 (CH), 127.1 (CH), 56.1 (CH), 42.6 (CH_2), 32.2 (CH_2).

5.2.4. Synthesis of Semicarbazones

Buffer A: 50 mM **159**, 150 mM NaCl, pH 5.0

Compound 158. 132 (200 mg, 0.400 mmol) was dissolved in CH_2Cl_2/TFA (1:1, 4 mL) and the reaction mixture was stirred at rt for 1 h. The reaction mixture was precipitated with Et_2O/pentane (1:1, 200 mL) and the crude product was filtered and washed three times with Et_2O/pentane (1:1, 200 mL). The crude colorless solid (TFA salt, 180 mg, 88 %) was used without further purification.

Compound 160. To a solution of **120** (5.9 mg, 22 µmol) in DMF (0.5 mL) were added **158** (11 mg, 22 µmol) and buffer A (4 mL) and the reaction mixture was stirred at rt for 1 h. The precipitate formed was filtered off and purified by RP flash column chromatography (BGB Scorpius® C_{18} 5.4 g, 10 mL/min, linear gradient 30 – 100% MeCN + 0.1% TFA in H_2O + 0.1% TFA) to afford **160** (11 mg, 79%) as a colorless solid. IR (neat): 3311 (br), 1691 (s), 1573 (s), 1479 (w), 1400 (w), 1194 (w), 1167 (w), 1101 (w); $[\alpha]_D^{20}$ +7.91 (*c* 1.00, EtOH); ^{1}H NMR (400 MHz, CD_3CN): 7.82 (s, 1H), 7.63 (d, $^3J_{H\text{-}H}$ = 8.1 Hz, 2H), 7.29 (d, $^3J_{H\text{-}H}$ = 8.1 Hz, 2H), 4.34 (s, 2H), 4.25 (dd, $^3J_{H\text{-}H}$ = 7.2, 5.4 Hz, 1H), 3.57 (s, 3H), 3.54 (dd, $^2J_{H\text{-}H}$ = 14.1, $^3J_{H\text{-}H}$ = 5.4 Hz, 1H), 3.43 (dd, $^2J_{H\text{-}H}$ = 14.1, $^3J_{H\text{-}H}$ = 7.2 Hz, 1H), 3.40 – 3.34 (m, 2H), 3.30 – 3.20 (m, 3H), 1.92 (s, 3H), 1.34 (s, 3H), 1.34 – 1.33 (m, 6H), 1.33 (s, 3H); ^{13}C NMR (101 MHz, CD_3CN): 175.5 (C), 174.1 (C), 171.7 (C), 171.6 (C), 170.2 (C), 157.2 (C), 141.5 (CH), 133.9 (C), 128.2 (CH), 127.5 (CH), 57.1 (C), 56.6 (CH), 56.2 (C), 52.4 (C), 52.1 (CH_3), 43.2 (CH_2), 42.9 (CH_2), 41.1 (CH_2), 25.2 (CH_3), 25.0 (CH_3), 24.8 (CH_3), 22.8 (CH_3).

Compound 161. To a solution of **157** (7.9 mg, 22 µmol) in DMF (0.5 mL) were added **158** (11 mg, 22 µmol) and buffer A (4 mL) and the reaction mixture was stirred at rt for 1 h. The precipitate formed was filtered off and purified by RP flash column chromatography (BGB Scorpius® C_{18} 5.4 g, 10 mL/min, linear gradient 5 – 100% MeCN + 0.1% TFA in H_2O + 0.1% TFA) to afford **161** (12 mg, 75 %) as a colorless solid. IR (neat): 3300 (br), 2980 (br), 1670 (s), 1549 (s), 1481 (w), 1448 (w), 1391 (w), 1203 (m), 1074 (m), 1048 (m), 891 (w), 851 (w),

775 (w); $[\alpha]_D^{20}$ +9.35 (*c* 1.00, EtOH); ^{1}H NMR (400 MHz, CD_3CN): 7.82 (s, 1H), 7.63 (d, $^3J_{H\text{-}H}$ = 8.3 Hz, 2H), 7.29 (d, $^3J_{H\text{-}H}$ = 8.3 Hz, 2H), 4.34 (s, 2H), 4.26 (dd, $^3J_{H\text{-}H}$ = 7.3, 5.5 Hz, 1H), 3.57 (s, 3H), 3.56 – 3.34 (m, 6H), 1.34 (s, 3H), 1.33 (s, 3H), 1.33 (s, 3H), 1.32 (s, 3H); ^{13}C NMR (101 MHz, CD_3CN): 176.0 (C), 174.7 (C), 173.0 (C), 172.7 (C), 170.7 (C), 157.5 (C), 142.5 (CH), 141.2 (C), 133.8 (C), 128.3 (CH), 127.6 (C), 57.7 (CH), 57.1 (C), 56.2 (C), 55.4 (CH), 52.4 (CH_3), 43.2 (CH_2), 40.9 (CH_2), 35.0 (CH_2), 25.2 (CH_3), 24.8 (CH_3), 24.6 (CH_3), 24.5 (CH_3), 22.6 (CH_3).

Compound 116. 139 (10 mg, 7.6 μmol) was dissolved in 4 M HCl in 1,4-dioxane (1 mL) and the reaction mixture was stirred at rt for 1 h, before the solvent was removed *in vacuo*. A solution of **120** (5.9 mg, 23 μmol) in DMF (750 μL) was added together with buffer A (7 mL), and the reaction mixture was stirred at rt for 16 h. The precipitate formed was filtered off and purified by RP flash column chromatography (BGB Scorpius® C_{18} 5.4 g, 10 mL/min, linear gradient 30 – 100% MeCN + 0.1% TFA in H_2O + 0.1% TFA) to afford **116** (8.3 mg, 62%) as a colorless solid. IR (neat): 3300 (br), 2980 (br), 1659 (s), 1544 (s), 1425 (m), 1388 (w), 1366 (w), 1281 (w), 1255 (w), 1211 (m), 1150 (m), 1057 (m), 724 (w), 676 (w); CD (TFE, 0.2 mM): 224 (–5.9), 210 (–7.6), 198 (+15.0); HPLC-MS: 1.87 min; 883 (100, $[M+2H]^{2+}$), 1764 (54, $[M+H]^+$); HRMS (ESI, +ve) calc. for $C_{75}H_{105}N_{21}O_{17}S_6$: 882.8234, found: 882.8198.

Compound 162. 139 (10 mg, 7.6 μmol) was dissolved in 4 M HCl in 1,4-dioxane (1 mL) and the reaction mixture was stirred at rt for 1 h, before the solvent was removed *in vacuo*. A solution of **156** (7.4 mg, 23 μmol) in DMF (750 μL) was added together with buffer A (7 mL), and the reaction mixture was stirred at rt for 16 h. The precipitate formed was filtered off and purified by RP flash column chromatography (BGB Scorpius® C_{18} 5.4 g, 10 mL/min, linear gradient 30 – 70% MeCN + 0.1% TFA in H_2O + 0.1% TFA) to afford **162** (11.0 mg, 75%) as a colorless solid. IR (neat): 3300 (br), 2980 (br), 1681 (s), 1662 (s), 1544 (s), 1388 (w), 1366 (w), 1254 (w), 1213 (m), 1056 (s); CD (TFE, 0.2 mM):

220 (–10.2), 209 (–13.4), 193 (+21.1); HPLC-MS: 2.23 min; 967 (100, $[M+2H]^{2+}$), 1933 (24, $[M+H]^{+}$); HRMS (ESI, +ve) calc. for $C_{87}H_{129}N_{21}O_{17}S_6$: 966.9173, found: 966.9145.

Compound 163. 139 (5.0 mg, 3.8 μmol) was dissolved in 4 M HCl in 1,4-dioxane (0.5 mL) and the reaction mixture was stirred at rt for 1 h, before the solvent was removed *in vacuo*. A solution of **157** (5.5 mg, 15 μmol) in DMF (380 μL) was added together with buffer A (4 mL), and the reaction mixture was stirred at rt for 16 h. The precipitate formed was filtered off and purified by RP flash column chromatography (BGB Scorpius® C_{18} 5.4 g, 10 mL/min, linear gradient 30 – 70% MeCN + 0.1% TFA in H_2O + 0.1% TFA) to afford **163** (4.3 mg, 55%) as a colorless solid. IR (neat): 3355 (br), 2985 (br), 1650 (s), 1575 (m), 1553 (m), 1408 (w), 1388 (w), 1366 (w), 1204 (w), 1157 (w), 1075 (m), 1050 (w); CD (TFE, 0.2 mM): 221 (–7.9), 213 (–8.0), 192 (+7.7); HPLC-MS: 1.89 min; 1024 (100, $[M+2Na]^{2+}$); HRMS (ESI, +ve) calc. for $C_{75}H_{105}N_{21}O_{17}Se_6$: 1024.6598, found: 1025.6662.

Compound 164. 152 (10 mg, 7.6 μmol) was dissolved in 4 M HCl in 1,4-dioxane (1 mL) and the reaction mixture was stirred at rt for 1 h, before the solvent was removed *in vacuo*. A solution of **120** (10.1 mg, 38.0 μmol) in DMF (380 μL) was added together with buffer A (4 mL), and the reaction mixture was stirred at rt for 16 h. The precipitate formed was filtered off and purified by RP flash column chromatography (BGB Scorpius® C_{18} 20 g, 20 mL/min, linear gradient 40 – 100% MeCN + 0.1% TFA in H_2O + 0.1% TFA) to afford **164** (9.6 mg, 72%) as a colorless solid. IR (neat): 3315 (br), 2976 (br), 1680 (s), 1657 (s), 1550 (m), 1541 (s), 1529 (m), 1404 (w), 1388 (w), 1366 (w), 1255 (w), 1227 (w), 1077 (m), 1052 (w); CD (TFE, 0.2 mM): 221 (–8.6), 209 (–11.0), 192 (+7.5); HPLC-MS: 1.77 min; 883 (100, $[M+2H]^{2+}$), 1764 (78, $[M+H]^{+}$); HRMS (ESI, +ve) calc. for $C_{75}H_{105}N_{21}O_{17}S_6$: 882.8234, found: 882.8198.

5.2.5. Synthesis of Antibiotic-COC Conjugates

Compound 204e was synthesized according to a procedure described in reference.[214]

Compounds 209, 210, 213 and 214 were synthesized according to procedures described in reference.[88]

Compound 211 was synthesized according to a procedure described in reference.[112]

Compound 212. was synthesized according to a procedure described in reference.[246]

Compound 215. 211 (6.8 mg, 17 μmol) was dissolved in DMF (200 μL), DIPEA (6.0 μL, 34 μmol) and propargylamine (2.2 μL, 34 μmol) were added and the reaction mixture was stirred at rt for 2 h. The crude reaction mixture was concentrated *in vacuo* and purified by flash column chromatography (Biotage® SNAP Ultra 10 g, 12 mL/min, linear gradient 0 – 10% MeOH in CH_2Cl_2) to yield **215** as an orange solid (4.1 mg, 72%). R_f (CH_2Cl_2 + 1% MeOH): 0.48; IR (neat): 3281 (br) 3063 (w), 2928 (m), 2856 (w), 1707 (w), 1641 (s), 1529 (s), 1419 (m), 1350 (m), 1239 (m), 1130 (w), 1029 (w), 923 (w), 642 (br); mp: 63 – 64 °C; ^{1}H NMR (400 MHz, $CDCl_3$): 5.60 (br s, 1H), 4.05 (dd, $^3J_{H\text{-}H}$ = 5.3 Hz, $^4J_{H\text{-}H}$ = 2.5 Hz, 2H), 3.95 – 3.86 (m, 1H), 3.32 (t, $^3J_{H\text{-}H}$ = 6.2 Hz, 2H), 3.03 – 2.90 (m, 1H), 2.57 – 2.47 (m, 1H), 2.23 (d, $^4J_{H\text{-}H}$ = 2.5 Hz, 1H), 2.21 (t, $^3J_{H\text{-}H}$ = 7.6 Hz, 2H), 1.88 – 1.60 (m, 4H), 1.50 – 1.40 (m, 2H); ^{13}C NMR (101 MHz, $CDCl_3$): 172.2 (C), 79.6 (C), 71.7 (CH), 52.7 (CH), 45.7 (CH_2), 36.1 (CH_2), 35.3 (CH_2), 29.8 (CH_2), 29.4 (CH_2), 29.2 (CH_2), 25.1 (CH_2); HRMS (ESI, +ve) calc. for $C_{11}H_{17}NOSe_2Na$: 361.9536, found: 361.9516.

Compound 204d. 204e (170 mg, 0.23 mmol) and KOH (21 mg, 0.37 mmol) were dissolved in CH_3CN (6 mL) and stirred at rt. After 10 min and complete dissolution of KOH, **212** (51 mg, 0.27 mmol) was added and the reaction mixture was. stirred overnight at rt. The reaction mixture was concentrated *in vacuo* and

purified by flash column chromatography (Biotage® SNAP Ultra 25 g, 25 mL/min, linear gradient 0 – 10% MeOH in CH_2Cl_2) to afford **204d** as a colorless solid (79 mg, 36%). R_f (CH_2Cl_2/MeOH 9:1): 0.43; HPLC-MS: 2.66 min; 1741 (20, $[2M+Na]^+$), 882 (80, $[M+Na]^+$), 860 (100, $[M+H]^+$); HRMS (ESI, +ve) calc. for $C_{42}H_{78}N_5O_{13}$: 860.5591, found: 860.5596.

Compound 204a. To a solution of **204d** (2.6 mg, 3 µmol) and **213** (1.2 mg, 6 µmol) in H_2O/THF 1:1 (100 µL) were added sodium ascorbate (6.6 µL, 100 mM in H_2O, 0.66 µmol), $CuSO_4 \cdot 5H_2O$ (6.6 µL, 100 mM in H_2O, 0.66 µmol) and TBTA (6.6 µL, 1 mM in THF, 6.6 nmol). The resulting mixture was stirred at rt for 1.5 h, concentrated *in vacuo* and purified by semi-preparative RP-HPLC (MeCN/H_2O + 0.1% TFA [50%, 5 min] then [50 to 95%, 35 min], R_t 28.5) to yield **204a** as a colorless solid (1.1 mg, 35%). HPLC-MS: 2.39 min; 1069 (100, $[M+Na]^+$), 1047 (45, $[M+H]^+$); HRMS (ESI, +ve) calc. for $C_{49}H_{87}N_6O_{14}S_2$: 1047.5716, found: 1047.5725.

Compound 204b. To a solution of **204d** (8.6 mg, 10 µmol) and **214** (3.6 mg, 15 µmol) in H_2O/THF 1:1 (100 µL) were added sodium ascorbate (30 µL, 100 mM in H_2O, 3 µmol), $CuSO_4 \cdot 5H_2O$ (30 µL, 100 mM in H_2O, 3 µmol) and TBTA (30 µL, 1 mM in THF, 0.03 µmol). The resulting mixture was stirred at rt for 1.5 h, concentrated *in vacuo* and purified by semi-preparative RP-HPLC (MeCN/H_2O + 0.1% TFA [60%, 5 min] then [60 to 95%, 35 min], R_t 29.3) to yield **204b** as a colorless solid (3.2 mg, 29%). HPLC-MS: 2.53 min; 1126 (100, $[M+Na]^+$), 1103 (20, $[M+H]^+$); HRMS (ESI, +ve) calc. for $C_{53}H_{95}N_6O_{14}S_2$: 1103.6342, found: 1103.6376.

Compound 204c. To a solution of **204d** (4.3 mg, 5 µmol) and **215** (2.0 mg, 5 µmol) in H_2O/THF 1:1 (100 µL) were added sodium ascorbate (13 µL, 100 mM in H_2O, 1.3 µmol), $CuSO_4 \cdot 5H_2O$ (13 µL, 100 mM in H_2O, 1.3 µmol) and TBTA (13 µL, 1 mM in THF, 0.013 µmol). The resulting mixture was stirred at rt for 1.5 h, concentrated *in vacuo* and purified by semi-preparative RP-HPLC (MeCN/H_2O + 0.1% TFA [60%, 5 min] then [60 to 95%, 35 min], R_t 30.5) to

yield **204c** as a light–yellow solid (2.0 mg, 33%). HPLC-MS: 2.56 min; 1221 (100, $[M+Na]^+$), 1199 (50, $[M+H]^+$); HRMS (ESI, +ve) calc. for $C_{53}H_{95}N_6O_{14}Se_2$: 1199.5246, found: 1199.5264.

Compound 205a. To a solution of **205d** (8 mg, 10 µmol) and DIPEA (7 µL, 40 µmol) in DMF (200 µL) was added a solution of **209** (10 mg, 40 µmol) in DMF (100 µL), and the resulting mixture was stirred at rt for 1 h. The completion of the reaction was confirmed by HPLC-MS analyses. The reaction mixture was purified by semi-preparative RP-HPLC (MeCN/H_2O + 0.1% TFA [30%, 5 min] then [30 to 95%, 35 min], R_t 20.5) to yield **205a** as a colorless solid (TFA salt, 5.7 mg, 49%). IR (neat): 3313 (br), 2923 (m), 2856 (m), 1739 (s), 1710 (s), 1644 (s), 1516 (s), 1440 (m), 1416 (m), 1362 (m), 1221 (s), 1161 (m), 1091 (m), 1031 (m), 802 (m), 751 (w), 732 (w), 647 (m); mp: 194 – 196 °C; ^{1}H NMR (400 MHz, $CDCl_3$): 7.47 (dd, $^3J_{F\text{-}H}$ = 14.1, $^4J_{H\text{-}H}$ = 2.6 Hz, 1H), 7.09 (dd, $^4J_{F\text{-}H}$ = 8.8, $^3J_{H\text{-}H}$ = 2.6 Hz, 1H), 7.03 – 6.99 (m, 1H), 6.92 (t, $^3J_{H\text{-}H}$ = 9.0 Hz, 1H), 6.11 (t, $^3J_{H\text{-}H}$ = 6.2 Hz, 1H), 4.81 – 4.75 (m, 1H), 4.14 (d, $^3J_{H\text{-}H}$ = 4.1 Hz, 2H), 4.04 (t, $^3J_{H\text{-}H}$ = 9.0 Hz, 1H), 3.82 (t, $^3J_{H\text{-}H}$ = 5.1 Hz, 2H), 3.79 – 3.69 (m, 2H), 3.67 – 3.56 (m, 3H), 3.56 – 3.48 (m, 2H), 3.40 (d, $^3J_{H\text{-}H}$ = 6.2 Hz, 4H), 3.37 – 3.26 (m, 3H), 3.10 – 3.04 (m, 4H), 2.90 – 2.84 (m, 2H), 2.05 (s, 3H); ^{13}C NMR (101 MHz, $CDCl_3$): 172.1 (C), 171.8 (C), 166.5 (C), 155.8 (d, $^1J_{F\text{-}C}$ = 245 Hz, C), 154.5 (C), 119.9 (d, $^3J_{F\text{-}C}$ = 3.8 Hz, CH), 114.1 (d, $^4J_{F\text{-}C}$ = 2.8 Hz, CH), 107.8 (d, $^2J_{F\text{-}C}$ = 26.1 Hz, CH), 72.0 (CH), 52.2 (CH), 50.9 (CH_2), 50.6 (CH_2), 47.8 (CH_2), 44.7 (CH_2), 42.8 (CH_2), 42.2 (CH_2), 41.6 (CH_2), 25.7 (CH_2), 25.5 (CH_2), 23.2 (CH_3); ^{19}F NMR (282 MHz, $CDCl_3$): –75.9 (1F), –120.0 (3F); HPLC-MS: 1.80 min; 526 (100, $[M+H]^+$); HRMS (ESI, +ve) calc. for $C_{22}H_{29}FN_5O_5S_2$: 526.1589, found: 526.1601.

Compound 205b. To a solution of **205d** (8 mg, 20 µmol) and DIPEA (7 µL, 40 µmol) in DMF (200 µL) was added a solution of **210** (12 mg, 40 µmol) in DMF (100 µL), and the resulting mixture was stirred at rt for 1 h. The completion of the reaction was confirmed by HPLC-MS. The reaction mixture was purified

by semi-preparative RP-HPLC (MeCN/H_2O + 0.1% TFA [40%, 5 min] then [40 to 95%, 35 min], R_t 27.4) to yield **205b** as a colorless solid (TFA salt, 3.4 mg, 32%). IR (neat): 3301 (br), 2923 (s), 2850 (w), 1733 (s), 1659 (s), 1637 (s), 1564 (m), 1518 (m), 1420 (m), 1225 (s), 1078 (w), 1030 (w), 810 (w), 755 (w), 631 (w); mp: 169 – 170 °C; ^{1}H NMR (400 MHz, $CDCl_3$): 7.48 (dd, $^3J_{F\text{-}H}$ = 14.1, $^4J_{H\text{-}H}$ = 2.6 Hz, 1H), 7.09 (dd, $^4J_{F\text{-}H}$ = 8.8, $^3J_{H\text{-}H}$ = 2.7 Hz, 1H), 6.96 (t, $^3J_{H\text{-}H}$ = 9.0 Hz, 1H), 6.64 (t, $^3J_{H\text{-}H}$ = 3.5 Hz, 1H), 5.98 (t, $^3J_{H\text{-}H}$ = 6.2 Hz, 1H), 4.81 – 4.74 (m, 1H), 4.11 (d, $^3J_{H\text{-}H}$ = 4.0 Hz, 2H), 4.03 (t, $^3J_{H\text{-}H}$ = 9.0 Hz, 1H), 3.83 (t, $^3J_{H\text{-}H}$ = 5.1 Hz, 2H), 3.80 – 3.68 (m, 2H), 3.67 – 3.53 (m, 4H), 3.24 – 3.03 (m, 6H), 2.53 – 2.41 (m, 1H), 2.30 (t, $^3J_{H\text{-}H}$ = 7.5 Hz, 3H), 2.03 (s, 3H), 1.96 – 1.87 (m, 1H), 1.75 – 1.62 (m, 4H), 1.57 – 1.41 (m, 2H); ^{13}C NMR (101 MHz, $CDCl_3$): 173.3 (C), 171.3 (C), 166.7 (C), 155.8 (d, $^1J_{F\text{-}C}$ = 247 Hz, C), 154.3 (C), 119.9 (d, $^3J_{F\text{-}C}$ = 3.6 Hz, CH), 114.0 (d, $^4J_{F\text{-}C}$ = 2.9 Hz, CH), 107.7 (d, $^2J_{F\text{-}C}$ = 26.3 Hz, CH), 72.0 (CH), 56.5 (CH), 47.8 (CH_2), 44.6 (CH_2), 42.2 (CH_2), 41.4 (CH_2), 40.4 (CH_2), 38.6 (CH_2), 36.3 (CH_2), 34.8 (CH_2), 29.0 (CH_2), 25.5 (CH_2), 23.3 (CH_3); ^{19}F NMR (282 MHz, $CDCl_3$): –75.9 (1F), –120.0 (3F); HPLC-MS: 2.16 min; 582 (100, $[M+H]^+$); HRMS (ESI, +ve) calc. for $C_{26}H_{37}FN_5O_5S_2$: 582.2215, found: 582.2222.

Compound 206a. To a solution of **206** (35 mg, 0.1 mmol) and DIPEA (26 µL, 0.1 mmol) in DMF (300 µL) was added a solution of **209** (27 mg, 0.11 mmol) in DMF (100 µL), and the resulting mixture was stirred at rt for 1.5 h. The completion of the reaction was confirmed by HPLC-MS. The reaction mixture was concentrated *in vacuo* and purified by reverse-phase column chromatography (Biotage® SNAP Ultra C_{18} 30 g, linear gradient 5 – 70% MeCN + 0.1% TFA in H_2O + 0.1% TFA) to yield **206a** as a colorless solid (29 mg, 61%). IR (neat): 3282 (br), 3063 (w), 2928 (m), 2856 (w), 1707 (w), 1641 (s), 1529 (s), 1420 (w), 1350 (m), 1239 (m), 1130 (w), 1029 (w), 923 (w), 642 (br); mp: 188 – 190 °C; ^{1}H NMR (400 MHz, CD_3OD): 8.91 (d, $^3J_{H\text{-}H}$ = 7.4 Hz, 1H), 8.71 (d, $^3J_{H\text{-}H}$ = 7.0 Hz, 1H), 7.48 – 7.41 (m, 2H), 7.41 – 7.29 (m, 3H), 5.61 – 5.50 (m, 2H),

5.45 (d, $^{3}J_{H\text{-}H}$ = 4.0 Hz, 1H), 4.31 (s, 1H), 3.48 – 3.32 (m, 4H), 3.27 – 3.18 (m, 1H), 1.55 (s, 3H), 1.47 (s, 3H); ^{13}C NMR (101 MHz, CD_3OD): 174.4 (C), 173.9 (C), 172.2 (C), 171.0 (C), 138.1 (C), 129.8 (CH), 129.5 (CH), 128.9 (CH), 71.9 (C), 68.7 (CH), 65.1 (CH), 60.0 (CH), 58.6 (CH), 52.6 (CH), 43.7 (CH_2), 43.5 (CH_2), 31.0 (CH_3), 27.3 (CH_3); HPLC-MS: 2.20 min; 481.9 (100, $[M+H]^+$); HRMS (ESI, +ve) calc. for $C_{20}H_{24}N_3O_5S_3$: 482.0873, found: 482.0853.

Compound 206c. To a solution of **206** (14 mg, 0.04 mmol) and DIPEA (12 µL, 0.08 mmol) in DMF (200 µL) was added a solution of **211** (19 mg, 0.044 mmol) in DMF (200 µL), and the resulting mixture was stirred at rt for 1.5 h. The completion of the reaction was confirmed by HPLC-MS. The reaction mixture was concentrated *in vacuo* and purified by reverse-phase column chromatography (Biotage® SNAP Ultra C_{18} 30 g, linear gradient 5 – 60% MeCN + 0.1% TFA in H_2O + 0.1% TFA) to yield **206c** as an orange solid (19.8 mg, 78%). IR (neat): 3305 (br), 2930 (m), 2482 (w), 1783 (s), 1736 (m), 1709 (s), 1640 (s), 1536 (m), 1497 (w), 1428 (s), 1361 (m), 1297 (m), 1220 (s), 1158 (m), 1131 (m), 1089 (w), 10130 (w), 316 (w), 884 (w), 798 (w), 726 (m), 698 (s), 648 (m), 529 (s); mp: 169 – 171 °C; ^{1}H NMR (400 MHz, $CDCl_3$ + 5% CD_3OD): 7.36 – 7.27 (m, 5H), 5.60 – 5.52 (m, 2H), 5.42 (d, $^{3}J_{H\text{-}H}$ = 4.1 Hz, 1H), 4.33 (s, 1H), 3.92 – 3.80 (m, 1H), 3.30 – 3.25 (m, 2H), 2.95 – 2.85 (m, 2H), 2.52 – 2.40 (m, 1H), 2.31 – 2.18 (m, 2H), 1.82 – 1.57 (m, 4H), 1.54 (s, 3H), 1.48 (s, 3H), 1.45 – 1.35 (m, 2H); ^{13}C NMR (101 MHz, $CDCl_3$ + 5% CD_3OD): 173.2 (C), 172.8 (C), 170.1 (C), 169.6 (C), 137.2 (C), 129.2 (CH), 128.7 (CH), 127.4 (CH), 70.7 (CH), 67.6 (CH), 64.5 (C), 58.5 (C), 56.8 (C), 52.3 (C), 45.7 (CH_2), 36.1 (CH_2), 36.1 (CH_2), 35.4 (CH_2), 31.2 (CH_3), 29.8 (CH_2), 29.5 (CH_2), 27.0 (CH_3), 25.3 (CH_2); HPLC-MS: 2.50 min; 634 (100, $[M+H]^+$); HRMS (ESI, +ve) calc. for $C_{24}H_{32}N_3O_5SSe_2$: 634.0388, found: 634.0404.

Compound 207d. To a solution of **207** (21 mg, 14 µmol) in DMF (400 µL) was added **216** (2.3 mg, 14 µmol) and DIPEA (4.5 µL, 28 µmol) in MeOH (400 µL), and the reaction mixture was stirred at 70 °C for 6 h. The mixture was

allowed to cool down to room temperature before the addition of sodium cyanoborohydride (3.5 mg, 56 µmol). After stirring at 70 °C for 16 h, the mixture was concentrated *in vacuo* and purified by semi-preparative RP-HPLC (MeCN/H_2O + 0.1% TFA [20%, 5 min] then [20 to 100%, 20 min]) to yield **207d** as a colorless solid (10.3 mg, 46%). HPLC-MS: 1.50 min; 1595 (50, $[M+H]^+$), 1064 (30, $[2M+3H]^{3+}$), 798 (100, $[M+2H]^{2+}$); HRMS (ESI, +ve) calc. for $C_{74}H_{83}Cl_2N_{12}O_{24}$: 797.2544, found: 797.2510 ($[M+2H]^{2+}$).

Compound 207a. To a solution of **207d** (3.5 mg, 2.2 µmol) and **213** (0.4 mg, 2.2 µmol) in H_2O/THF 1:1 (140µL) were added sodium ascorbate (30 µL, 100 mM in H_2O, 3 µmol), $CuSO_4 \cdot 5H_2O$ (30 µL, 100 mM in H_2O, 3 µmol) and TBTA (30 µL, 1 mM in THF, 0.03 µmol). The resulting mixture was stirred at rt for 3 h, concentrated *in vacuo* and purified by semi-preparative RP-HPLC (MeCN/H_2O + 0.1% TFA [30%, 5 min] then [30 to 100%, 20 min]) to yield **207a** as a colorless solid (1.2 mg, 31%). HPLC-MS: 1.56 min; 1782 (10, $[M+H]^+$), 1337 (5, $[3M+4H]^{4+}$), 1189 (40, $[2M+3H]^{3+}$), 892 (100, $[M+2H]^{2+}$); HRMS (ESI, +ve) calc. for $C_{81}H_{92}Cl_2N_{13}O_{25}S_2$: 1782.5146, found: 1782.5231.

Compound 207b. To a solution of **207d** (3.5 mg, 2.2 µmol) and **214** (0.5 mg, 2.2 µmol) in H_2O/THF 1:1 (140µL) were added sodium ascorbate (30 µL, 100 mM in H_2O, 3 µmol), $CuSO_4 \cdot 5H_2O$ (30 µL, 100 mM in H_2O, 3 µmol) and TBTA (30 µL, 1 mM in THF, 0.03 µmol). The resulting mixture was stirred at rt for 3 h, concentrated *in vacuo* and purified by semi-preparative RP-HPLC (MeCN/H_2O + 0.1% TFA [30%, 5 min] then [30 to 100%, 15 min]) to yield **207b** as a colorless solid (1.7 mg, 43%). HPLC-MS: 1.65 min; 1838 (25, $[M+H]^+$), 1471 (5, $[4M+5H]^{5+}$), 1379 (20, $[3M+4H]^{4+}$), 1226 (50, $[2M+3H]^{3+}$), 920 (100, $[M+2H]^{2+}$); HRMS (ESI, +ve) calc. for $C_{85}H_{100}Cl_2N_{13}O_{25}S_2$: 1838.5774, found: 1838.5821.

Compound 207c. To a solution of **207d** (1.6 mg, 1.0 µmol) and **215** (0.4 mg, 1.2 µmol) H_2O/THF 1:1 (110µL) were added sodium ascorbate (10 µL, 100 mM in H_2O, 1 µmol), $CuSO_4 \cdot 5H_2O$ (10 µL, 100 mM in H_2O, 1 µmol) and TBTA (10

µL, 1 mM in THF, 0.01 µmol). The resulting mixture was stirred at rt for 3 h, concentrated *in vacuo* and purified by semi-preparative RP-HPLC (MeCN/H_2O + 0.1% TFA [30%, 5 min] then [30 to 100%, 20 min]) to yield **207c** as a colorless solid (0.9 mg, 45%). HPLC-MS: 1.76 min; 1933 (40, $[M+H]^+$),1547 (10, $[4M+5H]^{5+}$), 1449 (40, $[3M+4H]^{4+}$), 1289 (55, $[2M+3H]^{3+}$), 967 (100, $[M+2H]^{2+}$), 645 (10, $[M+3H]^{3+}$); HRMS (ESI, +ve) calc. for $C_{85}H_{101}Cl_2N_{13}O_{25}Se_2$: 966.7375 ($[M+2H]^{2+}$), found: 966.7365.

Compound 208a. To a solution of **208** (2.4 mg, 1.5 µmol) in THF (200 µL) at 0 °C was added $NaHCO_3$ (7.5 µL, 1 M in H_2O, 7.5 µmol) and DMAP (1.5 µL, 0.1 M in H_2O, 0.15 µmol). After stirring at 0 °C for 5 min, a solution of **209** (1.1 mg, 4.5 µmol) in DMF (25 µL) was added. The resulting mixture was allowed to warm up to rt and stirred 16 h. The completion of the reaction was confirmed by HPLC-MS. The reaction mixture was concentrated *in vacuo* and purified by semi-preparative RP-HPLC (MeCN/H_2O + 0.1% TFA [20%, 5 min] then [20 to 100%, 15 min]) to yield **208a** as a colorless solid (1.6 mg, 62%). HPLC-MS: 2.60 min; 1752 (100, $[M-H]^-$); HRMS (ESI, +ve) calc. for $C_{76}H_{106}N_{17}O_{27}S_2$: 1752.6880, found: 1752.6902.

Compound 208b. To a solution of **208** (2.4 mg, 1.5 µmol) in THF (200 µL) at 0 °C was added $NaHCO_3$ (7.5 µL, 1 M in H_2O, 7.5 µmol) and DMAP (1.5 µL, 0.1 M in H_2O, 0.15 µmol). After stirring at 0 °C for 5 min, a solution of **210** (0.5 mg, 1.8 µmol) in DMF (25 µL) was added. The resulting mixture was allowed to warm up to rt and stirred 16 h. The completion of the reaction was confirmed by HPLC-MS. The reaction mixture was concentrated *in vacuo* and purified by semi-preparative RP-HPLC (MeCN/H_2O + 0.1% TFA [30%, 5 min] then [30 to 100%, 15 min]) to yield **208b** as a colorless solid (1.3 mg, 48%). HPLC-MS: 2.70 min; 1808 (100, $[M-H]^-$); HRMS (ESI, +ve) calc. for $C_{80}H_{114}N_{17}O_{27}S_2$: 1808.7506, found: 1808.7517.

Compound 208c. To a solution of **208** (2.4 mg, 1.5 µmol) in THF (200 µL) at 0 °C was added $NaHCO_3$ (7.5 µL, 1 M in H_2O, 7.5 µmol) and DMAP (1.5 µL,

0.1 M in H_2O, 0.15 μmol). After stirring at 0 °C for 5 min, a solution of **211** (1.8 mg, 4.5 μmol) in DMF (25 μL) was added. The resulting mixture was allowed to warm up to rt and stirred 16 h. The completion of the reaction was confirmed by HPLC-MS. The reaction mixture was concentrated *in vacuo* and purified by semi-preparative RP-HPLC (MeCN/H_2O + 0.1% TFA [20%, 5 min] then [20 to 100%, 15 min]) to yield **208c** as a colorless solid (1.8 mg, 62%). HPLC-MS: 2.70 min; 1901 (100, $[M-H]^-$); HRMS (ESI, +ve) calc. for $C_{80}H_{114}N_{17}O_{27}Se_2$: 1904.6395, found: 1904.6395.

5.2.6. Synthesis of Disulfides and Inhibitors

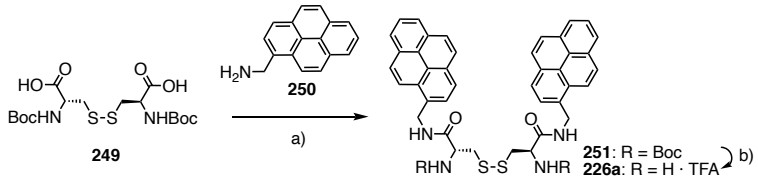

Scheme 29. (a) HBTU, Et_3N, DMF, rt, 20 min. (b) TFA, CH_2Cl_2, rt, 20 min, 2 steps, 72%.

Compound 251. To a solution of Boc-Cystine **249** (30 mg, 68 µmol) in DMF (0.7 mL) and CH_2Cl_2 (0.7 mL) were added HBTU (62 mg, 0.16 mmol), 2,4,6-collidine (22 µL, 0.17 mmol), **250** (HCl salt, 37 mg, 0.14 mmol) and Et_3N (20 µL, 0.14 mmol). The mixture was stirred for 20 min at rt and CH_2Cl_2 was evaporated under reduced pressure. The resulting suspension was diluted with H_2O (≈5 mL), sonicated, centrifuged, and the supernatant was discarded. The residue was suspended in MeOH (≈5 mL), sonicated, centrifuged, and the supernatant was discarded. The same procedure was repeated two more times. The poorly soluble product **251** (50 mg) was used in the next reaction without further purifications.

Compound 226a. To a suspension of **251** (50 mg) in CH_2Cl_2 (2 mL) were added *i*Pr_3SiH (80 µL, 0.26 mmol) and TFA (1 mL). The resulting solution was stirred at rt for 20 min, and then concentrated to dryness. The residue was triturated with Et_2O and purified by reverse phase flash chromatography (Claricep® C_{18} 12 g, linear gradient 20 – 80% CH_3CN + 0.1% TFA in H_2O + 0.1% TFA) to give **226a** (42 mg, 2 steps 72%) as a colorless solid. $[\alpha]_D^{20}$ –43 (*c* 0.79, MeOH); IR (neat): 3302 (w), 3041 (w), 1666 (s), 1554 (m), 1431 (w), 1204 (s), 1137 (m), 841 (s), 8001 (w), 757 (w), 724 (w), 708 (w), 681 (w); ^{1}H NMR (400 MHz, CD_3OD): 8.02 (dd, $^3J_{H\text{-}H}$ = 7.7 Hz, $^4J_{H\text{-}H}$ = 1.1 Hz, 2H), 7.96 – 7.88 (m, 6H), 7.86 (d, $^3J_{H\text{-}H}$ = 9.4 Hz, 2H), 7.83 (t, $^3J_{H\text{-}H}$ = 7.9 Hz, 2H), 7.77 (s, 4H), 7.68 (d, $^3J_{H\text{-}H}$ = 7.8 Hz, 2H), 4.81 (d, $^2J_{H\text{-}H}$ = 14.4 Hz, 2H), 4.54 (d, $^2J_{H\text{-}H}$ = 14.4

Hz, 2H), 4.21 (dd, $^{3}J_{H\text{-}H}$ = 7.7, 4.7 Hz, 2H), 3.31 – 3.26 (m, 2H), 3.02 (dd, $^{2}J_{H\text{-}H}$ = 14.8 Hz, $^{3}J_{H\text{-}H}$ = 7.7 Hz, 2H); ^{13}C NMR (101 MHz, CD_3OD): 168.5 (C), 132.6 (C), 132.4 (C), 131.8 (C), 131.1 (C), 130.0 (C), 129.1 (CH), 128.5 (CH), 128.4 (CH), 128.1 (CH), 127.0 (CH), 126.4 (CH), 126.3 (CH), 125.8 (C), 125.7 (CH), 125.6 (C), 123.4 (CH), 52.9 (CH), 42.9 (CH_2), 41.3 (CH_2); HRMS (ESI, +ve) calc. for $C_{40}H_{34}N_4O_2S_2$ $[M+H]^+$: 667.2197, found: 667.2214.

Compounds 85, **86**, **87**, **89**, **90** and **91** were synthesized according to procedures described in reference.[117]

Compound 92 was synthesized according to a procedure described in reference.[247]

Compound 93 was synthesized according to a procedure described in reference.[248]

5.3. Ring Opening in Organic Solvent

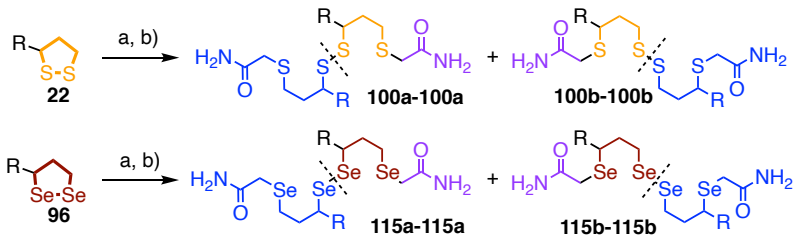

Scheme 30. a) 1. **94**, DIPEA; 2. **95**, CH_2Cl_2, –78 °C; b) 40 °C, reduced pressure. Dotted line = ESI-MS fragmentation.

General procedure for the ring opening reaction. To a solution of disulfide **22** or diselenide **96** (40 mM) in dry CH_2Cl_2 under nitrogen atmosphere was added DIPEA (3.0 equiv.). The reaction mixture was cooled down to –78 °C. Ethane- or *t*-butanethiol (**94** or **101**, 5.0 equiv.) was added to the reaction mixture, and solid iodoacetamide **95** (5.0 equiv.) was subsequently added after a delay Δt = 10, 20, 30, or 60 s. Additions of the thiol, DIPEA and iodoacetamide were repeated four times to improve conversion. The reaction was monitored by LCMS. Once maximum conversion was reached, the reaction mixture was warmed up to room temperature, washed twice with water and then with brine, and the organic layer was dried over Na_2SO_4, filtered and concentrated *in vacuo*. Upon concentration, products were found to dimerize to yield isomers **100a**/**b** (or **115a**/**b**). The crude mixture was purified by flash column chromatography (Biotage® SNAP Ultra 10 g, 0 – 10% MeOH in CH_2Cl_2) to afford a mixture of products **100a/b** (or **115a/b**). The ratios of both isomers were determined by ^{1}H NMR spectroscopy.

Compound 100a/b. Following the general procedure, methyl lipoate **22** was converted to dimers **100a**/**b**. The crude product was purified by flash column chromatography (Biotage® SNAP Ultra 10 g, 12 mL/min, linear gradient 0 – 10% MeOH in CH_2Cl_2 APCI mass detection *m/z* 557.2). Different delays Δt yielded

different ratios of regioisomers **100a**/**b** obtained as a light-yellow oil (2 – 40% yield). R_f (CH_2Cl_2/MeOH 9:1): 0.37; IR (neat): 3343 (br), 2921 (s), 2856 (m), 1734 (m), 1684 (m), 1457 (w), 1152 (br); ^{1}H NMR (400 MHz, $CDCl_3$, *n*/*n*: regio-isomeric peaks): 6.77 – 6.71 (m, 2H), 6.33 – 6.22 (m, 2H), 3.66 (s, 6H), 3.21/3.20 (s, 4H), 2.91 – 2.64 (m, 6H), 2.32 (t, $^3J_{H\text{-}H}$ = 7.3 Hz, 4H), 2.02 – 1.82 (m, 4H), 1.68 – 1.54 (m, 8H), 1.53 – 1.37 (m, 4H); ^{13}C NMR (101 MHz, $CDCl_3$, *n*/*n*: regio-isomeric peaks): 174.14/171.12 (C), 172.5/172.1 (C), 77.4 (CH), 56.4 (CH), 54.8 (CH), 51.7 (CH_3), 51.1/51.0 (CH), 50.7 (CH_3), 45.58/45.51 (CH), 45.47/45.42 (CH), 42.9 (CH_2), 40.3 (CH_2), 38.6 (CH_2), 36.6 (CH_2), 36.0 (CH_2), 35.96/35.87 (CH_2), 35.77/35.75 (CH_2), 34.29/34.24 (CH_2), 34.21/34.19 (CH_2), 34.0 (CH_2), 33.94/33.90 (CH_2), 33.62/33.55 (CH_2), 33.46/33.42 (CH_2), 30.39/ 30.32 (CH_2), 26.48/26.43 (CH_2), 26.18/ 26.14 (CH_2), 24.78/24.75 (CH_2), 18.8 (CH), 17.5 (CH); HPLC-MS: 2.42 min; 557 (100, $[M+H]^+$), 278 (20, $[M+2H]^{2+}$); HRMS (ESI, +ve) calc. for $C_{22}H_{41}N_2O_6S_4$: 557.1842, found: 557.1841.

Compound 115a/b. Following the general procedure, methyl diselenolipoate **96** was converted to dimers **115a**/**b**. The crude product was purified by flash column chromatography (Biotage® SNAP Ultra 10 g, 12 mL/min, linear gradient 0 – 10% MeOH in CH_2Cl_2, APCI mass detection *m/z* 741 – 747). Different delays Δt yielded different ratios of regioisomers of **115a**/**b** obtained as a light-yellow oil (2 – 20% yield). R_f (CH_2Cl_2/MeOH 9:1): 0.48; IR (neat): 3417 (br), 2930 (m), 2850 (m), 1736 (s), 1671 (s), 1435 (m), 1372 (m), 1192 (m), 1174 (s), 567 (m); ^{1}H NMR (400 MHz, $CDCl_3$, *n*/*n*: regio-isomeric peaks): 6.45 (s, 2H), 6.07 – 5.85 (m, 2H), 3.67 (s, 6H), 3.23/3.21 (s, 4H), 3.09 – 2.95 (m, 2H), 2.85 – 2.80 (m, 2H), 2.33 (t, $^3J_{H\text{-}H}$ = 7.3 Hz, 4H), 2.03 (s, 4H), 1.74 – 1.60 (m, 8H), 1.57 – 1.38 (m, 4H); ^{13}C NMR (101 MHz, $CDCl_3$): δ 174.25/174.22 (C), 173.0/172.7 (C), 77.4 (CH), 53.7 (CH), 52.7 (CH), 51.7 (CH_3), 46.3 (CH), 46.05/46.00 (CH), 45.8 (CH_2), 43.3 (CH_2), 36.96/36.90 (CH_2), 36.21/36.18 (CH_2), 35.73/35.69 (CH_2), 35.48/35.42, 34.02/33.97 (CH_2), 29.88/29.85 (CH_2), 29.5 (CH_2), 27.90/27.87 (CH_2), 27.44/27.39 (CH_2), 27.27/27.20 (CH_2), 25.64/25.59 (CH_2), 24.77/24.73

(CH_2), 23.76/23.73 (CH_2), 18.8 (CH), 17.6 (CH). HPLC-MS: 2.55 min; 745 (70, $[M+H]^+$), 372 (100, $[M+2H]^{2+}$); HRMS (ESI, +ve) calc. for $C_{22}H_{41}N_2O_6Se_4$: 748.9620, found: 748.9618.

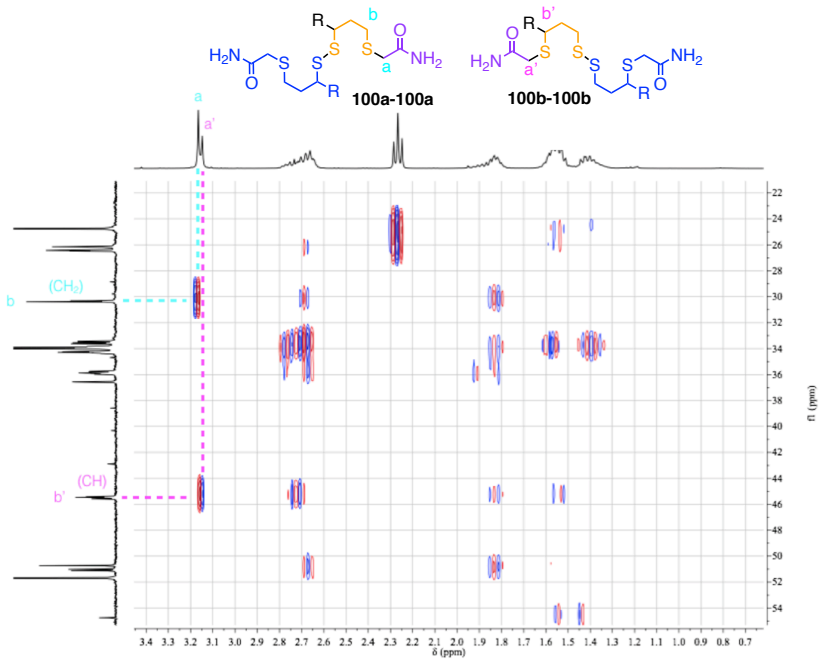

Figure 76. HMBC NMR spectrum of **100a/b** in $CDCl_3$ with important correlations.

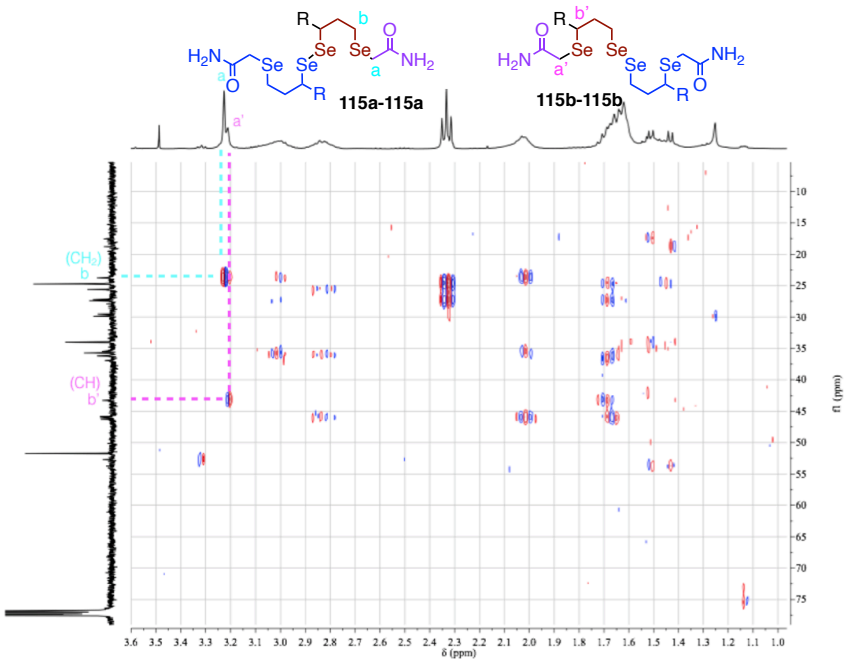

Figure 77. HMBC NMR spectrum of **115a/b** in $CDCl_3$ with important correlations.

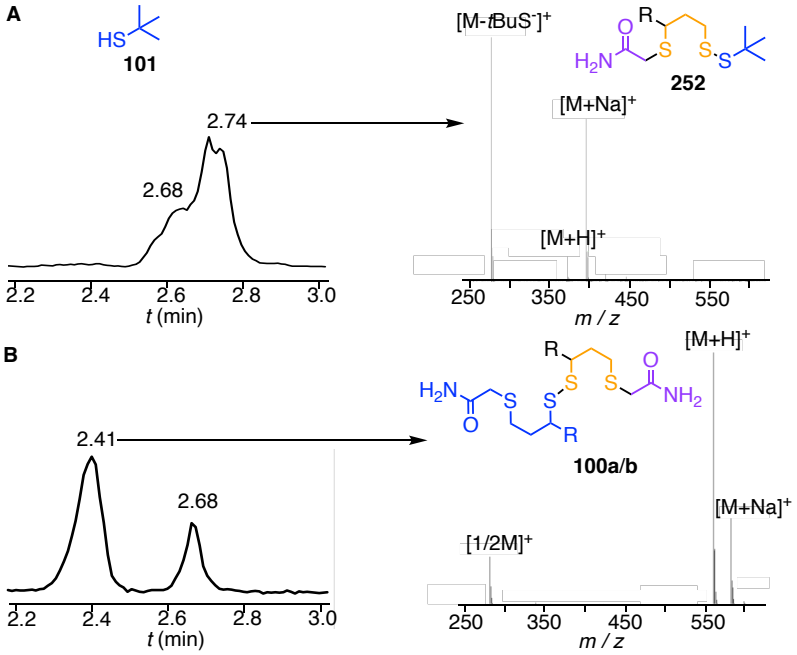

Figure 78. LCMS traces of the reaction mixture of **22** reacted with *t*BuSH **101** followed by iodoacetamide **95** before (A) and after workup (B).

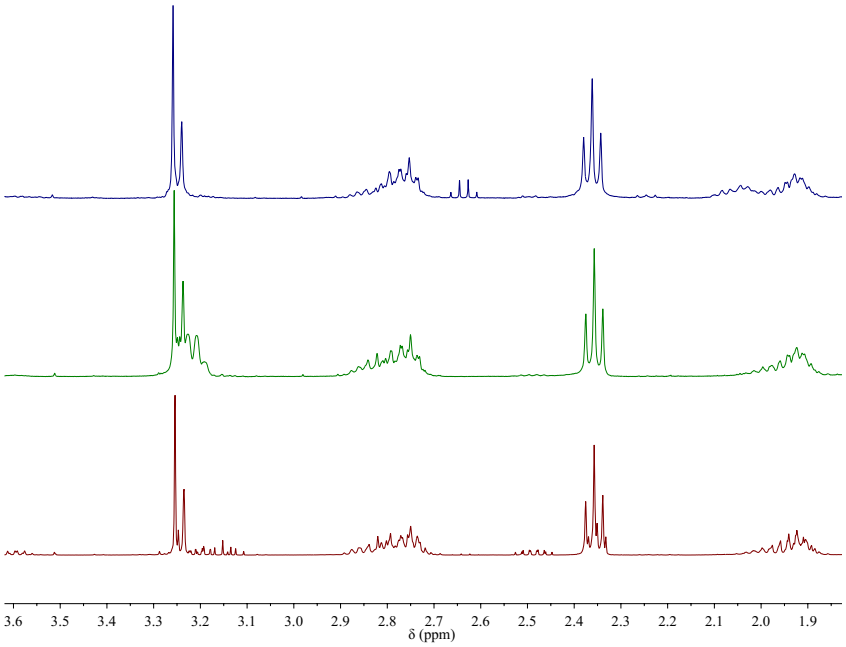

Figure 79. Comparison of the diagnostic region of the ^{1}H NMR spectra of **100a/b** obtained from enantiopure **22** and **94** (top) and enantiopure **22** and *t*BuSH **101** (middle) at equilibrium in CH_2Cl_2, and from racemic **22** and **94** at equilibrium in EtOAc (bottom).

5.4. Cascade Ring Opening

5.4.1. Ring Opening on the Monomer Level

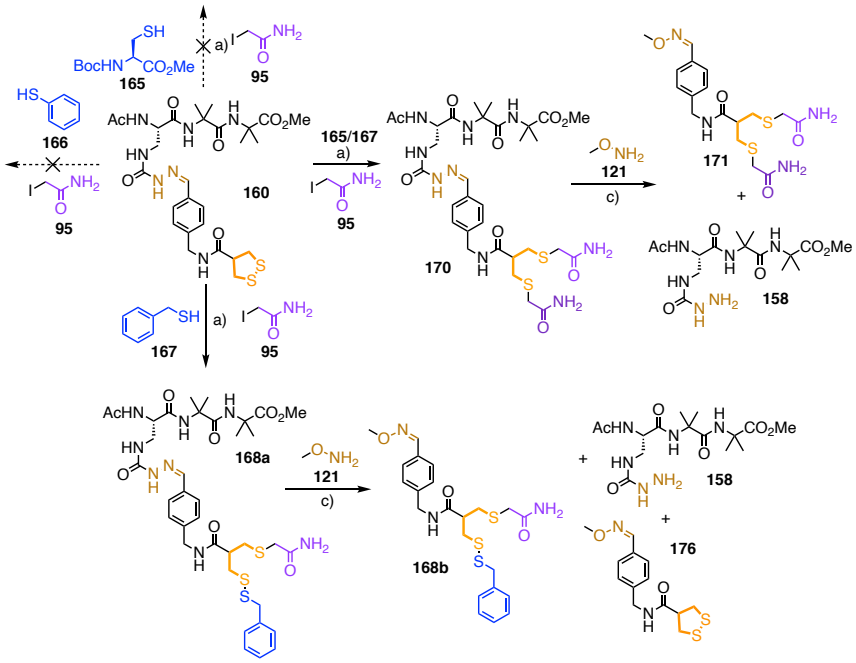

Scheme 31. a) 10 mM **160**, 50 – 500 mM **165-167**, buffer B, pH 8.7, rt, 1 h, then addition of **95**; b) 100 mM **121**, buffer A 16 h, rt.

Buffer B: 10 mM Tris, 1 mM EDTA, pH between 8.7 and 11 as specified.

Screening of initiators. To a solution of **160** in buffer B at pH 8.7 (10 mM, 100 µL, 1.0 µmol) was added **165**, **166** or **167** in DMF (10 µmol) and the reaction mixture was stirred at rt for 1 h. Then, iodoacetamide **95** was added (18.5 mg, 100 µmol) and the reaction mixture was stirred at rt for 15 min before being analyzed by HPLC-MS (method B5). **170**: 1.56 min; 754 (100, $[M+H]^+$), 776 (50, $[M+Na]^+$), 798 (30, $[M+2Na-H]^+$); **167**: 1.73 min; **160**: 1.96 min; 638 (100,

[M+H]$^+$), 669 (30, [M+Na+H$_2$O]$^+$); **168a**: 2.19 min, 819 (100, [M+H]$^+$), 841 (20, [M+Na]$^+$).

The reaction mixture was diluted with methoxylamine **121** in buffer A (100 mM, 400 µL, 40 µmol) and stirred at rt for 16 h before being analyzed by HPLC-MS (method B5). **158**: 1.14 min; 357 (48, [M-N$_2$H$_3$]$^+$), 389 (100, [M+H]$^+$), 411 (34, [M+Na]$^+$), 799 (54, [2M+Na]$^+$); **171**: 1.70 min; 413 (100, [M+H]$^+$), 435 (36, [M+Na]$^+$); **176**: 2.35 min; 297 (100, [M+H]$^+$); **168b**: 2.57 min, 478 (100, [M+H]$^+$).

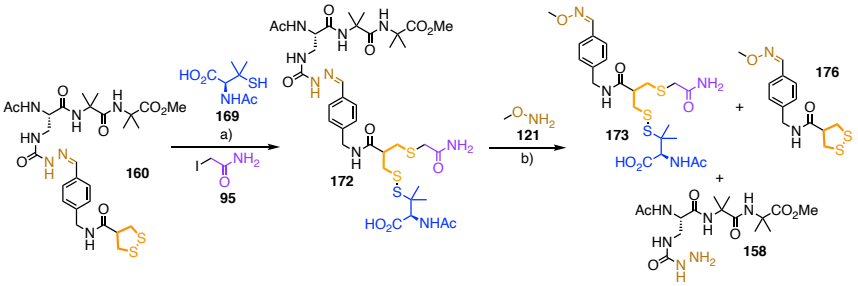

Scheme 32. a) 100 µM **160**, 200 µM – 50 mM **169**, TFE/buffer B, pH 9.0, rt, 1 h then addition of **95**; c) 100 mM **121**, buffer A, 16 h, rt.

Penicillamine as Initiator. To a solution of **160** in 1:1 TFE/buffer B at pH 9.0 (100 µM, 250 µL, 25 nmol) was added 2.5, 7.5 or 25 µL of **169** in DMF (10 mM, 25, 75 or 250 nmol) and the reaction mixture was stirred at rt for 1 h. Then, iodoacetamide **95** in water was added (1 M, 1µL, 1.0 µmol) and the reaction mixture was stirred at rt for 15 min.

The reaction mixture was diluted with methoxylamine **121** in buffer A (20 mM, 1.25 mL, 25.0 µmol) and stirred at rt for 16 h before being analyzed by HPLC-MS (method B5). **158**: 1.11 min; 357 (28, [M-N$_2$H$_3$]$^+$), 389 (50, [M+H]$^+$), 411 (46, [M+Na]$^+$), 799 (100, [2M+Na]$^+$); **173**: 1.95 min; 545 (100, [M+H]$^+$), 567 (34, [M+Na]$^+$), 1111 (28, [2M+Na]$^+$); **176**: 2.32 min; 297 (100, [M+H]$^+$).

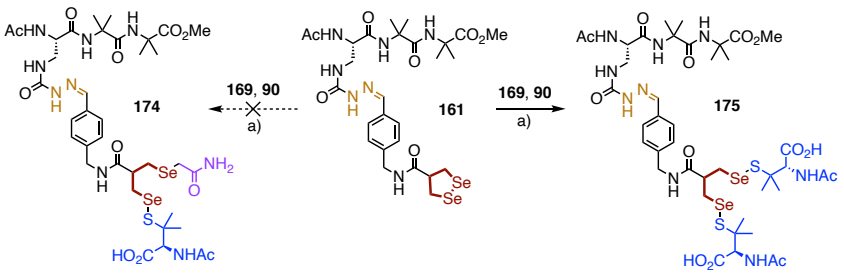

Scheme 33. a) 100 µM **161**, 2 mM **169**, TFE/buffer B, pH 9.0, rt, 1 h, then addition of **95**.

With Diselenolane-Containing Peptide. To a solution of **161** in 1:1 TFE/buffer B at pH 9.0 (100 µM, 250 µL, 25 nmol) was added 5, 15 or 50 µL of **169** in DMF (10 mM, 50, 150 or 500 nmol) and the reaction mixture was stirred at rt for 1 h. Then, iodoacetamide **95** in water was added (1 M, 1µL, 1.0 µmol) and the reaction mixture was stirred at rt for 15 min before being analyzed by HPLC-MS (method B30). **175**: 0.58 min; 1112/1114 (100, $[M+H]^+$), 1134/1136 (50, $[M+Na]^+$). **161**: 0.67 min; 732/734 (100, $[M+H]^+$), 1462/1464 (50, $[2M+H]^+$), 1484/1486 (42, $[2M+Na]^+$).

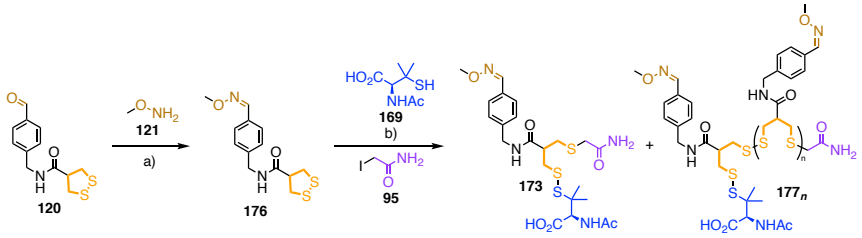

Scheme 34. a) **121**, buffer A, rt, 30 min, 95%; b) 100 µM – 30 mM **176**, 2 mM **169**, TFE/buffer B, rt, 1 h, then addition of **95**; c) 100 mM **121**, buffer A, 16 h, rt.

Compound 176. A solution of **120** (10.0 mg, 37.4 µmol) in DMF (100 µL) was diluted with a solution of **121** (5.61 mL, 112 µmol) in buffer A, and the

reaction mixture was stirred at rt for 30 min. The reaction mixture was extracted with EtOAc (10 mL), washed twice with brine, dried over Na_2SO_4 and concentrated *in vacuo* to afford **176** (10.5 mg, 95 %) as a yellow solid which was used without further purification. R_f (EtOAc): 0.66; IR (neat): 2985 s), 2953 (m), 2904 (s), 1651 (w), 1410 (m), 1396 (m), 1252 (m), 1221 (m), 1054 (s), 901 (w), 894 (w); ^{1}H NMR (400 MHz, $CDCl_3$): 8.66 (t, ^3J = 5.9 Hz, 1H), 8.19 (s, 1H), 7.55 (d, ^3J = 8.2 Hz, 2H), 7.29 (d, ^3J = 8.1 Hz, 2H), 4.30 (d, ^3J = 5.9 Hz, 2H), 3.87 (s, 3H), 3.45 – 3.34 (m, 4H), 3.27 – 3.21 (m, 1H); ^{13}C NMR (101 MHz, $CDCl_3$): 171.0 (C), 148.9 (CH), 141.6 (C), 131.0 (C), 128.1 (CH), 127.3 (CH), 70.2 (CH_2), 62.0 (CH), 51.8 (CH), 42.5 (CH_2).

Ring-Opening Polymerization Attempt on Monomer 176. To a solution of **169** in 1:1 TFE/buffer B at pH 9 (2 mM, 100 µL, 200 nmol) was added 1 µL (10 mM, 10 nmol), 3 µL (10 mM, 30 nmol), 1 µL (100 mM, 100 nmol), 3 µL (100 mM, 300 nmol), 10 µL (100 mM, 1.0 µmol) or 30 µL (100 mM, 3.0 µmol) of **176**, and the reaction mixture was stirred at rt for 30 min, before addition of iodoacetamide **95** in water (1.0 M, 5 µL, 5.0 µmol). The reaction mixture analyzed by HPLC-MS (method B30). **173**: 0.74 min; 545 (100, $[M+H]^+$), 567 (42, $[M+Na]^+$), 590 (38, $[M+2Na-H]^+$); **176**: 1.41 min; 279 (100, $[M+H-H_2O]^+$), 297 (16, $[M+H]^+$). No traces of **181** or **182** were observed.

5.4.2. Cascade Ring Opening on Trimers

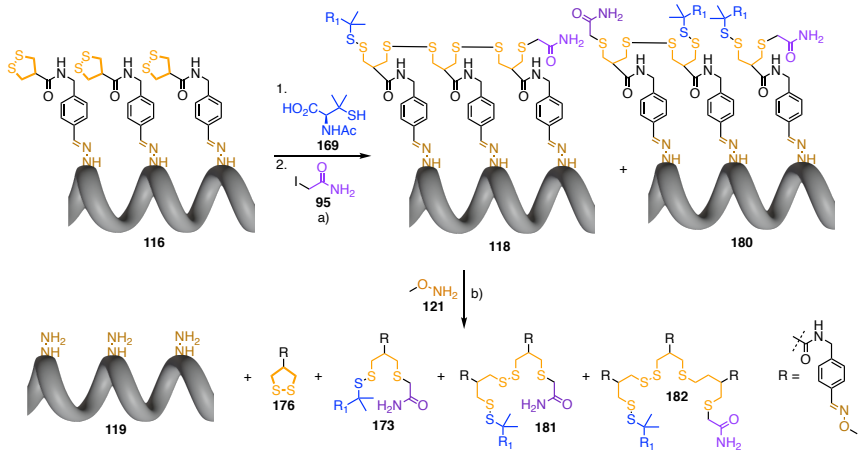

Scheme 35. a) 100 µM **116**, 1 – 5 mM **169**, buffer B, pH 8.7 – 11, H_2O/TFE 1:0 to 2:8, 0 °C to 80 °C, 30 min, then addition of **95**; b) 100 mM **121**, buffer A, 16 h, rt.

Templated Oligomerization of AspA on Nonapeptide 116. To a solution of **116** (100 µM, 50 µL, 5 nmol) in the appropriate buffer (1 M urea in buffer B, buffer B, TFE/buffer B 4:1, 3:2, 1:1, 2:3 or 1:4 at pH 8.7 to 11) was added **169** (10 mM, 5 to 25 µL, 50 to 250 nmol) and the reaction mixture was stirred at 0 °C, rt, 40 °C, 60 °C or 80 °C for 30 min, before addition of iodoacetamide **95** in water (1.0 M, 5 µL, 5.0 µmol). The reaction mixture analyzed by HPLC-MS (method B30). **180**: 1.29 min; 1131 (100, $[M+2H]^{2+}$); **118**: 1.39, 1.46, 1.50, 1.59 min; 1007 (100, $[M+2H]^{2+}$), 1020 (18, $[M+H+Na]^{2+}$); **116**: 1.85 min; 883 (100, $[M+2H]^{2+}$), 897 (66, $[M+H+Na]^{2+}$), 1764 (94, $[M+H]^{+}$), 1786 (48, $[M+Na]^{+}$), 1814 30, $[M+H]^{+}$).

The reaction mixture was diluted with methoxylamine **121** in buffer B (20 mM, 250 µL, 5.0 µmol) and stirred at rt for 16 h before being analyzed by HPLC-MS (method B30). **119**: 0.31 min; 1017 (40, $[M+H]^{+}$), 1039 (100, $[M+Na]^{+}$); **173**: 0.74 min; 545 (100, $[M+H]^{+}$), 567 (86, $[M+Na]^{+}$), 633 (90, [M+**159**+H]$^{+}$),

1110 (40, $[2M+Na]^+$), 1132 (40, $[2M+2Na-H]^+$); **176**: 1.41 min; 297 (80, $[M+H]^+$); **181**: 1.60 min; 841 (100, $[M+H]^+$), 863 (92, $[M+Na]^+$), 929 (52, [M+**159**+H]$^+$), 1702 (20, $[2M+Na]^+$), 1724 (40, $[2M+2Na-H]^+$); **182**: 1.98 min; 1137 (100, $[M+H]^+$), 1159 (70, $[M+Na]^+$), 1225 (62, [M+**159**+H]$^+$).

Yields (η) were estimated by comparing integrals of peaks in HPLC ($\lambda = 288$ nm) corresponding to compounds **173**, **176**, **181**–**182**.

The time allowed between addition of initiator **169** and terminator **95** was varied from 15 min to 24 h and did not influence the distribution of products.

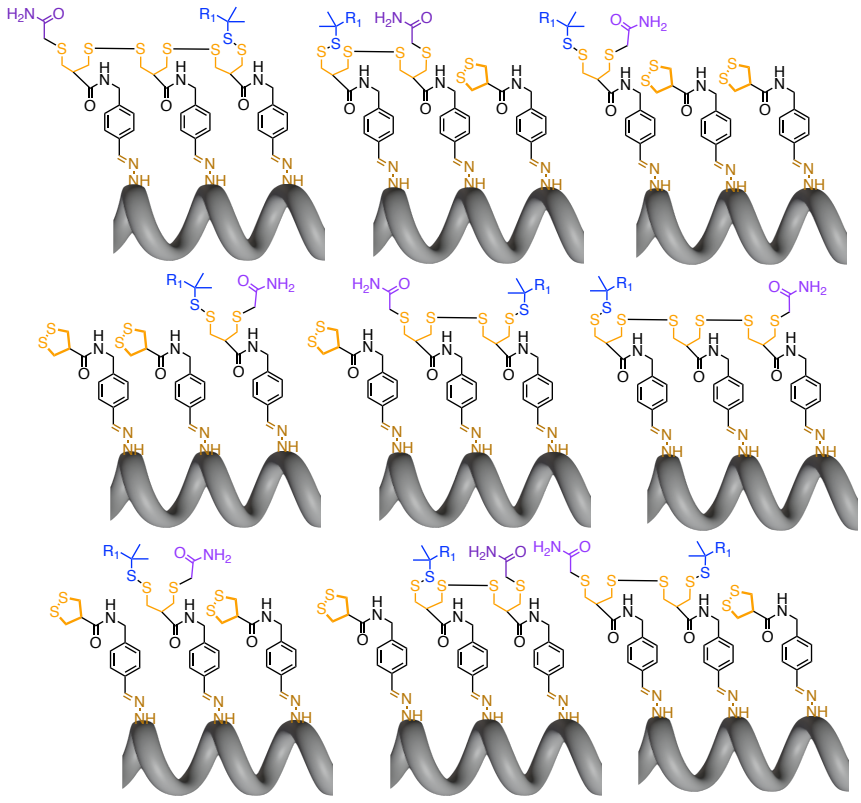

Figure 80. Structure of all possible isomers of **118**.

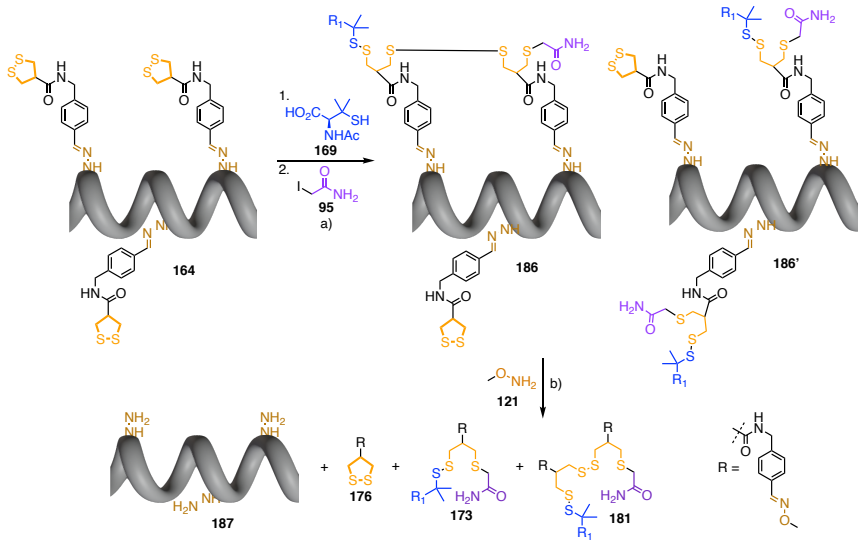

Scheme 36. a) 100 µM **164**, 1 – 5 mM **169**, buffer B, pH 8.7 – 11, H_2O/TFE 1:0 to 2:8, 0 °C to 80 °C, 30 min, then addition of **95**; b) 100 mM **121**, buffer A, 16 h, rt.

Anti-Templated Oligomerization on Nonapeptide 164. To a solution of **164** (100 µM, 50 µL, 5 nmol) in the appropriate buffer (1 M urea in buffer B, TFE/buffer B 1:1 or 4:1 at pH 9.0) was added **169** (10 mM, 10 µL, 100 nmol) and the reaction mixture was stirred at rt for 30 min, before addition of iodoacetamide **95** in water (1.0 M, 5 µL, 5.0 µmol). The reaction mixture analyzed by HPLC-MS (method B30). **186'**: 1.07 min; 1131 (100, $[M+2H]^{2+}$), 1153 (28, $[M+2Na]^{2+}$); **186**: 1.25, 1.38, 1.51 min; 1007 (100, $[M+2H]^{2+}$), 1019 (18, $[M+H+Na]^{2+}$), 1029 (18, $[M+2Na]^{2+}$); **164**: 1.78 min; 883 (100, $[M+2H]^{2+}$), 897 (56, $[M+H+Na]^{2+}$), 1764 (30, $[M+H]^{+}$), 1786 (38, $[M+Na]^{+}$), 1814 (20, $[M+H]^{+}$).

The reaction mixture was diluted with methoxylamine **121** in buffer A (20 mM, 250 µL, 5.0 µmol) and stirred at rt for 16 h before being analyzed by HPLC-MS (method B30). **187**: 0.31 min; 1017 (40, $[M+H]^{+}$), 1039 (100, $[M+Na]^{+}$); **173**: 0.74 min; 545 (100, $[M+H]^{+}$), 567 (86, $[M+Na]^{+}$), 633 (90, [M+**159**+H]$^{+}$),

1110 (40, $[2M+Na]^+$), 1132 (40, $[2M+2Na-H]^+$); **176**: 1.41 min; 297 (80, $[M+H]^+$); **181**: 1.60 min; 841 (100, $[M+H]^+$), 863 (92, $[M+Na]^+$), 929 (52, [M+**159**+H]$^+$), 1702 (20, $[2M+Na]^+$), 1724 (40, $[2M+2Na-H]^+$); **182**: 1.98 min; 1137 (100, $[M+H]^+$), 1159 (70, $[M+Na]^+$), 1225 (62, [M+**159**+H]$^+$).

Table 7. RO as a function of reaction conditions.[a]

Entry	[**169**]/ [**116**]	*T* (°C)	pH	[Urea]	% TFE	RO (%)[b]
1	10	rt	9.0	-	50	31
2	15	rt	9.0	-	50	36
3	20	rt	9.0	-	50	47
4	25	rt	9.0	-	50	44
5	30	rt	9.0	-	50	27
6	50	rt	9.0	-	50	20
7	20	rt	8.7	-	50	26
8	20	rt	9.0	-	50	31
9	20	rt	9.5	-	50	47
10	20	rt	10.0	-	50	67
11	20	rt	10.5	-	50	66
12	20	rt	11.0	-	50	53
13	20	0	9.0	-	80	59
14	20	25	9.0	-	80	52
15	20	40	9.0	-	80	30
16	20	60	9.0	-	80	27

Table 7. RO as a function of reaction conditions (continued).[a]

Entry	[**169**]/ [**116**]	*T* (°C)	pH	[Urea]	% TFE	RO (%)[b]
17	20	80	9.0	-	80	39
18[c]	20	rt	9.0	1.0 M	0	35
19	20	rt	9.0	1.0 M	0	54
20[c]	20	rt	9.0	-	50	13
21	20	rt	9.0	-	50	59
22[c]	20	rt	9.0	-	80	11
23	20	rt	9.0	-	80	54

[a]Reactions performed at 100 μM **116** or **164**. [b]Ring-opening yield RO = η_{173} + η_{181} + η_{182}. [c]On shifted templated **164** instead of **116**.

Table 8. Product distribution and T_{eff} as a function of reaction conditions.[a]

Entry	η_{176}[b]	η_{173}[b]	η_{181}[b]	η_{182}[b]	T_{eff}[c]	RO (%)[d]
1	69	7	21	3	1.11	31
2	64	14	19	3	0.82	36
3	53	19	24	3	0.75	47
4	56	16	24	3	0.85	44
5	73	10	15	2	0.83	27
6	80	13	4	3	0.31	20
7	74	8	15	3	0.98	26
8	69	13	16	2	0.75	31
9	53	15	28	4	0.93	47

Table 8. Product distribution and T_{eff} as a function of reaction conditions (continued).[a]

Entry	η_{176}[b]	η_{173}[b]	η_{181}[b]	η_{182}[b]	T_{eff}[c]	RO (%)[d]
10	33	19	45	3	1.00	67
11	34	23	38	5	0.87	66
12	47	20	28	4	0.81	53
13	41	14	38	8	1.13	59
14	48	15	30	6	1.00	52
15	70	13	14	2	0.71	30
16	73	20	6	1	0.15	27
17	61	35	4	0	–0.32	39
18[e]	65	21	15	0	0.45	35
19	46	32	22	0	0.44	54
20[e]	87	7	6	0	0.53	13
21	41	19	36	4	0.93	59
22[e]	89	9	2	0	–0.15	11
23	46	11	32	12	1.22	54

[a]Reactions performed at 100 μM **116** or **164**, entries match those of Table 7. [b]Yields calculated from integrals in HPLC. [c]Effective templation $T_{eff} = \log(\eta_{181} + \eta_{182} / \eta_{173}) + 0.60$ [d]Ring-opening yield RO = $\eta_{173} + \eta_{181} + \eta_{182}$. [e]On shifted templated **164** instead of **116**.

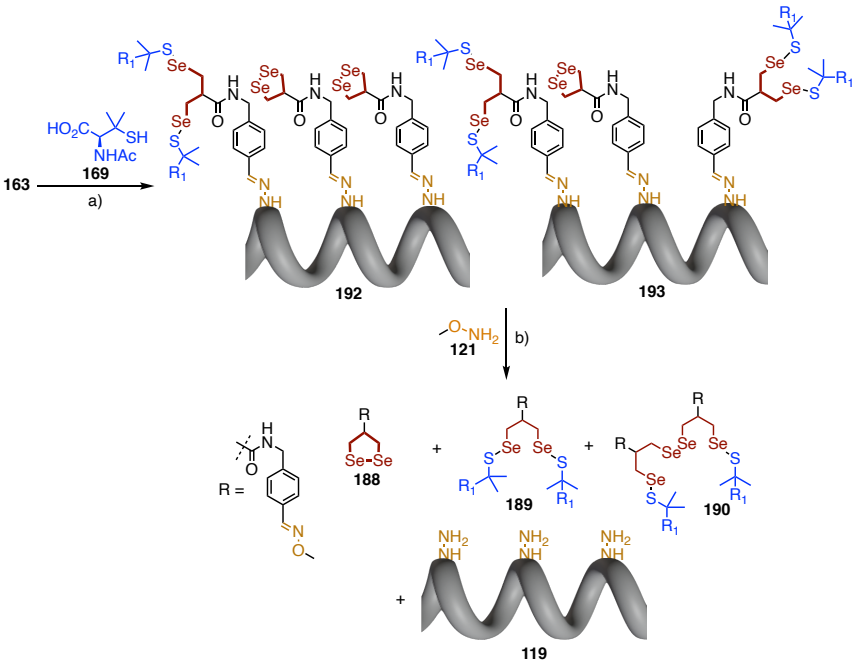

Scheme 37. a) 100 µM **163**, 200 µM – 2 mM **169**, TFE/buffer B 4:1, pH 9.0, rt, 30 min; b) 100 mM **121**, buffer A, 16 h, rt.

Templated Oligomerization on Diselenolane Nonapeptide 163. To a solution of **163** (100 µM, 50 µL, 5 nmol) in 4:1 TFE/buffer B at pH 9.0 was added **169** (10 mM, 1, 3, 5 or 10 µL, 10, 30, 50 or 100 nmol) and the reaction mixture was stirred at rt for 30 min. The reaction mixture analyzed by HPLC-MS (method B30). **193**: 1.55 min; 1025/1027 (30, $[M+2H-4*\mathbf{169}]^{2+}$), 1214/1216 (60, $[M+2H-2*\mathbf{169}]^{2+}$), 1404/1406 (100, $[M+2H]^{2+}$); **192**: 1.70 min; 1025/1027 (74, $[M+2H-2*\mathbf{169}]^{2+}$), 1214/1216 (100, $[M+2H]^{2+}$); **163**: 1.89 min; 1025/1027 (100, $[M+2H]^{2+}$). All isotopic patterns match with the calculated ones for 6 Se atoms.

The reaction mixture was diluted with methoxylamine **121** in buffer A (20 mM, 250 µL, 5.0 µmol) and stirred at rt for 16 h before being analyzed by HPLC-

MS (method B30). **119**: 0.31 min; 1017 (40, $[M+H]^+$), 1039 (100, $[M+Na]^+$); **189** 1.26 min; 771/773 (78, $[M+H]^+$), 793/795 (50, $[M+Na]^+$), 859/861 (100, [M+**159**+H]$^+$), 1562/1564 (36, $[2M+Na]^+$), all isotopic patterns match with the calculated ones for 2 Se atoms.; **188**: 1.45 min; 389/391 (100, $[M+H]^+$), all isotopic patterns match with the calculated ones for 2 Se atoms.; **190**: 1.83 min; 1162/1164 (30, $[M+H]^+$), 1183/1185 (100, $[M+Na]^+$), 1249/1251 (70, [M+**159**+H]$^+$), all isotopic patterns match with the calculated ones for 4 Se atoms.

Table 9. RO, product distribution and T_{eff} as a function of reaction conditions.[a]

Entry	[**169**]/ [**163**]	η_{188}[b]	η_{189}[b]	η_{190}[b]	T_{eff}[c]	RO (%)[d]
1	2	80	13	6	0.28	20
2	6	64	29	6	–0.05	36
3	10	57	40	3	–0.53	43
4	20	51	47	2	–0.74	49

[a]Reactions performed at 100 μM **163** in 4:1 TFE/buffer B at pH 9.0 at rt. [b]Yields calculated from integrals in HPLC. [c]Effective templation $T_{eff} = \log(\eta_{190} / \eta_{189}) + 0.60$ [d]Ring-opening yield RO = $\eta_{189} + \eta_{190}$.

5.4.3. Artificial Signal Transduction Through a Lipid Bilayer

5.4.3.1. Vesicle Preparation

A thin film was prepared by evaporating a solution of DPPC (5 mg) in $CHCl_3$ (2 mL) on a rotary evaporator (40 °C) and then *in vacuo* overnight. The film was then hydrated with 500 µL of SBD-F solution (1 mM in 10 mM Tris, 100 mM NaCl, pH 8.0), subjected to five freeze-thaw cycles (liquid N_2, 50 °C water bath) and extruded ten times though a polycarbonate membrane (pore size 200 nm, 50 °C). Extravesicular components were removed by size exclusion chromatography (PD MiniTrap Sephadex G-25) with 10 mM Tris, 100 mM NaCl, pH 8.0. Final conditions: 10 mM DPPC, inside 1 mM SBD-F, 10 mM Tris, 100 mM NaCl, pH 8.0, outside 10 mM Tris, 100 mM NaCl, pH 8.0. The vesicles were used within the day of preparation.

5.4.3.2. Cascade Ring Opening Through a Lipid Bilayer

In 2.5 mL glass cuvettes, solutions of the vesicles were prepared to reach a lipid concentration of 0.1 mM of DPPC in 10 mM Tris, 100 mM NaCl, pH 8.0. In two separate cuvettes, stock solutions of **116** or **139** (5 mM in DMF, 5 µL, 10 µM final concentration) were added and the cuvettes warmed up to 50 °C to allow for partitioning of the helix in the membrane. In a separate cuvette, the vesicles were destroyed by the addition of Triton-X (50 µL, 1% aq.) and the cuvette warmed up top 50 °C. Then, in all four cuvettes, glutathione was added (100 mM, 25 µL, 1 mM final concentration), and the reaction mixtures were stirred at 50 °C. Emission spectra of the four cuvettes were measured every 10 min over 24 h (λ_{exc} = 385 nm, slits 5:10 nm, plot λ_{em} = 535 nm).

5.5. High-Content High-Throughput Inhibitor Screening

5.5.1. General Procedure

HeLa Kyoto cells were seeded at 8 $\times 10^4$ cells/well in FluoroBrite DMEM + 10% FBS on µ-Plate 96-well Black ibiTreat sterile and kept at 37 °C with 5% CO_2 overnight. The next day, serial dilutions of the inhibitors in PBS (10x final concentration), OPS (10x in PBS) and a solution of Hoechst 33342 (100 µg/mL) in PBS were prepared freshly in a 96-well V-bottom plate. Then, cells were washed with PBS (3 x 3 mL/well) and the media was exchanged to FluoroBrite DMEM (4 x 150 µL/well) using a plate washer (Biotek EL406®), keeping a final volume of 135 µL/well. The inhibitor solutions from the V-bottom plate were added to the cells (15 µL/well, 10x final concentration in PBS) using an electronic multichannel pipette to reach a final volume of 150 µL/well. Cells were incubated for 1 h at 37 °C with 5% CO_2. After this, cells were washed again using the plate washer and OPS solution (10 x in PBS) from the V-bottom plate was added (15 µL/well) using an electronic multichannel pipette to reach a final volume of 150 µL/well. After 2 h of incubation at 37 °C with 5% CO_2, the solution of Hoechst 33342 from V-bottom plate was added (15 µL/well) using an electronic multichannel pipette. After 15 min of incubation at 37 °C with 5% CO_2, the liquid was removed and cells were fixed with 3% PFA (80 µL/well). The plate was washed with PBS (9 x 3 mL/well) and imaged using an automated confocal microscope.

For each experiment, 6 images at 20x were recorded per well using two channels: blue for Hoechst 33342 (excitation filter: 377/50 nm; emission filter: 477/60 nm) and red for Cy_5 (excitation filter: 620/50 nm; emission filter: 690/50 nm), as shown in Figure 81. Duplicates were performed for each condition.

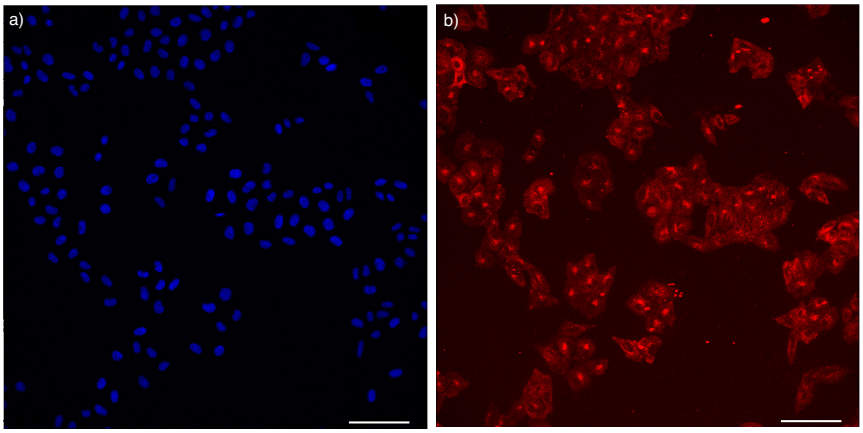

Figure 81. CLSM images of a) blue channel recording the Hoechst 33342 localization in the nuclei and b) red channel recording the signal from Cy_5-labelled OPS **218**. Scale bar = 100 µm.

5.5.2. Data Analysis

For each cell, the blue channel image is used for the segmentation of nuclei and whole cell body.

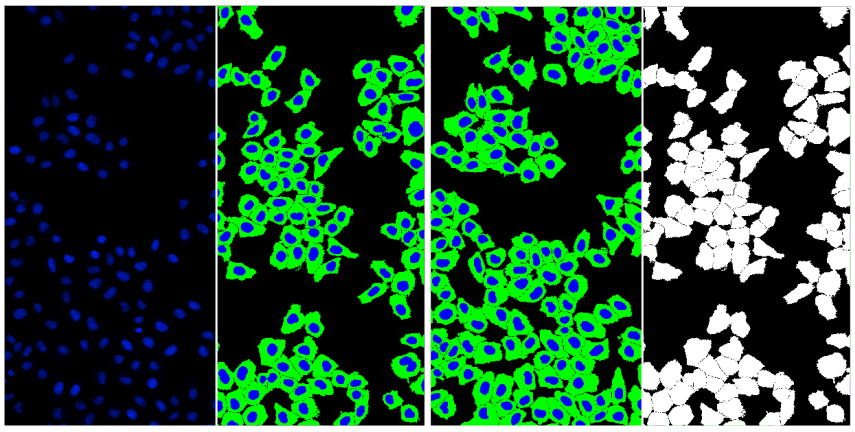

Figure 82. Segmentation of nuclei (blue mask) and cell body (green mask) using the blue channel.

Bright fluorescent aggregates were detected using a detection threshold of 5000 over the background intensity and grown to be removed.

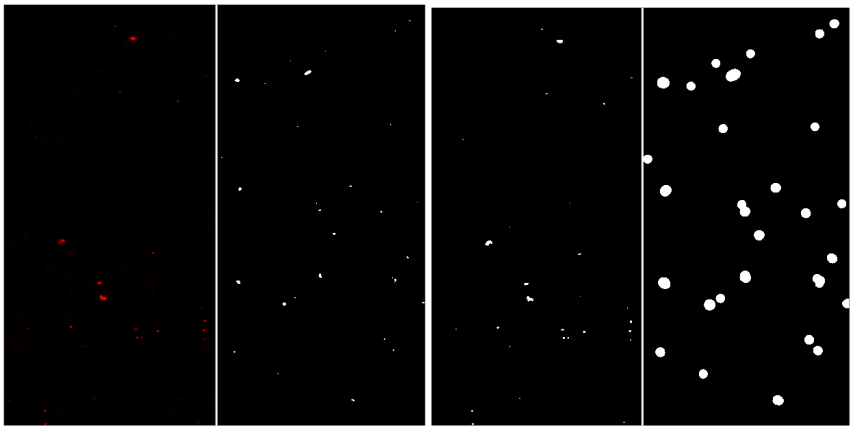

Figure 83. Detection of bright fluorescent aggregates using the red channel (left) and growth of the detected objects to be removed (right).

Masks of bright fluorescent aggregates were used as a proxy to remove all cells touched by them from the final quantification.

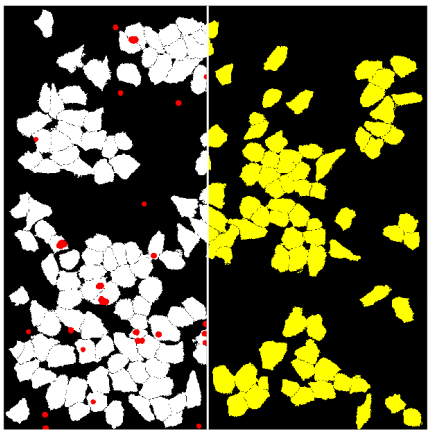

Figure 84. Detection of bright fluorescent aggregates using the red channel (left) and growth of the detected objects to be removed (right).

Cell body and dots masks were applied to extract the integrated (sum of the intensities of the pixels included in the mask) and average intensity values in the background.

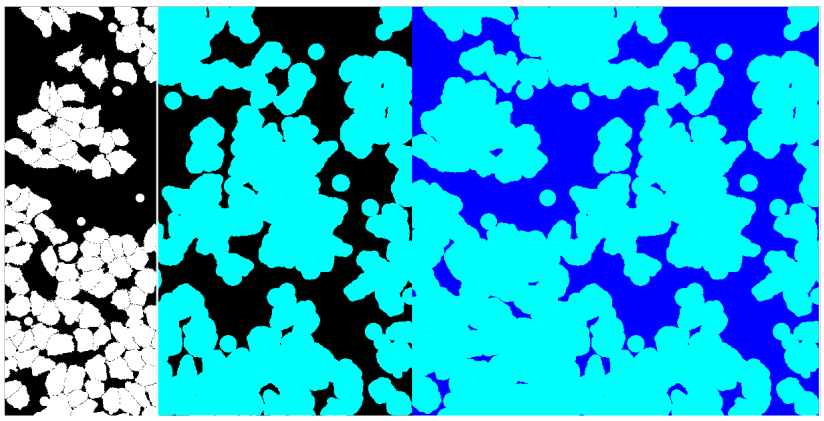

Figure 85. Mask (sky blue) applied for the quantification of the fluorescence intensity of background (dark blue) in the red channel image.

Integrated and average intensity of the detected and validated cells (~800 cells/well) was finally extracted from the mask.

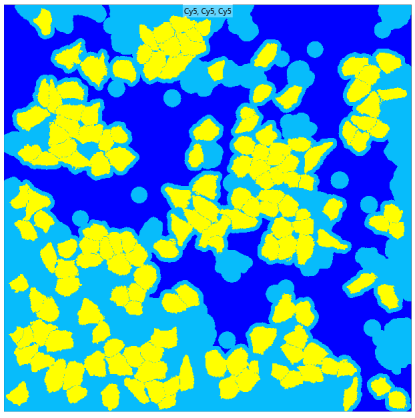

Figure 86. Analysis of the red channel image showing detected cells (yellow), excluded areas (sky blue) and background (dark blue).

Average fluorescent intensity values per cell (I) were calculated by subtracting average background intensity from average intensity of the whole cell. Average intensities I for each condition in the presence of inhibitors were normalized against that obtained without the addition of inhibitors (I_0) using equation (S1).

$$I_T = I / I_0 \qquad \text{(S1)}$$

Duplicates were performed for each condition and averaged. The resulting dependence of the relative fluorescent intensity values (I_T) to the concentration of inhibitors ($c_{inhibitor}$) was plotted and fitted with equation (S2) to retrieve the half maximal inhibitory concentration (IC_{50}) and the Hill coefficient (n). MIC values were estimated from the fit curve as the concentration at which 15% of uptake was inhibited.

$$I_{rel} = 1 / (1 + (IC_{50} / c_{inhibitor})^{-n}) \quad \text{(S2)}$$

Top-hat transformation of the red channel image is used to facilitate the segmentation of the dotted structures.

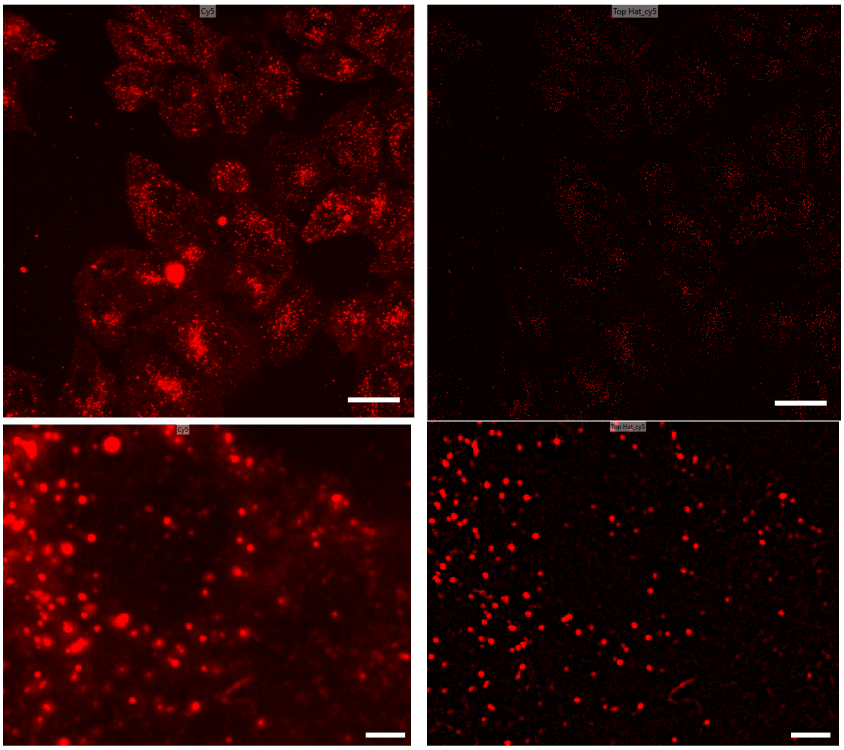

Figure 87. *Top-hat* transform (right) of the red channel image (left), scale bar = 30 µm. Bottom: zoomed in images, scale bar = 3.5 µm.

A mask based on the detected dots is applied to extract integrated and average intensity in the punctate structures, that most likely correspond to endosomes and lysosomes.

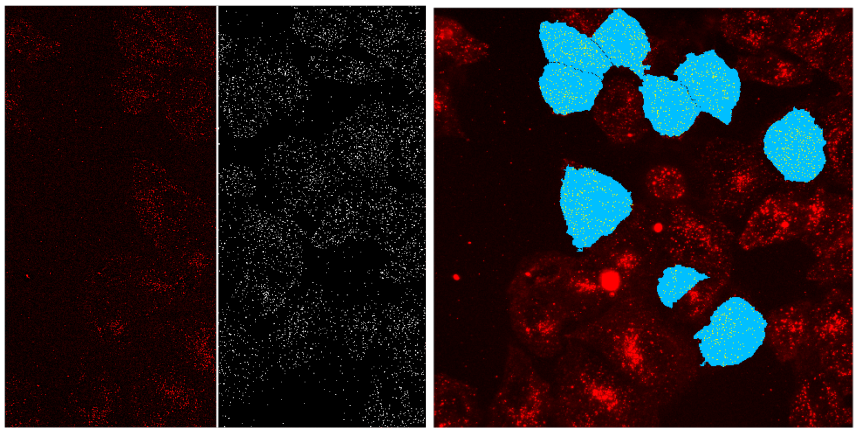

Figure 88. Segmentation of the dotted structures based on the *top-hat* transformation (left) and final mask applied on cells (right).

Data extracted from the "dots" mask are treated as described above for the cell mask.

5.5.3. Inhibitor Screening

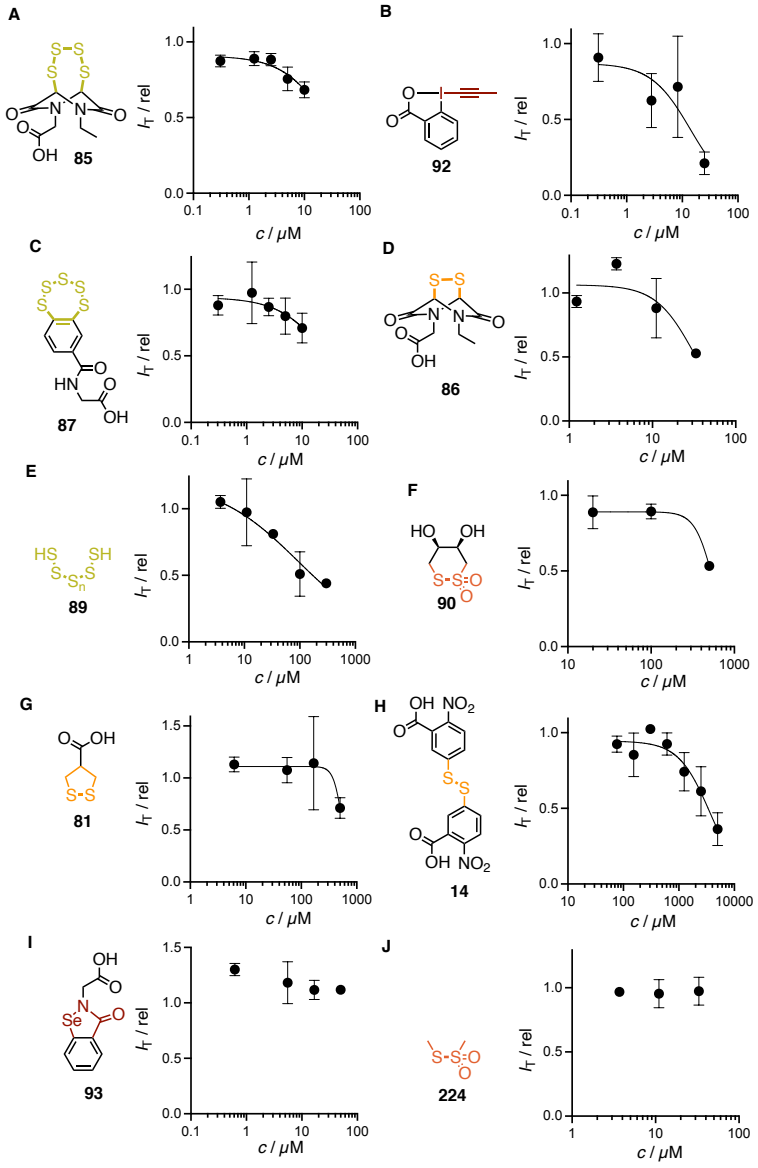

Figure 89. Automatically analyzed HCHT data showing relative fluorescence intensity ± SEM in HeLa Kyoto cells after preincubation with the different inhibitors for 1 h followed by washing and incubation with OPS **218** (250 mM for **14**, 500 nM for **86**, **89**-**93** and **224** or 1 µM for **85** and **87**) for 2 h.

5.6. Dynamic-Covalent Chemistry of OPS

5.6.1. HPLC Studies

Method A: Analytical HPLC were recorded using a JASCO LC-2000 Plus system equipped with quaternary pump (JASCO PU-2089), UV/Vis detector (JASCO UV-2077 Plus, λ_{abs} at 260 nm for detection) and fluorescence detector (JASCO FP-2020 Plus) equipped with a Jupiter 4u Proteo 90 Å 100 x 4.6 mm column, flow 0.5 mL/min with the following conditions: 95% H_2O/5% CH_3CN + 0.1% TFA for 2 min, then a linear elution gradient from 95% H_2O/5% CH_3CN + 0.1% TFA to 100% CH_3CN + 0.1% TFA in 8 min, 100% CH_3CN + 0.1% TFA for 3 min, then return to 95% H_2O/5% CH_3CN + 0.1% TFA.

Method B: Analytical HPLC were recorded using a JASCO LC-2000 Plus system equipped with quaternary pump (JASCO PU-2089), UV/Vis detector (JASCO UV-2077 Plus, λ_{abs} at 260 nm for detection) equipped with a Nucleosil 100-5 C_{18} AB column, flow 1.0 mL/min with the following conditions: linear elution gradient from 95% buffer/5% CH_3CN to 60% buffer/40% CH_3CN in 4 min, 60% buffer/40% CH_3CN for 1 min, then return to 95% buffer/5% CH_3CN. The buffer used was 100 mM TEAA, pH 7.5.

Method C: LCMS were recorded using a Thermo Scientific Accela HPLC equipped with a Thermo C_{18} Hypersil GOLD column (50 x 2.1 mm, 1.9 μm particles size) coupled with a LCQ Fleet three-dimensional ion trap mass spectrometer (ESI, Thermo Scientific) with a linear elution gradient from 95% H_2O / 5% CH_3CN + 0.1% TFA to 10% H_2O / 90% CH_3CN + 0.1% TFA in 4.0 min at a flow rate of 0.75 mL/min. UV (λ_{abs} = 260 nm) detection was used.

Compound 227a. To a solution of cystine **226a** in PBS (1 mM, 4.00 μL, 1.0 eq.) was added a solution of 5'-AMPS **225** in PBS buffer (111 μM (1 eq.), 1.11 mM (10 eq.), 11.1 mM (100 eq.), 36 μL, pH 7.4). HPLC chromatograms were measured after 30 min using method C. HRMS (ESI, +ve) calc. for $C_{30}H_{30}N_7O_7PS_2$ $[M+2H]^+$: 696.1459, found: 696.1446.

Compound 227b. To a solution of 5'-AMPS **225** in PBS (1 mM, 4.00 µL, 1.0 eq.) was added a solution of cystine **226b** in PBS buffer (111 µM (1 eq.), 1.11 mM (10 eq.), 11.1 mM (100 eq.), 111 mM (1000 equiv.), 36 µL, pH 7.4). HPLC chromatograms were measured after 30 min using method B. HRMS (ESI, -ve) calc. for $C_{19}H_{29}N_6O_{10}PS_2$ $[M]^-$: 595.1051, found: 595.1029.

Compound 228. Cysteine **228** was generated *in situ* by mixing cystine **226a** with 1 equivalent of TCEP. To a solution of cysteine **228** in PBS (1 mM, 4.00 µL, 1.0 eq.) was added a solution of 5'-AMPS **225** in PBS buffer (111 µM (1 eq.), 1.11 mM (10 eq.), 11.1 mM (100 eq.), 36 µL, pH 7.4). HPLC chromatograms were measured after 30 min using method C.

Compound 229. To a solution of 5'-AMPS **225** in PBS (1 mM, 4.00 µL, 1.0 eq.) was added a solution of DTNB **14** in PBS buffer (11.1 µM (0.1 eq.), 111 µM (1 eq.), 1.11 mM (10 eq.), 11.1 mM (100 eq.), 36 µL, pH 7.4). HPLC chromatograms were measured after 30 min using method A. HRMS (ESI, +ve) calc. for $C_{17}H_{17}N_6O_{10}PS_2$ $[M+2H]^+$: 561.0259, found: 561.0275.

Compound 230. To a solution of 5'-AMPS **225** in PBS (1 mM, 4.00 µL, 1.0 eq.) was added a solution of thiosulfonate **224** in PBS buffer (11.1 µM (0.1 eq.), 22.2 µM (0.2 eq.), 55.5 µM (0.5 eq.), 111 µM (1 eq.), 444 µM (4 eq.) or 1.11 mM (10 eq.), 36 µL, pH 7.4). HPLC chromatograms were measured after 30 min using method C. HRMS (ESI, +ve) calc. for $C_{11}H_{16}N_5O_6PS_2$ $[M+2H]^+$: 410.0353, found: 410.0367.

Compound 231. To a solution of 5'-AMPS **225** in PBS (1 mM, 4.00 µL, 1.0 eq.) was added a solution of **85** in PBS buffer (111 µM (1 eq.), 1.11 mM (10 eq.), 11.1 mM (100 eq.), 36 µL, pH 7.4). HPLC chromatograms were measured after 30 min using method B.

Compound 232. To a solution of 5'-AMPS **225** in PBS (1 mM, 4.00 µL, 1.0 eq.) was added a solution of **89** in PBS buffer (111 µM (1 eq.), 1.11 mM (10 eq.),

11.1 mM (100 eq.), 111 mM (1000 equiv.), 36 µL, pH 7.4). HPLC chromatograms were measured after 30 min using method B.

Library 234. To a solution of **66** in DMSO (100 µM, 4 µL, 1.0 eq.) was added a solution of **233** in PBS buffer (5.56 µM (0.5 eq.), 11.1 µM (1.0 eq.), 22.2 µM (2.0 eq.), 111 µM (10 eq.), or 1.11 mM (100 eq.), 36 µL, pH 7.4). HPLC chromatograms were measured after 30 min at rt using method A.

5.6.2. Activation of OPS Uptake

Activation of OPS was performed by incubating **218** (500 nM) with the corresponding concentration of activator in PBS buffer pH 7.4 for 30 min at 25 °C prior to incubation.

When purification was performed to remove excess activator, the solution (500 µL) was concentrated down to 50 µL through Amicon Ultra 0.5 mL 3 kDa cutoff centrifugal filters, and diluted back to 500 µL with fresh PBS buffer. This process was repeated 7 times to remove excess activator and yield the solution of activated OPS (50 µL, 5 µM). Incubation with cells was then performed as described above.

5.7. Abbreviations

5'-AMPS: Adenosine-5'-O-monophosphorothioate
ABC: Amine buffer-catalyst
Aib: α-aminoisobutyric acid
Alloc: Allyloxycarbonyl
APCI: Atmospheric pressure chemical ionization
ArM: Artificial metalloenzyme
AspA: Asparagusic acid
Boc: *tert*-butylcarbonyl
BPS: Benzopolysulfane
BS: *B. subtilis*
BSA: Bovine serum albumin
Calc: Calculated
CAPA: Chloroalkane penetration assay
cCPP: Cyclic cell-penetrating peptide
CD: Circular dichroism
CF: Ciprofloxacin
CLIC1: Chloride intracellular channel protein 1
CLSM: Confocal laser scanning microscopy
COC: Cyclic oligochalcogenides
COSY: Correlation spectroscopy
CPD: Cell-penetrating poly(disulfide)s
CPP: Cell-penetrating peptide
CPS: Cell penetrating streptavidin
CP_{50}: Half maximal cell penetration concentration
CryoROP: Cryo-ring-opening polymerization
CuAAC: Cu(I)-catalyzed azide–alkyne cycloaddition
Cy_5: Cyanine 5
Dap: Diaminopropionic acid
DCC: Dynamic covalent chemistry

DEPT: Distortionless enhancement by polarization transfer

DIPEA: Diisopropylethylamine

DMAP: 4-dimethylamino pyridine

DMEM: Dulbecco's modified eagle medium

DMF: Dimethylformamide

DMSO: Dimethylsulfoxide

DNA: Deoxyribonucleic acid

DPPC: 1,2-dipalmitoylphosphatidylcholine

DSL: 1,2-diselenolane

DTNB: 5,5'-dithiobis-(2-nitrobenzoic acid)

DTT: Dithiothreitol

EC: *E. coli*

EC_{50}: Half maximal effective concentration

EDTA: Ethylenediaminetetraacetic acid

EGFR: epidermal growth factor receptor

em: Emission

ESI: Electron spray ionization

ESKAPE: *E. faecium*, *S. aureus*, *K. pneumoniae*, *A. baumannii*, *P. aeruginosa*, *Enterobacter*

EtOAc: Ethyl acetate

ETP: Epidithiodiketopiperazine

ex: Excitation

FBS: Fetal bovine serum

FITC: Fluorescein isothiocyanate

Fmoc: Fluorenylmethyloxycarbonyl

GBP: Anti-GFP antibody

GFP: Green fluorescent protein

GSH: Glutathione

HATU: (1-[Bis(dimethylamino)methylene]-1H-1,2,3-triazolo[4,5-b]pyridinium 3-oxide hexafluorophosphate

HBTU: 2-(1H-Benzotriazole-1-yl)-1,1,3,3-tetramethyluronium hexafluorophosphate

HCCA: α-Cyano-4-hydroxycinnamic acid
HCHT: High-content high-throughput
HIV: Human immunodeficiency virus
HMBC: Heteronuclear multiple bond correlation
HPLC: High-pressure liquid chromatography
HRMS: High-resolution mass spectrometry
HSQC: Heteronuclear single quantum correlation
IC_{50}: Half maximal inhibitory concentration
IgG: Immunoglobulin G
IM: Inner membrane
IPS: Inorganic polysulfide
IR: Infrared
KM: Kanamycin
LCMS: Liquid chromatography–mass spectrometry
LipA: Lipoic acid
LUV: Large unilamellar vesicle
MALDI: Matrix-assisted laser desorption ionization
MIC: Minimum inhibitory concentration
MMFF: Molecular mechanics force field
MMTS: S-methyl methanethiosulfonate
MRSA: Methicillin-resistant *S. aureus*
MSN: Mesoporous silica nanoparticle
mRNA: Messenger RNA
MS: Mass spectrometry
NDI: Naphthalene diimide
NHS: N-hydroxysuccinimide
NMR: Nuclear magnetic resonance
NTA: Nitrilotriacetic acid
OD_{600}: Optical density at 600 nm
OM: Outer membrane
OPS: Oligonucleotide phosphorothioate

PAMAM: poly(amidoamine)
PBS: Phosphate buffer saline
PDI: Protein disulfide isomerase
PEG: Polyethylene glycol
PEI: Poly(ethyleneimine)
Pen: Penicillin
PFA: Paraformaldehyde
PM: Plasma membrane
PNA: Peptide nucleic acid
PO: Phosphodiester
PS: Phosphorothioate
QD: Quantum dot
R_f: Retardation factor
RGD: Arginylglycylaspartic acid
RNA: Ribonucleic acid
RO: Ring opening
RP: Reverse phase
R_t: Retention time
rt: Room temperature
SaV: Streptavidin
SBD-F: 7-fluorobenzofurazan-4-sulfonic acid ammonium salt
SCARB1: Scavenger receptor class B type 1
SDS: Sodium dodecyl sulfate
SEM: Standard error of the mean
siRNA: Silencing RNA
SNA: Spherical nucleic acid
S_NAr: Nucleophilic aromatic substitution
SPPS: Solid-phase peptide synthesis
Strep: Streptomycin
TAMRA: 5-carboxytetramethylrhodamine
TBTA: Tris((1-benzyl-1*H*-1,2,3-triazol-4-yl)methyl)amine

TCEP: (tris(2-carboxyethyl)phosphine

TEAA: Tetraethylammonium acetate

TFA: Trifluoroacetic acid

TFE: Trifluoroethanol

T_{eff}: Effective templation

T_f: Templation factor

TfR: Transferrin receptor

THF: Tetrahydrofuran

TLC: Thin-layer chromatography

TMS: Trimethylsilane

TOF: Time of flight

Tris: 2-amino-2-(hydroxymethyl)propane-1,3-diol

WHO: World health organization

Chapter 6

REFERENCES

[1] T. Harayama, H. Riezman, *Nat. Rev. Mol. Cell Biol.* **2018**, *19*, 281–296.

[2] M. D. Shultz, *J. Med. Chem.* **2019**, *62*, 1701–1714.

[3] M. Masi, M. Réfregiers, K. M. Pos, J.-M. Pagès, *Nat. Microbiol.* **2017**, *2*, 17001.

[4] H. Yin, *Angew. Chem. Int. Ed.* **2008**, *47*, 2744–2752.

[5] J. Bernardino de la Serna, G. J. Schütz, C. Eggeling, M. Cebecauer, *Front. Cell Dev. Biol.* **2016**, *4*, 106.

[6] P. D. Dobson, D. B. Kell, *Nat. Rev. Drug Discov.* **2008**, *7*, 205–220.

[7] P. Ughachukwu, P. Unekwe, *Ann. Med. Health Sci. Res.* **2012**, *2*, 191–198.

[8] R. L. Juliano, *Nucleic Acids Res.* **2016**, *44*, 6518–6548.

[9] N. Chaudhary, D. Weissman, K. A. Whitehead, *Nat. Rev. Drug Discov.* **2021**, *20*, 817–838.

[10] W. Palm, C. B. Thompson, *Nature* **2017**, *546*, 234–242.

[11] G. J. Doherty, H. T. McMahon, *Annu. Rev. Biochem.* **2009**, *78*, 857–902.

[12] J. P. Luzio, P. R. Pryor, N. A. Bright, *Nat. Rev. Mol. Cell Biol.* **2007**, *8*, 622–632.

[13] E. Uribe-Querol, C. Rosales, *Front. Immunol.* **2020**, *11*, 1066.

[14] J. Canton, *Front. Immunol.* **2018**, *9*, 2286.

[15] J. V. V. Arafiles, H. Hirose, M. Akishiba, S. Tsuji, M. Imanishi, S. Futaki, *Bioconjugate Chem.* **2020**, *31*, 547–553.

[16] M. Kaksonen, A. Roux, *Nat. Rev. Mol. Cell Biol.* **2018**, *19*, 313–326.

[17] Y. Sun, C. Kang, F. Liu, Y. Zhou, L. Luo, H. Qiao, *Drug Dev. Res.* **2017**, *78*, 283–291.

[18] I. Kemker, R. C. Feiner, K. M. Müller, N. Sewald, *ChemBioChem* **2020**, *21*, 496–499.

[19] V. T. Cong, R. D. Tilley, G. Sharbeen, P. A. Phillips, K. Gaus, J. J. Gooding, *Chem. Sci.* **2021**, *12*, 15407–15417.

[20] S. Du, S. S. Liew, L. Li, S. Q. Yao, *J. Am. Chem. Soc.* **2018**, *140*, 15986–15996.

[21] T. Bus, A. Traeger, U. S. Schubert, *J. Mater. Chem. B* **2018**, *6*, 6904–6918.

[22] T. F. Martens, K. Remaut, J. Demeester, S. C. De Smedt, K. Braeckmans, *Nano Today* **2014**, *9*, 344–364.

[23] B. S. Pattni, V. V. Chupin, V. P. Torchilin, *Chem. Rev.* **2015**, *115*, 10938–10966.

[24] C. Zylberberg, S. Matosevic, *Drug Deliv.* **2016**, *23*, 3319–3329.

[25] R. Tenchov, R. Bird, A. E. Curtze, Q. Zhou, *ACS Nano* **2021**, *15*, 16982–17015.

[26] V. Torchilin, *Curr. Drug Deliv.* **2005**, *2*, 319–327.

[27] R. Goswami, T. Jeon, H. Nagaraj, S. Zhai, V. M. Rotello, *Trends Pharmacol. Sci.* **2020**, *41*, 743–754.

[28] M. J. Mitchell, M. M. Billingsley, R. M. Haley, M. E. Wechsler, N. A. Peppas, R. Langer, *Nat. Rev. Drug Discov.* **2021**, *20*, 101–124.

[29] X. Sun, N. Zhang, *Mini-Rev. Med. Chem.* **2010**, *10*, 108–125.

[30] R. V. Benjaminsen, M. A. Mattebjerg, J. R. Henriksen, S. M. Moghimi, T. L. Andresen, *Mol. Ther.* **2013**, *21*, 149–157.

[31] K. E. Bujold, A. Lacroix, H. F. Sleiman, *Chem* **2018**, *4*, 495–521.

[32] A. Lacroix, H. F. Sleiman, *ACS Nano* **2021**, *15*, 3631–3645.

[33] H. Ding, J. Li, N. Chen, X. Hu, X. Yang, L. Guo, Q. Li, X. Zuo, L. Wang, Y. Ma, C. Fan, *ACS Cent. Sci.* **2018**, *4*, 1344–1351.

[34] E. Vivès, P. Brodin, B. Lebleu, *J. Biol. Chem.* **1997**, *272*, 16010–16017.

[35] P. A. Wender, D. J. Mitchell, K. Pattabiraman, E. T. Pelkey, L. Steinman, J. B. Rothbard, *Proc. Natl. Acad. Sci. U.S.A.* **2000**, *97*, 13003–13008.

[36] J. B. Rothbard, T. C. Jessop, R. S. Lewis, B. A. Murray, P. A. Wender, *J. Am. Chem. Soc.* **2004**, *126*, 9506–9507.

[37] N. Sakai, S. Matile, *J. Am. Chem. Soc.* **2003**, *125*, 14348–14356.

[38] M. Di Pisa, G. Chassaing, J.-M. Swiecicki, *Biochemistry* **2015**, *54*, 194–207.

[39] H. D. Herce, A. E. Garcia, J. Litt, R. S. Kane, P. Martin, N. Enrique, A. Rebolledo, V. Milesi, *Biophys. J.* **2009**, *97*, 1917–1925.

[40] H. D. Herce, A. E. Garcia, M. C. Cardoso, *J. Am. Chem. Soc.* **2014**, *136*, 17459–17467.

[41] H. A. Rydberg, M. Matson, H. L. Åmand, E. K. Esbjörner, B. Nordén, *Biochemistry* **2012**, *51*, 5531–5539.

[42] J. S. Appelbaum, J. R. LaRochelle, B. A. Smith, D. M. Balkin, J. M. Holub, A. Schepartz, *Chem. Biol.* **2012**, *19*, 819–830.

[43] G. Lättig-Tünnemann, M. Prinz, D. Hoffmann, J. Behlke, C. Palm-Apergi, I. Morano, H. D. Herce, M. C. Cardoso, *Nat. Commun.* **2011**, *2*, 453.

[44] Z. Qian, T. Liu, Y.-Y. Liu, R. Briesewitz, A. M. Barrios, S. M. Jhiang, D. Pei, *ACS*

Chem. Biol. **2013**, *8*, 423–431.

[45] J. M. Wolfe, C. M. Fadzen, R. L. Holden, M. Yao, G. J. Hanson, B. L. Pentelute, *Angew. Chem. Int. Ed.* **2018**, *57*, 4756–4759.

[46] C. M. Fadzen, J. M. Wolfe, C.-F. Cho, E. A. Chiocca, S. E. Lawler, B. L. Pentelute, *J. Am. Chem. Soc.* **2017**, *139*, 15628–15631.

[47] P. A. Wender, J. B. Rothbard, T. C. Jessop, E. L. Kreider, B. L. Wylie, *J. Am. Chem. Soc.* **2002**, *124*, 13382–13383.

[48] C. B. Cooley, B. M. Trantow, F. Nederberg, M. K. Kiesewetter, J. L. Hedrick, R. M. Waymouth, P. A. Wender, *J. Am. Chem. Soc.* **2009**, *131*, 16401–16403.

[49] C. J. McKinlay, R. M. Waymouth, P. A. Wender, *J. Am. Chem. Soc.* **2016**, *138*, 3510–3517.

[50] C. Douat, C. Aisenbrey, S. Antunes, M. Decossas, O. Lambert, B. Bechinger, A. Kichler, G. Guichard, *Angew. Chem. Int. Ed.* **2015**, *54*, 11133–11137.

[51] K. Pulka-Ziach, S. Antunes, C. Perdriau, B. Kauffmann, M. Pasco, C. Douat, G. Guichard, *J. Org. Chem.* **2018**, *83*, 2530–2541.

[52] L. L. Vezenkov, V. Martin, N. Bettache, M. Simon, A. Messerschmitt, B. Legrand, J.-L. Bantignies, G. Subra, M. Maynadier, V. Bellet, M. Garcia, J. Martinez, M. Amblard, *ChemBioChem* **2017**, *18*, 2110–2114.

[53] E.-K. Bang, G. Gasparini, G. Molinard, A. Roux, N. Sakai, S. Matile, *J. Am. Chem. Soc.* **2013**, *135*, 2088–2091.

[54] G. Gasparini, E.-K. Bang, G. Molinard, D. V. Tulumello, S. Ward, S. O. Kelley, A. Roux, N. Sakai, S. Matile, *J. Am. Chem. Soc.* **2014**, *136*, 6069–6074.

[55] Y. Zhang, Y. Qi, S. Ulrich, M. Barboiu, O. Ramström, *Mater. Chem. Front.* **2020**, *4*, 489–506.

[56] S. Ulrich, *Acc. Chem. Res.* **2019**, *52*, 510–519.

[57] C. Bouillon, Y. Bessin, F. Poncet, M. Gary-Bobo, P. Dumy, M. Barboiu, N. Bettache, S. Ulrich, *J. Mater. Chem. B* **2018**, *6*, 7239–7246.

[58] N. Laroui, M. Coste, D. Su, L. M. A. Ali, Y. Bessin, M. Barboiu, M. Gary-Bobo, N. Bettache, S. Ulrich, *Angew. Chem. Int. Ed.* **2021**, *60*, 5783–5787.

[59] P. K. Hashim, K. Okuro, S. Sasaki, Y. Hoashi, T. Aida, *J. Am. Chem. Soc.* **2015**, *137*, 15608–15611.

[60] P. K. Hashim, K. Okuro, T. Aida, *J. Control. Release* **2017**, *259*, e101.

[61] A. Kohata, P. K. Hashim, K. Okuro, T. Aida, *J. Am. Chem. Soc.* **2019**, *141*, 2862–2866.

[62] J. M. Priegue, D. N. Crisan, J. Martínez-Costas, J. R. Granja, F. Fernandez-Trillo, J. Montenegro, *Angew. Chem. Int. Ed.* **2016**, *55*, 7492–7495.

[63] I. Louzao, R. García-Fandiño, J. Montenegro, *J. Mater. Chem. B* **2017**, *5*, 4426–4434.

[64] K. A. Andersen, T. P. Smith, J. E. Lomax, R. T. Raines, *ACS Chem. Biol.* **2016**, *11*, 319–323.

[65] A. Bandyopadhyay, K. A. McCarthy, M. A. Kelly, J. Gao, *Nat. Commun.* **2015**, *6*, 6561.

[66] Q. Laurent, R. Martinent, B. Lim, A.-T. Pham, T. Kato, J. López-Andarias, N. Sakai, S. Matile, *JACS Au* **2021**, *1*, 710–728.

[67] E. P. Feener, W. C. Shen, H. J. Ryser, *J. Biol. Chem.* **1990**, *265*, 18780–18785.

[68] H. J. Ryser, R. Mandel, F. Ghani, *J. Biol. Chem.* **1991**, *266*, 18439–18442.

[69] H. J. Ryser, E. M. Levy, R. Mandel, G. J. DiSciullo, *Proc. Natl. Acad. Sci. U.S.A.* **1994**, *91*, 4559–4563.

[70] A. Kichler, J. S. Remy, O. Boussif, B. Frisch, C. Boeckler, J. P. Behr, F. Schuber, *Biochem. Biophys. Res. Commun.* **1995**, *209*, 444–450.

[71] S. Aubry, F. Burlina, E. Dupont, D. Delaroche, A. Joliot, S. Lavielle, G. Chassaing, S. Sagan, *FASEB J.* **2009**, *23*, 2956–2967.

[72] A. G. Torres, M. J. Gait, *Trends Biotechnol.* **2012**, *30*, 185–190.

[73] R. Breslow, *Ann. N. Y. Acad. Sci.* **1964**, *98*, 445–452.

[74] A. Kisanuki, Y. Kimpara, Y. Oikado, N. Kado, M. Matsumoto, K. Endo, *J. Polym. Sci. A: Polym. Chem.* **2010**, *48*, 5247–5253.

[75] Q. Zhang, C.-Y. Shi, D.-H. Qu, Y.-T. Long, B. L. Feringa, H. Tian, *Sci. Adv.* **2018**, *4*, eaat8192.

[76] Y. Deng, Q. Zhang, B. L. Feringa, H. Tian, D.-H. Qu, *Angew. Chem. Int. Ed.* **2020**, *59*, 5278–5283.

[77] Q. Zhang, Y.-X. Deng, H.-X. Luo, C.-Y. Shi, G. M. Geise, B. L. Feringa, H. Tian, D.-H. Qu, *J. Am. Chem. Soc.* **2019**, *141*, 12804–12814.

[78] Y. Liu, Y. Jia, Q. Wu, J. S. Moore, *J. Am. Chem. Soc.* **2019**, *141*, 17075–17080.

[79] Andrzej. Sadownik, James. Stefely, S. L. Regen, *J. Am. Chem. Soc.* **1986**, *108*, 7789–7791.

[80] M. Balakirev, G. Schoehn, J. Chroboczek, *Chem. Biol.* **2000**, *7*, 813–819.

[81] Z. Zhang, Q. Liu, Z. Sun, B. K. Phillips, Z. Wang, M. Al-Hashimi, L. Fang, M. A. Olson, *Chem. Mater.* **2019**, *31*, 4405–4417.

[82] G. A. Barcan, X. Zhang, R. M. Waymouth, *J. Am. Chem. Soc.* **2015**, *137*, 5650–5653.

[83] K. Margulis, X. Zhang, L.-M. Joubert, K. Bruening, C. J. Tassone, R. N. Zare, R. M. Waymouth, *Angew. Chem. Int. Ed.* **2017**, *56*, 16357–16362.

[84] J. Zhou, L. Sun, L. Wang, Y. Liu, J. Li, J. Li, J. Li, H. Yang, *Angew. Chem. Int. Ed.* **2019**, *58*, 5236–5240.

[85] N. Sakai, M. Lista, O. Kel, S. Sakurai, D. Emery, J. Mareda, E. Vauthey, S. Matile, *J. Am. Chem. Soc.* **2011**, *133*, 15224–15227.

[86] E.-K. Bang, S. Ward, G. Gasparini, N. Sakai, S. Matile, *Polym. Chem.* **2014**, *5*, 2433–2441.

[87] N. Chuard, G. Gasparini, A. Roux, N. Sakai, S. Matile, *Org. Biomol. Chem.* **2015**, *13*, 64–67.

[88] P. Morelli, S. Matile, *Helv. Chim. Acta* **2017**, *100*, e1600370.

[89] P. Morelli, E. Bartolami, N. Sakai, S. Matile, *Helv. Chim. Acta* **2018**, *101*, e1700266.

[90] P. Morelli, X. Martin-Benlloch, R. Tessier, J. Waser, N. Sakai, S. Matile, *Polymer Chemistry* **2016**, *7*, 3465–3470.

[91] G. Gasparini, S. Matile, *Chem. Commun.* **2015**, *51*, 17160–17162.

[92] E. Derivery, E. Bartolami, S. Matile, M. Gonzalez-Gaitan, *J. Am. Chem. Soc.* **2017**, *139*, 10172–10175.

[93] Y. Okamoto, R. Kojima, F. Schwizer, E. Bartolami, T. Heinisch, S. Matile, M. Fussenegger, T. R. Ward, *Nat. Commun.* **2018**, *9*, 1943.

[94] J. Fu, C. Yu, L. Li, S. Q. Yao, *J. Am. Chem. Soc.* **2015**, *137*, 12153–12160.

[95] L. Qian, J. Fu, P. Yuan, S. Du, W. Huang, L. Li, S. Q. Yao, *Angew. Chem. Int. Ed.* **2018**, *57*, 1532–1536.

[96] X. Qin, C. Yu, J. Wei, L. Li, C. Zhang, Q. Wu, J. Liu, S. Q. Yao, W. Huang, *Adv. Mater.* **2019**, *31*, 1902791.

[97] C. Yu, L. Qian, J. Ge, J. Fu, P. Yuan, S. C. L. Yao, S. Q. Yao, *Angew. Chem. Int. Ed.* **2016**, *55*, 9272–9276.

[98] P. Yuan, X. Mao, K. C. Chong, J. Fu, S. Pan, S. Wu, C. Yu, S. Q. Yao, *Small* **2017**, *13*, 1700569.

[99] X. Mao, P. Yuan, C. Yu, L. Li, S. Q. Yao, *Angew. Chem. Int. Ed.* **2018**, *57*, 10257–10262.

[100] P. Yuan, H. Zhang, L. Qian, X. Mao, S. Du, C. Yu, B. Peng, S. Q. Yao, *Angew. Chem. Int. Ed.* **2017**, *56*, 12481–12485.

[101] P. Yuan, X. Mao, X. Wu, S. S. Liew, L. Li, S. Q. Yao, *Angew. Chem. Int. Ed.* **2019**, *58*, 7657–7661.

[102] J. Guo, T. Wan, B. Li, Q. Pan, H. Xin, Y. Qiu, Y. Ping, *ACS Cent. Sci.* **2021**, *7*, 990–1000.

[103] J. Lu, H. Wang, Z. Tian, Y. Hou, H. Lu, *J. Am. Chem. Soc.* **2020**, *142*, 1217–1221.

[104] G. Gasparini, G. Sargsyan, E.-K. Bang, N. Sakai, S. Matile, *Angew. Chem. Int. Ed.* **2015**, *54*, 7328–7331.

[105] D. Abegg, G. Gasparini, D. G. Hoch, A. Shuster, E. Bartolami, S. Matile, A. Adibekian, *J. Am. Chem. Soc.* **2017**, *139*, 231–238.

[106] A. Tirla, M. Hansen, P. Rivera-Fuentes, *Synlett* **2018**, *29*, 1289–1292.

[107] A. Tirla, P. Rivera-Fuentes, *Biochemistry* **2019**, *58*, 1184–1187.

[108] N. Chuard, G. Gasparini, D. Moreau, S. Lörcher, C. Palivan, W. Meier, N. Sakai, S. Matile, *Angew. Chem. Int. Ed.* **2017**, *56*, 2947–2950.

[109] R. Martinent, D. Du, J. López-Andarias, N. Sakai, S. Matile, *ChemBioChem* **2021**, *22*, 253–259.

[110] R. Martinent, S. Tawffik, J. López-Andarias, D. Moreau, Q. Laurent, S. Matile, *Chem. Sci.* **2021**, *12*, 13922–13929.

[111] L. Zong, E. Bartolami, D. Abegg, A. Adibekian, N. Sakai, S. Matile, *ACS Cent. Sci.* **2017**, *3*, 449–453.

[112] N. Chuard, A. I. Poblador-Bahamonde, L. Zong, E. Bartolami, J. Hildebrandt, W. Weigand, N. Sakai, S. Matile, *Chem. Sci.* **2018**, *9*, 1860–1866.

[113] E. Bartolami, D. Basagiannis, L. Zong, R. Martinent, Y. Okamoto, Q. Laurent, T. R. Ward, M. Gonzalez-Gaitan, N. Sakai, S. Matile, *Chem. Eur. J.* **2019**, *25*, 4047–4051.

[114] Y. Cheng, L. Zong, J. López-Andarias, E. Bartolami, Y. Okamoto, T. R. Ward, N. Sakai, S. Matile, *Angew. Chem. Int. Ed.* **2019**, *58*, 9522–9526.

[115] J. López-Andarias, J. Saarbach, D. Moreau, Y. Cheng, E. Derivery, Q. Laurent, M. González-Gaitán, N. Winssinger, N. Sakai, S. Matile, *J. Am. Chem. Soc.* **2020**, *142*, 4784–4792.

[116] R. Martinent, J. López-Andarias, D. Moreau, Y. Cheng, N. Sakai, S. Matile, *Beilstein J. Org. Chem.* **2020**, *16*, 2007–2016.

[117] Y. Cheng, A.-T. Pham, T. Kato, B. Lim, D. Moreau, J. López-Andarias, L. Zong, N. Sakai, S. Matile, *Chem. Sci.* **2021**, *12*, 626–631.

[118] B. Lim, Y. Cheng, T. Kato, A. Pham, E. Le Du, A. K. Mishra, E. Grinhagena, D. Moreau, N. Sakai, J. Waser, S. Matile, *Helv. Chim. Acta* **2021**, *104*, e2100085.

[119] L. Y. Kong, K. Zeng, Y. Zhang, J. Shao, J. Yan, J.-Y. Liao, W. Wang, X. Dai, Q. Weng, S. Yao, S. Zeng, L. Qian, *Chem. Commun.* **2022**, *in press*, DOI 10.1039.D1CC06840G.

[120] L. K. McKenzie, R. El-Khoury, J. D. Thorpe, M. J. Damha, M. Hollenstein, *Chem. Soc. Rev.* **2021**, *50*, 5126–5164.

[121] S. T. Crooke, S. Wang, T. A. Vickers, W. Shen, X. Liang, *Nat. Biotechnol.* **2017**, *35*, 230–237.

[122] Q. Laurent, N. Sakai, S. Matile, *Helv. Chim. Acta* **2019**, *102*, e1800209.

[123] A. D. Clauss, S. F. Nelsen, M. Ayoub, J. W. Moore, C. R. Landis, F. Weinhold, *Chem. Educ. Res. Pract.* **2014**, *15*, 417–434.

[124] P. C. Hiberty, B. Braïda, *Angew. Chem. Int. Ed.* **2018**, *57*, 5994–6002.

[125] R. Singh, G. M. Whitesides, *J. Am. Chem. Soc.* **1990**, *112*, 6304–6309.

[126] X. Zhang, R. M. Waymouth, *J. Am. Chem. Soc.* **2017**, *139*, 3822–3833.

[127] E. H. Smith, *J. Chem. Soc., Perkin Trans. 1* **1984**, 523–527.

[128] K. Tittmann, *FEBS J.* **2009**, *276*, 2454–2468.

[129] H. M. A. Hassan, B. A. Maltman, *Bioorg. Chem.* **2012**, *40*, 6–9.

[130] Y. S. Yang, P. A. Frey, *Biochemistry* **1986**, *25*, 8173–8178.

[131] G. S. Pulcu, N. S. Galenkamp, Y. Qing, G. Gasparini, E. Mikhailova, S. Matile, H. Bayley, *J. Am. Chem. Soc.* **2019**, *141*, 12444–12447.

[132] J. Hildebrandt, T. Niksch, R. Trautwein, N. Häfner, H. Görls, M.-C. Barth, M. Dürst, I. B. Runnebaum, W. Weigand, *Phosphorus Sulfur Silicon Relat. Elem.* **2017**, *192*, 182–186.

[133] D. Steinmann, T. Nauser, W. H. Koppenol, *J. Org. Chem.* **2010**, *75*, 6696–6699.

[134] B. Rasmussen, A. Sørensen, H. Gotfredsen, M. Pittelkow, *Chem. Commun.* **2014**, *50*, 3716–3718.

[135] N. Metanis, D. Hilvert, *Chem. Sci.* **2015**, *6*, 322–325.

[136] J. C. Lukesh, B. VanVeller, R. T. Raines, *Angew. Chem. Int. Ed.* **2013**, *52*, 12901–12904.

[137] M. von Delius, E. M. Geertsema, D. A. Leigh, *Nat. Chem.* **2010**, *2*, 96–101.

[138] M. von Delius, E. M. Geertsema, D. A. Leigh, D.-T. D. Tang, *J. Am. Chem. Soc.* **2010**, *132*, 16134–16145.

[139] A. G. Campaña, A. Carlone, K. Chen, D. T. F. Dryden, D. A. Leigh, U. Lewandowska, K. M. Mullen, *Angew. Chem. Int. Ed.* **2012**, *51*, 5480–5483.

[140] A. G. Campaña, D. A. Leigh, U. Lewandowska, *J. Am. Chem. Soc.* **2013**, *135*, 8639–8645.

[141] S. Q. Jing, I. S. Trowbridge, *EMBO J.* **1987**, *6*, 327–331.

[142] Y. Cheng, O. Zak, P. Aisen, S. C. Harrison, T. Walz, *Cell* **2004**, *116*, 565–576.

[143] D. R. Littler, S. J. Harrop, W. D. Fairlie, L. J. Brown, G. J. Pankhurst, S. Pankhurst, M. Z. DeMaere, T. J. Campbell, A. R. Bauskin, R. Tonini, M. Mazzanti, S. N. Breit, P. M. G. Curmi, *J. Biol. Chem.* **2004**, *279*, 9298–9305.

[144] H. Singh, *FEBS Lett.* **2010**, *584*, 2112–2121.

[145] T. S. Mansour, V. Potluri, R. R. Pallepati, V. Basetti, M. Keesara, A. G. Moghudula, P. Maiti, *Bioorganic Med. Chem. Lett.* **2019**, *29*, 1435–1439.

[146] M. E. Falzone, M. Malvezzi, B.-C. Lee, A. Accardi, *J. Gen. Physiol.* **2018**, *150*, 933–947.

[147] N. P. Bethel, M. Grabe, *Proc. Natl. Acad. Sci. U.S.A.* **2016**, *113*, 14049–14054.

[148] C. Alvadia, N. K. Lim, V. Clerico Mosina, G. T. Oostergetel, R. Dutzler, C. Paulino, *eLife* **2019**, *8*, e44365.

[149] C. M. Miller, A. J. Donner, E. E. Blank, A. W. Egger, B. M. Kellar, M. E. Østergaard, P. P. Seth, E. N. Harris, *Nucleic Acids Res.* **2016**, *44*, 2782–2794.

[150] R. Martinent, Q. Laurent, N. Sakai, S. Matile, *Chimia* **2019**, *73*, 304–307.

[151] Y. Yong Tan, *Prog. Polym. Sci.* **1994**, *19*, 561–588.

[152] S. Połowiński, *Prog. Polym. Sci.* **2002**, *27*, 537–577.

[153] C. R. South, M. Weck, *Macromolecules* **2007**, *40*, 1386–1394.

[154] A. M. van Herk, *Biomacromolecules* **2020**, *21*, 4379–4387.

[155] Y. Brudno, D. R. Liu, *Chem. Biol.* **2009**, *16*, 265–276.

[156] N. ten Brummelhuis, *Polym. Chem.* **2015**, *6*, 654–667.

[157] D. Núñez-Villanueva, M. Ciaccia, G. Iadevaia, E. Sanna, C. A. Hunter, *Chem. Sci.* **2019**, *10*, 5258–5266.

[158] M. Ciaccia, D. Núñez-Villanueva, C. A. Hunter, *J. Am. Chem. Soc.* **2019**, *141*, 10862–10875.

[159] D. Núñez-Villanueva, M. Ciaccia, C. A. Hunter, *RSC Adv.* **2019**, *9*, 29566–29569.

[160] D. Núñez-Villanueva, C. A. Hunter, *Org. Biomol. Chem.* **2019**, *17*, 9660–9665.

[161] D. Núñez-Villanueva, C. A. Hunter, *Chem. Sci.* **2021**, *12*, 4063–4068.

[162] S. H. Gellman, *Acc. Chem. Res.* **1998**, *31*, 173–180.

[163] A. Violette, M. C. Averlant-Petit, V. Semetey, C. Hemmerlin, R. Casimir, R. Graff, M. Marraud, J.-P. Briand, D. Rognan, G. Guichard, *J. Am. Chem. Soc.* **2005**, *127*, 2156–2164.

[164] A. Salaün, M. Potel, T. Roisnel, P. Gall, P. Le Grel, *J. Org. Chem.* **2005**, *70*, 6499–6502.

[165] D. Seebach, D. F. Hook, A. Glättli, *Biopolymers* **2006**, *84*, 23–37.

[166] H.-D. Arndt, B. Ziemer, U. Koert, *Org. Lett.* **2004**, *6*, 3269–3272.

[167] D.-W. Zhang, X. Zhao, J.-L. Hou, Z.-T. Li, *Chem. Rev.* **2012**, *112*, 5271–5316.

[168] M. Tomsett, I. Maffucci, B. A. F. Le Bailly, L. Byrne, S. M. Bijvoets, M. G. Lizio, J. Raftery, C. P. Butts, S. J. Webb, A. Contini, J. Clayden, *Chem. Sci.* **2017**, *8*,

3007–3018.

[169] G. W. Collie, R. Bailly, K. Pulka-Ziach, C. M. Lombardo, L. Mauran, N. Taib-Maamar, J. Dessolin, C. D. Mackereth, G. Guichard, *J. Am. Chem. Soc.* **2017**, *139*, 6128–6137.

[170] B. Mensa, Y. H. Kim, S. Choi, R. Scott, G. A. Caputo, W. F. DeGrado, *Antimicrob. Agents Chemother.* **2011**, *55*, 5043–5053.

[171] M. De Poli, W. Zawodny, O. Quinonero, M. Lorch, S. J. Webb, J. Clayden, *Science* **2016**, *352*, 575–580.

[172] Y. H. Lau, P. de Andrade, Y. Wu, D. R. Spring, *Chem. Soc. Rev.* **2015**, *44*, 91–102.

[173] M. T. J. Bluntzer, J. O'Connell, T. S. Baker, J. Michel, A. N. Hulme, *Pept. Sci.* **2021**, *113*, e24191.

[174] M. Oba, Y. Nagano, T. Kato, M. Tanaka, *Sci. Rep.* **2019**, *9*, 1349.

[175] K. Yanagisawa, T. Morita, S. Kimura, *J. Am. Chem. Soc.* **2004**, *126*, 12780–12781.

[176] V. Diemer, J. Maury, B. A. F. Le Bailly, S. J. Webb, J. Clayden, *Chem. Commun.* **2017**, *53*, 10768–10771.

[177] F. G. A. Lister, B. A. F. Le Bailly, S. J. Webb, J. Clayden, *Nat. Chem.* **2017**, *9*, 420–425.

[178] R. A. Brown, V. Diemer, S. J. Webb, J. Clayden, *Nat. Chem.* **2013**, *5*, 853–860.

[179] J. E. Jones, V. Diemer, C. Adam, J. Raftery, R. E. Ruscoe, J. T. Sengel, M. I. Wallace, A. Bader, S. L. Cockroft, J. Clayden, S. J. Webb, *J. Am. Chem. Soc.* **2016**, *138*, 688–695.

[180] Z. C. Girvin, S. H. Gellman, *J. Am. Chem. Soc.* **2020**, *142*, 17211–17223.

[181] D. Larsen, A. M. Kietrys, S. A. Clark, H. S. Park, A. Ekebergh, E. T. Kool, *Chem. Sci.* **2018**, *9*, 5252–5259.

[182] J. Kalia, R. T. Raines, *Angew. Chem. Int. Ed.* **2008**, *47*, 7523–7526.

[183] W. Drożdż, C. Bouillon, C. Kotras, S. Richeter, M. Barboiu, S. Clément, A. R. Stefankiewicz, S. Ulrich, *Chem. Eur. J.* **2017**, *23*, 18010–18018.

[184] F. Zieleniewski, D. N. Woolfson, J. Clayden, *Chem. Commun.* **2020**, *56*, 12049–12052.

[185] G. Tsuji, T. Misawa, M. Doi, Y. Demizu, *ACS Omega* **2018**, *3*, 6395–6399.

[186] A. Dirksen, S. Dirksen, T. M. Hackeng, P. E. Dawson, *J. Am. Chem. Soc.* **2006**, *128*, 15602–15603.

[187] S. Tsukagoshi, R. Mikami, K. Arai, *Chem. Asian J.* **2020**, *15*, 2646–2652.

[188] P. Luo, R. L. Baldwin, *Biochemistry* **1997**, *36*, 8413–8421.

[189] C. Toniolo, A. Polese, F. Formaggio, M. Crisma, J. Kamphuis, *J. Am. Chem. Soc.* **1996**, *118*, 2744–2745.

[190] P. A. Fernandes, M. J. Ramos, *Chem. Eur. J.* **2004**, *10*, 257–266.

[191] A. D. Peters, S. Borsley, F. della Sala, D. F. Cairns-Gibson, M. Leonidou, J. Clayden, G. F. S. Whitehead, I. J. Vitórica-Yrezábal, E. Takano, J. Burthem, S. L. Cockroft, S. J. Webb, *Chem. Sci.* **2020**, *11*, 7023–7030.

[192] R. Bekus, T. Schrader, *ChemistryOpen* **2020**, *9*, 667–682.

[193] S. Lascano, K.-D. Zhang, R. Wehlauch, K. Gademann, N. Sakai, S. Matile, *Chem. Sci.* **2016**, *7*, 4720–4724.

[194] Q. Laurent, M. Berthet, Y. Cheng, N. Sakai, S. Barluenga, N. Winssinger, S. Matile, *ChemBioChem* **2020**, *21*, 69–73.

[195] C. Nathan, *Nat. Rev. Microbiol.* **2020**, *18*, 259–260.

[196] P. Holmstrup, B. Klausen, *Oral Dis.* **2017**, *24*, 291–295.

[197] J. N. Pendleton, S. P. Gorman, B. F. Gilmore, *Expert Rev. Anti Infect. Ther.* **2013**, *11*, 297–308.

[198] M. F. Richter, P. J. Hergenrother, *Ann. N.Y. Acad. Sci.* **2019**, *1435*, 18–38.

[199] P. A. Smith, M. F. T. Koehler, H. S. Girgis, D. Yan, Y. Chen, Y. Chen, J. J. Crawford, M. R. Durk, R. I. Higuchi, J. Kang, J. Murray, P. Paraselli, S. Park, W. Phung, J. G. Quinn, T. C. Roberts, L. Rougé, J. B. Schwarz, E. Skippington, J. Wai, M. Xu, Z. Yu, H. Zhang, M.-W. Tan, C. E. Heise, *Nature* **2018**, *561*, 189–194.

[200] A. Gupta, S. Mumtaz, C.-H. Li, I. Hussain, V. M. Rotello, *Chem. Soc. Rev.* **2019**, *48*, 415–427.

[201] U. E. Schaible, S. H. E. Kaufmann, *Nat. Rev. Microbiol.* **2004**, *2*, 946–953.

[202] C. Ratledge, L. G. Dover, *Annu. Rev. Microbiol.* **2000**, *54*, 881–941.

[203] R. C. Hider, X. Kong, *Nat. Prod. Rep.* **2010**, *27*, 637.

[204] T. A. Wencewicz, M. J. Miller, *J. Med. Chem.* **2013**, *56*, 4044–4052.

[205] C. Ji, M. J. Miller, *BioMetals* **2015**, *28*, 541–551.

[206] T. A. Wencewicz, M. J. Miller, *Antibacterials* in *Topics in Medicinal Chemistry* (Springer, Berlin, Heidelberg) **2017**, 151–183.

[207] R. Liu, P. A. Miller, S. B. Vakulenko, N. K. Stewart, W. C. Boggess, M. J. Miller, *J. Med. Chem.* **2018**, *61*, 3845–3854.

[208] Q. Laurent, L. K. Batchelor, P. J. Dyson, *Organometallics* **2018**, *37*, 915–923.

[209] Q. Yu, J. Szymanowski, S. C. B. Myneni, J. B. Fein, *Chem. Geol.* **2014**, *373*, 50–58.

[210] D. Michelon, S. Abraham, B. Ebel, J. De Coninck, F. Husson, G. Feron, P. Gervais, R. Cachon, *FEBS J.* **2010**, *277*, 2282–2290.

[211] J.-C. Gasc, S. G. D'Ambrieres, A. Lutz, J.-F. Chantot, *J. Antibiot.* **1991**, *44*, 313–330.

[212] G. Dhanda, P. Sarkar, S. Samaddar, J. Haldar, *J. Med. Chem.* **2018**, *62*, 3184–3205.

[213] S. D. Taylor, M. Palmer, *Bioorg. Med. Chem.* **2016**, *24*, 6253–6268.

[214] F. G. Glansdorp, R. J. Spandl, J. E. Swatton, O. Loiseleur, M. Welch, D. R. Spring, *Org. Biomol. Chem.* **2008**, *6*, 4120–4124.

[215] M. Ghosh, M. J. Miller, *Bioorg. Med. Chem.* **1996**, *4*, 43–48.

[216] I. S. Shchelik, K. Gademann, *ACS Med. Chem. Lett.* **2021**, *12*, 1898–1904.

[217] Y. Halfon, D. Matzov, Z. Eyal, A. Bashan, E. Zimmerman, J. Kjeldgaard, H. Ingmer, A. Yonath, *Sci. Rep.* **2019**, *9*, 11460.

[218] T. A. Wencewicz, U. Möllmann, T. E. Long, M. J. Miller, *BioMetals* **2009**, *22*, 633–648.

[219] C. Ji, M. J. Miller, *Bioorg. Med. Chem.* **2012**, *20*, 3828–36.

[220] I. S. Shchelik, K. Gademann, *bioRxiv* **2021**, doi.org/10.1101/2021.11.03.467114.

[221] J. Felber, L. Poczka, S. Busker, U. Theisen, L. Zeisel, M. S. Maier, K. Loy, C. Brandstädter, K. Scholzen, K. Becker, E. Arnér, J. Ahlfeld, O. Thorn-Seshold, *chemRxiv*, **2020**, doi.org/10.26434/chemrxiv.13483155.v1.

[222] J. G. Felber, L. Zeisel, L. Poczka, K. Scholzen, S. Busker, M. S. Maier, U. Theisen, C. Brandstädter, K. Becker, E. S. J. Arnér, J. Thorn-Seshold, O. Thorn-Seshold, *J. Am. Chem. Soc.* **2021**, *143*, 8791–8803.

[223] J. T. Mika, A. J. Thompson, M. R. Dent, N. J. Brooks, J. Michiels, J. Hofkens, M. K. Kuimova, *Biophys. J.* **2016**, *111*, 1528–1540.

[224] P. Loison, N. A. Hosny, P. Gervais, D. Champion, M. K. Kuimova, J.-M. Perrier-Cornet, *Biochim. Biophys. Acta Biomembr.* **2013**, *1828*, 2436–2443.

[225] N. Purkayastha, S. Capone, A. K. Beck, D. Seebach, J. Leeds, K. Thompson, H. E. Moser, *Chem. Biodivers.* **2015**, *12*, 179–193.

[226] B. Geueke, K. Namoto, I. Agarkova, J.-C. Perriard, H.-P. E. Kohler, D. Seebach, *ChemBioChem* **2005**, *6*, 982–985.

[227] D. T. Cohen, C. Zhang, C. M. Fadzen, A. J. Mijalis, L. Hie, K. D. Johnson, Z. Shriver, O. Plante, S. J. Miller, S. L. Buchwald, B. L. Pentelute, *Nat. Chem.* **2019**, *11*, 78–85.

[228] A. Antonoplis, X. Zang, M. A. Huttner, K. K. L. Chong, Y. B. Lee, J. Y. Co, M. R. Amieva, K. A. Kline, P. A. Wender, L. Cegelski, *J. Am. Chem. Soc.* **2018**, *140*, 16140–16151.

[229] Q. Laurent, R. Martinent, D. Moreau, N. Winssinger, N. Sakai, S. Matile, *Angew. Chem. Int. Ed.* **2021**, *60*, 19102–19106.

[230] F. Eckstein, *Nucleic Acid Ther.* **2014**, *24*, 374–387.

[231] W. B. Wan, P. P. Seth, *J. Med. Chem.* **2016**, *59*, 9645–9667.

[232] S. T. Crooke, P. P. Seth, T. A. Vickers, X. Liang, *J. Am. Chem. Soc.* **2020**, *142*, 14754–14771.

[233] P. A. Frey, R. D. Sammons, *Science* **1985**, *228*, 541–545.

[234] S. T. Crooke, T. A. Vickers, X. Liang, *Nucleic Acids Res.* **2020**, *48*, 5235–5253.

[235] S. Wang, N. Allen, T. A. Vickers, A. S. Revenko, H. Sun, X.-H. Liang, S. T. Crooke, *Nucleic Acids Res.* **2018**, *46*, 3579–3594.

[236] N. Oka, T. Wada, *Chem. Soc. Rev.* **2011**, *40*, 5829.

[237] Y. Huang, K. W. Knouse, S. Qiu, W. Hao, N. M. Padial, J. C. Vantourout, B. Zheng, S. E. Mercer, J. Lopez-Ogalla, R. Narayan, R. E. Olson, D. G. Blackmond, M. D. Eastgate, M. A. Schmidt, I. M. McDonald, P. S. Baran, *Science* **2021**, *373*, 1265–1270.

[238] R. S. Goody, F. Eckstein, *J. Am. Chem. Soc.* **1971**, *93*, 6252–6257.

[239] G. Sengle, A. Jenne, P. S. Arora, B. Seelig, J. S. Nowick, A. Jäschke, M. Famulok, *Bioorg. Med. Chem.* **2000**, *8*, 1317–1329.

[240] V. G. Metelev, O. A. Borisova, E. M. Volkov, T. S. Oretskaya, N. G. Dolinnaya, *Nucleic Acids Res.* **2001**, *29*, 4062–4069.

[241] V. Janout, B. Jing, S. L. Regen, *Bioconjugate Chem.* **2002**, *13*, 351–356.

[242] V. G. Metelev, E. A. Kubareva, O. V. Vorob'eva, A. S. Romanenkov, T. S. Oretskaya, *FEBS Lett.* **2003**, *538*, 48–52.

[243] H. M. Seifert, K. Ramirez Trejo, E. V. Anslyn, *J. Am. Chem. Soc.* **2016**, *138*, 10916–10924.

[244] Ø. Jacobsen, H. Maekawa, N.-H. Ge, C. H. Görbitz, P. Rongved, O. P. Ottersen, M. Amiry-Moghaddam, J. Klaveness, *J. Org. Chem.* **2011**, *76*, 1228–1238.

[245] A. Yagishita, T. Ueno, H. Esumi, H. Saya, K. Kaneko, K. Tsuchihara, Y. Urano, *Bioconjugate Chem.* **2017**, *28*, 302–306.

[246] S. A. Caldarelli, S. El Fangour, S. Wein, C. Tran van Ba, C. Périgaud, A. Pellet, H. J. Vial, S. Peyrottes, *J. Med. Chem.* **2013**, *56*, 496–509.

[247] R. Frei, M. D. Wodrich, D. P. Hari, P.-A. Borin, C. Chauvier, J. Waser, *J. Am. Chem. Soc.* **2014**, *136*, 16563–16573.

[248] W. B. Jin, C. Xu, Q. Cheng, X. L. Qi, W. Gao, Z. Zheng, E. W. C. Chan, Y.-C. Leung, T. H. Chan, K.-Y. Wong, S. Chen, K.-F. Chan, *Eur. J. Med. Chem.* **2018**, *155*, 285–302.